Innate Immunity and Bone Remodeling
during *Staphylococcus aureus* Osteomyelitis

By

Nicole Elizabeth Putnam

Dissertation

submitted to the Faculty of the

Graduate School of Vanderbilt University

in partial fulfillment of the requirements

for the degree of

DOCTOR OF PHILOSOPHY

in

Microbiology and Immunology

June 30, 2019

Nashville, Tennessee

Approved:

Eric P. Skaar, Ph.D., M.P.H.

Julie A. Rhoades (Sterling), Ph.D.

Isaac P. Thomsen, M.D.

Jeffrey C. Rathmell, Ph.D.

Daniel J. Moore, M.D., Ph.D.

James E. Cassat, M.D., Ph.D.

ACKNOWLEDGEMENTS

To my mentors, colleagues, and collaborators at Vanderbilt. I could not have done this without you all. Thank you first and foremost to Dr. Jim Cassat, for allowing me to be one of his first trainees. This was a very exciting time and project. Thank you for being a great mentor and role model, and for helping me develop my writing and presentation skills. Thank you for encouraging me to write independently, but also providing thorough and consistent feedback. I am thankful you allowed me to travel to conferences, and shared in the excitement over posters and presentations. Thank you to my lab mates and research assistants for making the work atmosphere warm and friendly, even when the days and weeks got chaotic. I thank Aimee Potter, Caleb Ford, Chris Peek, Tom Spoonmore, Jenna Petronglo, and Casey Butrico for their intellectual contributions to my research, and Andrew Hendrix, Jacob Curry, and Laura Fulbright for providing resources and organization. Thank you to the Skaar lab members for welcoming me into their science community – for expertise, advice, and friendship. Thank you all for talking science and non-science, and to all of my Vanderbilt friends for the fun times and memories.

To my thesis committee members: thank you for your perceptive advice over the past few years, your support, and helping me develop as a scientist. Thank you to Dr. Eric Skaar for serving as my committee chair, and for giving me the opportunity to use the Microbial Pathogenesis Mini-Sabbatical to learn critical techniques and analyses in bone biology. Thank you to committee member Dr. Julie Rhoades (Sterling), Alyssa Merkel, Dr. Rachelle Johnson, and Josh Johnson for conveying their extensive knowledge towards bone histology sectioning, staining, and histomorphometry. I couldn't have completed this

TABLE OF CONTENTS

LIST OF TABLES

LIST OF FIGURES

LIST OF ABBREVIATIONS

ACK	ammonium chloride potassium
agr	accessory gene regulator
AMPs	antimicrobial peptides
αMEM	Alpha modification minimal essential medium Eagle
BM	bone marrow
BMMs	bone marrow macrophages
CA	community-acquired
CFUs	colony-forming units
CGD	chronic granulomatous disease
DAMPs	damage associated molecular patterns
DMEM	Dulbecco's modified Eagle medium
DNA	deoxyribonucleic acid
ECM	extracellular matrix
FBS	fetal bovine serum
HKLM	heat-killed *Listeria monocytogenes*
LTA-SA	lipoteichoic acid from *S. aureus*
MRSA	methicillin-resistant *S. aureus*
NETs	neutrophil extracellular traps
NO	nitric oxide
NOD	nucleotide-binding oligomerization domain
NSG	non-obese diabetic-*scid IL2Rγ*
OBs	osteoblasts
OCs	osteoclasts
OD	optical density
ODN	CpG oligonucleotide
OPG	osteoprotegerin
P/S	penicillin/streptomycin
PAM_2CSK_4	synthetic diacylated lipopeptide
PAM_3CSK_4	synthetic triacylated lipopeptide
PAMPs	pathogen-associated molecular patterns
PBS	phosphate buffered saline
PGN-SA	peptidoglycan from *S. aureus*
PRRs	pattern recognition receptors
PSMα	alpha-type phenol soluble modulins
PVL	Panton-Valentine Leukotoxin
qRT-PCR	quantitative real-time-polymerase chain reaction
RANKL	cytokines receptor activator of NFκB ligand
RNA	ribonucleic acid
RNS	reactive nitrogen species
ROS	reactive oxygen species
RPMI	Roswell Park Memorial Institute medium
SEAP	secreted alkaline phosphatase
Spa	staphylococcal protein A

TLRs	toll-like receptors
Tm	melting temperature
TRAP	tartrate-resistant acid phosphatase
TSA	tryptic soy agar
TSB	tryptic soy broth
TSM	tris sucrose magnesium chloride buffer
TSST-1	toxin shock syndrome toxin-1
v/v	volume per volume
WBM	whole bone marrow
WT	wild-type

INTRODUCTION

Staphylococcus aureus causes a wide range of diseases that together embody a significant public health burden due to the variety of clinical manifestations and complications during infection. Aided by metabolic flexibility and a large virulence repertoire, *S. aureus* can hematogenously disseminate and infect various tissues, including skin, lung, heart, and bone, among others. Resident cells at each tissue site mount an immune response through recognition of bacterial components and danger signals from cellular damage. This response leads to the production of proinflammatory cytokines, chemokines, and lipid mediators. The localized immune response enhances leukocyte infiltration and activation, leading to the phagocytosis and killing of bacteria. The hallmark lesions of staphylococcal infections are abscesses, which denote the powerful innate immune responses to tissue invasion, as well as the ability of staphylococci to persist within these lesions. The innate immune response develops from resident tissue cells, and specific immune cells are recruited to produce antimicrobial effectors and sequester bacteria to prevent spreading. In this introduction, I review the innate immune responses to *S. aureus*, focusing on the interactions that occur in bone, which serves as a paradigm for invasive disease.

The research questions outlined in this dissertation investigate how innate immune signaling influences antibacterial host responses and bone remodeling alterations during *S. aureus* osteomyelitis. More specifically, Chapter I (Introduction) summarizes (1) specific details on bone as a target tissue of infection, (2) the key components necessary to mount an innate immune response to *S. aureus* in the context of invasive infections, (3) an

overview of osteo-immunologic crosstalk between the immune and skeletal systems, (4) the ability of *S. aureus* to induce pathology and modulate host immune responses, and (5) a summary of innate effector cells and mechanisms necessary for bacterial control as elucidated from *S. aureus* skin infections. Collectively, Chapter I provides the rationale for the studies described within this thesis.

Based on this background information, in this thesis I test the central hypothesis that *MyD88-dependent immune pathways are necessary for antibacterial responses during S. aureus osteomyelitis, but this dependence may have detrimental effects on bone homeostasis through the modulation of skeletal cell differentiation*. In Chapter II, I test how inflammatory stimuli perturb osteoclast differentiation, in which I also outline the development of assays to define the ability of *S. aureus* to influence changes in osteoclast lineage cells. Chapter III presents data on how *S. aureus* influences trabecular bone remodeling and skeletal cell changes *in vivo,* while also testing the ability of the innate immune components MyD88 and IL-1R to influence bone remodeling and immune responses. Furthermore, Chapter IV defines the influence of TLR2 and TLR9 on bone remodeling and antibacterial immunity as defined by *in vitro* and *in vivo* analyses. Together, this thesis establishes how MyD88, TLR2, TLR9, and IL-1R modulate the host immune response and influence bone remodeling in response to *S. aureus* osteomyelitis.

A portion of the following section (*Chapter I, Innate immunity to Staphylococcus aureus: Evolving paradigms in invasive infection*) was originally published in *The Journal of Immunology*. (June 2018).

Brandt SL*, Putnam NE*, Cassat JE[#], Serezani CH[#]. 2018. Innate immunity to *Staphylococcus aureus*: Evolving paradigms in soft tissue and invasive infections. *J Immunol*. 200(12):3871-3880.

CHAPTER I

INNATE IMMUNITY TO *STAPHYLOCOCCUS AUREUS*:

EVOLVING PARADIGMS IN INVASIVE DISEASE

Introduction

Staphylococcus aureus is a Gram-positive bacterium that colonizes approximately 30% of the population [1]. Despite this relatively innocuous lifestyle, *S. aureus* is capable of breaching tissue barriers, circulating through the bloodstream, and infecting nearly every organ system in the body. *S. aureus* is the most common cause of bacterial skin and soft tissue infections in the United States [2, 3]. Other infection sites include but are not limited to bone, lung, kidney, and heart. A critical tenant in the battle against staphylococcal infections is to understand host risk factors, including those that parse out individuals capable of local control of infection, versus those that progress to invasive disease.

Burden of *S. aureus* infections

In the early 1880's, Dr. Alexander Ogston examined purulent material from patients with soft tissue infection [4, 5]. Following Ogston's landmark discovery, it has become clear that *S. aureus* is the predominant bacterial pathogen causing purulent infections in both superficial and deep tissues. Infections caused by *S. aureus* range from relatively harmless folliculitis to life-threatening sepsis. However, if not properly treated, less serious infections could progress to more complicated infection through spread into the bloodstream or translocation to deep tissues and organs [6]. Historically, most invasive *S. aureus* cases were due to hospital-acquired infections, but over the past few decades

community-acquired (CA) *S. aureus* strains have become a common cause of infection in otherwise healthy individuals [7]. These CA strains are thought to be able to cause severe infections in immunocompetent populations in part due to a higher abundance of virulence factors. Based on epidemiologic data from 2012 in the United States, approximately 80,000 invasive methicillin-resistant *S. aureus* (MRSA) infections occur each year, leading to over 11,000 deaths [8]. Invasive infections can encompass body sites such as the lung, heart, and bone. Although much has been learned regarding the architecture of staphylococcal abscesses and the major cellular contributors to pyogenic immune responses [9], many questions remain unanswered. In the sections that follow, we review the key events underlying effective recognition and microbiologic control of *S. aureus* bone infection, as *S. aureus* is responsible for the vast majority of all human osteomyelitis cases [10], and also serves as a paradigm for invasive disease.

Skeletal cell remodel bone and are innate sensors of bacterial pathogens

Osteoblast and osteoclast ontogeny and function

Skeletal cells have specialized roles to maintain bone structure, which is continually remodeling. Osteoblasts are derived from mesenchymal stem cells, and function as bone-forming cells that lay down an extracellular matrix, predominantly made of type I collagen. Osteoblasts then mineralize this matrix, incorporating hydroxyapatite crystals to give the bone its rigid tissue structure. When bone becomes old or damaged, this matrix can be degraded by osteoclasts derived from myeloid lineage cells. Osteoclasts function by forming a localized resorption compartment on bone with a low pH into which they secrete enzymes to mobilize mineral and digest the organic matrix, and coordinate resorption with

recruitment of bone-forming osteoblasts, to continually remodel bone and maintain a healthy extracellular matrix (ECM) [11-13].

Homeostatic bone remodeling is regulated by cytokines and systemic cues

Bone remodeling is regulated under tight homeostatic control. Osteoblasts and their descendant lineage osteocytes that become encased in bone matrix are key modulators of bone remodeling, with the ability to respond to systemic and local cues such as hormones, vitamins, and minerals. Under normal flux the cytokines receptor activator of NFκB ligand (RANKL) and osteoprotegerin (OPG) help precisely balance osteoblast and osteoclast activities. Osteoblast and osteocytes produce RANKL and OPG at varying ratios to favor either bone resorption or formation [14-16], although RANKL is also expressed by activated lymphocytes [17-20]. Increased production of the TNF-family cytokine RANKL signals through the RANK receptor on myeloid lineage cells to promote osteoclast differentiation and bone resorption [15] **(Figure 1)**. Thus, mice deficient in RANK or RANKL do not have osteoclasts, resulting in very dense bones, or severe osteopetrosis [21, 22]. In this way, RANKL is a key factor in monocyte cellular fate, as these cells can differentiate either into inflammatory macrophages or bone-resorbing osteoclasts depending on the environmental milieu. However, a decreased RANKL:OPG ratio will slow bone resorption, leading to a net anabolic effect by bone-forming osteoblasts. Tight regulation of osteoclastogenesis is imposed by osteoblasts through production of the soluble decoy receptor OPG that acts as an important physiologic inhibitor of osteoclastogenesis, and OPG-deficient mice exhibit osteoporosis [23]. To induce osteoclastogenesis RANK signaling must occur on a myeloid lineage cell in the presence

of M-CSF, and with co-stimulation through immunoglobulin-like receptors TREM2 or OSCAR [24]. Complex signaling pathways during osteoclast differentiation lead to the activation of transcription factors NFκB, AP-1, and NFATc1, among others, to induce osteoclast-specific genes [25-29] **(Figure 2)**.
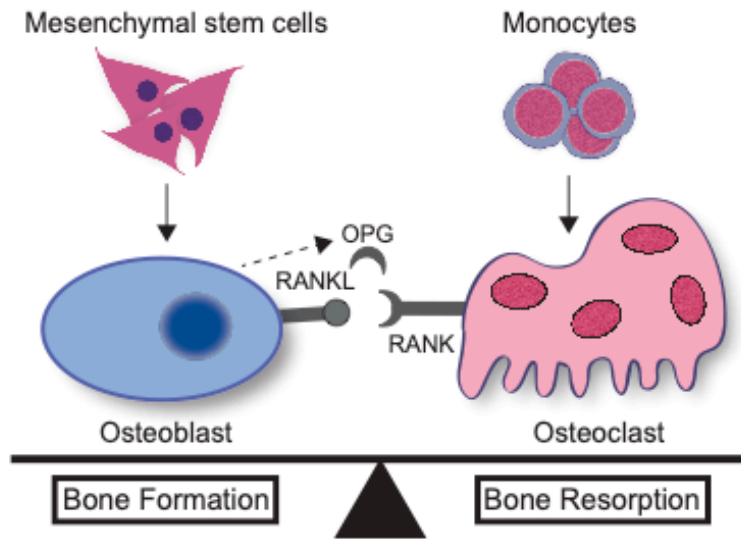
Figure 1. Homeostatic bone remodeling occurs through communication between osteoblast and osteoclast lineage cells. Mesenchymal stem cells give rise to osteoblasts that are responsible for forming and mineralizing the extracellular matrix of bone. Osteoblast lineage cells are also the primary producers of the TNF-family cytokines RANKL and OPG, which control bone resorption by promoting and inhibiting osteoclast differentiation, respectively. Osteoclasts arise from myeloid lineage cells of hematopoietic origin through multinucleation. Osteoclasts are functionally able to resorb bone by demineralizing and degrading bone matrix.
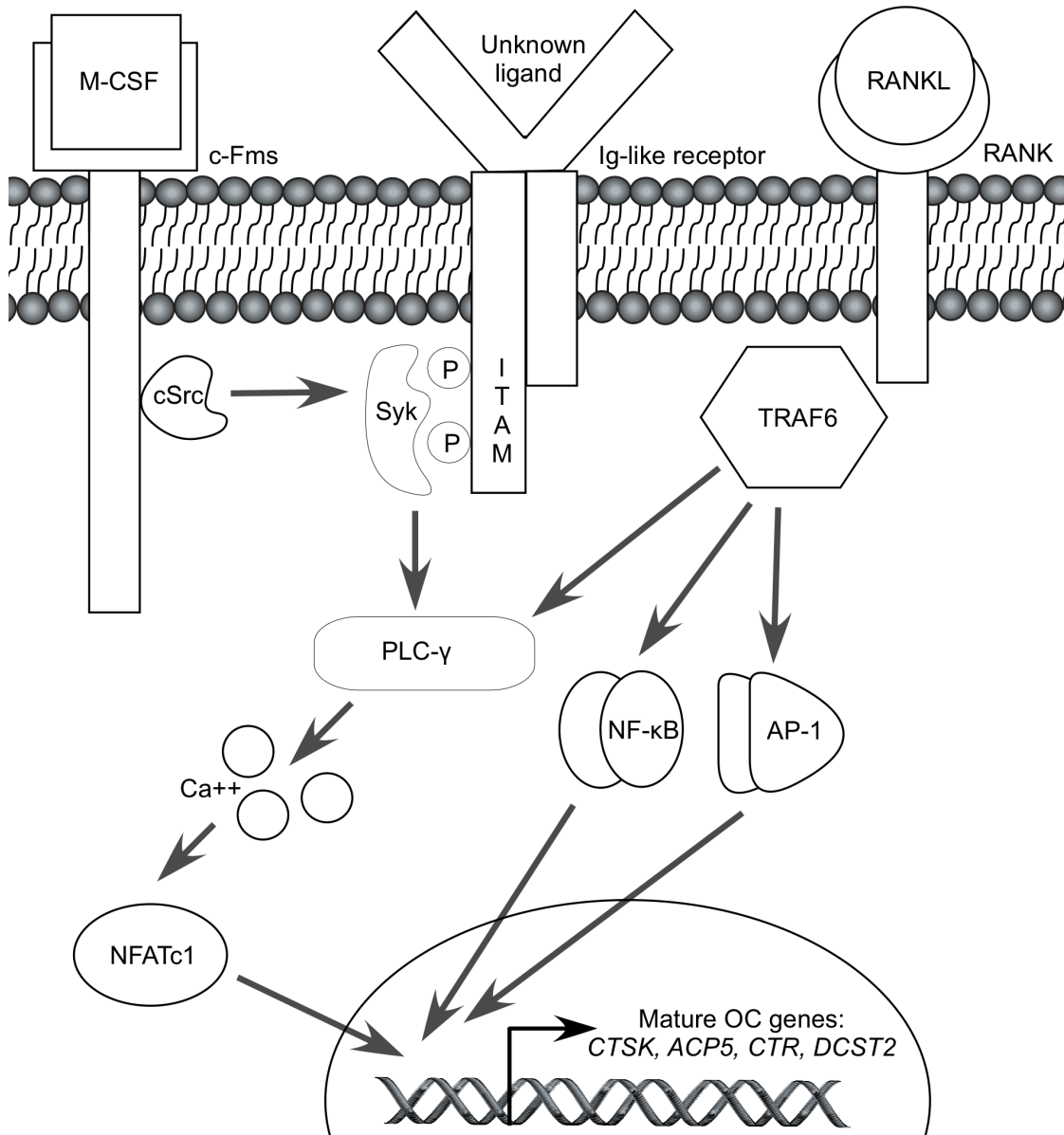
Figure 2. Osteoclast differentiation requires RANKL signaling in the presence of M-CSF and co-stimulation from an Ig-like receptor.

In a simplified version of osteoclast signaling: M-CSF signaling through its receptor, c-FMS, leads to activation of cSrc kinase to phosphorylate ITAMS on a co-stimulatory Ig-like receptor, allowing for Syk kinase docking. Syk kinase and TRAF6-mediated signaling activate phospholipase C (PLC)-γ to cleave the substrate PIP_2. This reaction leads to cytoplasmic mobilization of calcium and activation of the canonical osteoclast transcription factor, NFATc1. RANK signaling through TRAF6 activates additional transcription factors necessary for osteoclastogenesis, including canonical and non-canoncial NFκB and AP-1. In the nucleus, these transcription factors work together to induce osteoclast-specific genes, *CTSK* (cathepskin K), *TRAP* (tartrate-resistant acid phosphatase), *CTR* (calcitonin receptor), and *DCST2* (DC-STAMP), among others.

Bone as a target tissue for *S. aureus* infection

The skeletal environment is complex, and it is unclear how *S. aureus* is so well equipped to survive in this niche. *S. aureus* is capable of colonizing skeletal tissues following hematogenous dissemination, via direct inoculation following trauma, or by spread of a contiguous infection. Upon colonization of bone, *S. aureus* is capable of establishing chronic infection, often surviving within traditional abscess lesions in the bone marrow **(Figure 3A and 3C)** or invading directly into damaged bone through the network of osteocytic canaliculi [30]. In addition to invading into healthy bone tissue, *S. aureus* can also invade and adhere to pieces of devitalized bone known as sequestra, creating a niche for chronic infection [30] **(Figure 3D and 3E)**. The mechanisms used by staphylococci to persist within bone are an area of ongoing investigation [31-35]. However, the events leading to detection of invading staphylococci by the immune system in bone are poorly understood in comparison to studies in skin. Moreover, innate immune responses to bacterial pathogens in bone lead to profound effects on bone remodeling, which in turn dramatically influence the outcome of infection [31, 36-40].
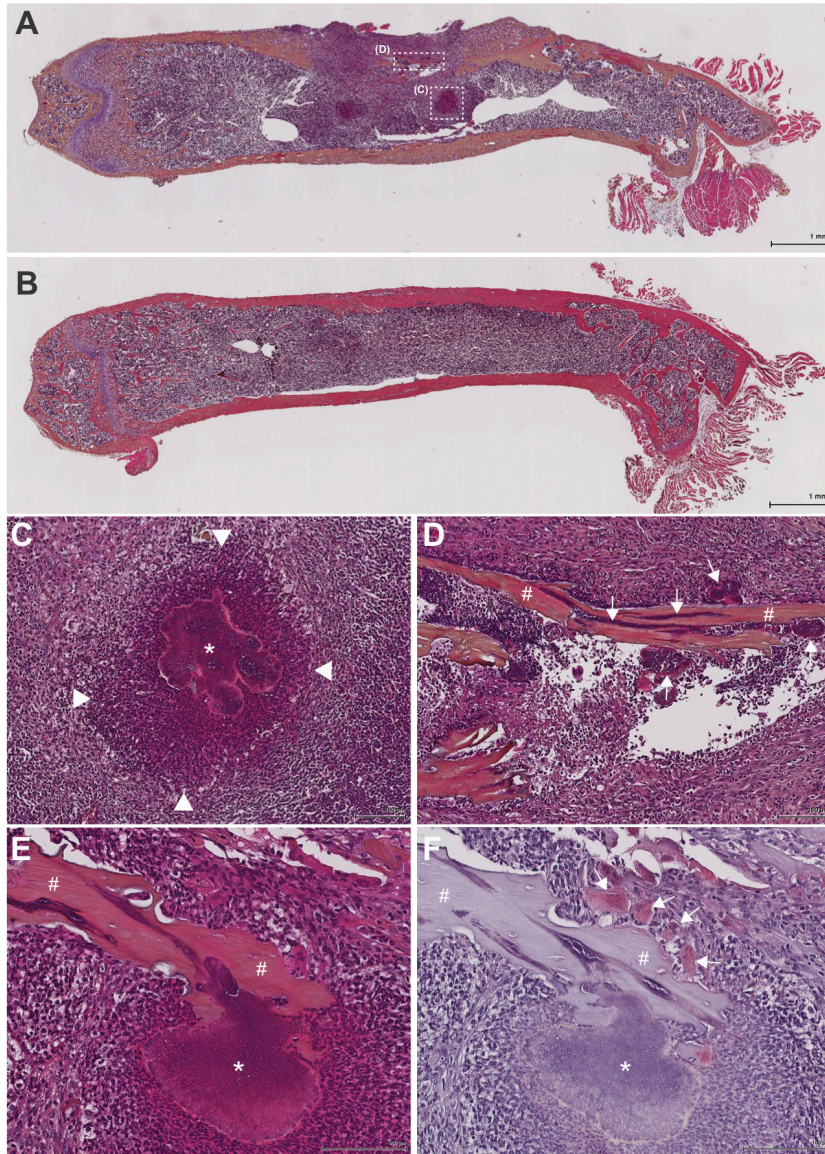
Figure 3. *S. aureus* **forms traditional abscesses in bone marrow but also grows directly on and invades into living and dead bone fragments.**
Murine femurs were extracted, fixed in neutral buffered formalin, and dehydrated in 70% ethanol. Following decalcification in 20% EDTA (pH 7.4), femurs were processed and embedded in paraffin. Femurs infected with *S. aureus* **(A)** or mock infected with PBS **(B)** were sectioned and stained with a modified H&E stain prior to imaging at original magnification X1. Different abscess morphologies, including a traditional abscess (box C) in the bone marrow **(C)** and sequestra (box D) along cortical bone fragments **(D)**, were observed in the *S. aureus*-infected femurs upon imaging at original magnification X10. Arrowheads in (C) denote the boundaries of the abscess's neutrophilic infiltrate. * denotes the staphylococcal abscess community surrounded by an eosinophilic pseudocapsule in the center of the abscess. # in (D) denotes a non-viable piece of cortical bone (sequestrum) with tiny adherent clusters of staphylococci (arrows) both on the surface of and within the

sequestrum. **(E and F)** A second murine osteomyelitis sample was stained with both modified H&E **(E)** and tartrate-resistant acid phosphatase (mature osteoclast marker) **(F)** to demonstrate that *S. aureus* can also adhere to segments of living cortical bone (denoted by #), as osteoclasts (arrows) are visualized remodeling the same fragment of cortical bone. * denotes a large cluster of staphylococci directly adherent to the bone segment.

Skeletal cells as innate sensors of bacterial pathogens

S. aureus has an extraordinary virulence repertoire that facilitates binding to host tissues, subsequent tissue invasion, host cell death, and bacterial dissemination [41-44]. *S. aureus* is a Gram-positive pathogen and therefore has a thick peptidoglycan wall studded with lipoteichoic acids, surface adhesins, and immunomodulatory proteins. Staphylococci also secrete toxins, proteases, and other degradative enzymes that facilitate tissue invasion, host cell death, and dissemination. Yet these virulence factors also serve as potent stimuli for activation of innate immune responses.

Staphylococcal adhesins allow binding to extracellular matrix components found in bone, including fibronectin and collagen [45]. Select adhesins also promote endocytic uptake into nonprofessional phagocytic cells, such as osteoblasts [45, 46]. Once internalized, *S. aureus* can escape into the cytoplasm by lysing the endosome [47-50]. This close association with bone cells triggers immune responses, as osteoblasts, osteoclasts, and their precursor cells express a repertoire of pattern recognition receptors (PRRs) [51-56], each capable of detecting pathogen associated molecular patterns (PAMPs) and initiating downstream immune responses.

Much like the epithelium, bone cells can express antimicrobial peptides (AMPs) that serve as an early defense to protect against invasion by pathogenic bacteria [57]. In bone samples isolated from humans and mice with osteomyelitis, AMPs were increased relative to healthy bones [58]. *In vitro* studies have also shown that *S. aureus* supernatants and IL-1 are able to enhance AMP expression from human and murine osteoblasts via the p38 MAPK and NFκB pathways [58, 59]. In a murine model of post-traumatic *S. aureus*

osteomyelitis, Yoshii et al. [60] found high levels of IL-1, IL-6, and TNFα in bone early after infection, with TNFα remaining elevated for the 28-day course of infection.

PRRs on bone cells that sense *S. aureus* include toll-like receptors (TLRs) and nucleotide-binding oligomerization domain (NOD) receptors. Specifically, TLR2 recognition of peptidoglycan and lipoteichoic acid [54, 61, 62], TLR9 endosomal recognition of bacterial DNA [63], and NOD-mediated recognition of cytoplasmic bacteria following escape from the endosome [64]. Similar to the interactions with resident skin cells, *S. aureus* activates TLR2 on osteoblasts *in vitro*, leading to release of AMPs and cell death [58, 65]. Once internalized, *S. aureus* in osteoblasts can be killed in the endosome through TLR9-mediated induction of oxidative stress, though not as robustly as professional phagocytes [66, 67]. *S. aureus* also triggers expression of NOD2 by osteoblasts, [64, 68], and cooperation between TLR2 and NOD2 induces RANKL production [52, 53, 69]. Finally, the NLRP3 inflammasome can be activated in myeloid cells by *S. aureus* peptidoglycan and bone particles [70, 71]. Consequently, recognition of *S. aureus* by multiple PRRs on bone cells induces a robust inflammatory response and alters bone remodeling **(Figure 4)**. *S. aureus* recognition by PRRs, such as TLR2 and NOD2, allows for shared innate mechanisms between resident skin and bone cells, emphasizing the importance of response to general bacterial motifs.
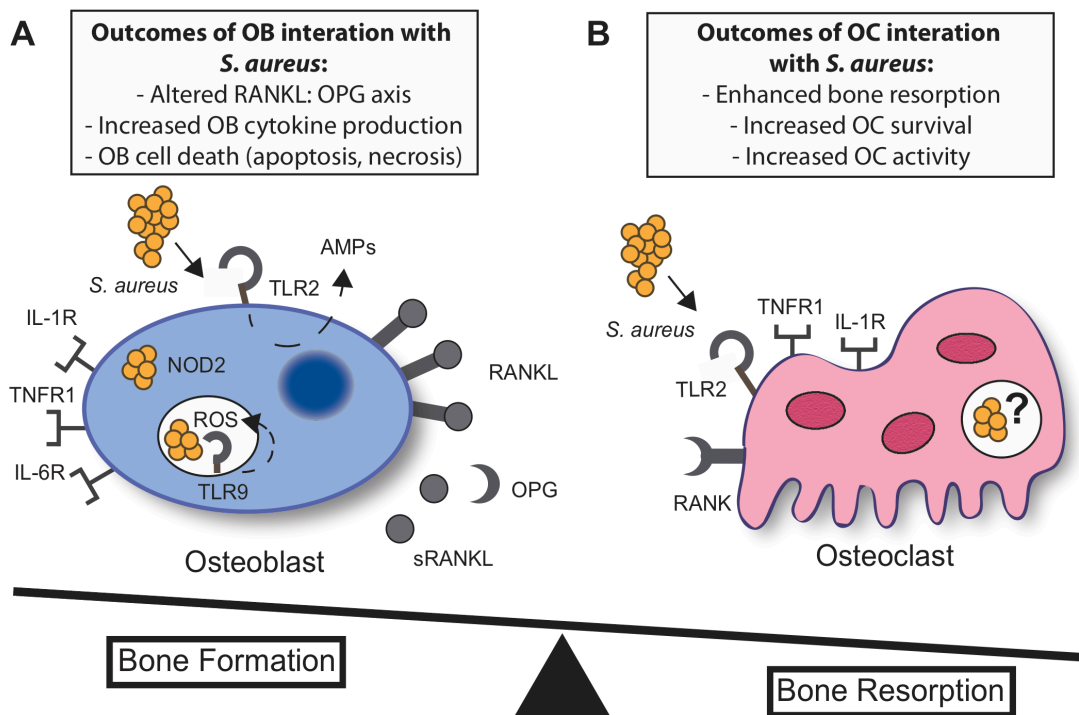
Figure 4. Outcomes of skeletal cell interactions with *S. aureus.*
(A-B) Bone remodeling activities of osteoblasts (OBs) and osteoclasts (OCs) are altered following interactions between innate immune receptors and *S. aureus*. **(A)** In osteoblasts, TLR2 recognition of extracellular *S. aureus* leads to production of AMPs, TLR9 detection of bacterial CpG DNA in the endosome induces an antimicrobial ROS response, and NOD2 sensing of cytoplasmic *S. aureus* occurs following escape from the endosome. The culmination of osteoblastic innate recognition results in production of proinflammatory cytokines, such as TNFα, IL-1, and IL-6. These cytokines allow osteoblasts to favor increased production of RANKL and decreased release of the RANKL inhibitory cytokine OPG. The increased RANKL:OPG ratio and pro-inflammatory cytokine production have a net effect to enhance osteoclast differentiation. However, osteoblast activation and the effects of staphylococcal toxins may also result in osteoblast dell death through apoptosis and necrosis. RANKL production allows for enhanced differentiation of osteoclast precursors. Pro-inflammatory cytokines, such as TNFα, IL-1, can signal directly onto osteoclast precursors to increase osteoclast survival and bone resorption activity. **(B)** Osteoclast expression and ligation of TLR2 have been shown to allow for the further differentiation down the osteoclast lineage; however, this occurs only in cells that have first been stimulated with RANKL. Whether or not *S. aureus* can invade osteoclasts of activate endosomal or cytoplasmic PRRs remains to be determined.

Host immunity to *S. aureus* during skeletal infection

Osteomyelitis as a paradigm for invasive staphylococcal infection

S. aureus has the remarkable ability to invade and establish infection at various sites throughout the body. The metabolic flexibility and large repertoire of immune evasion and virulence strategies employed by staphylococci allow these bacteria to seed various tissues and gain nutrients to sustain infection. Of the many tissues that *S. aureus* is capable of colonizing, bone is one of the most frequently infected, and unfortunately, one of the most debilitating manifestations of disease.

S. aureus is by far the most common cause of osteomyelitis [10, 72]. Treatment regimens include prolonged antimicrobial therapy in conjunction with surgery to remove infected or devitalized bone. These surgical procedures are necessary given that *S. aureus* triggers profound bone destruction, which is accompanied by a loss of vascular architecture, and thus decreased delivery of antimicrobials to the site of infection. *S. aureus* is also the most common cause of septic arthritis, which can trigger subchondral bone destruction or even osteomyelitis if contiguous spread occurs [73, 74]. Osteomyelitis is therefore paradigmatic for invasive staphylococcal infections that are recalcitrant to treatment and carry considerable morbidity. In the following sections, we detail advances in our understanding of the innate immune responses to *S. aureus* infection of bone.

Downstream of PRRs, signaling through MyD88 is critical for osteoclastogenesis induced by PAMPs and IL-1 [51, 75]. MyD88 and IL-1R are important for bacterial control on implants in a post-arthroplasty model of infection [76], just as they are also crucial for neutrophil recruitment and *S. aureus* clearance in cutaneous infection models [77]. Furthermore, IL-1R-deficient mice were found to have a higher frequency and severity of

septic arthritis in a systemic *S. aureus* model [78]. The role of TLR2 in *S. aureus* infection is largely dependent on the model system employed and the target tissue examined (see section on skin infections below). However, TLR2 enhances bone resorption in response to injection of heat-killed *S. aureus* but not a lipoprotein-deficient strain [79]. This evidence supports a mechanism whereby TLR2 senses systemic bacterial components and can mediate changes in bone homeostasis. These studies corroborate that MyD88-dependent PRRs and cytokines are critical for bone remodeling and control of *S. aureus* infection.

Animal models of osteomyelitis

In 2013, our laboratory developed a unique murine model of bacterial osteomyelitis [31]. Contrary to other experimental osteomyelitis infections, this model induces a unicortical defect in the bone rather than a larger fracture that requires fixation. This increases precision by allowing for direct inoculation into the intramedullary canal of the femur and does not confound bacterial burden by introducing an implant. Additionally, mouse models are genetically tractable, as there are many readily available reagents specific for murine cells. Our infection model is advantageous for other reasons, including that we can precisely calculate colony-forming units (CFUs) and we have developed imaging analyses to accurately quantify bone remodeling. Many other experimental models of *S. aureus* osteomyelitis use larger mammalian hosts, including rabbits, rats, dogs, sheep, pigs, and goats [80-89]. Osteomyelitis animal models can also vary in their etiology from establishing bone infection downstream of hematogenous dissemination or fracture [36, 84, 86, 90], or associated with the implantation of a foreign device [30, 85, 87, 91-93]. Thus, as animal models of osteomyelitis can be used to define critical immune

responses leading to inflammation and alterations in bone remodeling [31, 33, 35, 36, 80, 94-97], there may be inherent differences between comparisons.

Murine models of staphylococcal infection also have certain limitations. The contribution of individual toxins to disease pathogenesis is controversial when considering data from different animal models. For example, the Panton-Valentine Leukotoxin (PVL) activity is restricted to the human and rabbit C5a receptor; thus the effects of this toxin cannot be elucidated using murine models, but a rabbit model is well suited for discovery of toxin effects during infection [81, 82, 98]. Similarly, other staphylococcal bi-component toxins have species-specific interactions with receptors; therefore not all animal models are appropriate to measure toxin effects [99]. Moreover, humanized mice (NSG mice reconstituted with a human hematopoietic system) used in *S. aureus* infection models have been shown to exhibit increased pathogenesis relative to WT mice [100], which could also provide an improved experimental platform to study *S. aureus* toxin-mediated pathogenesis.

Staphylococcal immune response in humans

Individuals with diseases that impact innate immunity are at increased risk of staphylococcal infection. Genetic diseases that predispose individuals to *S. aureus* infections include chronic granulomatous disease (CGD) [101], deficiencies in MyD88 [102], IRAK-4 [103], TIRAP [104], and RAC2 [105]; Wiskott-Aldrich Syndrome [106], leukocyte adhesion deficiencies [106], severe congenital neutropenia [106]; and allelic variants of cytokines IL-1α, IL-4, and IL-6 [107, 108]; among others. In patients with CGD, there is a failure to produce an antimicrobial respiratory burst in phagocytes due to

mutations in the NADPH oxidase complex [109]. CGD patients are therefore exquisitely susceptible to catalase-producing microorganisms, including *S. aureus*, and suffer from recurrent infections in skin, bone, lungs, and other tissues [109]. MyD88, IRAK-4, and TIRAP deficiency lead to a failure to transduce PRR- and IL-1R-associated signals, thereby significantly hampering immune responses to select pathogens. Interestingly, these patients experience infections with a narrow range of pathogens, most notably *S. aureus* and *Streptococcus pneumoniae*, and tend to improve with age [104, 110].

Increased risk of *S. aureus* infection has also been associated with co-morbidities, such as diabetes [111, 112], malnutrition [113], bone marrow transplantation [114], and HIV infection [115]. In general, these conditions are associated with extreme dysregulation of the immune response. Although individuals with malnutrition [113, 116], newborns [117, 118] and bone-marrow transplant recipients [119] are functionally immunocompromised, subjects with uncontrolled diabetes [120-122], obesity [123, 124], and advanced age [125, 126] exhibit chronic low-grade inflammation and are also susceptible to infection. However, the common ground that favors *S. aureus* infection remains to be determined.

The emerging field of osteoimmunology

Reciprocal interactions between the skeleton and the immune system

The intricate cellular interactions that lead to bone remodeling took many decades to delineate and are still an active area of research. In the late 1980s, osteoblasts were linked to the regulation of osteoclastogenesis, even before the primary signals for osteoclastogenesis had been identified [127-129]. M-CSF was identified as a critical factor

supporting osteoclastogenesis, in keeping with the observation that osteoclasts arise from myeloid cells during co-culture experiments [130, 131]. These early discoveries paved the way for the identification RANKL as the canonical osteoclast differentiating factor [14, 15], as well as the discovery of a related inhibitory molecule OPG [132, 133].

The field of osteoimmunology, in which the effects of various immune cell-derived factors and cytokines on bone homeostasis were examined, emerged from work dating back to the 1970s [134, 135]. TNFα, IL-1, and IL-6 favor bone resorption by promoting osteoclast differentiation and function. Indeed, IL-1 was initially described as osteoclast activating factor due to its effects on bone [136, 137]. IL-1, IL-6, and TNFα trigger osteoblast lineage cells to upregulate RANKL [138], whereas IL-1 and TNFα can also act on mature osteoclasts to promote differentiation, survival, and bone resorbing activity [139-141]. However, both TNFα and IL-1 can only affect osteoclast precursors that have first been primed with RANKL [142, 143]. Interestingly, bone remodeling mediated through TNFα is in part driven by its ability to alter osteoblastic expression of IL-1 and the IL-1R [144]. Cytokines can also indirectly impact bone resorption by osteoclasts, as both IL-1 and IL-6 increase production of RANKL by osteoblasts [138]. In addition to these cytokines, T_H17 cells contribute to bone loss during arthritis, as IL-17 triggers RANKL production and osteoclastogenesis [145, 146]. In contrast to IL-1, IL-6, TNFα, and IL-17, anti-inflammatory and T_H2 cytokines are anti-osteoclastogenic. IL-4 and IL-13 are generally suppressive to skeletal cells, reducing activities of both osteoblast and osteoclast lineage cells, as they inhibit osteoblast proliferation, favor production of OPG, and decrease RANK expression on osteoclasts [147-150]. Similarly, IL-10 can signal directly onto preosteoclasts to suppress RANKL-induced transcription factors [151, 152]. The net

20

effects of these cytokines in the skeleton favor bone resorption by shifting the axis towards enhanced osteoclast numbers and activity.

Osteo-immunologic crosstalk impacts bone health in numerous human diseases

The various effects of RANKL and other pro-inflammatory cytokines to influence bone biology and immune function have led to the classification of a field that merges these two disciplines, called osteoimmunology. Many human diseases have significant skeletal effects driven by inflammation, including conditions characterized by localized inflammation, such as rheumatoid arthritis, multiple myeloma, and tumor-induced bone disease. However, chronic inflammation present in patients with chronic conditions such as inflammatory bowel disease and systemic lupus erythematosus can also advance bone loss. Interactions between skeletal cells during inflammation are multifactorial, but studies in these fields show overlapping importance of cytokines such as TNFα [153, 154], IL-1 [155], IL-6 [156, 157], IL-11 [158], and IL-17 [145, 159-163]. Interestingly, these fields became more entwined when it was discovered that activated B and T lymphocytes release RANKL, which can induce osteoclastogenesis, leading to bone loss and joint destruction [17, 19].

S. aureus-induced pathogenesis during skeletal infection

S. aureus secreted virulence factors

S. aureus pathogenesis is partially dependent on the elaboration of secreted virulence factors, including cytolytic toxins and proteins that modify immune functions. In experimental models of osteomyelitis, several *S. aureus* proteins have been shown to

impact bone architecture and contribute to comorbidities, such as sepsis. During bone infection, abscess formation in the bone marrow and around devitalized bone leads to a hypoxic environment, which subsequently alters quorum sensing and toxin production [32]. Along with many other staphylococcal toxins and proteases, the alpha-type phenol soluble modulins (PSMα) toxins are regulated by the accessory gene regulator (*agr*) quorum sensing system. PSMα toxins are small, amphipathic pore-forming toxins that are relatively promiscuous in their ability to induce toxicity among several cell types and species [32, 164]. In a murine model of post-traumatic osteomyelitis, PSMα toxins are responsible for killing primary bone cells *in vitro* and that killing enhances bone destruction *in vivo* [31, 32]. However, a *S. aureus* strain lacking the PSMα toxins still incites substantial bone damage, causing approximately 70% of the bone loss that is observed in femurs infected with a wild-type *S. aureus* strain [31]. In rabbit and murine models of experimental osteomyelitis, inactivation of *agr* further reduced bone destruction [31, 80]. However, significant cortical bone loss still occurred even with this virulence-attenuated strain during osteomyelitis [31].

Bone destruction mediated by *S. aureus* is multifaceted. PVL can mediate bone cell death through the lysis of myeloid cells, including osteoclasts, after binding the C5a receptor [165]. Meanwhile, PVL contributes to increased pathogenesis to enhance early bacterial survival in bone and promote bacterial spread to nearby muscles and joints in a rabbit model of osteomyelitis [82]. *S. aureus* strains expressing PVL are associated with more severe local disease and a greater systemic inflammatory response in children with osteomyelitis [165, 166] . Furthermore, bone destruction during *S. aureus* infection can also be triggered by the superantigen toxin shock syndrome toxin-1 (TSST-1) and the

antibody-binding protein staphylococcal protein A (Spa), which both activate osteoclast signaling to enhance bone resorption [40, 165, 167].

To impede the early host defenses, *S. aureus* produces a repertoire of toxins that to damage biological membranes, including hemolysins and leukotoxins. Release from the phagosome and lysis of incoming innate immune cells allows *S. aureus* to avoid many host anti-bacterial effector mechanisms. Yet, the contribution of staphylococcal toxins regarding disease severity and pathogenesis varies based on the infection site and the repertoire of virulence factors expressed by the infecting *S. aureus* strains.

The ability of biofilm to modulate innate immune responses

Many *S. aureus* clinical isolates from infections are found to have a dysfunctional *agr* system [168]. These *agr*-deficient strains are characterized by low virulence factor production and enhanced biofilm formation [169, 170]. In individual cases, it is unclear whether colonizing bacteria are *agr*-deficient or the bacterial population have evolved in the host towards a biofilm-forming, toxin-limited state. However, serially isolation and sequencing of colonies from patient wounds over time have shown mixed populations with respect to *agr* functionality in consecutive samples [168]. Additionally, many isolates with non-functional *agr* systems appear to have developed simultaneously rather than sequentially, as *agr* mutants were reflective of various genetic alterations, including deletions, missense mutations, and frameshifts [168]. Bacteria that form biofilms are often more resistant to clearance by the host immune response, leading to a chronic infection. Neutrophils are the principal innate effector against *S. aureus*, and are still thought to be critical for the clearance of bacterial biofilms [171]. However, studies have shown that *S.*

aureus biofilms can negatively affect phagocytosis by macrophages and attenuate inflammation *in vivo* [172].

Innate immune responses to *S. aureus*:

Lessons learned from studying skin infections

Key players involved in bacterial recognition and innate immunity

A plethora of research has been focused on defining the innate immune responses to *S. aureus* cutaneous infections. Critical steps in anti-staphylococcal immunity are outlined in this section. An active innate immune response is mounted in response to the invading bacteria once *S. aureus* has obstructed mechanical tissue barriers. Tissue resident macrophages can phagocytose and kill *S. aureus* efficiently by producing reactive oxygen and nitrogen species (ROS and RNS), AMPs, and chelating proteins that starve bacteria of essential nutrients [173, 174]. However, the main mechanisms of bacterial clearance require a large influx of leukocytes and phagocytosis of bacterial cells by innate effector cells.

Resident tissue cells and endothelial cells lining blood vessels that supply the tissue are typically the first cells that encounter pathogens during infection, and such cells recognize PAMPs via different PRRs, such as TLRs and NOD-1 and -2 [175-177]. Signaling through these receptors induces activation of transcription factors, such as NFκB and AP-1 to generate cytokines, chemokines, and antimicrobial effector mechanisms [177-179] **(Figure 5, left)**.

24
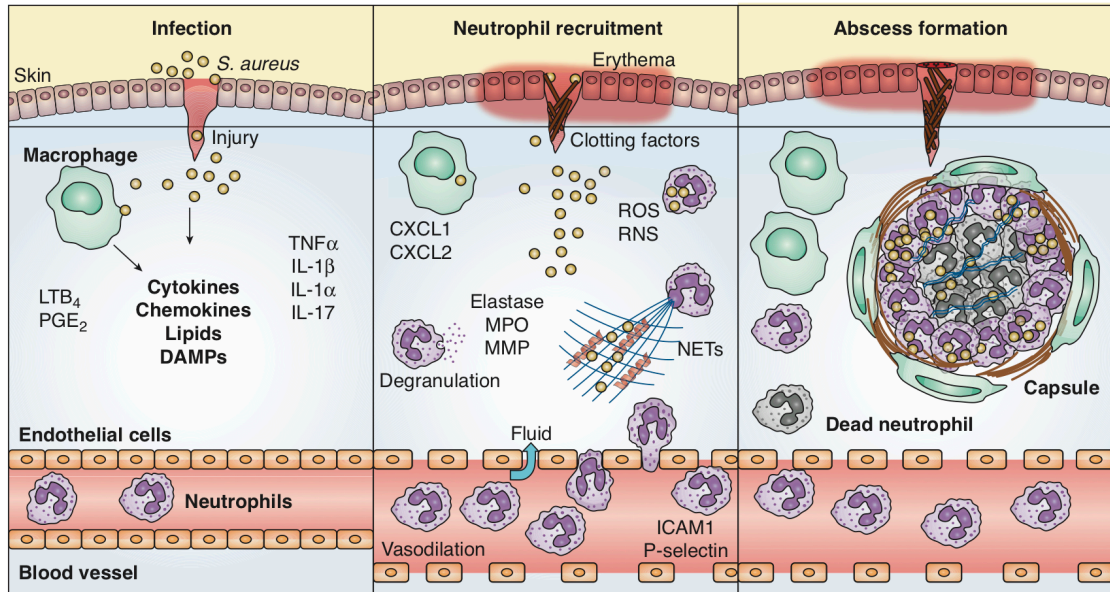
Figure 5. Innate immune responses to *S. aureus* during infection.
Left panel, *S. aureus* infects skin after breaching the epithelial layers. Keratinocytes and skin-resident macrophages produce inflammatory mediators that promote neutrophil responses. Middle panel, neutrophils are recruited to the skin where they phagocytose bacteria, undergo degranulation, and produce extracellular traps that aid in bacterial killing. Right panel, *S. aureus* infection is contained by abscess formation. Live and dead neutrophils and bacteria are found within the abscess. The abscess becomes encapsulated with fibrous material and surrounded by macrophages.

Staphylococcal-sensing TLRs of unique interest are the TLRs 1, 2, 6, and 9 because they have been implicated in osteoblast recognition of staphylococcal components and signal through MyD88 [180]. Extracellular TLR1/2 and TLR2/6 heterodimers are known to engage *S. aureus* cell wall components, specifically lipopeptides and peptidoglycan [181, 182], and *S. aureus* CpG DNA stimulates TLR9 during bacterial replication in the endosome [183]. These TLRs utilize the signaling adapter MyD88 to induce robust and efficient transcriptional programs that lead to inflammatory responses to *S. aureus* in different models of infections. Mice deficient in MyD88 are highly susceptible to *S. aureus* skin infection as evidenced by increased bacterial load, poor inflammatory response, and enhanced mortality or morbidity in various models of disease [77, 184-186]. TLR2 and TLR9 can recognize bacterial products and allow resident cells to produce neutrophil chemoattractants, AMPs, such as pore-forming cathelicidin LL-37 (human) or cathelicidin-related AMP (mouse) and defensins, and pro-inflammatory cytokines such as TNFα and IL-6 [178, 187]. Moreover, TLR2 is highly expressed on the cell surface of resident macrophages and recruited neutrophils and monocytes, which promptly respond to *S. aureus* and further stimulate cytokine production and phagocytosis. Therefore, it is expected that TLR2 is critical for both systemic and localized *S. aureus* infection. However, in some infection models, the role of TLR2 is controversial. Although Miller et al. [77] demonstrated that TLR2 is dispensable to control *S. aureus* infection, Hoebe et al. showed that *Tlr2*^{-/-} mice are more susceptible to infection [188]. Distinct bacterial strains express unique virulence factors and toxins that could underlie different TLR2 requirements. Furthermore, the infection inoculum varies between these studies. If TLR2 is required for fine tuning the immune response, higher amounts of bacteria (as used by

Miller et al.) could override the TLR2 requirement to induce an efficient response, whereas lower doses of the bacteria could require TLR2 to mount a robust immune response. Phagocytosis and internalization of *S. aureus* sequesters the bacterium into the host cell endosome, where TLR9 is expressed. TLR9 induction of IL-1α has been described in patients with atopic dermatitis, that have accumulated *S. aureus* in keratinocyte lysosomes [189]. Taken together, these data suggest that TLRs promote early antibacterial events during *S. aureus* infection.

     S. aureus has the ability to escape the host cell endosome by lysing the membrane and entering the cytoplasm [45, 48, 50]. Here, the intracellular PRRs NOD1 and NOD2 can detect bacterial peptidoglycan to induce inflammatory responses, production of antimicrobial peptides and increased phagocyte antimicrobial effector functions. NOD2 recognize the muramyl-dipeptide derived from peptidoglycan during *S. aureus* infection. Furthermore, *Nod2*$^{-/-}$ mice are highly susceptible to *S. aureus* skin and systemic infections when compared to WT counterparts [190-194].

     Resident stromal cells and endothelial cells at the site of infection are activated by *S. aureus* to release constitutively produced IL-1α, whereas tissue resident macrophages are the primary producers of IL-1β [195]. These tissue resident macrophages assist in the initial clearance of *S. aureus,* and in conjunction with perivascular macrophages, they regulate the recruitment of neutrophils and monocytes to the site of infection [196, 197]. Moreover, the secretion of chemoattractants required for neutrophil recruitment is dependent on IL-1R and MyD88 signaling [77]. IL-1 cytokines play a central role in recruitment of neutrophils by signaling through the IL-1R on skin and endothelial cells to increase chemotactic molecules such as CXCL1, CXCL2, and IL-8 [76, 77, 198, 199].

Furthermore, the complement cascade results in the production of the potent neutrophil chemoattractant C5a and supports opsonization of bacterial cells to augment phagocytosis by innate effector cells, though *S. aureus* has many complement evasion strategies [200-202]. Bacterial factors, such as the PSM toxins, can also serve as a mechanism to recruit and lyse neutrophils *in vivo* [203, 204].

IL-1β is produced as an inactive pro-IL-1β, which requires proteolytic processing to be functional. The NLRP3 inflammasome is a major mechanism that processes IL-1β and facilitates antimicrobial activities and enhances immune effector functions [205]. NLRP3 inflammasomes are multi-subunit protein complexes involving NLRP3, ASC, and caspase-1. Once assembled, caspase-1 is activated and cleaves pro-IL-1β to form mature IL-1β. Effective IL-1β processing by NLRP3 requires two signals: 1) TLR activation to induce expression of *Il1b* and 2) activation signal to induce inflammasome assembly and activity. Alternatively, IL-1β can also be processed in noncanonical NLRP3 activation, mediated through caspase-11 activation or via serine proteases from neutrophils and bacterial proteases in an inflammasome-independent mechanism [206]. The majority of IL-1β produced in the skin of *S. aureus* infected mice is processed primarily through NLRP3 inflammasome activity [199]. IL-1β is important for neutrophil recruitment and bacterial clearance during *S. aureus* infections [199] and for abscess formation [207].

Neutrophils are the primary cellular defense mechanism deployed during *S. aureus* infection. These cells make up the largest portion of circulating leukocytes and are effectively recruited to the site of infection, where opsonization of bacteria by complement C3 and C5 convertases facilitate phagocytic killing by neutrophils. Neutrophils are inherently short-lived cells, however, recognition of bacterial PAMPs and host DAMPs

28

through TLRs can prolong their survival, promote phagocytosis, ROS production, and granule release [208-210]. In addition to microbicidal activities and neutrophil extracellular trap (NET) formation carried out by neutrophils, they are a critical component of abscess formation, thought to sequester *S. aureus* bacteria to prevent dissemination of infection [9]. Once neutrophils arrive to the site of infection, they ingest *S. aureus* and attempt to control microbial growth by producing different antimicrobial effectors [174, 211, 212]. Neutrophils are short-lived cells that readily undergo apoptosis and need to be cleared from the site of infection.

Phagocytosis of bacteria and neutrophil activation prompts apoptosis, though *S. aureus* has also been described to enhance neutrophil necrosis, leading to secretion of damage associated molecular patterns (DAMPs) and further inflammation [213]. With a large repertoire of virulence factors, *S. aureus* can induce cell death of resident cells. The accumulation of dead cells and debris requires clearance by macrophages through a process called efferocytosis, which itself has been proposed as an innate antimicrobial mechanism to contribute to clearance of infected apoptotic cells [214]. These cells are also involved in the clearance of dead cells in the site of infection, which is essential for the resolution of the infection [173, 174]. Macrophage activity during clearance of the infected site is altered depending on whether the cellular debris resulted from apoptotic or necrotic cells, with inflammatory cell death supporting enhanced MHC II presentation and T cell activation [215]. After bacteria and debris are eliminated, fibroblasts and macrophages produce molecules to aid in the ECM remodeling.

Effector mechanisms of bacterial control

S. aureus can be ingested into the cell using receptors that recognize both opsonized and nonopsonized bacteria [174, 216, 217]. When coated with opsonins (e.g. C3b and IgG), S. aureus elicits different antimicrobial effector functions [218]. ROS (such as O_2^-, H_2O_2 and HOCl) are produced quickly following phagocytosis through the actions of NADPH oxidase and myeloperoxidase, and can directly kill bacteria or facilitate further killing by other mechanisms [219, 220]. The inducible nitric oxide synthase (iNos) produces nitric oxide (NO), a major RNS that has various antimicrobial and immunomodulatory functions [221]. Both genetic deletion and pharmacologic inhibition of NO formation render mice highly susceptible to S. aureus infection [222, 223].

Neutrophils kill pathogens by producing toxic components within granules that are released in a process known as neutrophil degranulation [224]. Degranulation induces the secretion of specific granules containing AMPs and defensins. These cationic peptides interact and disrupt bacterial membranes. Degranulation also leads to secretion of azurocidin, cathepsins, lactoferrin, lysozymes, proteinase-3, and elastase [201, 225]. As an additional effector mechanism to control S. aureus infection, neutrophils secrete DNA rich structures known as NETs. NETs are produced in a MyD88- and TLR2-dependent manner and are necessary for containing S. aureus in the skin to prevent bacteremia [226] **(Figure 5, middle)**. NETs limit the spread of pathogens because they are rich in antimicrobial molecules such as antimicrobial peptides, cathepsins, elastase, histones, and proteases [227]. However, S. aureus destroys NETs, and the degradation product 2'-deoxy-adenosine induces apoptosis in macrophages, which increases bacterial survival in the abscess [228].

Immune mechanisms of abscess formation

Abscesses are the hallmark inflammatory lesions during *S. aureus* infection, and function to restrain and eliminate the pathogen [9, 174, 229]. Abscess formation is a dynamic event that involves different features over time. The abscess core contains fibrin, viable and necrotic neutrophils, tissue debris, and live bacteria **(Figure 5, right)**. Abscess maturation is accompanied by formation of a fibrous capsule at the periphery; however, if the abscess is not tightly organized, systemic spread of infection may occur via the bloodstream [9, 174, 229]. Macrophages are localized to the periphery of the abscess in areas near the fibrous capsule, which may suggest a role in neutrophil chemotaxis toward and egress from the abscess [9, 174].

The immune mechanisms involved in abscess formation are beginning to be uncovered. Although fibroblasts synthesize collagen, and fibrin is synthesized from fibrinogen by thrombin, the role of phagocytes and their mediators involved in abscess formation and maturation is poorly understood. Cho et al. [207] have shown that neutrophil-derived IL-1β is required for *S. aureus*-induced abscess formation. Recently, Feuerstein et al. [184] suggested that resident macrophages expressing MyD88 contribute to abscess maturation. The lipid mediator leukotriene B$_4$ (LTB$_4$) is also essential for neutrophil direction to the infectious focus, microbial killing, and fibrous capsule formation [230]. Furthermore, an ointment containing LTB$_4$ increases *S. aureus* clearance and decreases lesion size [230]. These findings correlate with increased neutrophil recruitment, abscess formation, ROS production, and IL-1β generation. Although there is much more to learn regarding the host-derived products that contribute to formation of abscess, a

considerable amount of research has focused on the staphylococcal factors that promote survival within abscesses.

Among the *S. aureus* virulence factors involved in abscess formation, staphylocoagulase (Coa), von Willebrand factor binding protein (vWbp) and clumping factor A (ClfA) are all required for abscess formation. These proteins promote coagulation leading to fibrin generation and the formation of a pseudocapsule surrounding "staphylococcal abscess communities" within individual abscess lesions [9, 231]. Taken together, understanding the immune responses to *S. aureus* in skin, as well as host and bacterial mechanisms of abscess formation and survival, will aid in understanding the dynamics of staphylococcal pathogenesis and invasive infection.

Conclusions

In conclusion, innate immunity to *S. aureus* infection is multifaceted and likely tissue specific. Decades of research on staphylococcal pathogenesis in skin have elucidated important roles for PRRs, as well as for specific cytokine signaling pathways such as IL-1. However, innate immune responses that mediate control of bacterial burdens in bone remain undefined, as do the consequences of inflammation on tissue remodeling during *S. aureus* osteomyelitis. The work in this thesis was based on the overarching hypothesis that MyD88-dependent innate immune receptors, including TLR2, TLR9 and IL-1R, mediate control of bacterial burdens locally and prevent bacterial dissemination, but that they may also contribute to bone loss through increased osteoclastogenesis. Many triggers of altered bone loss have been postulated based on *in vitro* findings, but remain unsubstantiated *in vivo*. Changes in bone architecture during *S. aureus* osteomyelitis may be due to the

sustained presence of bacteria in bone, local inflammation, or activated immune pathways on skeletal cells. In order to better define how *S. aureus* perturbs bone remodeling, I characterized cytokines and chemokines present in the infected femur to provide context of the inflammatory environment and to inform future studies. I expanded the assays in our laboratory to reveal how osteoclast differentiation is affected by *S. aureus in vitro,* and tested the role of MyD88-dependent pathways on *S. aureus*-mediated changes in osteoclastogenesis. Finally, I assessed how bone loss, osteoclast number, and actively resorbing osteoclast surface were altered during *S. aureus* osteomyelitis, and how TLR2, TLR9, and IL-1R influence bone remodeling *in vivo.* Overall, this thesis elucidates critical anti-bacterial responses in bone and the consequences of the resulting innate immune response on bone remodeling.

A portion of the following section (*Chapter II, Bacterial stimuli influence the*

differentiation of bone-resorbing osteoclasts in vitro)

was originally published in *The Journal of Immunology.* (June 2018).

Brandt SL*, Putnam NE*, Cassat JE[#], Serezani CH[#]. 2018. Innate immunity to

Staphylococcus aureus: Evolving paradigms in soft tissue and invasive infections. *J*

Immunol. 200(12):3871-3880.

CHAPTER II

BACTERIAL STIMULI INFLUENCE THE DIFFERENTIATION
OF BONE-RESORBING OSTEOCLASTS *IN VITRO*

Introduction

Bacterial osteomyelitis can cause serious complications from alterations in bone remodeling, including large areas of bone destruction, aberrant bone formation, and local vasculature damage. Altered bone remodeling can also be induced by other inflammatory disorders; understanding how bacterial-induced inflammation impacts bone remodeling will enhance understanding of how systemic inflammatory disorders affect bone health. The presence of *S. aureus* in bone disrupts normal, homeostatic bone remodeling [31, 39, 40, 45, 80, 232]. Although PSMα toxins were found to induce direct skeletal cell death, *in vivo* experiments have shown that toxin-deficient *S. aureus* strains still induce dramatic alterations in bone physiology [31]. These results indicate that there are multiple mechanisms leading to changes in bone during *S. aureus* osteomyelitis.

Osteomyelitis is at the cusp of the emerging field of osteoimmunology, which highlights the interplay between bone biology and immunology [26, 180, 233]. RANKL-dependent osteoclastogenesis is a well-defined process, and it is often hypothesized that crosstalk between osteoclastogenic signaling pathways and inflammatory stimuli, including canonical and non-canonical NFκB pathways may occur [15, 234]. Local erosion of bone and teeth occurs in inflammatory bone disorders such as periodontal disease and rheumatoid arthritis [56, 235, 236], and systemic inflammatory diseases of the bowel and lung can also lead to bone loss [180, 237]. Notably, local inflammation of bone also occurs

subsequent to the establishment of *S. aureus* osteomyelitis [60, 238, 239]. Thus, inflammatory-induced bone resorption activities by osteoclasts may be responsible for potentiating pathologic bone destruction [180, 237]. These observations insinuate that enhanced bone loss occurs in part when osteoclast differentiation is favored.

On a cellular basis, both osteoblast and osteoclast lineage cells express PRRs, although their contribution to changes in bone physiology and pathogen clearance have not been defined during osteomyelitis. Sensing of conserved molecular patterns on *S. aureus* by PRRs initiate innate immune responses during infection, leading to activation of transcription factors that are also involved in osteoclast differentiation. In regards to *S. aureus*, reports on osteoclastogenic effects are unclear due to the use of various pre-osteoclast cultures and stimulation methods [140, 240-242].

To better understand how *S. aureus* triggers bone destruction, research described in this chapter focuses on how innate immune sensing by bone cells might perturb osteoclast differentiation. *We hypothesized that differentiation of bone-resorbing osteoclasts could be enhanced directly through sensing of bacterial stimuli and indirectly through cytokine induction.* In experiments described in this chapter, we investigate how *S. aureus* alters the differentiation of myeloid cells into bone-resorbing osteoclasts with a focus on PAMPs and inflammation **(Figure 6)**. To accomplish this investigation, we used bacterial supernatants, cell wall extracts, TLR agonists, and *in vitro* osteoclastogenesis assays to monitor the effects of PAMPs on osteoclast differentiation. To further investigate whether the inflammatory milieu modulates osteoclastogenesis through the production and action of specific cytokines, we tested specific cytokine blockade conditions. Finally, we explore the role of myeloid lineage cells to respond to *S. aureus* through the production of

inflammatory transcripts and cytokines. These data implicate direct PRR sensing on myeloid lineage cells in disrupting basic bone homeostasis, which relates current findings to the scenario of *S. aureus* osteomyelitis.

Materials and methods

Bacterial strains and growth conditions

The wild-type *S. aureus* strain used in these studies is an erythromycin-sensitive derivative of the USA300 type LAC clinical isolate (AH1263) [243]. The toxin-deficient strain LACΔ*psmα1-4* (herein referred to as Δ*psm*) was described previously [31, 244]. *S. epidermidis* strain NRS6 is a clinical isolate from the NARSA library made available through BEI Resources and obtained as a gift from the Skaar laboratory. All staphylococci were routinely grown on trypic soy agar (TSA) or shaking in tryptic soy broth (TSB) with or without 10 µg/mL erythromycin. The *E. coli* strain used in these experiments is the laboratory strain DH5α.
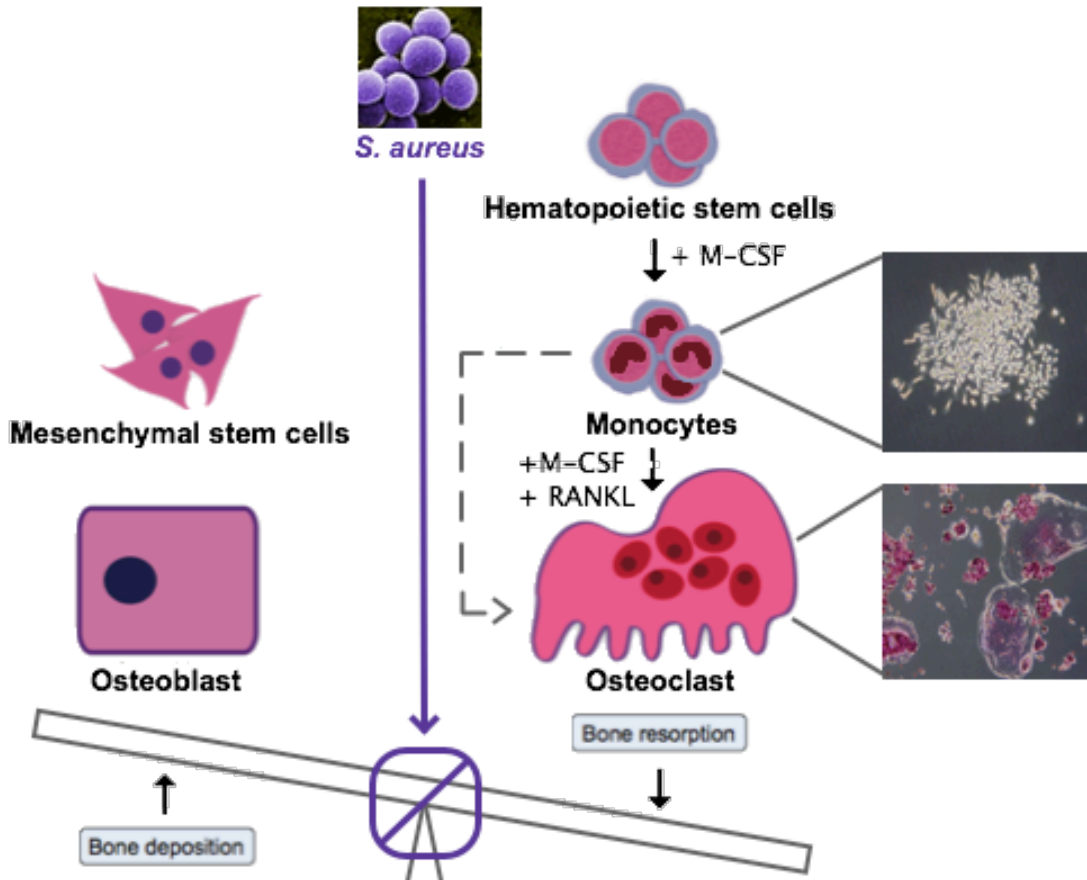
Figure 6. We hypothesize that *S. aureus* perturbs bone remodeling by altering the interactions between skeletal cells.

The communication between mesenchymal-derived osteoblast lineage cells and hematopoietic-derived osteoclast lineage cells normally maintains bone homeostasis. Osteoblasts are responsible for forming the mineralized matrix of bone. Osteoclasts develop from the M-CSF derived myeloid population of cells, with differentiation driven by the canonical cytokine, RANKL. During *S. aureus* osteomyelitis, bone remodeling is altered. Where aberrant bone formation and bone loss both occur during infection, the hypotheses in this chapter aim to elucidate how *S. aureus* perturbs bone remodeling through altering interactions between skeletal cells. The majority of this chapter focuses on the osteoclast lineage transition from monocyte/macrophages shown in the top right photo into multinucleated osteoclasts that stain positively for the presence of the osteoclast-marker tartrate-resistant acid phosphatase (TRAP), shown in the bottom right photo.

Preparation of bacterial supernatants

To prepare concentrated bacterial supernatants, bacterial cells were grown overnight in RPMI supplemented with 1% casamino acids at 37°C using a 1:5 ratio of liquid media to flask size (250 mL or 1 L Erlenmeyer flask were used), with shaking at 180 rpm. Three bacterial colonies per 50 mL of media were inoculated into each flask, and the flask was stoppered to create a hypoxic environment that promotes toxin production, as previously described [32]. After 15 hours of growth, bacterial cultures were centrifuged at 8000 x g for 8 minutes at 4°C with a fixed angle rotor. Supernatants were pooled and filter sterilized with a 0.22 μM filter. Amicon Ultra 50 mL concentration tubes were then filled with 15 mL of the filter sterilized supernatant and centrifuged at 4000 x g for 30-45 minutes at 4°C. This was done three times in succession, decanting the filtrate each time, until the concentrated supernatant remaining above the filter reached approximately 1.5 mL. Concentrated supernatants were then pooled, filter sterilized again with a 0.22 μM filter, and aliquoted to freeze at -80°C for a single thaw and use.

Bacterial cell wall isolation

A 5 mL overnight culture at stationary phase was pelleted at 4000 x g for 5 minutes. TSM buffer (100 mM Tris, pH 7; 500 mM sucrose; 10 mM $MgCl_2$) and 40 μg/mL lysostaphin were gently mixed with the bacterial cell pellet and incubated at 37°C for 1 hour. Tubes were spun at 13000 rpm for 2 minutes and the supernatant, containing the cell wall, was collected and filter sterilized through a 0.45 μM filter. Cell wall fractions were stored at 4°C until use.

Cell lines, primary cell isolation, and cell maintenance

RAW264.7 cells are a monocyte/macrophage adherent cell line (ATCC, Manassas, VA, TIB-71) that were used for their ability to differentiate into multinucleated osteoclasts with RANKL supplementation. These cells were routinely cultured in DMEM supplemented with 10% fetal bovine serum (FBS) and 1X Penicillin/Streptomycin (P/S). Cells were scraped off the plate and into a single cell suspension for subculture and plating. The mc3T3 adherent mouse pre-osteoblast cell line (ATCC, Manassas, VA, CRL-2593) was cultured in αMEM, 10% FBS, and 1X P/S. Cells were harvested using 0.25% Trypsin/EDTA. THP-1 Blue NFκB Cells (InvivoGen, San Diego, CA) are a human monocyte cell line that grows in suspension and contains an NFκB-inducible reporter, leading to the release of a secreted alkaline phosphatase (SEAP). SEAP activity can be measured by adding the QUANTI-Blue (InvivoGen, San Diego, CA) substrate into the cell culture media. THP-1 Blue cells were thawed and grown in RPMI supplemented with 10% FBS, 1% P/S, and 100 µg/mL normocin. Cells were subcultured and blastocidin was added into the culture medium at 10 µg/mL to select for cells containing the reporter construct.

To obtain primary cells, 8- to 13-week old male mice were sacrificed by CO_2 asphyxiation, confirmed dead by observation, and cervically dislocated as a secondary method of euthanasia. Femurs from wild-type C57BL/6 (WT) mice (The Jackson Laboratory, Bar Harbor, ME, Stock #: 000664) were extracted and the muscle surrounding the femur was removed. Femurs were stored in PBS on ice until ready for skeletal cell isolation. To isolate whole bone marrow (WBM), the epiphyses (ends) of femurs were cut off and discarded. To collect bone marrow (BM), cold, unsupplemented αMEM was flushed through the medullary cavity into a tube using a 27-gauge needle and 10 mL Luer-

Lock syringe. Cells were pelleted at 1500 rpm for 5 minutes, and incubated for 10 minutes at room temperature in Ammonium Chloride Potassium (ACK) Lysing Buffer (Lonza, Walkersville, MD). The reaction was quenched with 10 mL PBS, and cells were pelleted, counted, and either immediately used in cell culture or frozen.

WBM was cultured in αMEM (without ascorbic acid), 10% FBS, 1X P/S, and 10 nM 1α, 25-dihydroxyvitamin D_3 (Sigma, Saint Louis, MO, D1530) to model a co-coculture system or was used to enrich for bone marrow macrophages (BMMs) by plating between 8-13x10^6 cells per 10 cm dish in media supplemented with 100 ng/mL recombinant murine M-CSF (R&D Systems, Minneapolis, MN, 416-ML) for 4 days. After 4 days in culture, enriched BMMs were scraped into a single cell suspension to plate for immediate use or to freeze down for later use. Osteoclast precursors were derived from BMMs after treatment with 1:20 CMG14-12 supernatant (equivalent to 20 ng/mL recombinant murine M-CSF activity) and 35 ng/mL recombinant murine RANKL (R&D Systems, Minneapolis, MN, 462-TR) for 2 days [28].

To isolate primary osteoblasts from WT, *Myd88*$^{-/-}$ (The Jackson Laboratory, Bar Harbor, ME, Stock #: 009088), and *Tlr2*$^{-/-}$ (The Jackson Laboratory, Bar Harbor, ME, Stock #: 004650) mice, the diaphysis (flushed of bone marrow) was cut lengthwise into strips, and then cut crosswise to create several small bone fragments. In a conical tube, the minced bone tissue was washed three times in PBS by successive centrifugations at 1500 rpm for 5 minutes. Digestion media was prepared fresh, containing 20 mg of type II collagenase (Worthington Biochemical Corporation, Lakewood, NJ, #LS004176) and a final concentration of 0.01% Trypsin/EDTA in PBS. Bone fragments were incubated in 2 mL digestion media at 37°C for 45 minutes two times, and washed three more times in

PBS. Digested bone fragments were then added to a 10 cm dish with αMEM (without ascorbic acid), 10% FBS, and 1X P/S. Importantly, only half of the media was replaced every 2-3 days to allow for cell-derived growth factors to remain in the media. Over time in culture, osteoblastic cells began to migrate out of the bone fragments. Between 10 and 14 days, cells were between 50-80% confluent. At this time bone fragments were discarded, and cells were trypsinized and plated for use or frozen. All culture media was sterilized through a 0.22 μM filter, all FBS was heat-killed, all primary cells were frozen in 90% FBS and 10% DMSO, all cell lines were frozen in 90% media and 10% DMSO, and all cells were cultured in an incubator at 37ºC 5% CO_2.

Cell viability and toxicity

Primary BMMs and osteoblasts were plated at 50,000 or 10,000 cells per well, respectively, in a 96-well plate and were cultured overnight at 37°C 5% CO_2. LAC and Δ*psm* supernatants, or vehicle controls were used to stimulate cells at a final volume / volume ranging between 2.5 – 20% per well for 22 hours, at which point media was removed and CellTiter 96 Aqueous One Solution Cell Proliferation Assay (MTS) (Promega, Madison, WI) was added to the media at a final concentration of 10%, and the cells incubated for an additional 2 hours at 37ºC 5% CO_2. Similarly, the plates containing THP-1 Blue NFκB reporter cells were spun down to pellet cells in suspension. At 22 hours post-stimulation, media and stimuli were removed and cells were incubated for 2 hours with a 10% CellTiter 96 Aqueous One Solution. Each plate was read at an absorbance of 490 nm, where an increased absorbance corresponds to higher cellular metabolic activity

from the cells in culture. Absorbance readings were corrected for background, and the percent viability of treated cells compared vehicle control was calculated.

To test for the viability of myeloid cells in response to various doses of *S. aureus* supernatants (LAC, Δ*psm*) or vehicle control, we stimulated RAW264.7 cells in culture and monitored their metabolic activity over 5 days as a proxy for cell proliferation over time. 7,500 RAW264.7 cells were plated per well in a 12-well plate, with one plate to be read on each day. At each time point, media was removed from the cells and a 10% CellTiter 96 Aqueous One Solution was incubated with the cells for 2 hours at 37ºC 5% CO_2. From each well, 200 µL was removed and added to a 96-well plate to read the absorbance at 490 nm. After correcting for background, the absorbance for each condition was plotted over time.

NFκB activity using THP-1 Blue cells

Human THP-1 Blue cells were used to determine NFκB activity per manufacturer's instructions. Cells were resuspended at 5×10^5 cells/mL and 200 µL of this cell suspension was added to each well of a 96-well plate to result in 100,000 cells/well. Stimulation was added to each well, including water (negative control), heat-killed *Listeria monocytogenes* (HKLM) (positive control), TLR agonists, and various bacterial fractions and supernatants. Human TLR1-9 Agonist kit (InvivoGen, San Diego, CA, product #: tlrl-kit1hw) were used to stimulate specific TLRs, such as synthetic tri- and di-acylated lipopeptides PAM_3CSK_4 (TLR1/2) and PAM_2CSK_4 (TLR2/6), a synthetic unmethylated oligonucleotide ODN2006 (TLR9), as well as purified bacterial components including *Escherichia coli* lipopolysaccharide (LPS) (TLR4), *S. aureus* peptidoglycan (PG) (TLR2), and *S. aureus*

lipoteichoic acid (LTA) (TLR2). Bacterial cell wall fractions were tested from *S. aureus* strain LAC and *S. epidermidis*, alongside a vehicle control containing TSM buffer and lysostaphin. Bacterial supernatants from LAC, Δ*psm*, *S. epidermidis*, and the DH5α strain of *E. coli* were also tested for NFκB activity. At 21 hours post-stimulation, 180 µL of pre-warmed QUANTI-Blue substrate was added to a 96-well plate containing 20 µL of the cell culture medium from stimulated THP-1 Blue NFκB reporter cell. The plate was incubated for an additional 3 hours at 37ºC 5% CO_2, and SEAP activity was then measured spectrophotometrically at 630 nm.

Osteoclastogenesis assays

RAW264.7 cells were plated at 250 cells per well in a 96-well plate format or 7,500 cells per well in a 12-well format for osteoclastogenesis assays to prevent overgrowth in the week-long assay. In order to determine the ability of TLR agonists, bacterial cell wall extracts, and bacterial supernatants to induce osteoclastogenesis in RAW264.7 cells, they were stimulated with these components at the time of plating, at day 2 with fresh media, and cells were TRAP stained at day 6. The extent of osteoclastogenesis was determined by staining cells with reagents from the Acid Phosphatase, Leukocyte (TRAP) Kit (Sigma, Saint Louis, MO, 378-A) and counting TRAP$^+$ multinucleated (>3 nuclei) cells.

For osteoclastogenesis assays with primary cells, an osteoclast precursor population was first generated by pre-committing 50,000 BMMs per well in a 96-well plate with 1:20 CMG14-12 supernatants as a source of M-CSF [28] and 35 ng/mL RANKL for 2 days. Mature osteoclasts were formed in culture after 6-7 days of continuous M-CSF and RANKL stimulation. To determine the osteoclastogenic response of enriched BMMs and

osteoclast precursors to *S. aureus* supernatants, we developed two different assays. Osteoclast precursors were either pre-committed with RANKL for 48 hours before they were stimulated with *S. aureus* supernatants for 4 days, or BMMs that had not been pre-committed were stimulated with *S. aureus* supernatants for 24 hours before stimulation with RANKL for 5 days. All primary myeloid cultures had continuous M-CSF treatment. TRAP$^+$ multinucleated cells were counted manually at 10X, with the assistance of OsteoMeasure software (OsteoMetrics, Inc., Decatur, GA) or by taking serial images of the entire well (18 total) and using the FIJI Cell Counter Plugin.

Recombinant murine TNFα (R&D Systems, Minneapolis, MN, 410-MT) was added to osteoclast precursors at 10 ng/mL to determine the ability to enhance osteoclastogenesis. Additionally, RANKL and TNFα inhibitors were added to elucidate the ability of RANKL and TNFα to influence *S. aureus*-enhanced osteoclast differentiation. Anti-RANKL (R&D Systems, Minneapolis, MN, AF462) was used within the reported range for the neutralization dose 50 (ND$_{50}$) for 30 ng/mL RANKL at 21 ng/mL. Anti-TNFα (R&D Systems, Minneapolis, MN, AF410) was used at 4 µg/mL to target an ND$_{50}$ for 10 ng/mL TNFα.

Additionally, the complex cellular milieu of WBM was adapted into a co-culture system based on the presence of both myeloid and stromal cells. In this system, WBM was plated at 0.5 million cells or 3 million cells per well in 96-well plates or 24-well plates, respectively. In both formats, WBM cells were cultured in αMEM (without ascorbic acid), 10% FBS, 1X P/S, and 10 nM 1α, 25-dihydroxyvitamin D$_3$ (Sigma, Saint Louis, MO, D1530). Vitamin D$_3$ (calcitriol) in this assay induces osteoblastic RANKL production, and thus, no exogenous RANKL or M-CSF was added to these cultures. For two weeks, half

of the media was removed and replenished with fresh media every 2-3 days. During the second week, cells were stimulated with 2.5-5% Δ*psm* supernatant. WBM co-cultures were TRAP stained two weeks later to look for osteoclastogenic induction.

Transcriptional changes in osteoclast lineage cells in response to RANKL and *S. aureus* supernatant stimulation

BMMs, pre-osteoclasts, and osteoclasts were generated as described above in a 96-well plate format. At day 7 in culture, RNA was harvested from myeloid cells treated with RANKL (osteoclasts) or untreated (BMMs). To determine the immune response of BMMs versus early osteoclasts, BMMs and osteoclast precursors, generated with 2 days of RANKL treatment, were stimulated with Δ*psm* and vehicle (RPMI) for four hours before harvesting RNA. The RNeasy Mini Kit (Qiagen, Germantown, MD, 74104) with RNase-free DNase treatment (Qiagen, 79254) was used to harvest RNA from cells. After washing with PBS, cells were lysed with Buffer RLT supplemented with β-mercaptoethanol. The lysate from 15 wells with the same stimulation conditions were pooled, and cells were further homogenized through QIAshredder spin columns (Qiagen, Germantown, MD, 79654). Per the manufacturer's directions, 70% ethanol was added to the homogenate and loaded onto a RNeasy mini spin column, where an on-column DNase treatment was performed, and the resulting RNA washed and eluted in RNase-free water. Total RNA was quantified using the Take3 micro-volume plate (BioTek, Winooski, VT) and a BioTek plate reader. The First-Strand Synthesis cDNA system (Promega, Madison, WI, M-MLV) was used to convert 1 µg of RNA into cDNA in a buffered reaction with a recombinant RNase inhibitor, the M-MLV reverse transcriptase enzyme, random hexamers for

annealing, and dNTPs. Reactants were incubated for one hour at 37ºC. For quantitative Real-Time-Polymerase Chain Reaction (qRT-PCR) amplification of mRNA transcripts, SYBR Green Supermix was used with a 12.5 µL final reaction volume. cDNA was diluted 1:100, and 1 µL was added to reactions for housekeeping genes, whereas 2.5 µL was added per reaction for other target genes. Forward and reverse primers were used at a final concentration of 2 µM. Primers were used to detect the presence of RNA transcripts for the genes *Gapdh*, *Acp5*, *Ctsk*, *B2m*, *Tnfsf1a,* and *Nos2* (Table 1).

Table 1. Primers for qRT-PCR detection of mRNA transcripts.

Gene Product	Primer	5' to 3' Sequence	Tm (ºC)
GAPDH	mGapdhFw	ACCCAGAAGACTGTGGATGG	56.6
	mGapdhRv	TTCAGCTCAGGGATGACCTT	55.8
TRAP	mAcp5Fw	CAGCTCCCTAGAAGATGGATTCAT	56.1
	mAcp5Rv	GTCAGGAGTGGGAGCCATATG	57.2
Cathepsin K	mCtskFw	ATGTGGGTGTTCAAGTTTCTGC	56
	mCtskRv	CCACAAGATTCTGGGGACTC	55.1
B2m	mB2MFw	CTGCTACGTAACACAGTTCCACCC	61.5
	mB2MRv	CATGATGCTTGATCACATGTCTCG	57.3
TNFα	mTNFaFw	CCTGTAGCCCACGTCGTAG	61.5
	mTNFaRv	GGGAGTAGACAAGGTACAACCC	61.4
iNos	mNos2Fw	CACCTTGGAGTTCACCCAGT	57.1
	mNos2Rv	ACCACTCGTACTTGGGATGC	57.1

Primers were used to detect the presence of RNA transcripts for the genes *Gapdh*, *Acp5*, *Ctsk, B2m, Tnfsf1a,* and *Nos2*. Listed in this table are the respective gene products, forward (Fw) and reverse (Rv) primer sequences, and corresponding melting temperature (Tm).

Cytokine detection via Luminex

BMM and pre-osteoclast cytokine responses to S. aureus supernatant stimulation. BMMs and pre-osteoclasts were generated in a 96-well plate format. Cells were stimulated with Δ*psm* supernatant or vehicle control in triplicate. At 24 hours, cells were washed twice with PBS and fresh media (αMEM, 10% FBS, 1X P/S, and 1:20 CMG14-12) was replenished. All conditions were incubated for another 24 hours at 37ºC 5% CO_2, and supernatants were collected and stored at -80ºC until analyzed.

Luminex platform. Supernatants were thawed slowly from -80ºC, by storing at -20ºC overnight, and at 4ºC two hours before starting. The Milliplex Map Kit – Mouse Cytokine/Chemokine Magnetic Bead Panels (Millipore Sigma, Burlington, MA, MCYTOMAG-70K-PMX32) was used per the manufacturer's directions. Briefly, the plates were washed, samples were centrifuged to pellet particulate matter from supernatant, and quality controls and standards were prepared. Standards, quality controls, or samples were added to each well. Media was added to standards and quality controls, and assay buffer was added to sample wells to equilibrate a baseline mixture of assay buffer and cell culture media in each well. Detection beads were sonicated and added to each well. Plates were sealed, wrapped in foil, and left to shake overnight at 4ºC. The following day, with the use of a magnetic base, wells were washed with wash buffer, incubated with detection antibodies followed by streptavidin-phycoerythrin, washed, and resuspended in sheath fluid. The samples were run using the FLEXMAP 3D system. Data was analyzed by confirming quality control values, assessing standard curve generation, and verifying appropriate variance (CV) values between duplicate wells.

Results

Signaling crosstalk between immunologic pathways and pathways necessary for skeletal cell differentiation becomes an important consideration in the context of bacterial bone infection. This potential crosstalk led me to ask how *S. aureus* influences skeletal cell differentiation and bone homeostasis. To answer this question, we developed and conducted a variety of *in vitro* assays to ask how skeletal cells sense and respond to bacterial and inflammatory components. The majority of these assays focused on the perturbation of myeloid lineage cells as they differentiated into mature osteoclasts. However, we also began to explore how osteoblasts react to *S. aureus* in monoculture and co-culture systems. In this chapter, we describe how *S. aureus* or other bacterial components perturb osteoclast and osteoblast lineage cells in regards to cell differentiation status and immunologic capacity in terms of cytokine production.

Bacterial stimuli stimulate monocytes to activate NFκB and increase their proliferative capacity

Previous work from our laboratory characterized the ability of PSMα toxins to induce cell death in a variety of cell lines, including RAW264.7 cells, a murine monocyte/macrophage cell line, and mc3T3 cells, a murine pre-osteoblast cell line [32]. In order to develop *in vitro* cell culture models, we first tested the susceptibility of primary murine skeletal cells isolated from WT mice to cell death induced by *S. aureus* supernatants. We used concentrated *S. aureus* supernatant preparations as reported previously [31, 32], and incubated WT BMMs with either wild-type *S. aureus* or PSMα-deficient supernatants at increasing doses ranging from 2.5 to 10% volume/volume. The

results confirmed that PSMα toxins induce death of primary BMMs in a dose-dependent manner, where at 10% final supernatant concentration in the cell culture media, all the WT BMMs were non-viable after 24 hours post-intoxication **(Figure 7A)**. Furthermore, when testing primary osteoblasts obtained from WT and immunodeficient animals, all cell types were sensitive to PSMα-induced cytotoxicity **(Figure 7B)**. These data indicated that in order to retain viable cells in culture, we should utilize PSMα-deficient supernatants in our *in vitro* assays.
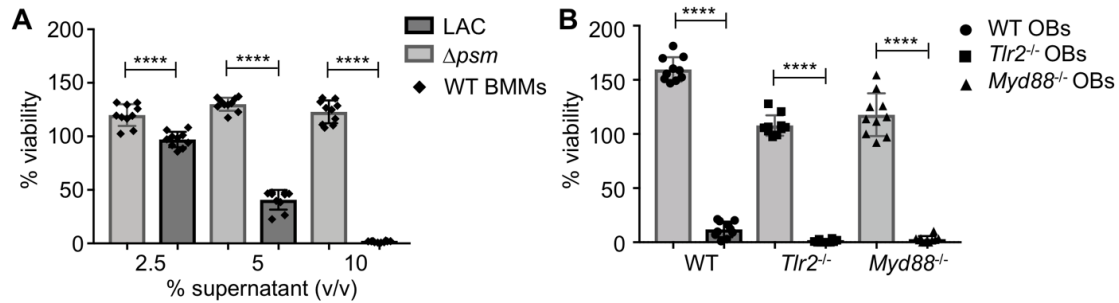
Figure 7. Alpha-type PSMs are toxic to primary skeletal cells.
(A-B) Viability of skeletal cells after treatment with *S. aureus* supernatants (LAC, Δ*psm)* relative to vehicle control was determined by the ability of cells to metabolize the CellTiter 96 Aqueous One dye, as enumerated by optical density at 490 nm (OD_{490}). Percent viability was calculated relative to the OD_{490} of vehicle control. **(A)** WT BMMs were treated with increasing doses of concentrated supernatants from LAC (dark grey) and toxin-deficient Δ*psm* (light grey) supernatants, ranging from 2.5%, 5%, to 10% supernatant volume/media volume or a vehicle control (RPMI). WT BMMs (diamonds) were plated at 50,000 cells/well in a 96-well plate, and each treatment condition was plated in 10 replicates. **(B)** Primary osteoblasts (OBs) were harvested from WT (circles), *Tlr2*^{-/-} (squares), and *Myd88*^{-/-} (triangles) femurs and plated at 10,000 cells per well in a 96-well plate. Cells were treated with LAC (dark grey) and toxin-deficient Δ*psm* (light grey) supernatants or vehicle at 20% volume/volume in 10 replicates per condition. Multiple *t*-tests were used to compare viability between supernatants at each dose and were corrected for multiple comparisons using the Holm-Sidak methods. Unpaired *t*-tests were used to compare viability between each osteoblast genotype. **** *p* < 0.0001.

51

When assaying cell lines and primary cells for toxicity, we calculated percent viability based on the relative cell metabolic rate compared to cells stimulated with vehicle. In some cases, cells were calculated to have much greater than 100% viability. When present, this phenotype was consistent, more robust in cell lines as previously reported [32], and was diminished in immunodeficient cells **(Figure 7A and 7B)**. These data led us to believe that there was an enhanced proliferative response that may be downstream of NFκB transcription factor activation. NFκB signaling is critical for many cellular response systems, including cellular proliferation, osteoclast differentiation, and promotion of innate immune responses. This led us to ask whether *S. aureus* supernatants induce NFκB activity, and if so, what types of general bacterial components stimulate NFκB.

To test which types of bacterial components are able to activate NFκB transcription factor activity, we stimulated a human THP-1 monocytic cell line containing an NFκB reporter system with diverse purified or synthetic TLR ligands, crude staphylococcal cell wall extracts, or supernatants from various bacterial strains. For viability and NFκB activity, concentrations of TLR agonists per the manufacturer's suggestions, with an additional dose used outside this range for PAM_3CSK_4 and PAM_2CSK_4. Cell viability assays of each condition indicated there was only cell death associated with *S. aureus* LAC supernatant, and there was no appreciable cell death with any other stimulation condition **(Figure 8A, 8C, and 8E)**. NFκB activity was measured by a colorimetric change, which could be quantified by reading OD_{630}. Prominent NFκB activity occurred in response to the synthetic peptides PAM_3CSK_4 and PAM_2CSK_4. PAM_2CSK_4 acted as a more potent stimulator, with NFκB activity similar to the positive control (HKLM) at a much lower dose than PAM_3CSK_4 **(Figure 8B)**. LPS appeared to induce some NFκB activity at high

52

doses, but had much weaker magnitude **(Figure 8B)**. Furthermore, NFκB activity was induced by staphylococcal cell wall extracts and supernatants, as well as *E. coli* strain DH5α supernatants. *S. aureus* LAC supernatants at sub-cytotoxic doses could still stimulate NFκB activity. However, not all the PRR agonists tested activated NFκB transcription in this assay, including the TLR9 agonist ODN2006, purified peptidoglycan from *S. aureus,* and purified lipoteichoic acid from *S. aureus*. Overall, these results support that components from Gram-negative and Gram-positive bacteria, and more specifically, staphylococcal cell wall components and concentrated supernatants activate NFκB transcription factor activity, but the purified Gram-positive cell wall components supplied by the manufacturer do not.
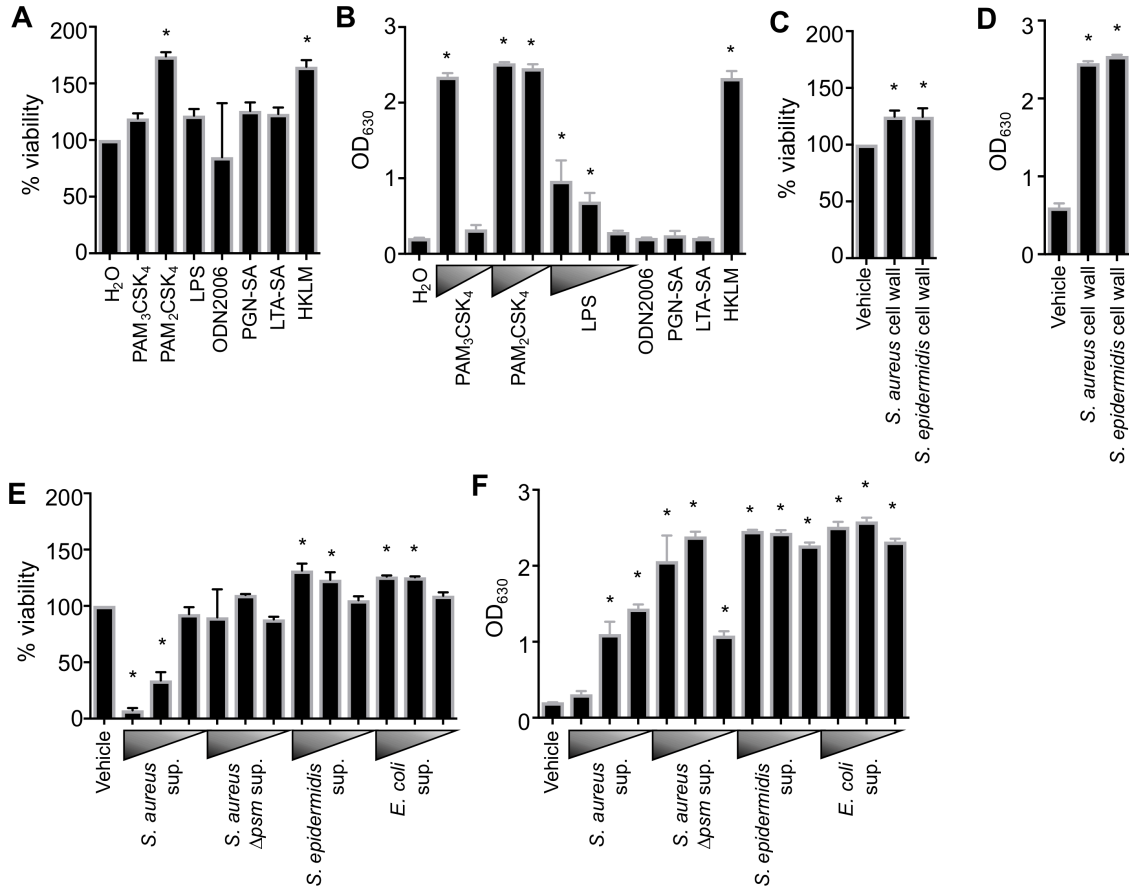
Figure 8. TLR agonists, bacterial supernatants, and bacterial cell wall fractions induce NFκB transcription factor activity in human osteoclast progenitors.
(A-F) $1x10^5$ human THP-1 monocytes were treated with various stimulatory conditions and monitored for viability using Cell Titer 96 Aqueous One dye relative to a vehicle control **(A, C, E)** or NFκB reporter activity as measured by the enzymatic conversion of the QUANTI-Blue substrate in the supernatant at OD_{630} **(B, D, F)**. Wedges under bar graphs indicate stimulation conditions (as numbered) with multiple stimulation concentrations tested, with wedge reflecting highest to lowest concentration. **(A, B)** TLR agonists were added to cells as follows: H_2O vehicle control, PAM_3CSK_4 at 1 µg/mL and/or 10 ng/mL, PAM_2CSK_4 at 1 µg/mL and/or 10 ng/mL, LPS at 4.5 µg/mL, 2 µg/mL, and/or 10 ng/mL, ODN2006 at 5 µM, PGN-SA at 1 µg/mL, LTA-SA at 1 µg/mL, and HKLM positive control. Viability **(A)** reflects PAM_3CSK_4, PAM_2CSK_4, and LPS at the highest dose, whereas NFκB reporter activity **(B)** shows all doses. **(C, D)** Crude cell wall extracts were tested where the vehicle control, TSM buffer + lysostaphin at 10µL, *S. aureus* LAC cell wall at 10 µL, and *S. epidermidis* cell wall at 10 µL for viability **(C)** and NFκB reporter activity **(D)**. **(E, F)** Various bacterial supernatants were tested for effects on viability **(E)** and NFκB reporter activity **(F)**, including the vehicle control (RPMI) at 10µL, concentrated supernatants from LAC at 2 µL, 1 µL, or 0.25 µL, Δ*psm* at 10 µL, 2 µL, or 0.25 µL, *S. epidermidis* at 10 µL, 2µL, or 0.25 µL, and *E. coli* DH5α at 10 µL, 2 µL, or 0.25 µL (16). Comparisons between conditions on each panel were conducted using a one-way ANOVA with Dunnett's multiple comparisons test. * $p < 0.0001$.

Notably, the downstream consequences of NFκB activity include proliferation, osteoclast differentiation, and cytokine induction. To test the effects of proliferation on these cells, the growth kinetics of RAW264.7 myeloid cells were measured for 5 days in response to increasing doses of vehicle and *S. aureus* LAC or PSMα-deficient supernatants. In all conditions, vehicle-treated cells steadily proliferate over the course of the 5 days in culture. At all doses of Δ*psm* supernatants, cells proliferate above the vehicle-maximum by day 3 post-stimulation, after which the signal plateaus or drops, likely reflecting cell overgrowing **(Figure 9A-D)**. Cells treated with sub-toxic doses of LAC supernatant (1.25% and 2.5%) show a similar trend **(Figure 9A and 9B)**. However, higher doses of LAC stimulation cause immediate cell death **(Figure 9C and 9D)**. Taken together, these data support that *S. aureus* stimulation enhances NFκB activity and its downstream effect on proliferation.
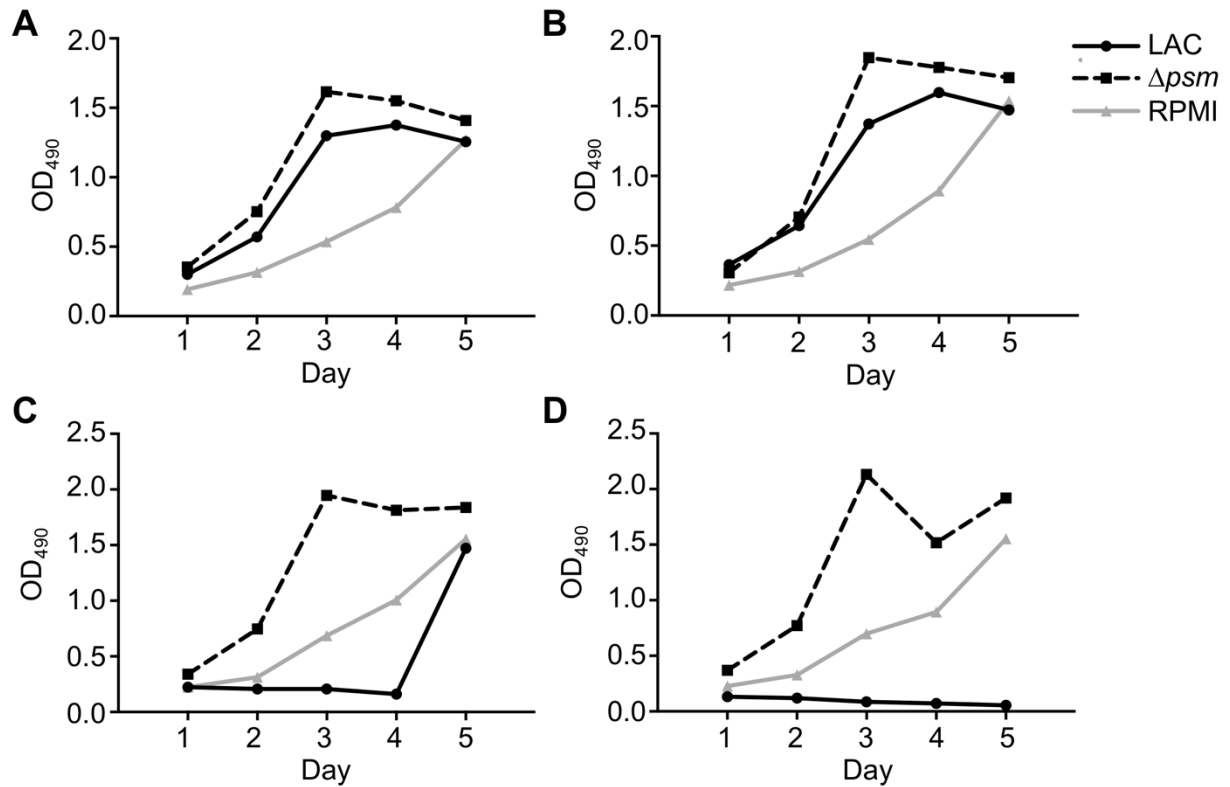
Figure 9. Toxin-deficient *S. aureus* supernatants enhance proliferation of a murine myeloid cell line.
(A-D) The RAW264.7 murine macrophage/monocyte cell line was plated at 250 cells per well in a 96-well plate, where vehicle (RPMI; solid grey) or concentrated supernatants from LAC (solid black) or Δ*psm* (dashed black) supernatants were added at concentrations of 1.25% **(A)**, 2.5% **(B)**, 5% **(C)**, and 12.5% **(D)** at the time of plating, and replenished in fresh media at day 2. After plating and stimulating cells, CellTiter 96 Aqueous One dye was added to one plate replicate each day for 5 days, and plates were read at OD$_{490}$ as a proxy for cell proliferation over time.

Bacterial stimuli promote osteoclast differentiation of myeloid cell lines and RANKL-committed primary cells

Next, we tested the ability of bacterial supernatants to induce osteoclastogenesis from RAW264.7 cells. In this assay, we treated the cells with vehicle or supernatants from *S. aureus* Δ*psm*, *S. epidermidis,* or *E. coli* DH5α. In all supernatant conditions compared to vehicle, we observed that post bacterial-stimulation, cells expressed the osteoclast marker TRAP **(Figure 10A-D)**. In response to *E. coli* DH5α supernatants, we observed particularly large, multinucleated cells with expansive cytoplasm **(Figure 10D)**. We then went on to test the osteoclastogenic potential of a panel of TLR agonists, compared to the water vehicle used to reconstitute the agonists **(Figure 11A)** and low or high doses of RANKL **(Figure 11B and 11C)**. In this assay, we used concentrations of TLR agonists based on viability data and NFκB activity, or on other reports [62, 245]. We found that although purified *S. aureus* LTA and PGN failed to induce robust NFκB activity, each stimulus could induce osteoclastogenesis in RAW264.7 cells **(Figure 11D and 11E)**. However, the TLR9 agonist ODN2006 was also unable to stimulate NFκB activity, and it did not induce osteoclastogenesis **(Figure 11F)**. The synthetic lipoproteins that engage TLR2 heterodimers, PAM$_3$CSK$_4$ and PAM$_2$CSK$_4$, and the agonist for TLR4, LPS, were found to have both NFκB stimulating activity and various amounts of TRAP-positivity **(Figure 11G-11I).** Interestingly, the vehicle control for cell wall extraction had a low level of TRAP-positivity **(Figure 11J)**. This vehicle included lysostaphin, a staphylococcal enzyme isolated from *S. simulans*, that may have other bacterial PAMPs in the preparation. In comparison to this vehicle, crude cell wall extracts from staphylococcal species *S. aureus* and *S. epidermidis* both exhibited a greater ability to drive osteoclast differentiation

(Figure 11K and 11L). These results broadly support that staphylococcal cell walls and TLR agonists induce osteoclastogenesis.
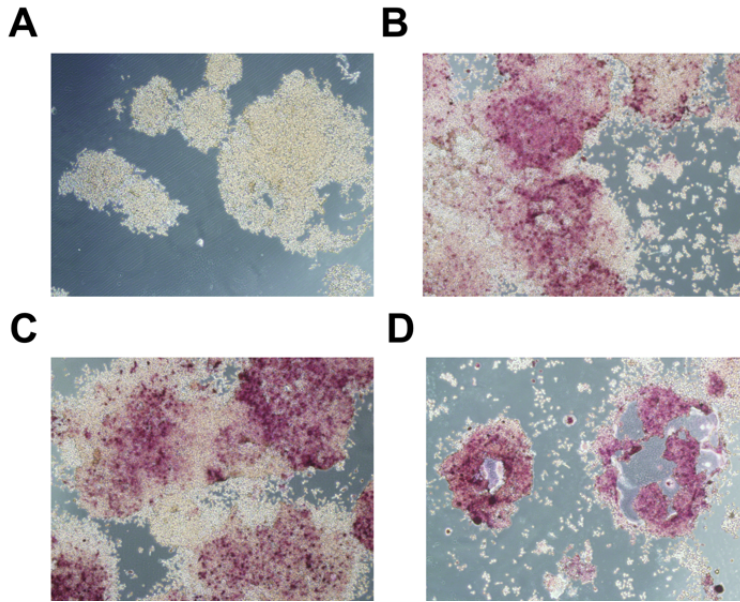
Figure 10. Bacterial supernatants from *S. aureus, S. epidermidis,* and *E. coli* induce osteoclastogenesis in the RAW264.7 monocyte/macrophage cell line.
(A-D) RAW264.7 cells were plated at 250 cells per well in a 96-well plate, where 1% (v/v) of each, vehicle (RPMI; **A**) and concentrated supernatants from LACΔ*psm* **(B)**, *S. epidermidis* **(C)**, or *E. coli* DH5α **(D)** were added to each well with fresh media at day 1, 4, and 6. At day 7 in culture, cells were TRAP stained and imaged at 10X. TRAP positivity is indicated by a pink-purple color change.
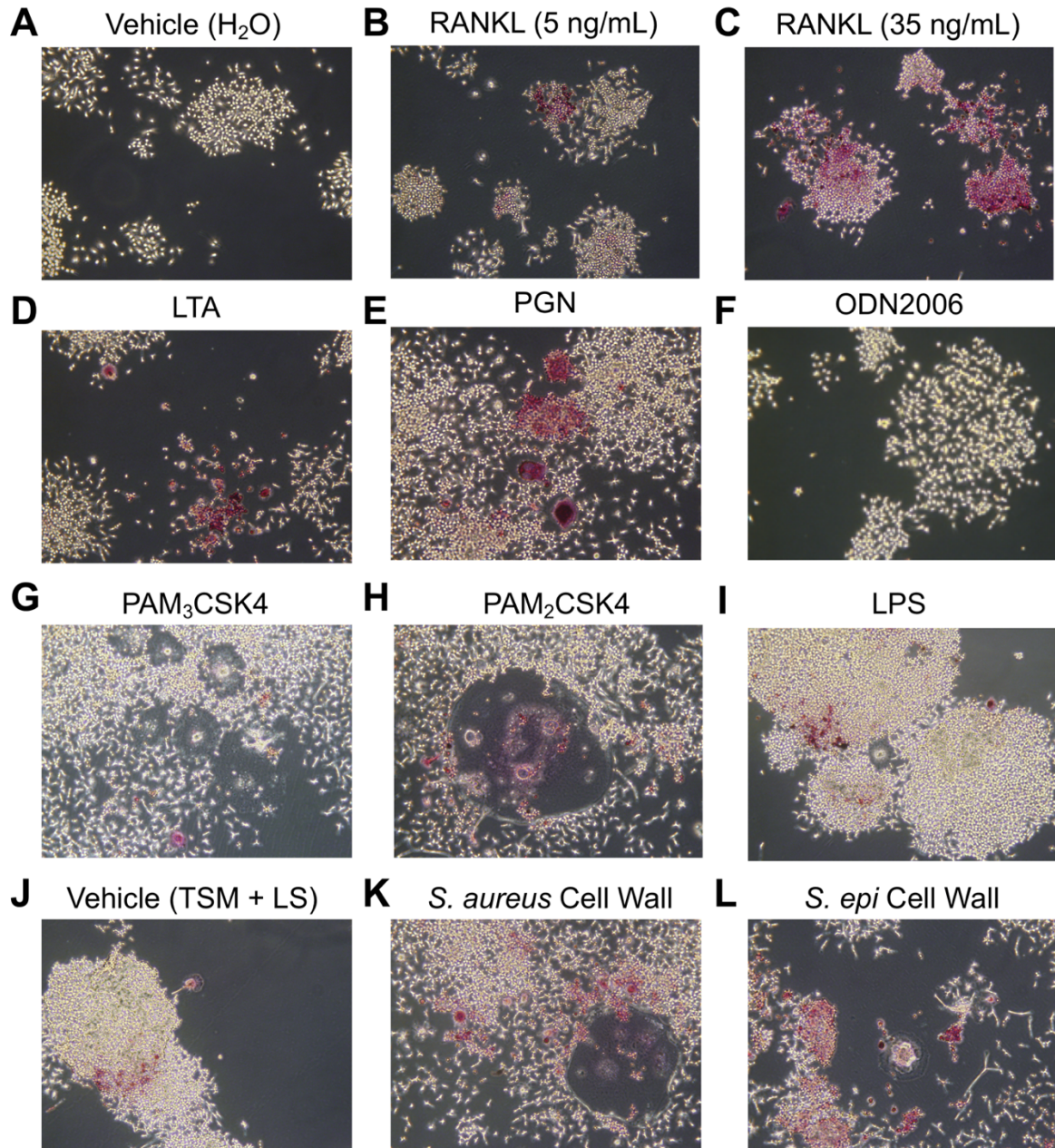
Figure 11. Cell wall components and TLR agonists induce osteoclastogenesis.
(A-L) RAW264.7 cells were plated at 7,500 cells per well in 12-well plates and stimulated
with vehicle or bacterial stimuli at the time of plating and at day 2 with fresh media. **(A-I)**
Purified TLR agonists tested for osteoclastogenic enhancement compared to negative
control (H_2O; **A**), and positive control (RANKL; **B, C**), including LTA-SA at 2 µg/mL
(D), PGN-SA at 20 µg/mL **(E)**, ODN2006 at 5µM **(F)**, PAM_3CSK4 at 300 ng/mL **(G)**,
PAM_2CSK4 at 300 ng/mL **(H)** and LPS at 10 µg/mL **(I)**. **(J-L)** Crude cell wall extractions
were tested for ability to induce osteoclastogenesis relative to vehicle control (TSM buffer
+ lysostaphin; **J**), including *S. aureus* LAC cell wall at 10 µL **(K)** and *S. epidermidis* cell
wall at 10 µL **(L)**. Stimuli were added to each well with fresh media at day 2. At day 6 in
culture, cells were TRAP stained and imaged at 10X.

60

While cell lines were useful for preliminary experiments, primary cells are a more dependable model system that requires canonical signals for viability and differentiation. To better replicate osteoclastogenesis in culture, we generated osteoclasts from BMMs treated with M-CSF and RANKL. After 7 days in culture, cells treated with only M-CSF remained TRAP negative and mononuclear, whereas cells treated with RANKL were all TRAP positive and many were multinucleated **(Figure 12A and 12B)**. In agreement with this, we determined that cells treated with RANKL were of osteoclast origin, as indicated by their increased levels of osteoclast transcripts, including the genes for TRAP and Cathepsin K **(Figure 12C)**. In order to determine how *S. aureus* perturbs primary osteoclast differentiation, I developed an assay where precursor cells from a population of BMMs were treated with RANKL for two days, and were continuously treated with M-CSF. RANKL was removed at two days and replaced with RPMI vehicle stimulation. Six days into the assay, it appeared that these primary cells had received enough RANKL signaling and activity to allow some of the cells to become TRAP positive, with some multinucleation **(Figure 13A)**. However, when the osteoclast precursor population was subjected to increasing doses of *S. aureus* Δ*psm* supernatant, we observed an increase in the number of TRAP$^+$ multinucleated cells formed *in vitro* **(Figure 13B and 13E)**. Excitingly, this increase occurred to a similar extent as osteoclastogenesis driven by RANKL alone **(Figure 13C and 13E)**. These data indicate that, similar to cell lines that do not require canonical stimulation with M-CSF and RANKL, *S. aureus* stimulation allows primary osteoclast precursor cells to continue through osteoclastogenesis. Furthermore, with continuous RANKL treatment, *S. aureus* Δ*psm* supernatant can further enhance osteoclastogenesis **(Figure 13D and 13E)**.
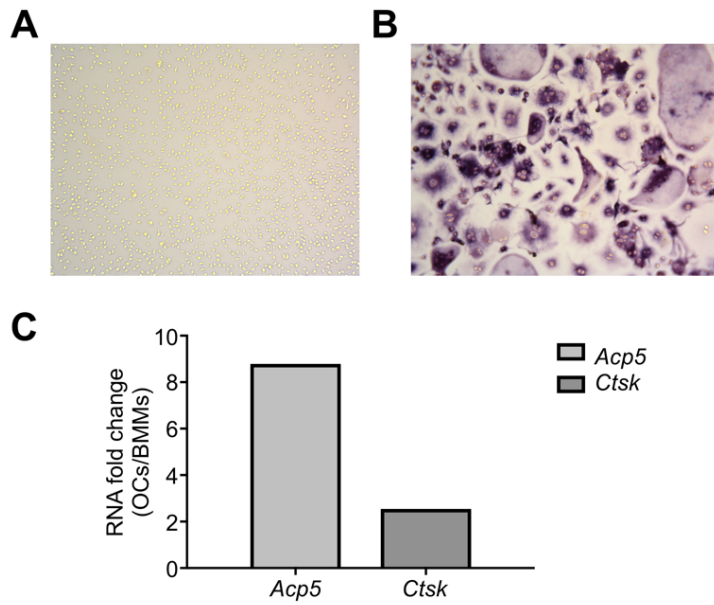
Figure 12. RANKL-derived osteoclasts express expected osteoclast markers *Acp5* and *Ctsk*.
(A-C) WT BMMs were plated at 50,000 cells per well in a 96-well plate and stimulated with M-CSF (BMMs; **A**) or M-CSF and 35 ng/mL recombinant murine RANKL (OCs; **B**). Fresh media and reagents were replenished at days 1, 4, and 6. At day 7 in culture, cells were TRAP stained and imaged at 10X. Buffer RLT was added to 15 wells per condition (BMMs or OCs) and lysed cells were pooled to harvest RNA. qRT-PCR was run to amplify mRNA transcripts for *Gapdh*, *Acp5,* and *Ctsk. Gapdh* was used to calculate relative values for each cellular condition, and the relative fold increase of *Acp5* and *Ctsk* osteoclast genes are reported **(C)**.
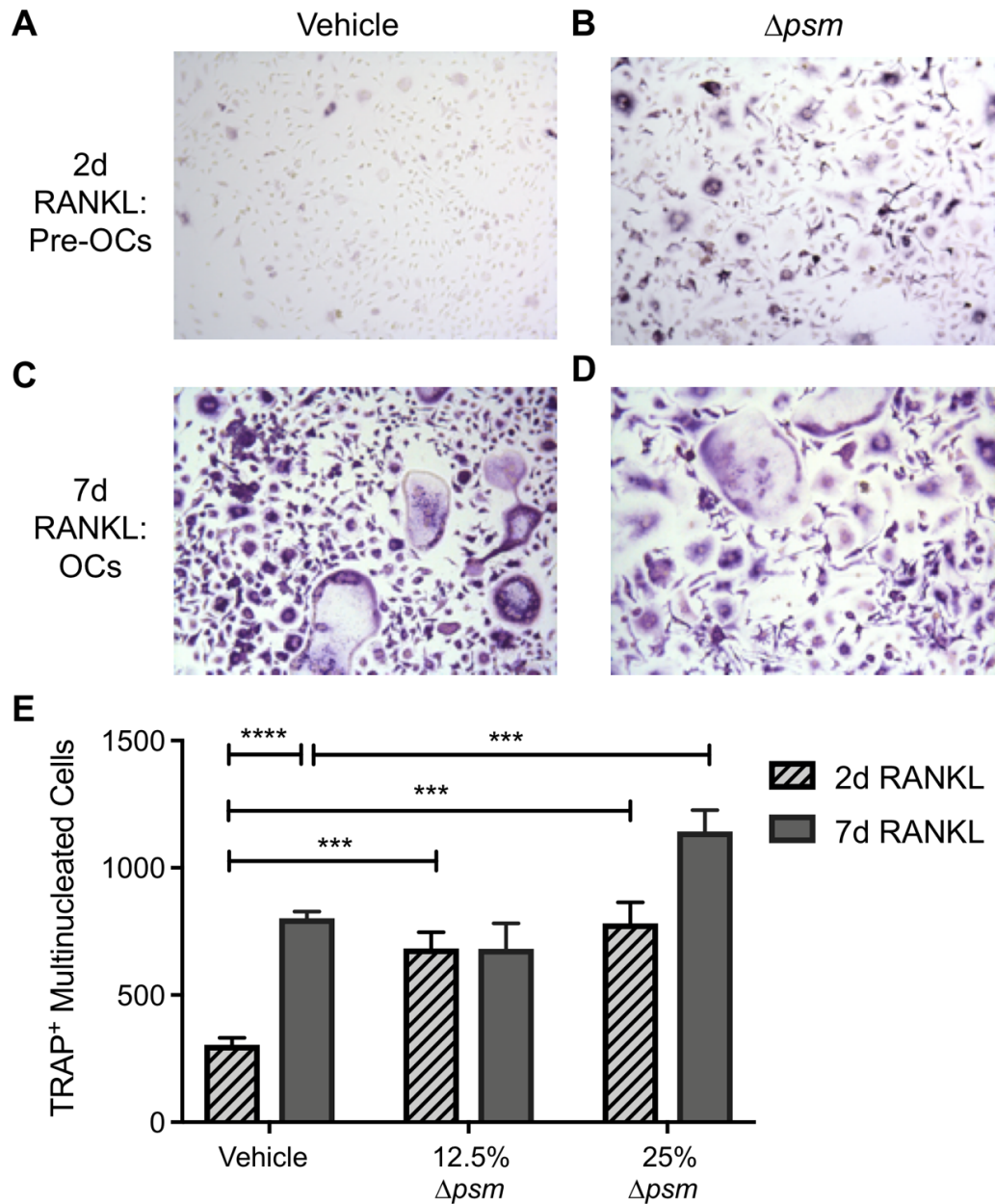
Figure 13. RANKL-stimulated osteoclast lineage cells are enhanced by *S. aureus* stimulation. (A-E) WT primary BMMs were pre-committed with 35 ng/mL RANKL for 2 days (Pre-OCs) **(A, B)** or continuously treated with 35 ng/mL RANKL for 7 days (OCs) **(C, D)**. Pre-OCs were stimulated at day 2 in culture with vehicle **(A)** or *S. aureus* Δ*psm* supernatant **(B)** at 12.5% in cell culture media, or OCs were continuously treated with RANKL were stimulated at days 1, 4, and 6 in culture with vehicle **(B)** or *S. aureus* Δ*psm* supernatant **(D)** at 12.5% in cell culture media. Cells were TRAP stained at day 6 **(A, B)** or day 7 **(C, D)** and TRAP+ multi-nucleated cells were manually quantified using OsteoMeasure software **(E)**. A two-way ANOVA compared the effects of *S. aureus* stimulation and RANKL stimulation on the magnitude of TRAP+ multinucleated cells formed in culture. *** $p < 0.001$, **** $p < 0.0001$.

Due to the robust osteoclastogenesis with continuous RANKL treatment, we chose to use the pre-osteoclast state to assess modulation of osteoclast differentiation. To expand on these data, we found that osteoclastogenesis occurred in a dose-dependent manner **(Figure 14A-G)**. From these results it appears that *S. aureus* enhances osteoclast differentiation; however, we also wondered how *S. aureus* stimulation of myeloid cells prior to commitment to the osteoclast lineage might influence osteoclastogenesis. The starting BMM culture contains precursor cells that are also able to differentiate into inflammatory macrophages. In order to address conflicting reports on how inflammatory stimuli influence osteoclastogenesis, primary WT BMMs were stimulated first with vehicle or *S. aureus* Δ*psm* supernatants for 24 hours and then given RANKL for the remaining 6 days in culture. RANKL for the course of 6 days leads to numerous TRAP$^+$ cells and is sufficient for the formation of TRAP$^+$ multinucleated cells after vehicle treatment **(Figure 15A)**. Unlike stimulation of osteoclast precursors, we observed inhibition of osteoclastogenesis when BMMs were stimulated with supernatant prior to RANKL treatment **(Figure 15B-G)**. These opposing phenotypes highlight the ability of naïve BMMs to undergo cell fate decisions to begin differentiation down a pathway that prevents osteoclast differentiation.
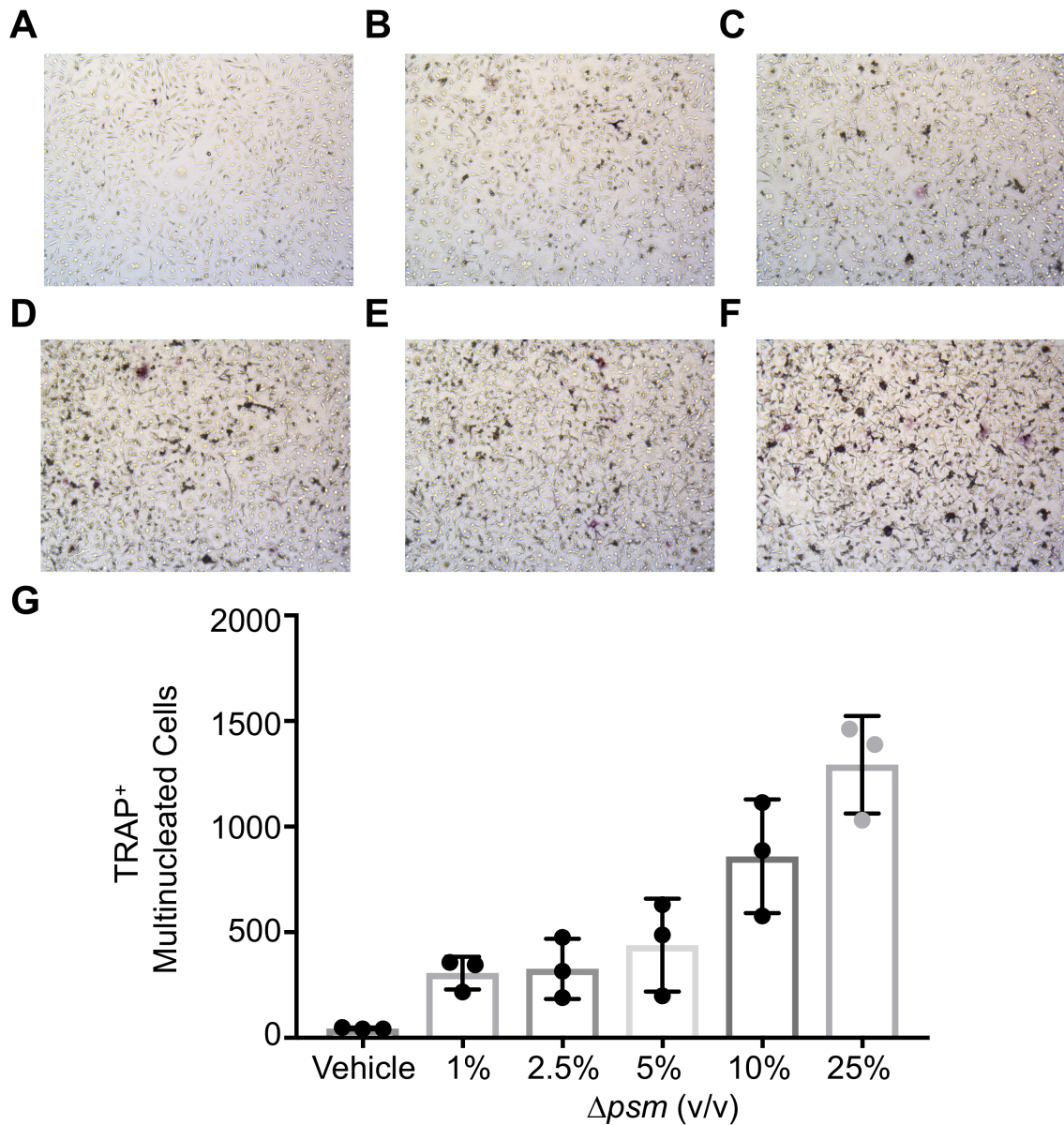
Figure 14. *S. aureus* enhances osteoclast differentiation from primary WT osteoclast precursors.
(A-G) WT pre-osteoclasts were generated by plating 50,000 BMMs and treated them for 2 days with M-CSF and 35 ng/mL RANKL. At day 2 post-plating, cells were washed 2 times with PBS, and fresh media and M-CSF were added cells. Vehicle (RPMI; **A**) or LAC*Δpsm* concentrated supernatants were added in increasing amounts at 1% **(B)**, 2.5% **(C)**, 5% **(D)**, 12.5% **(E)**, or 25% **(F)** (v/v). At day 6 in culture, cells were TRAP stained and imaged at 10X, and TRAP+ multinucleated cells were counted from triplicate wells **(G)**.
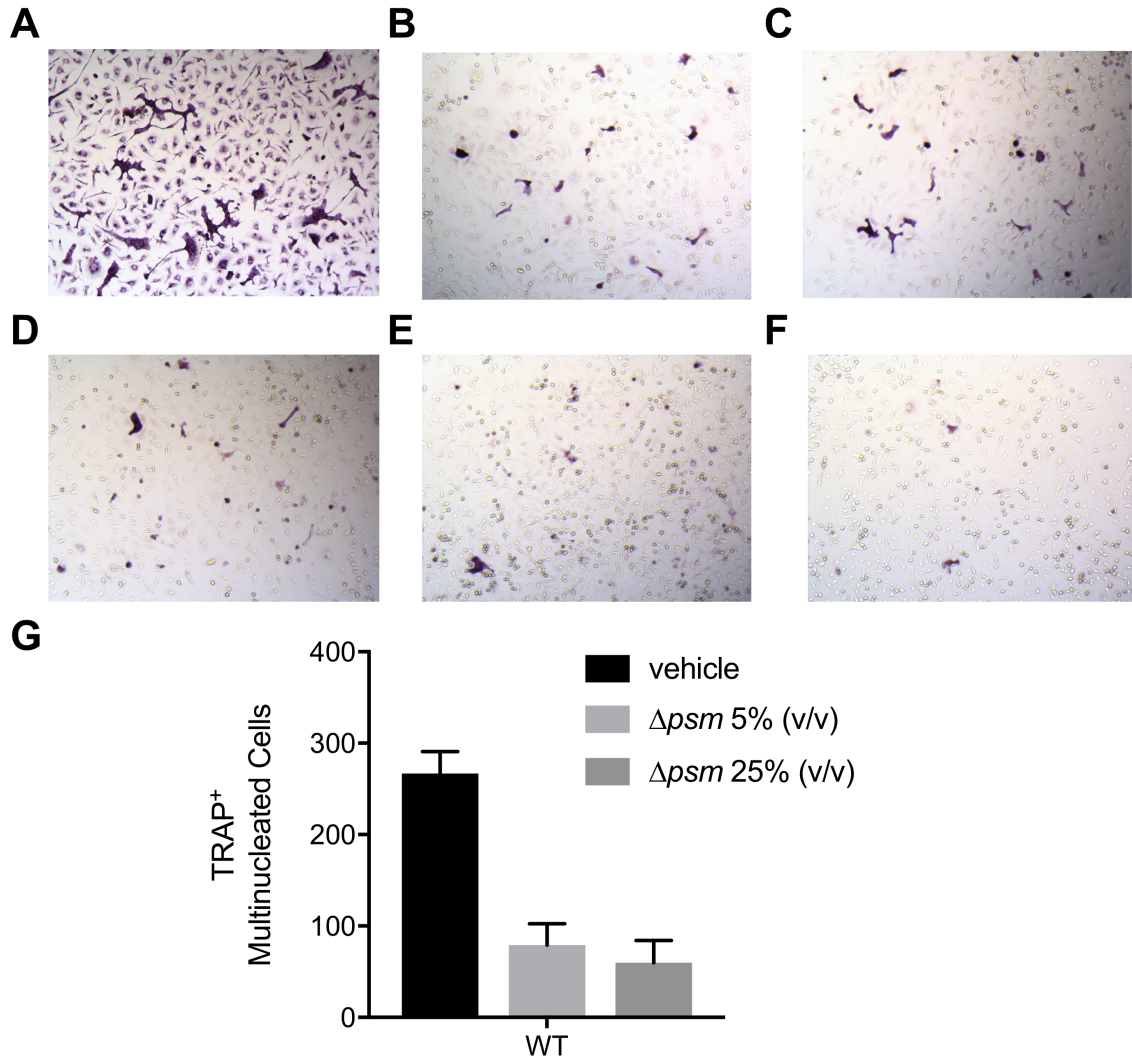
Figure 15. WT BMMs pre-stimulated with bacterial supernatants show inhibited ability to undergo osteoclastogenesis.
(A-G) WT BMMs were plated at 50,000 cells per well and treated with M-CSF and vehicle (RPMI; **A**) or LACΔ*psm* concentrated supernatants were added in increasing amounts at 1% **(B)**, 2.5% **(C)**, 5% **(D)**, 12.5% **(E)**, or 25% **(F)** (v/v). At 24 hours after stimulation, cells were washed with PBS and fresh media was replenished with M-CSF and 35 ng/mL RANKL. At day 6 in culture, cells were TRAP stained and imaged at 10X, and TRAP$^+$ multinucleated cells were counted from triplicate wells in vehicle-treated, 5%, or 25% Δ*psm*-treated conditions **(G)**.

There has been debate in the field of bone biology as to what constitutes canonical or non-canonical osteoclastogenesis. As primary cells are harvested from bone marrow, they are inherently not RANKL-naïve given their close association in the bone marrow with osteoblast-lineage cells that produce RANKL. Canonical osteoclast differentiation is thought to be due to the combinatorial signals from the c-FMS receptor, the RANK receptor, and co-stimulatory Ig-like receptors OSCAR and TREM2. However, noncanonical osteoclast differentiation has referred to signals that are reportedly RANKL-independent. In order to test whether or not *S. aureus* supernatants are triggering canonical or non-canonical osteoclastogenesis, we used pre-osteoclast and osteoclast differentiation conditions with or without *S. aureus* Δ*psm* supernatants in the presence of anti-RANKL antibody treatment. In the PBS control, we observed TRAP$^+$ mononuclear osteoclast precursors and mature TRAP$^+$ multinucleated osteoclasts **(Figure 16A and 16B)**. In contrast, anti-RANKL treatment diminished osteoclast differentiation **(Figure 16A and 16B)**. However, it appears that some osteoclast differentiation still occurs in the context of *S. aureus* Δ*psm* supernatant stimulation in the presence of anti-RANKL treatment **(Figure 16B)**. These data indicate that osteoclast promotion through treatment with *S. aureus* supernatants is dependent on RANKL pre-commitment of myeloid cells down the osteoclast lineage.
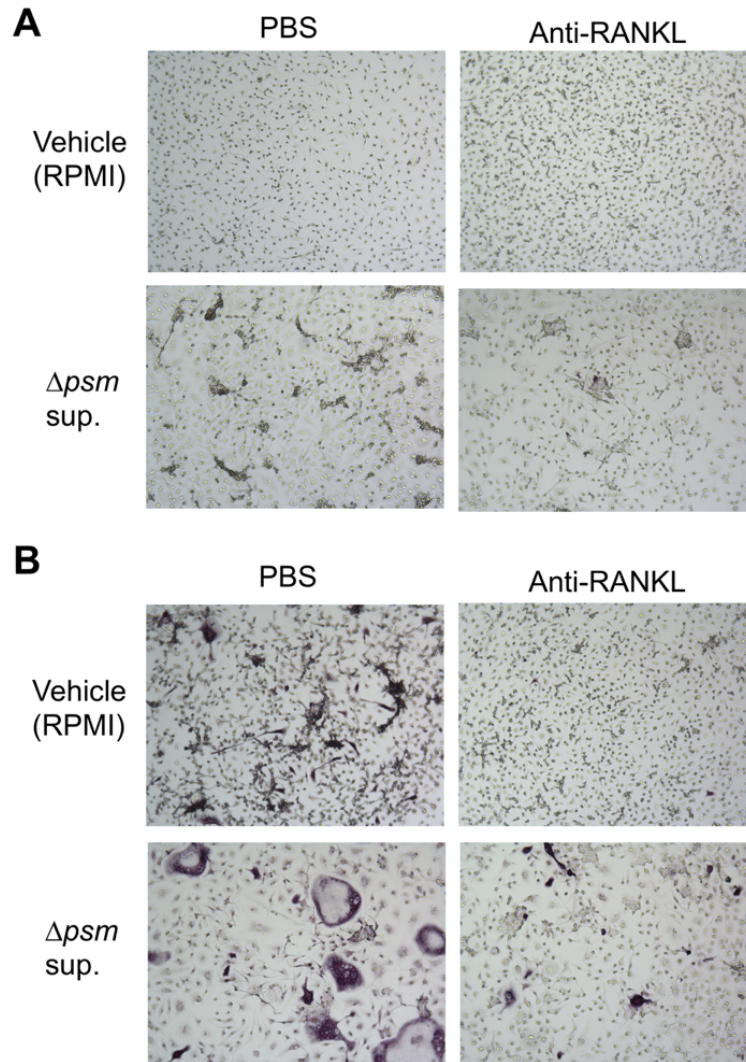
Figure 16. *S. aureus*-enhanced osteoclastogenesis from primary bone marrow cells is dependent on RANKL pre-commitment.
(A-B) WT BMMs were plated at 50,000 cells per well in a 96-well plate with M-CSF and RANKL for 2 days to generate osteoclast precursors **(A)** or M-CSF and continuous RANKL **(B)**. PBS (negative control; left column) or anti-RANKL antibody at 21 ng/mL (right column) were added alongside *S. aureus* to test RANKL blockade on osteoclastogenesis. **(A)** At day 2 osteoclast precursors were generated, washed with PBS twice, and RPMI (top row) or Δ*psm* supernatants (bottom row) at 5% volume/volume and PBS or anti-RANKL were added to culture. Cells were TRAP stained at day 6. **(B)** In continuous RANKL treatment, RPMI (top row) or Δ*psm* supernatants (bottom row) were added to cells at 5% volume/volume one day after plating, with PBS or anti-RANKL. All reagents were replenished on days 4 and 6. Cells were TRAP stained at day 7.

TNF-family cytokines have been reported as potent inducers of non-canonical osteoclastogenesis [246]. In order to test whether *S. aureus* supernatant was inducing non-canonical osteoclastogenesis through TNFα, we treated osteoclast precursors with TNFα as a positive control, supernatant vehicle control, or Δ*psm* supernatant and then added anti-TNFα to the culture. As expected, TNFα enhanced osteoclastogenesis from osteoclast precursors compared to vehicle **(Figure 17A and 17B)**, and anti-TNFα treatment blocked TNFα-mediated osteoclastogenesis **(Figure 17D and 17E)**. Importantly, we found that *S. aureus*-enhanced osteoclastogenesis occurred even in the presence of inhibitory concentrations of anti-TNFα **(Figure 17C and 17F)**. These data suggest that *S. aureus* supernatant-enhanced osteoclastogenesis is not due to the production of TNFα.

While the previous studies have elucidated the influence of myeloid-lineage signaling pathways in *S. aureus*-enhanced osteoclastogenesis, a monoculture system is inherently simplistic when considering complex skeletal cell communication as it occurs in bone. We established a co-culture system that has a combination of cells with osteoblastic and osteoclastic potential, using the active form of (1,25)-dihydroxy vitamin D$_3$ (calcitriol) to activate the production of growth factors and RANKL from osteoblast lineage cells to drive osteoclastogenesis. We found that after two weeks in culture with vehicle stimulation, the co-culture system was able to generate osteoclasts **(Figure 18A and 18C)**. Before perturbation with bacterial stimulation, cells were cultured for a week to allow for osteoblast production of growth factors and RANKL, thus creating a network of skeletal cell communication *in vitro*. During the second week in culture, the addition of *S. aureus* Δ*psm* supernatant enhanced osteoclastogenesis over that of vehicle control,

suggesting that *S. aureus* supernatants can stimulate also osteoclastogenesis in co-cultures without the addition of exogenous M-CSF or RANKL **(Figure 18A-D)**.
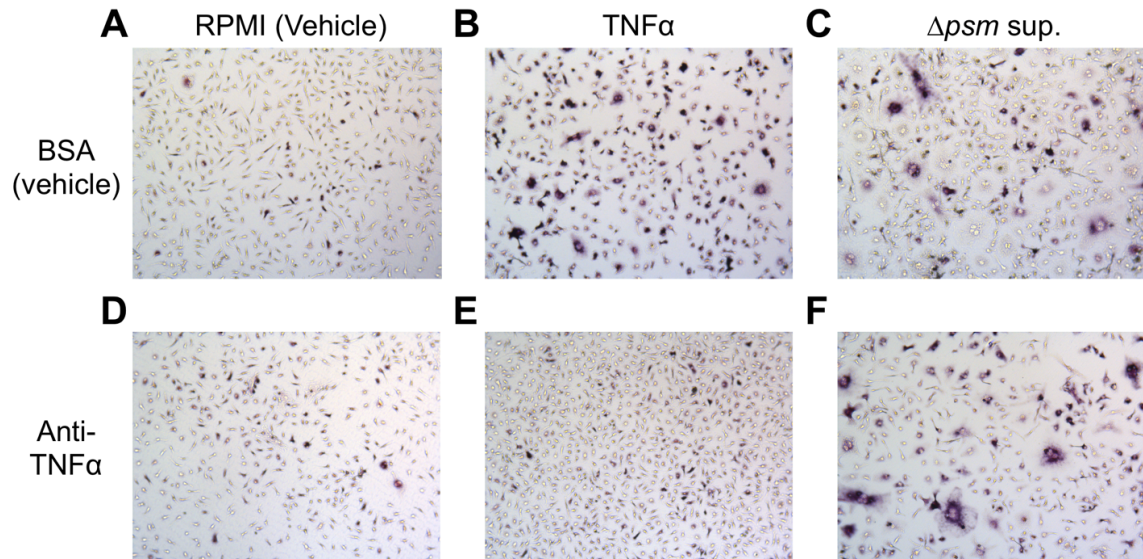
Figure 17. *S. aureus*-enhanced osteoclastogenesis is not dependent on TNFα.
(A-H) WT osteoclast precursors were generated with M-CSF and RANKL for 2 days in culture, washed with PBS, after which fresh media and M-CSF were replenished with BSA vehicle **(A-C)** or 4µg/mL Anti-TNFα antibody **(D-F)**, vehicle (RPMI; **A, D**), 10 ng/mL recombinant TNFα **(B, E)**, LAC∆*psm* supernatant **(C, F)**. Cells were TRAP stained at day 6 and imaged at 10X.
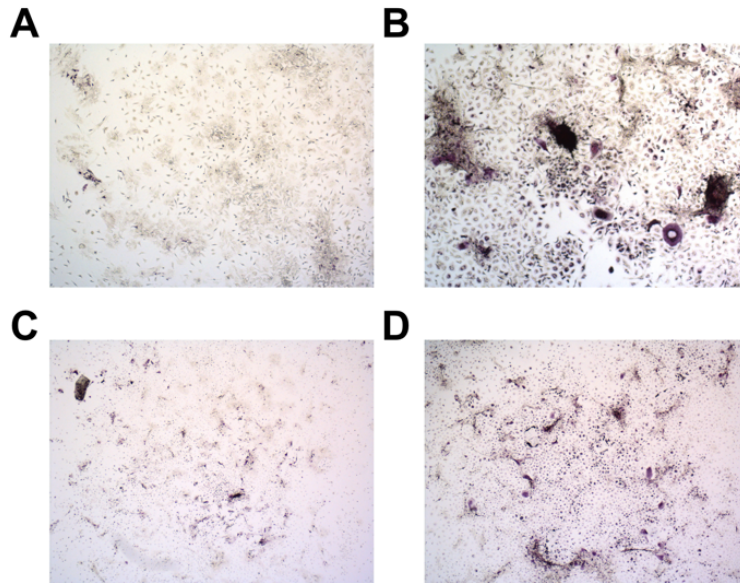
Figure 18. *S. aureus* can enhance osteoclastogenesis in a primary co-culture system.
(A-D) WT WBM was plated with 10 nM (1,25)-dihydroxy vitamin D_3 and half the media was changed every 2-3 days for 2 weeks. Cells were plated at 0.5 million cells per well in 96-well plates **(A, B)** or 3 million cells per well in 24-well plates **(C, D)**. When media was changed during the second week in culture, vehicle (**A, C**) or Δ*psm* supernatants **(B, D)** were added in culture at 5% (v/v) in 24-well plates and 2.5% volume/volume to cells in 96-well plates. At day 14 in culture, cells were TRAP stained and imaged at 4X.

BMMs and osteoclast precursors have overlapping and divergent immune responses in response to *S. aureus* stimulation

To further explore how stimulation with bacterial supernatants alters inflammatory gene expression, we conducted preliminary assays to compare inflammatory gene transcripts and cytokine production between BMMs and osteoclast precursors. Our rationale for this experiment was that bacterial stimulation might have different effects on monocyte lineage cells depending on their differentiation state during osteoclastogenesis. Such differences in inflammatory gene expression might indicate differences in the ability to serve as immune effector cells. Thus, we cultured BMMs or osteoclast precursors and stimulated both cell populations with *S. aureus* Δ*psm* supernatants to assess their capacity to promote inflammatory changes. We measured this inflammatory effect by looking at transcriptional changes in inflammatory genes encoding the cytokine TNFα or enzyme iNos. These factors are observed in various cell types, but increased values of both characterize polarization into the inflammatory "M1" macrophage lineage. As expected, *S. aureus*-stimulated BMMs have highly abundant levels of these transcripts in relation to vehicle stimulation **(Figure 19A and 19B)**. Furthermore, RANKL pre-commitment for 2 days does not completely ablate the ability of osteoclast precursors to upregulate inflammatory transcripts *Tnfsf1a* and *Nos2* compared to vehicle **(Figure 19A and 19B)**. These data indicate that *S. aureus* potently increases transcription of inflammatory components in both BMMs and pre-osteoclasts. These data also indicate that differentiation status may determine the extent of gene expression, but these experiments should be extended.
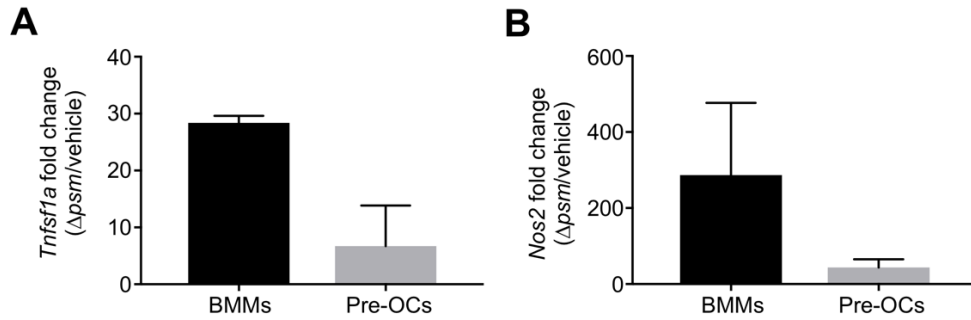
Figure 19. BMMs and osteoclast precursors upregulate inflammatory macrophage transcripts in response to *S. aureus* stimulation.

To determine transcript levels of *Tnfsf1a* **(A)** and *Nos2* **(B)** genes in WT BMMs and osteoclast precursors, BMMs and pre-osteoclasts (Pre-OCs) were stimulated with Δ*psm* supernatant or vehicle for 4 hours before pooling RNA from 15 wells in triplicate. qRT-PCR was performed using primers for the *B2m* housekeeping gene, *Tnfsf1a*, and *Nos2*. After correcting for expression relative to *B2m,* the fold change in transcript levels was calculated as Δ*psm* supernatant stimulation relative to vehicle for each cell type. Unpaired *t*-tests did not find statistical differences between *Tnfsf1a* fold changes ($p = 0.0513$) or *Nos2* fold changes ($p = 0.2144$).

Finally, to characterize the inflammatory output from BMMs and osteoclast precursors, we performed a cytokine profiling experiment. Cytokines were measured as they accumulated in the growth medium between 24-48 hours post-stimulation with vehicle or *S. aureus* Δ*psm* supernatant. BMMs and osteoclast precursors released significantly higher levels of IL-10, MIP-1α, MIP-1β, MIP-2, RANTES, and TNFα in response to *S. aureus* stimulation than when stimulated with vehicle **(Figure 20N, 20AA-EE)**. Within this group of cytokines, BMMs produced higher levels of MIP-1α and RANTES than osteoclast precursors **(Figure 20AA and 20DD)**, whereas osteoclast precursors produced more abundant levels of MCP-1 than BMMs **(Figure 20Y)**. Additionally, BMMs were also able produce significantly more IL-6 after *S. aureus* stimulation than vehicle stimulation **(Figure 20K)**, and osteoclast precursors showed significantly higher levels of G-CSF, IL-2, IL-5, KC, and MCP-1 when stimulated with *S. aureus* **(Figure 20B, 20G, 20J, 20U, 20Y)**. These data indicate that BMMs and osteoclast precursors retain some overlapping ability to respond to *S. aureus*, however, they also have distinct abilities to produce specific cytokines.
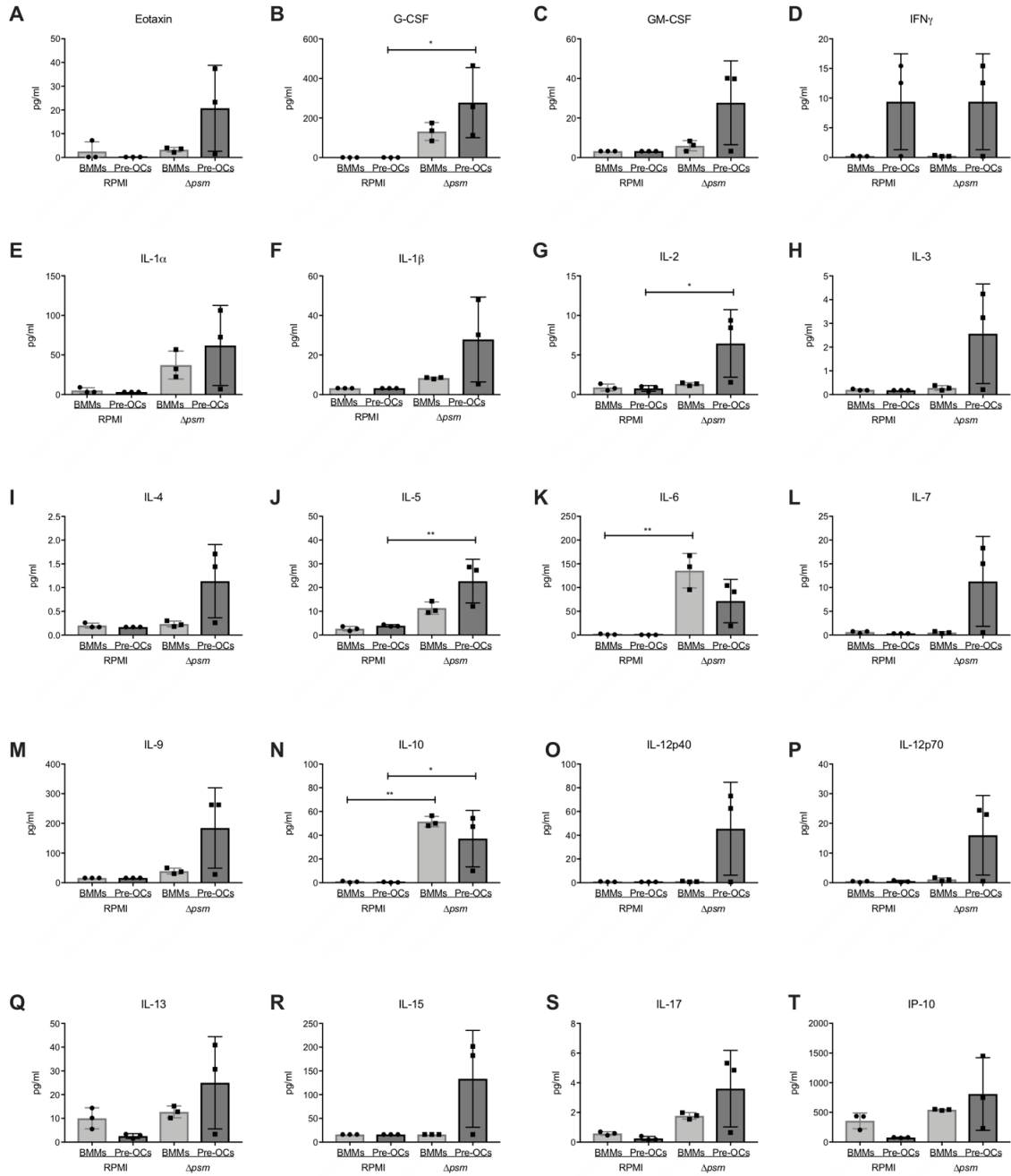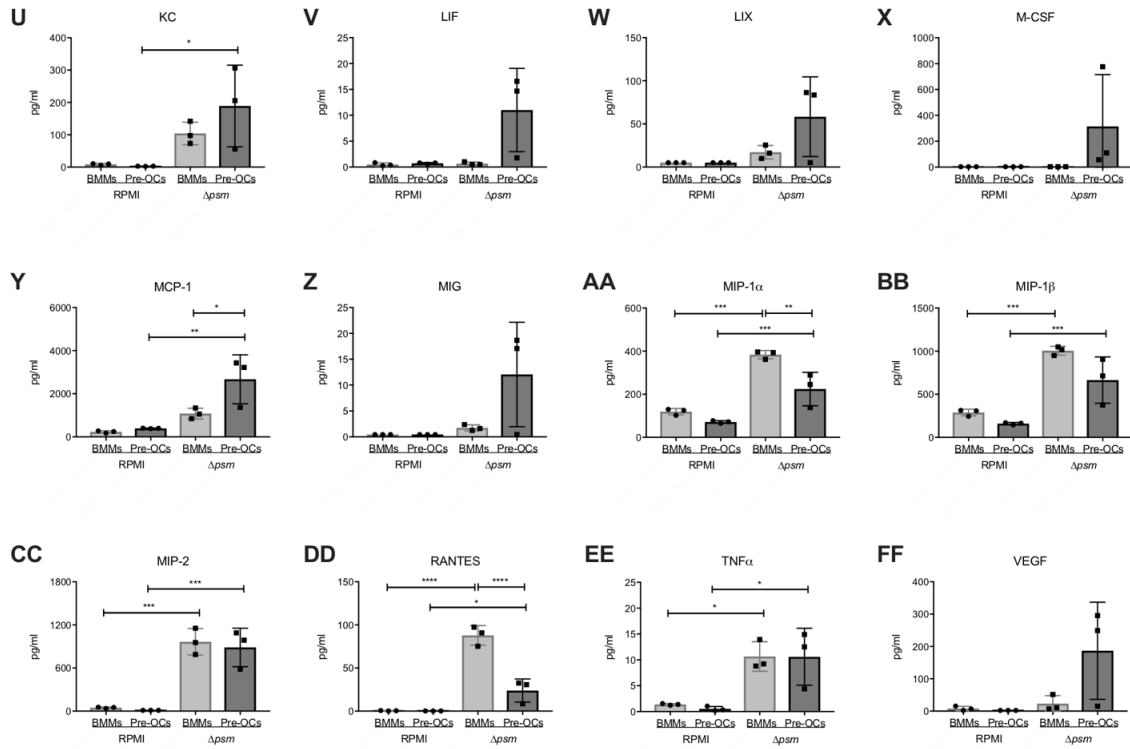
Figure 20. BMMs and Pre-OCs differentially produce select cytokines in response to _S. aureus_ stimulation.

(A-FF) WT BMMs and osteoclast precursors (Pre-OCs) were generated in 96-well plates by plating 50,000 BMMs and stimulating them with M-CSF with or without RANKL, respectively for 2 days. At this time, cells were stimulated with vehicle (RPMI) or Δ*psm* supernatants for 24 hours. At 24 hours post-stimulation, cells were washed with PBS and fresh media with M-CSF was replenished to allow stimulated cells to continue to produce cytokines in media. 24hrs after the media change, supernatants from each well were collected and frozen at -80ºC until they were thawed and analyzed on the Luminex platform. Cytokine levels were compared between groups using a one-way ANOVA and Sidak's multiple comparisons test for comparison made between cell type and stimulation within a cytokine. * $p < 0.05$, ** $p < 0.01$, *** $p < 0.001$, **** $p < 0.0001$.

Discussion

The complex signaling cascades that converge to allow myeloid cells to differentiate into osteoclasts have been characterized over decades of work [247]. Classically, RANKL signals through the RANK receptor of myeloid cells to drive osteoclast differentiation [15]. Osteoclast differentiation also requires activation of transcription factors for canonical and non-canonical NFκB, AP-1, and the major transcriptional regulator NFATc1, among others [25-27, 233]. In our work, we have found that stimulation of the RAW264.7 murine monocyte/macrophage cell line with concentrated staphylococcal supernatants, *S. aureus* cell wall fractions, and TLR agonists can drive osteoclast differentiation without the addition of exogenous RANKL. Furthermore, we confirmed that many of the stimulatory conditions that induce osteoclastogenesis *in vitro* also lead to early NFκB activation, and a sustained increase in proliferation of these monocytes suggest that these stimuli elicit functional changes following NFκB activation.

While informative, these early experiments require cautious interpretation of the results because they were performed with cell lines. Although these cells bypass the requirement for exogenous RANKL to form TRAP$^+$ multinucleated cells, this occurrence is likely an artifact of using an immortalized cell line. In order to increase the rigor of these studies, we fine-tuned *in vitro* osteoclastogenesis assays using primary cell cultures. This step was critical, as primary cells require viability signals through c-FMS receptor by M-CSF and osteoclast differentiation in culture requires signaling through the RANK receptor, by RANKL.

Years of contradictory findings have clouded the interpretation on how bacterial stimulation perturbs osteoclast differentiation. In regards to *S. aureus*, reports on osteoclastogenic effects are unclear due to the use of various culture models and stimulation methods [25, 140, 240-242, 247-250]. The goal of these studies was to provide clarity on the mechanism by which bacterial stimuli alter osteoclastogenesis using primary skeletal cells and a clinically relevant strain of *S. aureus*. We used an isolate of *S. aureus* (LAC, a USA300-type strain) that represents the most common lineage causing bone infections, which may help clarify previous studies using laboratory strains. To avoid toxin-mediated cell death, cells were stimulated with PSM-deficient *S. aureus* supernatants.

The hypothesis that overlapping immune and skeletal cell signaling pathways perturb osteoclastogenesis was tested with two assays. We hypothesized that different outcomes would occur based on the sequence of stimulation with bacterial supernatant or RANKL. To test this hypothesis, we pre-committed cells with 2 days of RANKL before stimulating with *S. aureus* supernatants, or conversely, stimulated myeloid cells with *S. aureus* before supplementing with RANKL for 5 days to allow cells sufficient time to undergo osteoclast differentiation. Our findings indicate that indeed, *S. aureus* is able to enhance *and* impede osteoclastogenesis, but the effects are solely dependent on the timing of stimuli. Other papers have characterized that these opposing phenotypes are time-dependent using purified TLR agonists [55]. We are thus able to expand on these findings through providing bacterial supernatants from a clinically relevant *S. aureus* strain, the most common causative agent of bacterial osteomyelitis [251]. When myeloid cells are

first stimulated with the canonical differentiation factor RANKL, *S. aureus* alone is able to push these cells to continue down the osteoclast differentiation pathway [25, 240].

Positive regulation of osteoclastogenesis can also occur through indirect alteration of osteoblast function or due to cytokines that signal onto skeletal cells in an autocrine or paracrine manner [236]. Cytokines IL-1 and TNFα favor osteoclast differentiation indirectly through an increase of the RANKL/OPG ratio [155, 236, 252]. In addition to IL-1 and TNFα, the cytokines IL-6, IL-11, IL-15, and IL-17 have been identified as "pro-osteoclastogenic" and function to stimulate bone resorption [180, 237]. These cytokines can directly alter osteoclastogenic potential of pre-osteoclasts by enhancing their ability to undergo differentiation [141, 144], promoting cell-cell fusion [253], increasing osteoclast survival [242, 253], promoting intracellular signaling (TRAF6, PLC-γ) [254], activating osteoclastogenic transcription factors, and enhancing receptor (RANK, c-Fms) expression. As RANKL is a TNF-family cytokine, there are an abundance of studies focusing on the ability of TNFα to enhance osteoclastogenesis [69, 141, 142, 144, 246, 255-258]. Our results confirm that TNFα enhances osteoclastogenesis from primary osteoclast precursors *in vitro*. To test whether *S. aureus*-enhanced osteoclastogenesis is due to paracrine effects of TNFα production, we used an anti-TNFα antibody in our assays. Here we show that anti-TNFα does not inhibit the ability of *S. aureus* to enhance osteoclast differentiation from precursors. Furthermore, anti-RANKL treatment confirmed that RANKL signaling on primary cells is necessary for *S. aureus*-mediated osteoclastogenesis.

In contrast, when myeloid cells are first stimulated with *S. aureus* supernatants for just 24 hours before being provided RANKL, their ability to differentiate into osteoclasts is inhibited, which may recapitulate scenarios where osteoclastogenesis is negatively

regulated [248-250]. In addition to OPG, early IL-10 and GM-CSF signaling can prevent the development of osteoclast precursor cells, and several "anti-osteoclastogenic" cytokines can prevent osteoclast differentiation, including IL-4, IL-13, IL-27, and type I and II interferons [249]. Negative regulation of osteoclastogenesis can also occur through decreased receptor expression (RANK, c-Fms, OSCAR, TREM2), decreased RANKL and M-CSF production, suppression of intracellular signaling, increased anti-osteoclastogenic transcription factors, or increased OPG levels [249]. From our BMM cytokine levels, the increase in abundance of IL-10 may be responsible for the *in vitro* inhibition of osteoclastogenesis following BMM stimulation with Δ*psm* supernatants. IL-10 has been shown to suppress the early commitment of myeloid precursors into osteoclast precursors through inhibition of NFATc1, c-Fos, and c-Jun expression [151, 152]. However, it is also possible that quantification of cytokines from supernatants produced between 24-48 hours post-stimulation excluded the detection of important cytokines produced by BMMs and osteoclast precursors in the first 24 hours.

The unique cellular milieu present in bone marrow means that *S. aureus* infection results in the juxtaposition of bacteria, myeloid and lymphoid precursors, and skeletal cells. In order to test whether we can recapitulate *S. aureus*-enhanced osteoclastogenesis in a more complex culture system, we developed a WBM co-culture assay in which vitamin D$_3$ supplementation drives osteoblast-lineage cells to produce factors necessary for skeletal cell viability *in vitro*, as well as RANKL to mediate osteoclast formation. Here, we support our monoculture findings to show that *S. aureus* leads to enhanced osteoclastogenesis in a co-culture system. These results provide the context that *in vivo*, where skeletal cells are

81

continuously remodeling bone, the reservoir of osteoclast precursors represent a pool of cells that can be subject to enhanced osteoclastogenesis and ultimately trigger bone loss.

Finally, our findings that reciprocal stimulation of RANKL and *S. aureus* Δ*psm* supernatants conversely influence cell fate decisions on osteoclast differentiation *in vitro* led us to then inquire as to how macrophage and osteoclast precursor populations vary in their production of immune transcripts and cytokines. We found that in response to *S. aureus* supernatants, both BMMs and osteoclast precursors expressed mRNA transcripts *Tnfsf1a* and *Nos2* that are characteristic of M1 inflammatory macrophages. Although there was no statistical difference between the fold-changes relative to vehicle treatment, the difference in magnitude between BMMs and osteoclast precursors was large enough to provide the rationale that BMMs and osteoclast precursors may have intrinsically different capacities to respond to inflammatory stimuli. Future studies should investigate how myeloid lineage cells, including BMMs, osteoclast precursors, and mature osteoclasts, vary in their ability to mount immune transcripts indicative of anti-bacterial immune responses.

To begin to address how the cytokine and chemokine responses of BMMs and pre-osteoclasts differ to *S. aureus* stimulation, we measured inflammatory analytes in culture supernatants in response to vehicle or Δ*psm* supernatants. However, *S. aureus* produces antibody-binding proteins that might confound cytokine detection kits that are antibody-based. To avoid any false-positive signals, we stimulated cells for 24 hours, washed the supernatants from the cells, and allowed cells to produce cytokines in the media between 24-48 hours. Therefore, the cytokine measurements do not represent the immediate cytokines released between stimulation and 24 hours, but rather represent sustained release kinetics into day 2 post-stimulation. Interestingly, we found that BMMs and pre-osteoclasts

maintain some overlap in their cytokine production, with both cell types releasing IL-10, MIP-1α, MIP-1β, MIP-2, RANTES, and TNFα. Relative to vehicle control, BMMs also produced significantly higher levels of IL-6 when exposed to *S. aureus*, whereas osteoclast precursors treated with Δ*psm* supernant produced higher levels of G-CSF, IL-2, IL-6, KC, and MCP-1. These data suggest that while some common cytokines are produced by BMMs and osteoclast precursors in response to *S. aureus* stimulation, just 2 days of RANKL pre-commitment allows their immune responses to diverge. Although these data are preliminary, they provide foundational knowledge to support the interrogation into how osteoclast lineage cells undergoing differentiation vary in their capacity to mount anti-staphylococcal immune responses.

Data in this chapter clarify some of the discrepancies surrounding how bacterial stimulation perturbs osteoclastogenesis. We confirmed that many Gram-positive bacterial components influence osteoclast differentiation in myeloid lineage cells. *In vitro* osteoclastogenesis assays allowed us to show that osteoclast enhancement can only occur robustly once cells have been pre-committed to the osteoclast lineage with RANKL. Conversely, the ability of *S. aureus* to inhibit osteoclastogenesis from RANKL-naïve cells suggests that myeloid lineage cells undergo cell fate decisions that influence their capacity to differentiate. Accordingly, the ability of BMMs and osteoclast precursors to mount immune responses varied, as measured by *Tnfsf1a* and *Nos2* transcripts and cytokine production. Moreover, while osteoclastogenesis can be enhanced by TNFα, it does not appear that osteoclast enhancement downstream of *S. aureus* is due to the paracrine effect of TNFα in culture. To expand on these findings, the roles of MyD88, IL-1 cytokines and

the IL-1R, and *S. aureus* sensing TLR2 and TLR9 on antibacterial immunity and osteoclast-driven bone loss are investigated in the following chapters.

A version of the following section (*Chapter III,* MyD88 and IL-1R signaling mediate antibacterial immunity and osteoclast-driven bone loss during *Staphylococcus aureus* osteomyelitis) was originally published in *PLoS Pathogens* (April 2019).

CHAPTER III

MyD88 AND IL-1R SIGNALING MEDIATE ANTIBACTERIAL IMMUNITY AND OSTEOCLAST-DRIVEN BONE LOSS DURING *STAPHYLOCOCCUS AUREUS* OSTEOMYELITIS

Introduction

Osteomyelitis, or inflammation of bone, is most commonly caused by invasive bacterial infection [251]. *S. aureus* is the most frequently isolated etiologic agent of both acute and chronic bacterial osteomyelitis [10, 259]. *S. aureus* can colonize bone through hematogenous dissemination, contamination of bone following surgical or accidental trauma, or direct spread from a surrounding soft tissue infection [10, 260]. Bone represents a unique niche for invading bacterial pathogens as it is constantly undergoing turnover by bone-forming osteoblasts and bone-resorbing osteoclasts. Bone also represents an important immunological niche, as bone marrow houses hematopoietic stem cells that give rise to lymphocytes and myeloid cells [180]. Bone infections rarely resolve without medical intervention, and are difficult to treat due to the widespread antimicrobial resistance of *S. aureus* as well as induction of bone damage that effectively limits antibiotic delivery and immune cell influx [10, 259].

Osteomyelitis elicits pathologic bone remodeling, which, in addition to contributing to treatment failure, can enhance the likelihood of complications such as pathologic fractures [10, 31, 32, 40, 61, 79, 80]. In order to explore mechanisms of bone loss during osteomyelitis, we previously established a murine model of post-traumatic osteomyelitis [31]. Using this model, we found that pore-forming PSMα toxins mediate

approximately 30% of the bone loss observed in our murine model of osteomyelitis, with direct cytolytic effects on bone-forming osteoblasts [31, 32]. Thus, the majority of bone loss still ensued even with the toxin-deficient strain. These findings indicate that while bacterial factors directly contribute to bone damage, a substantial proportion of bone loss during osteomyelitis may be caused by host factors [37].

To maintain skeletal strength and structure, bone must be continuously remodeled by bone-forming osteoblasts and bone-resorbing osteoclasts [15, 16]. Bone remodeling occurs as a part of normal vertebrate physiology, but the kinetics of bone remodeling can be substantially altered in response to local and systemic inflammation [235]. Osteomyelitis, in particular, is associated with abundant levels of pro-inflammatory cytokines such as TNFα, IL-1β, and IL-6 [60, 180]. These pro-inflammatory cytokines promote skeletal cell differentiation *in vitro*, both directly by stimulating bone-resorbing osteoclasts and indirectly by promoting osteoblast production of RANKL to drive osteoclastogenesis [51, 235, 236]. IL-1 in particular was formerly referred to as "osteoclast activating factor," reflecting the ability of IL-1α and IL-1β to signal on osteoclast lineage cells to increase osteoclast viability and resorptive capacity [134, 136, 140, 242, 261, 262]. Through these mechanisms, pro-inflammatory cytokines contribute to bone loss *in vivo* in non-infectious models of rheumatoid arthritis [14, 236, 263], although less is known about their influence on bone loss during osteomyelitis. These observations led us to hypothesize that *S. aureus* osteomyelitis triggers enhanced bone loss through pro-inflammatory cytokine production and signaling.

IL-1 cytokines signal downstream of the IL-1R through the adapter protein MyD88, which also transduces signals from various Toll-like receptors (TLRs) after ligation by

conserved microbial motifs known as pathogen-associated molecular patterns (PAMPs). Thus, MyD88 is a critical component of the innate immune system, by relaying signals through the IL-1R and many TLRs. Prior research has highlighted a prominent role for MyD88 and IL-1R signaling in the activation of immune responses that are necessary to control *S. aureus* infection in other animal models of infection [76, 77, 199, 264-269]. In part, this occurs through the ability of IL-1 to mediate neutrophil recruitment and promote proper abscess formation for containment of *S. aureus* [77, 199]. Moreover, IL-1 plays a critical role in potentiating granulopoiesis, which occurs primarily in the bone marrow [270, 271]. The expansion and recruitment of granulocytes, such as neutrophils, are regulated in part by an IL-1R-dependent mechanism by which IL-1 signals onto endothelial cells in the bone marrow to release G-CSF [272-274]. Thus, MyD88 and the IL-1R form a critical signaling cascade that is necessary to mount an effective immune response to invading pathogens.

Importantly, osteoblasts and osteoclasts express innate immune receptors through which these cells sense and respond to PAMPs and inflammatory cytokines in cell culture [263]. Given the important role of IL-1 in anti-staphylococcal immunity, as well as compelling evidence demonstrating that IL-1 signaling impacts bone cells *in vitro, we hypothesized that MyD88 and IL-1R signaling are required for efficient antibacterial immune responses during osteomyelitis, but paradoxically may also promote pathologic bone loss*. To test this hypothesis, we used a murine model of *S. aureus* osteomyelitis, high resolution imaging, histologic analyses, and *in vitro* skeletal cell assays. We show that IL-1 is abundantly produced in bone in response to *S. aureus* infection, and that MyD88 and IL-1R signaling are required to limit staphylococcal burdens during osteomyelitis.

Furthermore, *S. aureus* incites bone loss *in vivo* through an IL-1R-mediated increase in osteoclastogenesis. Our findings reveal that while MyD88 and IL-1R signaling are necessary for antibacterial responses in bone, they also contribute to *S. aureus*-stimulated osteoclastogenesis and host-mediated bone loss during osteomyelitis.

Materials and methods

Ethics section

All experiments involving animals were reviewed and approved by the Institutional Animal Care and Use Committee at Vanderbilt University Medical Center on the animal protocols M12059 and M1800055. All experiments were performed according to NIH guidelines, the Animal Welfare Act, and US Federal law. The murine model of osteomyelitis required inhalational anesthesia with isoflurane (1–5%). Post-operative analgesia (buprenorphine 0.5–0.1 mg/kg) was provided pre-operatively and every 8–12 hours for 48 hours post-infection. Mice were euthanized by CO_2 asphyxiation with secondary confirmation by cervical dislocation and observation of heart rate and breathing.

Animal use

C57BL/6J (Stock #: 000664), *Myd88$^{-/-}$* (Stock #: 009088), and *Il1r1$^{-/-}$* (Stock #: 003245) mice were purchased through The Jackson Laboratory. *Il1a$^{-/-}$* and *Il1b$^{-/-}$* mice were generated as described [275]. WT mice were bred with *Myd88$^{-/-}$* or *Il1r1$^{-/-}$* mice to produce *Myd88$^{+/-}$* or *Il1r1$^{+/-}$* mice, respectively. Heterozygous mice were bred together to create mice carrying knockout (-/-), heterozygous (+/-), or wild-type (+/+) alleles for *Myd88* or *Il1r1*. Heterozygous breeding was done to reduce the confounding influence of microbiome

effects associated with genotypes and maintenance of separate mouse colonies. Resulting littermates were earpunched and genotyped through Transnetyx, Inc. (Cordova, TN).

Bacterial strain and growth conditions

All infections were conducted with an erythromycin-sensitive derivative the USA300 type *S. aureus* LAC clinical isolate (AH1263) [243]. The toxin-deficient strain LAC$\Delta psm\alpha1$-4 (Δpsm) has been previously described and was used for *in vitro* assays to prevent cell death [31, 244]. Bacteria were routinely grown on tryptic soy agar (TSA) or shaking in tryptic soy broth (TSB) with or without 10 µg/mL erythromycin as detailed previously [31]. To prepare concentrated supernatants, Δpsm was grown overnight in RPMI supplemented with 1% casamino acids [32].

Post-traumatic osteomyelitis infection

The murine model of osteomyelitis was performed as described previously [31, 32]. AH1263 was sub-cultured from an overnight culture, grown for 3 hours, and then adjusted in PBS to a concentration of approximately 1×10^6 CFUs in 2 µL PBS, unless diluted 1:10 or 1:100 to deliver inoculum doses of 1×10^5 or 1×10^4 CFUs, respectively. Osteomyelitis was induced in 5- to 8-week old male and female mice following the introduction of a unicortical bone defect using a 21G needle, into which 2 µL of bacterial suspension or PBS (mock infection) was injected into the intermedullary canal. Muscle fascia and skin were closed with sutures and mice were given buprenorphine analgesic every 12 hours for 48 hours, with daily monitoring until the experimental end point. Mice were euthanized if they

met human endpoints, including inability to ambulate, inability to eat or drink, loss of greater than 20% body weight, and/or hunched posture.

Micro-computed tomography (µCT) of cortical and trabecular bone

Femurs were harvested 14 days post-infection and fixed for 48 hours in neutral buffered formalin at 4°C. Bones were scanned using a µCT50 (Scanco Medical, Switzerland) and analyzed with µCT Tomography V6.3-4 software (Scanco USA, Inc., Wayne, PA). To expand previous µCT50 analyses that assessed only the cortical bone of the femoral diaphysis [31], here the diaphysis and distal epiphysis of each femur were visualized in the scout-view radiographs and imaged with 10.0 µm voxel size at 70 kV, 200 µA, and an integration time of 350 ms in a 10.24 mm view. Each imaging scan resulted in 1088 slices (10.88 mm) of the femur that included the diaphysis surrounding the inoculation site, trabecular bone in the distal femur, and excluded the proximal epiphysis. Three-dimensional volumetric analyses were conducted by contouring transverse image slices in the region of interest. The diaphysis of each femur was comprised of 818 image slices. These image slices were used to quantify cortical bone destruction (mm^3) and reactive bone formation (mm^3) surrounding the cortical bone inoculation site as described previously [31]. Trabecular bone measurements were obtained in the distal femur by advancing proximally past the growth plate 30 slices. 101 slices were analyzed with an inclusive contour drawn along the endosteal surface to include trabeculae and exclude the cortical bone. Trabecular bone volume per total volume (%), trabecular number (1/mm), trabecular thickness (mm), and trabecular spacing (mm) were determined by segmentation of the image with a lower threshold of 329 mg HA/ccm, sigma 1.3, and support 1.

Bone histology and histomorphometric analysis of osteoclasts in trabecular bone

After µCT imaging, femurs were decalcified for three days in 20% EDTA at 4°C. Decalcified bones were processed and embedded in paraffin before sectioning at 4µm thickness through the infectious nidus and bone marrow cavity using a Leica RM2255 microtome. Sectioned femurs were stained with a modified hematoxylin and eosin (H&E) that included orange G and phloxine for enhanced bone contrast, tartrate-resistant acid phosphatase (TRAP) stain with hematoxylin counterstain, or 3,3'-diaminobenzidine (DAB) immunohistochemistry to detect myeloperoxidase (MPO). OsteoMeasure software (OsteoMetrics, Inc., Decatur, GA) was used to manually analyze TRAP-stained histologic sections at a region of interest encompassing the trabeculae proximal to the growth plate in the distal femur. Osteoclast number, osteoclast surface, and bone perimeter were calculated and reported per ASBMR standards [276]. A Leica SCN400 Slide Scanner was used to scan stained femur sections in brightfield at 20X. Images were uploaded to and imaged with the Digital Imaging Hub (Leica Biosystems, Buffalo Grove, IL) and Tissue Image Analysis 2.0 (Tissue IA 2.0) (Leica Microsystems, Buffalo Grove, IL) was used to analyze callus area of infected femurs at 20X.

Determination of bone formation rate with double calcein labeling

WT and $Il1r1^{-/-}$ mice were intraperitoneally injected with 20 mg/kg calcein on days 8 and 12 post-infection with 10^5 CFUs. Femurs were subsequently harvested, formalin fixed, and dehydrated prior to embedding in poly(methyl methacrylate) for sectioning, and counterstained with toluidine blue. Fluorescent labels were identified as single- or double-labeled surface. Fluorescent labels and trabecular bone were traced in the distal femur using

OsteoMeasure software, and the mineralizing surface per bone surface (MS/BS), mineral apposition rate (MAR), and bone formation rate per bone surface (BFR/BS) were calculated per ASBMR standards [276].

CFU enumeration

At various time points post-infection, tissues were harvested and homogenized using a BulletBlender and NAVY lysis tubes (Next Advance, Inc., Averill Park, NY) at 4°C. To enumerate bacterial CFUs in infected femurs, the whole femur or only the regions encompassing the trabecular bone (i.e. metaphyses and epiphyses) were homogenized in PBS. To maximize cytokine signals in femur homogenates, CelLytic Buffer MT Cell Lysis Reagent (Sigma, Saint Louis, MO) was substituted for PBS to specifically lyse mammalian cells. Livers and kidneys were homogenized in PBS. Femur and organ homogenates were vortexed, serially diluted in PBS, and plated on TSA for bacterial enumeration. Femur homogenates lysed in CelLytic Buffer MT and PBS showed no difference in recoverable bacterial burdens.

Multiplexed cytokine detection

Following homogenization, femur homogenates were centrifuged at 4000 x g for 5 minutes to remove debris and the supernatant was stored at -80°C for subsequent analysis using Milliplex MAP multiplex magnetic bead-based antibody detection kits (EMD Millipore, Billerica, MA) according to the manufacturer's protocols. Cytokine quantification from bone homogenates was performed using the 32-plex Mouse

Cytokine/Chemokine Magnetic Bead Panel (MCYTMAG-70K-PX32) on the FLEXMAP 3D instrument. The quality controls for IL-13 failed, and these data were excluded.

Cytokine levels from femurs homogenized in 500 µL volume were read as pg/mL. Femur homogenates reported as relative values were homogenized in PBS, whereas cytokines values corrected for total protein were homogenized in CelLytic Buffer to maximize cytokine signals. Total protein (mg/mL) was quantified using the Pierce BCA Protein Assay Kit (ThermoFisher Scientific, Waltham, MA) per manufacturer's directions. Infected $Il1r1^{-/-}$ femurs were up to two times larger than WT infected femurs and four times larger than mock infected WT and $Il1r1^{-/-}$ femurs. Cytokine levels are therefore reported as pg cytokine/mg protein to control for femur size differences between infected $Il1r1^{-/-}$ and WT femurs.

Flow cytometry

Following *S. aureus* infection (10^5 CFUs), femurs from WT and $Il1r1^{-/-}$ mice were harvested at 1, 3, 5, and 14 days post-infection. Whole bone marrow (WBM) was flushed through a 70 µm nylon cell strainer (Falcon, Corning, New York) and red blood cells (RBCs) were lysed using the Ammonium Chloride Potassium (ACK) Lysing Buffer (Lonza, Walkersville, MD). Bone marrow (BM) mononuclear cells were counted and 1 million cells were plated per well and washed in PBS supplemented with 3% FBS and 0.1% sodium azide (FACS buffer). Cells were incubated with Anti-CD16/CD32 (Biolegend, 1:100, clone 93, San Diego, CA) to block non-specific antibody staining. Cells were then incubated with a mixture of murine-specific cell surface antibodies on ice, including Anti-Ly6G-PE (Biolegend, 1:3200, clone 1A8), Anti-Ly6C-PE-Dazzle 594

(Biolegend, 1:1600, clone HK1.4), Anti-CD68-PE-Cy7 (Biolegend, 1:100, clone FA-11), Anti-CD11b-APC (Tonbo 1:4800, clone M1/70, San Diego, CA), and Anti-CD45-AlexaFluor 700 (Biolegend, 1:400, clone 30-F11). Cells were washed two times in FACS buffer, resuspended in 2% paraformaldehyde solution, and run on a 3-laser BD LSRII flow cytometer the following day. Single BM cells were identified from successive gates, including side scatter-area by forward scatter-area (SSC-A x FSC-A), forward scatter area by height (FSC-A x FSC-H), and side scatter area by height (SSC-A x SSC-H). Next, $CD45^+$ cells, $CD11b^+$ cells, and $Ly6G^+LyC^{lo}$ cells (neutrophils) were gated sequentially.

Osteoclastogenesis assays

WBM was flushed from femurs of 8- to 13-week old male mice using α-MEM media. Following RBC lysis, WBM was resuspended in a 90% FBS and 10% DMSO solution and frozen in liquid nitrogen until thawed for use. BMMs were enriched by plating 8 to 13 million cells per 10 cm dish in α-MEM, 10% FBS, 1X Penicillin/Streptomycin (P/S), and 100 ng/mL recombinant murine M-CSF (R&D Systems, Minneapolis, MN, 416-ML) for 4 days. Non-adherent cells were removed and adherent cells were washed with PBS, scraped into fresh media, and counted prior to plating. Enriched BMMs were plated at a density of 50,000 cells/well in 96-well plates, and media (α-MEM, 10% FBS, 1X P/S) was supplemented 1:20 with CMG14-12 as an M-CSF source [28]. Osteoclastogenesis assays were performed with RANKL-primed osteoclast precursors, which were generated by plating BMMs in 35 ng/mL recombinant murine RANKL (R&D Systems, Minneapolis, MN, 462-TR) for 2 days. Prior to stimulation, RANKL-primed osteoclast precursors (WT, *Myd88*$^{-/-}$, *Il1r1*$^{-/-}$, *Il1a*$^{-/-}$, and *Il1b*$^{-/-}$) were washed twice with PBS. RANKL-primed

osteoclast precursors were stimulated with either a vehicle control (1% casamino acid-supplemented RPMI) or Δ*psm* supernatant. M-CSF was supplemented into the media containing each stimulation. To confirm the proposed role of IL-1β (R&D Systems, Minneapolis, MN, 410-ML) on osteoclastogenesis, 10 ng/mL IL-1β was added to RANKL pre-committed osteoclast precursors.

To test the specific role of IL-1R inhibition on *S. aureus*-enhanced osteoclast differentiation, osteoclastogenesis assays in WT and *Il1r1*$^{-/-}$ cells were conducted with the addition of a vehicle control (0.1% low endotoxin BSA) or 1 µg/mL recombinant murine IL-1ra (Novus Biologicals, LLC, Littleton, CO, NBP2-35105) during the 2 days of RANKL pre-commitment or during the 4 days of Δ*psm* supernatant stimulation. On day 6 in culture, all RPMI- and *S. aureus*-stimulated osteoclastogenesis assays were fixed with a 4% formaldehyde and 0.05% Triton X-100 solution in PBS (10 minutes) and 1:1 acetone:ethanol (1 minute), before TRAP staining with reagents from the Acid Phosphatase, Leukocyte (TRAP) Kit (Sigma, Saint Louis, MO, 378A). In control osteoclastogenesis assays without *S. aureus* supernatant stimulation, cells were stimulated at the time of plating with 1:20 CMG14-12 and 35ng/mL RANKL. Fresh media, CMG14-12, and RANKL were replenished on days 4 and 6 in culture, with cells TRAP stained on day 7. TRAP$^+$ multinucleated cells were counted manually at 10X, with OsteoMeasure software (OsteoMetrics, Inc., Decatur, GA) or the FIJI Cell Counter Plugin.

Statistical analysis

Data analysis and statistical tests were conducted using Graph Pad Prism software. Unpaired *t*-tests were used to compare CFU burdens, measurements of bone architecture

using μCT and histology, cytokine levels, neutrophil abundance, and TRAP[+] multinucleated cell counts when two groups were being compared. Log-rank Mantel Cox tests compared survival curves between genotypes for each *S. aureus* inoculum. A one-way ANOVA with Tukey's multiple comparison test compared CFU burdens from femurs between multiple genotypes. A two-way ANOVA was used with Fisher's Least Significant Difference (LSD) test to compare the effects of genotype and infection status between histomorphometry measurements. A repeated measures two-way ANOVA with Tukey's multiple comparisons test was used to compare TRAP[+] multinucleated cell counts between genotype at each Δ*psm* supernatant dose. Repeated measures two-way ANOVAs with Dunnett's multiple comparisons test were conducted on TRAP[+] cell counts from each genotype, to compare Δ*psm* supernatant dosage effects. A three-way ANOVA with Tukey's multiple comparisons test was used to compare cell genotype, IL-1ra pre-treatment, and IL-1ra treatment alongside Δ*psm* supernatant stimulation. *P* values of less than 0.05 were considered statistically significant. Details on number of data points, experimental replicates, calculated standard deviation, and statistical significance for each experiment are described in figure legends.

Results

S. aureus osteomyelitis alters cortical and trabecular bone remodeling

To determine changes in bone remodeling that occur during osteomyelitis, we compared architectural bone parameters between infected and mock infected wild-type (WT) C57BL/6J mice in a post-traumatic model of *S. aureus* bone infection [31]. We focused our analyses on two distinct anatomical sites of the infected femurs representing

the two major architectural types of bone: cortical bone that comprises the mid-region (diaphysis) of the long bone and trabecular bone found in the distal femur (metaphysis and epiphysis) **(Figure 21A-C)**. We previously observed that mock infected WT mice display a rapid cortical bone healing response at the surgical site, in which the induced bone defect in the femoral diaphysis is replaced with new bone by 2 weeks post-surgery [31]. In contrast to this sterile cortical bone repair, mice infected with *S. aureus* develop osteomyelitis, are unable to restore the cortical bone defect, and experience extensive cortical bone loss surrounding the site of inoculation **(Figure 22A and 22B)**. Moreover, *S. aureus* infected femurs show reactive cortical bone formation surrounding the site of inoculation **(Figure 22C)** [31].
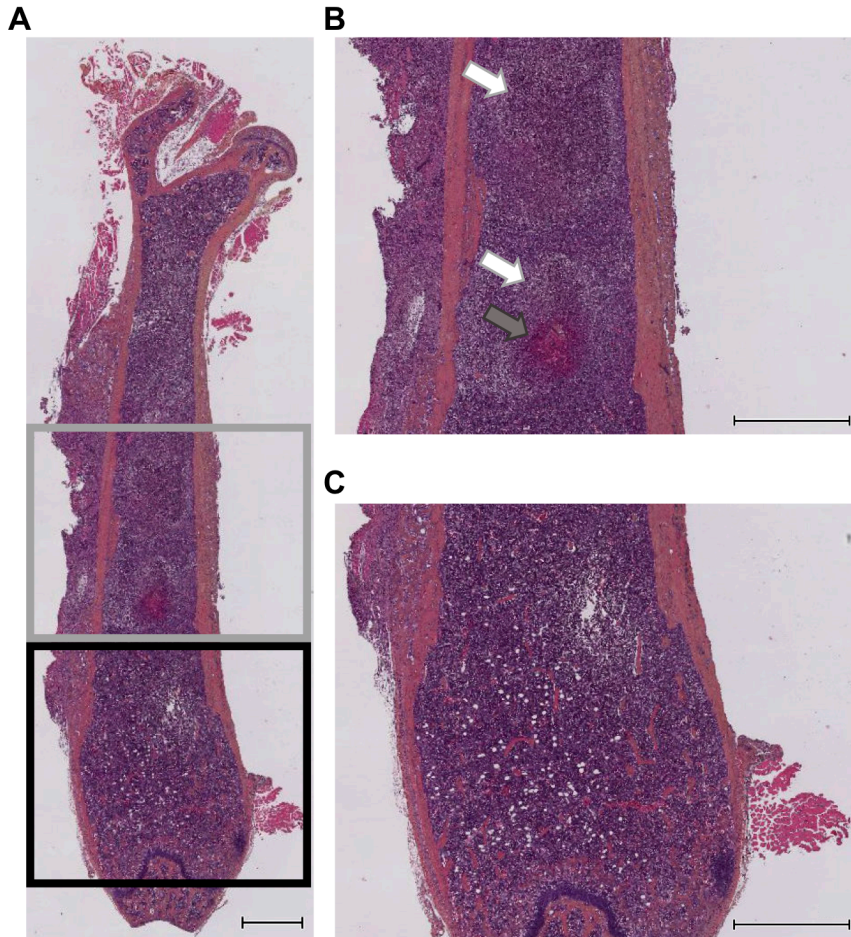
Figure 21. Cortical and trabecular bone architecture of *S. aureus* infected femurs via histology. (A-C) Femurs were harvested from female WT mice (*n* = 5) 14 days after *S. aureus* infection (10^6 CFUs). Representative modified H&E section of an infected female WT femur, imaged at 0.58X (scale bar = 1mm) **(A)** shown with a grey box surrounds the central portion of the diaphysis and the extent of abscess formation, and a black box surrounds trabecular bone in the distal femur, or imaged at 1.28X (scale bar = 1 mm) **(B, C)**. **(B)** Diaphysis and medullary cavity as outlined in the grey box, showing abscesses as indicated by white arrows and a *S. aureus* microcolony by a grey arrow. **(C)** Distal femur containing trabecular bone as outlined in the black box.
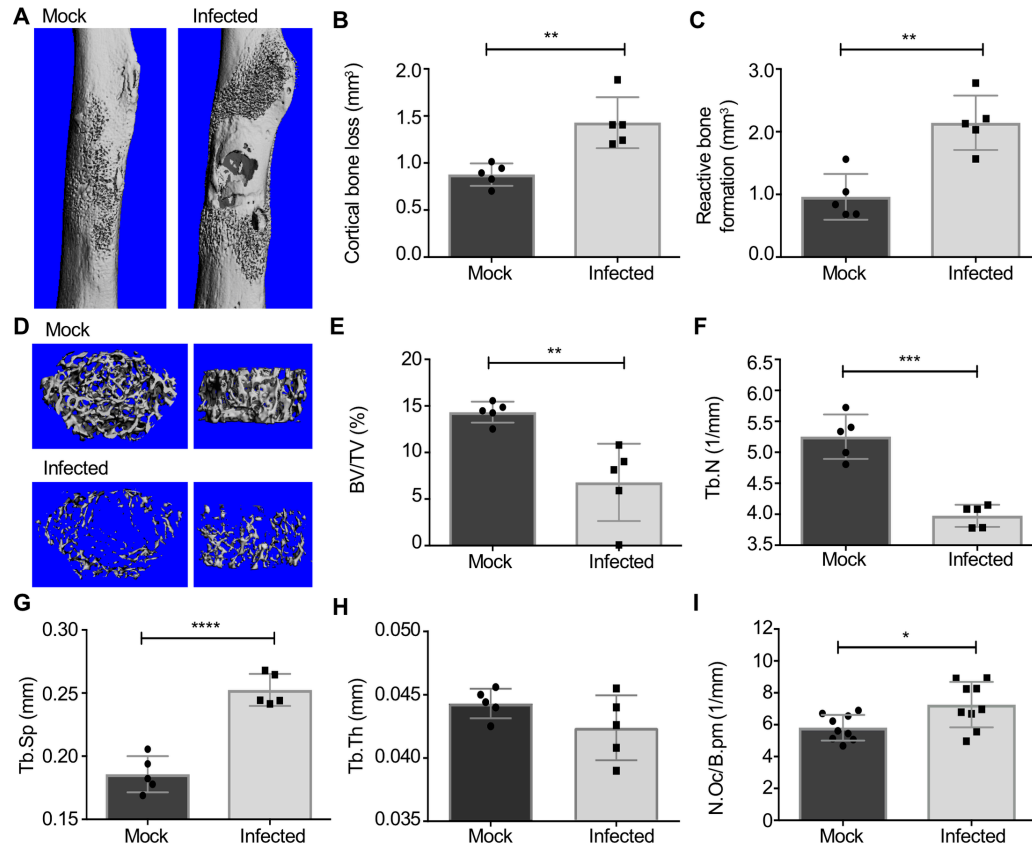
Figure 22. *S. aureus* **osteomyelitis alters cortical and trabecular bone remodeling. (A-H)** Mock infection or osteomyelitis was induced in female wild-type C57BL/6J (WT) mice via intraosseous inoculation with PBS or *S. aureus*. At 14 days post-infection, femurs were harvested, fixed in neutral buffered formalin, and scanned with a µCT50 at 10 µm resolution ($n = 5$ mice per group). **(A)** Anteroposterior view of the femur at the inoculation site in representative mock infected and *S. aureus* infected femurs. **(B, C)** Cortical bone loss (mm^3) **(B)** and reactive bone formation (mm^3) **(C)** were quantified via µCT. **(D)** Representative three-dimensional top down (left) and side (right) views of trabecular bone architecture in mock infected and *S. aureus* infected femurs. **(E-H)** Trabecular bone indices, including three-dimensional measurements of trabecular bone volume/total volume (BV/TV) (%) **(E)**, trabecular number (Tb.N) (1/mm) **(F)**, trabecular spacing (Tb.Sp) (mm) **(G)**, and trabecular thickness (Tb.Th) (mm) **(H)** were measured via µCT. After scanning, femurs were decalcified, processed, and embedded in paraffin for histologic sectioning and tartrate resistant acid phosphatase (TRAP) staining. **(I)** Histomorphometric analyses of trabecular bone in the distal femur proximal to the growth plate compared the number of osteoclasts per bone perimeter (N.Oc/B.pm) (1/mm) between mock infected and *S. aureus* infected femurs ($n = 9$ mice per group). Symbols represent individual data points from each mouse (Mock = circles; Infected = squares), the top line of each bar represents the mean, and error bars represent standard deviation. Unpaired *t*-tests were used to compare µCT and histomorphometry measurements between mock infected and *S. aureus* infected femurs. * $p < 0.05$, ** $p < 0.01$, *** $p < 0.001$, **** $p < 0.0001$.

S. aureus osteomyelitis induced dramatic alterations in cortical bone surrounding the infectious focus, which was initiated in the middle of the femoral diaphysis. However, trabecular bone, located at the ends of the long bones, is the major site of homeostatic bone remodeling [277]. In order to elucidate how inflammation during osteomyelitis leads to alterations in trabecular bone architecture, we also performed micro-computed tomography (μCT) imaging on trabecular bone in the distal femur. To determine the amount of trabecular bone that was lost during osteomyelitis, we calculated the trabecular bone volume per total volume (BV/TV), which is a standard measure of bone volume and architecture [276]. *S. aureus* infected femurs exhibited a dramatic loss in trabecular bone, with BV/TV markedly decreased in infected femurs compared to mock infected femurs **(Figure 22D and 22E)**. The observed decrease in BV/TV during infection is reflective of a decline in the number of bony trabeculae, which in turn increases the overall volume of space between trabeculae **(Figure 22F and 22G)**. Trabecular thickness was not significantly reduced in infected relative to mock infected femurs **(Figure 22H)**. Although skeletal histology revealed that the area of the femur encompassing the trabecular bone did not have apparent abscess formation **(Figure 21C)**, viable *S. aureus* cells were recoverable from the femoral epiphyses encompassing the trabecular bone **(Figure 23)**. These data collectively reveal that *S. aureus* osteomyelitis induces changes in bone turnover throughout the entire infected femur, which is reflected in a significant loss of cortical and trabecular bone.
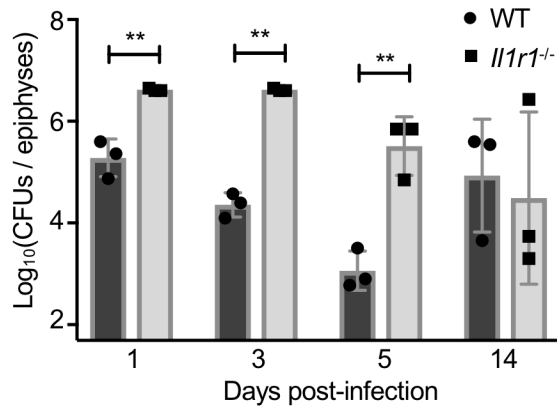
Figure 23. *S. aureus* burdens are detectable from femoral metaphyses and epiphyses during *S.* osteomyelitis. Femurs were harvested from female WT and *Il1r1*$^{-/-}$ mice at days 1, 3, 5, and 14 days after *S. aureus* infection (10^5 CFUs) ($n = 3$ per genotype). Distal and proximal femoral epiphyses were homogenized to quantify bacterial burdens in areas encompassing trabecular bone. *S. aureus* CFUs were detectable in the ends of WT and *Il1r1*$^{-/-}$ femurs at all time points. Symbols represent individual data points from each mouse (WT = circles; *Il1r1*$^{-/-}$ = squares), the top of each bar represents the mean, and error bars represent the standard deviation. Multiple *t*-tests were used to compare CFU burdens between WT and *Il1r1*$^{-/-}$ mice at each time point. ** $p < 0.01$.

One common mechanism of bone loss is mediated by an increase in the number of bone-resorbing osteoclasts residing on the bone surface. To examine whether the inflammation associated with *S. aureus* osteomyelitis enhances numbers of osteoclasts *in vivo*, we collected histologic sections of infected femurs for histomorphometry, which enables quantification of the number of osteoclasts and osteoclast resorbing surface relative to intact trabecular bone. Histomorphometric analysis showed an increased number of osteoclasts per bone perimeter (N.OC/B.pm) in *S. aureus* infected femurs relative to mock infected femurs, suggesting that enhancement of osteoclastogenesis might be one mechanism underlying trabecular bone loss during osteomyelitis **(Figure 22I)**. Taken together, these data indicate that *S. aureus* osteomyelitis perturbs normal bone homeostasis to induce pathologic bone remodeling in both cortical and trabecular bone.

Longitudinal cytokine profiling defines the local inflammatory milieu during *S. aureus* osteomyelitis

Previous studies have shown that toxin-deficient *S. aureus* strains retain the ability to alter bone remodeling, albeit to a lesser extent than WT *S. aureus*, implicating inflammation as a potential mediator of dysregulated bone remodeling during osteomyelitis [31, 32]. To characterize the local inflammatory environment during *S. aureus* osteomyelitis, we conducted longitudinal, multiplexed cytokine profiling of *S. aureus* and mock infected femurs over the course of 14 days. Relative to mock infected femurs, *S. aureus* infected femurs have more abundant levels of cardinal pro-inflammatory cytokines including v **(Figure 24)**. While both IL-1α and IL-1β are highly produced in infected femurs, IL-1β had a higher fold change than IL-1α throughout the timecourse when

comparing *S. aureus* infected to mock infected femurs. Furthermore, infected femurs have increased levels of cytokines that support myeloid cell chemotaxis and expansion, including KC (CXCL1), G-CSF, M-CSF, MCP-1 (CCL2), MIP-1α (CCL3), MIP-1β (CCL4), and MIP-2 (CXCL2), compared to mock infected femurs **(Figure 24)**. Cytokine profiling of *S. aureus* osteomyelitis demonstrated that inflammatory cytokines, chemokines, and growth factors are greatly increased in infected femurs by day 1 and throughout infection.

	Days post-infection				
	Day 1	Day 4	Day 7	Day 10	Day 14
IL-1α	1.62	1.03	2.33	3.06	2.44
IL-1β	5.00	4.08	5.50	3.54	3.82
IL-2	0.22	-0.44	0.42	-1.51	-0.40
IL-3	-0.65	1.81	1.72	1.49	1.25
IL-4	-0.24	-0.02	0.31	0.56	2.31
IL-5	0.41	0.70	1.91	2.45	1.26
IL-6	3.66	1.96	3.76	0.92	1.22
IL-7	0.29	0.36	0.09	-0.10	0.41
IL-9	-5.48	-1.29	-0.69	-0.58	-0.44
IL-10	0.95	2.35	2.48	1.90	0.96
IL-12p40	0.75	3.69	1.81	0.38	-0.62
IL-12p70	0.90	2.46	1.10	1.06	1.71
IL-15	-0.39	0.57	0.02	-1.06	0.45
IL-17	0.67	3.39	5.53	5.59	5.82
IFNγ	-1.47	3.55	-0.18	3.49	0.96
LIF	1.36	1.42	1.57	1.85	1.25
TNFα	1.75	2.10	2.32	2.89	2.88
G-CSF	5.06	4.54	4.83	4.95	5.64
GM-CSF	0.15	0.85	0.98	0.58	0.70
M-CSF	3.28	2.27	1.04	2.58	2.60
VEGF	-0.60	1.44	0.95	1.18	1.03
CCL2 / MCP-1	1.02	2.79	3.33	3.14	2.69
CCL3 / MIP-1α	1.70	1.35	2.77	3.03	4.22
CCL4 / MIP-1β	1.32	0.20	1.80	1.87	2.23
CCL5 / RANTES	0.10	0.20	1.14	1.42	1.07
CCL11 / Eotaxin	-0.35	0.41	0.69	0.90	0.82
CXCL1 / KC	3.19	2.38	2.82	3.53	3.46
CXCL2 / MIP-2	5.71	4.74	8.72	5.85	7.80
CXCL5 / LIX	-2.96	0.35	-2.25	-2.85	-3.02
CXCL9 / MIG	-0.32	1.23	2.28	2.52	1.78
CXCL10 / IP-10	-1.35	-0.71	-0.10	0.92	0.30

-5   0   5

Log $_2$ fold change (*S. aureus* infected / mock infected)

Figure 24. Longitudinal cytokine profiling defines the local inflammatory milieu during *S. aureus* osteomyelitis. Cytokine profiling was performed on homogenates from mock and *S. aureus* infected femurs from female WT mice. Groups of mock or *S. aureus* infected mice (*n* = 3 per time point) were sacrificed on days 1, 4, 7, 10, and 14 post-infection. Relative cytokine levels are represented as Log$_2$(*S. aureus* infected/mock infected) to reflect changes in cytokine production between sterile and infected bones. Dark blue shading represents increasing cytokine fold-changes observed in *S. aureus* infected femurs compared to mock infected femurs. Dark grey shading represents a decreasing cytokine fold-changes in *S. aureus* infected femurs compared to mock infected femurs.

The innate immune signaling adapter MyD88 and IL-1R signaling are critical for the control of bacterial burdens during *S. aureus* osteomyelitis

A rapid and robust cytokine response to *S. aureus* in bone led us to focus on identifying host signaling pathways that are responsible for coordinating an innate immune response. Given the central role for the signaling adapter MyD88 in pathogen recognition and induction of innate immune responses, we first sought to determine how MyD88 signaling influences staphylococcal burdens and host morbidity and mortality during osteomyelitis. *Myd88*$^{-/-}$ mice have enhanced susceptibility to, and morbidity from, bacterial infection [77, 184, 278]. We therefore inoculated these mice with a range of *S. aureus* colony forming units (CFUs), from 10^4-10^6. Although bacterial inocula up to 10^6 CFUs did not cause mortality in WT mice, *Myd88*$^{-/-}$ mice were exquisitely susceptible to *S. aureus* osteomyelitis, with mortality observed even at inocula as low as 10^4 CFUs **(Figure 25A)**. For infected *Myd88*$^{-/-}$ mice that met humane endpoints prior to the experimental endpoint or succumbing to disease, bacterial CFUs were enumerated at that time in the femur, liver, and kidneys. At the time of early sacrifice, *Myd88*$^{-/-}$ mice had between 10^7-10^8 *S. aureus* CFUs in the femur, kidneys, and liver, which was significantly increased over CFUs recovered from WT mice **(Figure 26)**. At the experimental endpoint (day 14 post-infection), surviving *Myd88*$^{-/-}$ mice not only had significantly elevated bacterial burdens in the infected femur, but also experienced more bacterial dissemination to the kidneys and liver **(Figure 25B)**. Consequently, the inability to prevent systemic bacterial dissemination results in significantly increased mortality in *Myd88*$^{-/-}$ mice. Taken together, these data demonstrate a critical role for MyD88-dependent immune responses during *S. aureus* osteomyelitis.

106
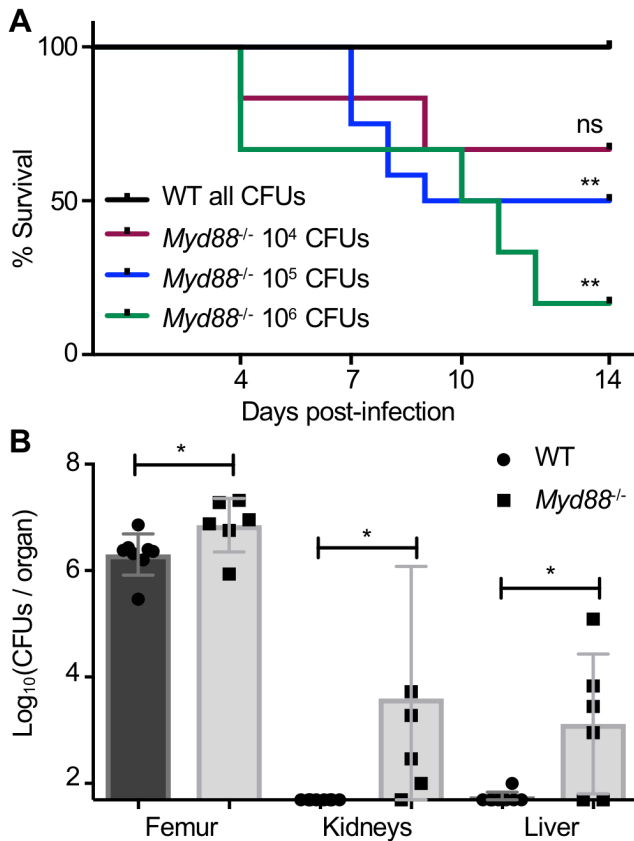
Figure 25. The innate immune signaling adapter MyD88 is critical for the control of bacterial burdens and systemic dissemination during *S. aureus* osteomyelitis. (A-B) Osteomyelitis was established in female WT and *Myd88*^{-/-} mice, following infection with varying *S. aureus* inocula: 10^6 CFUs (WT $n = 5$, *Myd88*^{-/-} = 6), 10^5 CFUs (WT $n = 10$, *Myd88*^{-/-} = 12; duplicate experiments), 10^4 CFUs (WT $n = 6$, *Myd88*^{-/-} = 6). Bacterial burdens were quantified from the infected femur, as well as both kidneys and the liver as a measure of bacterial dissemination. **(A)** Over the 14-day course of infection, mice were monitored for humane endpoints, and if necessary, mice were euthanized and mortality was recorded. Log-rank Mantel Cox test was used to compare WT and *Myd88*^{-/-} survival curves due to infection mortality for each *S. aureus* inoculum. ** $p < 0.01$, ns = not significant. **(B)** Bacterial burdens were enumerated in surviving mice at day 14 post-infection in duplicate experiments, following inoculation with 10^5 *S. aureus* CFUs (WT $n = 8$, *Myd88*^{-/-} $n = 6$; duplicate experiments). Symbols represent individual data points from each mouse (WT = circles; *Myd88*^{-/-} = squares), the top line of each bar represents the mean, and error bars represent standard deviation. Unpaired *t*-tests were used to compare CFU burdens between WT and *Myd88*^{-/-} organ homogenates. * $p < 0.05$, ns = not significant.
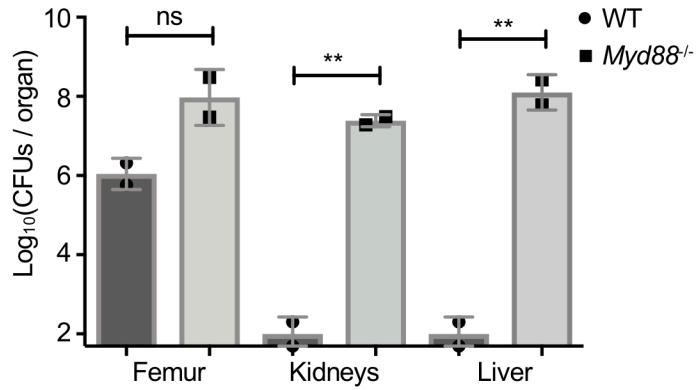
Figure 26. *Myd88⁻ᐟ⁻* **mice euthanized at humane endpoints exhibit greater *S. aureus* dissemination compared to WT mice.** Following infection with 10^5 *S. aureus* CFUs, female *Myd88⁻ᐟ⁻* mice that lost greater than 20% of their body weight were humanely euthanized at day 8 and day 9 post-infection with a randomly chosen female WT comparator ($n = 2$ per genotype) to compare bacterial burdens enumerated from the infected femurs, and to determine dissemination to the kidneys and liver. Symbols represent individual data points from each mouse (WT = circles; *Myd88⁻ᐟ⁻* = squares), the top of each bar represents the mean, and error bars represent the standard deviation. Unpaired *t*-tests were used to compare CFU burdens between WT and *Myd88⁻ᐟ⁻* organ homogenates. ** $p < 0.01$, ns = not significant.

Myd88⁻ᐟ⁻ mice have altered intestinal barrier function and are severely immunocompromised, and therefore may have significant microbiome differences relative to WT mice [75, 279, 280]. When considered in concert with recent studies suggesting that the microbiome may regulate bone mass [281-284], these observations prompted us to breed *Myd88⁻ᐟ⁻* and *Myd88⁺ᐟ⁺* littermate controls from a heterozygous colony and compare these littermate controls for susceptibility to osteomyelitis. We also examined the influence of sex as a biologic variable in these experiments. In line with results from mice bred in separate colonies, significant mortality from osteomyelitis was observed in male *Myd88⁻ᐟ⁻* mice, but not *Myd88⁺ᐟ⁺* littermate controls **(Figure 27A)**. Of note, at day 14 post-infection, male *Myd88⁻ᐟ⁻* mice had no difference from *Myd88⁺ᐟ⁺* littermate controls in recovered CFUs from infected femurs **(Figure 27B)**. This observation could indicate sex-dependent differences in osteomyelitis pathogenesis, or alternatively may reflect selection bias from removal of mice that succumbed to infection **(Figure 27A)**. In contrast to male mice, female *Myd88⁻ᐟ⁻* mice exhibited significantly higher bacterial burdens in the infected femur when compared *Myd88⁺ᐟ⁺* littermate controls **(Figure 27C)**. These experiments confirm that MyD88 is critical for the control of bacterial burdens and systemic dissemination during osteomyelitis independently of any confounding variables associated with separate colony maintenance.
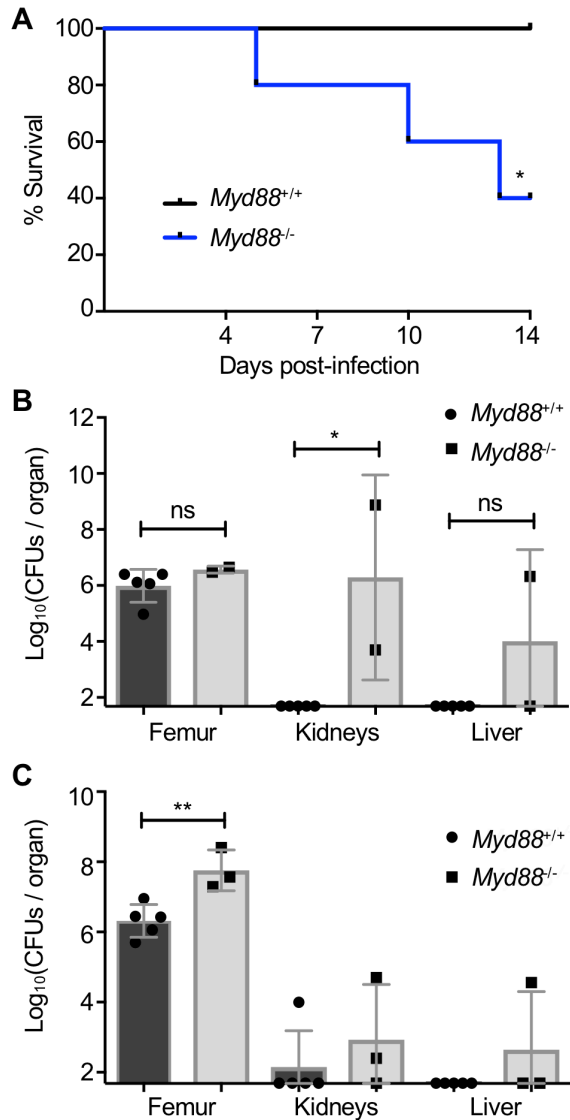
Figure 27. MyD88 protects against local *S. aureus* burdens and dissemination during *S. aureus* osteomyelitis in male and female *Myd88*⁺/⁺ and *Myd88*⁻/⁻ littermates. (A-C) *Myd88*⁺/⁻ mice were bred to produce *Myd88*⁺/⁺ and *Myd88*⁻/⁻ littermate controls. Male (*n* = 5 each genotype) and female (*n* = 5 *Myd88*⁺/⁺; *n* = 3 *Myd88*⁻/⁻) littermate controls were infected with 10^6 *S. aureus* CFUs to establish osteomyelitis. All groups were monitored for severe weight loss and signs of sepsis. **(A)** Male *Myd88*⁺/⁺ (*n* = 5) *Myd88*⁺/⁺ (*n* = 5) and *Myd88*⁺/⁺ (*n* = 5) mice survived until day 14. Log-rank Mantel Cox test was used to compare male *Myd88*⁺/⁺ and *Myd88*⁻/⁻ survival curves due to infection mortality. * $p < 0.05$. **(B, C)** Bacterial burdens were enumerated from the infected femur, kidneys and liver from male **(B)** and female **(C)** mice at day 14 post-infection. Symbols represent individual data points from each mouse (*Myd88*⁺/⁺ = circles; *Myd88*⁻/⁻ = squares), the top line of each bar represents the mean and error bars represent standard deviation. Unpaired *t*-tests were used to compare CFU burdens between *Myd88*⁺/⁺ and *Myd88*⁻/⁻ organ homogenates. * $p < 0.05$, ** $p < 0.01$, ns = not significant.

In the absence of MyD88 signaling, mice are unable to control *S. aureus* infection, indicating that upstream receptors that signal through MyD88, including *S. aureus*-recognizing TLRs and IL-1R, may be important for antibacterial protection. The high levels of IL-1 and IL-1-regulated cytokines present in *S. aureus* infected femurs led us to investigate the contribution of IL-1R signaling to anti-staphylococcal immunity in bone. We subjected WT and *Il1r1*^{-/-} mice to *S. aureus* osteomyelitis. In contrast to the extreme systemic morbidity observed in *MyD88*^{-/-} mice suffering from osteomyelitis, *Il1r1*^{-/-} mice had less morbidity when compared to WT mice, in that they lost significantly less weight over the course of infection **(Figure 28A)**. To determine the role of IL-1R and the relative contributions of IL-1 isoforms (IL-1α or IL-1β) to control bacterial burdens in bone, WT, *Il1r1*^{-/-}, *Il1a*^{-/-}, and *Il1b*^{-/-} mice were subjected to *S. aureus* osteomyelitis. Enumeration of bacterial burdens revealed that *Il1r1*^{-/-} mice harbored significantly higher bacterial burdens in infected femurs than WT, *Il1a*^{-/-}, and *Il1b*^{-/-} mice **(Figure 28B)**. *Il1a*^{-/-} and *Il1b*^{-/-} mice sustained bacterial burdens that were not significantly different from WT mice **(Figure 28B)**. Unlike *MyD88*^{-/-} mice, *Il1r1*^{-/-} mice were protected from significant systemic dissemination to the liver or kidneys **(Figure 28C)**. To determine whether differences in WT and *Il1r1*^{-/-} strains were due to background genotype or separate colony maintenance, heterozygous *Il1r1*^{+/-} mice were bred to generate *Il1r1*^{+/+} and *Il1r1*^{-/-} littermate controls. Infection of littermates with 10^6 *S. aureus* CFUs confirmed that *Il1r1*^{-/-} mice sustained higher bacterial burdens in bone compared to *Il1r1*^{+/+} mice **(Figure 28D)**. We next investigated the kinetics of bacterial clearance between WT and *Il1r1*^{-/-} mice. For this analysis we chose a lower *S. aureus* inoculum of 10^5 CFUs in an attempt to equilibrate bacterial burdens at day 14 post-infection. In both WT and *Il1r1*^{-/-} mice, the initial *S. aureus*

inoculum of 10^5 CFUs replicates to approximately 10^7 CFUs by day 1 post-infection **(Figure 28E)**. In WT mice, bacterial burdens decreased by greater than 1 log between days 3 and 5 post-infection. In contrast, bacterial burdens in *Il1r1$^{-/-}$* mice were essentially unchanged through day 5 post-infection, and only declined between days 5 and 10 post-infection. Accordingly, WT and *Il1r1$^{-/-}$* mice had significantly different bacterial burdens at day 5 post-infection with this lower inoculum, even though bacterial burdens were roughly equivalent at the final time point (day 14). These data reveal differences in infection kinetics between WT and *Il1r1$^{-/-}$* mice, and suggest that *Il1r1$^{-/-}$* mice might have a delay in bacterial control during osteomyelitis.
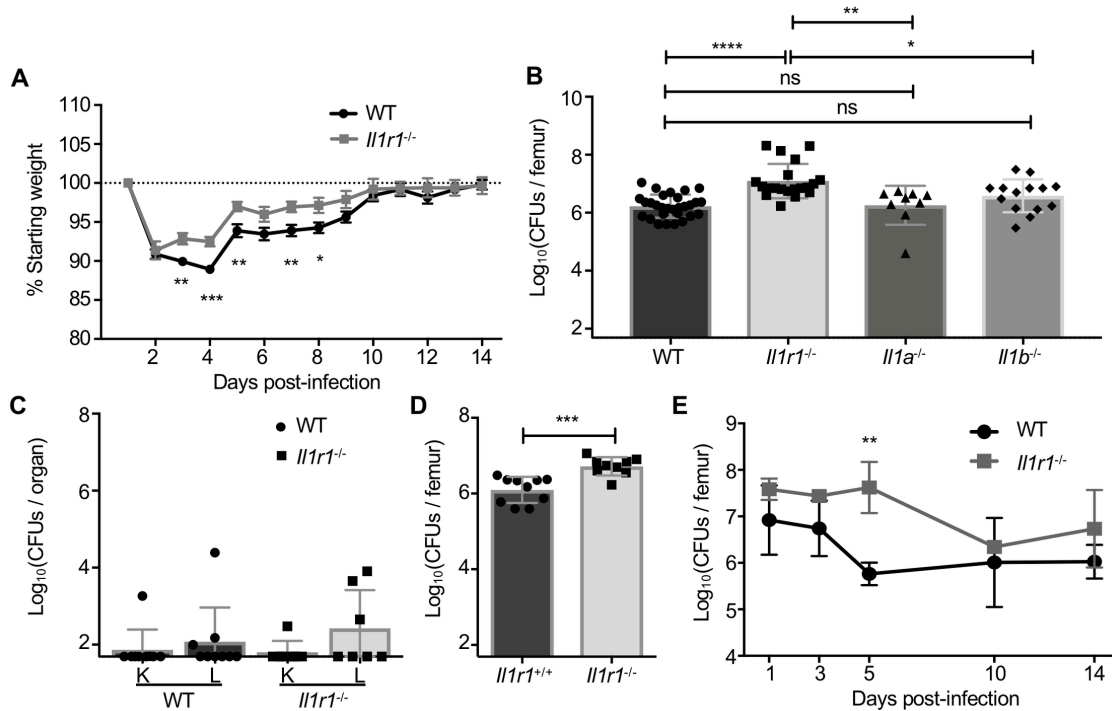
Figure 28. IL-1R signaling contributes to antibacterial immunity in bone. (A) Percent starting weight was monitored daily in triplicate experiments with 10^6 *S. aureus* CFU infection of female WT and *Il1r1*$^{-/-}$ mice (WT $n = 15$, *Il1r1*$^{-/-}$ $n = 13$). **(B-C)** At day 14 post-infection with 10^6 *S. aureus* CFU, bacterial burdens were enumerated from the infected femurs (WT $n = 29$, *Il1r1*$^{-/-}$ $n = 20$, *Il1a*$^{-/-}$ $n = 9$, *Il1b*$^{-/-}$ $n = 14$; six independent experiments) **(B)** or kidneys (K) and liver (L) (WT $n = 9$, *Il1r1*$^{-/-}$ $n = 7$; duplicate experiments) **(C)** of each mouse. **(D)** A subsequent experiment with a 10^6 *S. aureus* CFU inoculum was conducted in *Il1r1*$^{+/+}$ and *ll1r1*$^{-/-}$ mice bred as littermates from a heterozygous colony (*Il1r1*$^{+/+}$ $n = 10$, *ll1r1*$^{-/-}$ $n = 9$; duplicate experiments). **(E)** Following a lower 10^5 *S. aureus* CFU inoculum, bacterial burdens were enumerated from infected femurs of WT and *Il1r1*$^{-/-}$ mice on days 1, 3, 5, 10, and 14 post-infection ($n = 3$ mice per genotype per time point). On bar graphs, symbols represent individual data points from a single mouse (WT and *Il1r1*$^{+/+}$ = circles; *Il1r1*$^{-/-}$ = squares; *Il1a*$^{-/-}$ = triangles, *Il1b*$^{-/-}$ = diamonds) and the mean is represented by the top line of the bar. On timecourse graphs, symbols represent the mean. On all graphs, error bars represent the standard deviation. Unpaired *t*-tests compared weight recovery and CFU burdens between WT and *Il1r1*$^{-/-}$ mice and between *Il1r1*$^{+/+}$ and *Il1r1*$^{-/-}$ femurs. A one-way ANOVA with Tukey's multiple comparisons test was used to compare bacterial burdens harvested from femurs between mice of all genotypes. For kidney and liver burdens, separate *t*-tests compared WT and *Il1r1*$^{-/-}$ burdens from each organ site. * $p < 0.05$, ** $p < 0.01$, *** $p < 0.001$, **** $p < 0.0001$, ns = not significant.

In other *S. aureus* infection models, IL-1 coordinates neutrophil recruitment and is necessary for sequestration of *S. aureus* into mature abscesses [77, 199]. We therefore hypothesized that the delay in bacterial clearance in *Il1r1*$^{-/-}$ mice subjected to osteomyelitis was related to differences in abscess maturation and neutrophil abundance. To visualize immune cell infiltration and abscess structure, we conducted myeloperoxidase (MPO) staining on histologic sections of infected femurs at day 14 post-infection. *Il1r1*$^{-/-}$ mice with osteomyelitis have differential MPO staining in comparison to WT controls, suggesting these mice have disorganized abscess structure **(Figure 29A)**. WT mice have MPO$^+$ cells that surround and encompass the abscess, whereas *Il1r1*$^{-/-}$ mice show extensive MPO$^+$ staining throughout the femur. To assess changes in inflammatory signatures that correspond to differences in infection kinetics, infected femur homogenates from WT and *Il1r1*$^{-/-}$ mice were analyzed using multiplexed cytokine analysis. In comparison to WT mice, *Il1r1*$^{-/-}$ mice had significantly decreased abundance of neutrophil growth factors G-CSF and GM-CSF and lower levels of the neutrophil chemokine CXCL1 at day 1 post-infection, a timepoint that precedes early bacterial control in WT mice between days 3 and 5 **(Figure 29B-D, Figure 28E)**. GM-CSF and CXCL1 levels then decline in WT mice by day 5 post-infection. In contrast, *Il1r1*$^{-/-}$ mice display significantly higher levels of GM-CSF and CXCL1 at day 5 post-infection when compared to WT mice, prior to the decrease in bacterial burdens that occurs between days 5 and 10 post-infection **(Figure 29C and 29D, Figure 28E)**. Moreover, there are global changes in cytokine abundance when comparing WT and *Il1r1*$^{-/-}$ mice **(Table 2)**. These data suggest that WT mice have an early influx and/or expansion of neutrophils, important for the control of bacterial burdens and normal abscess formation.
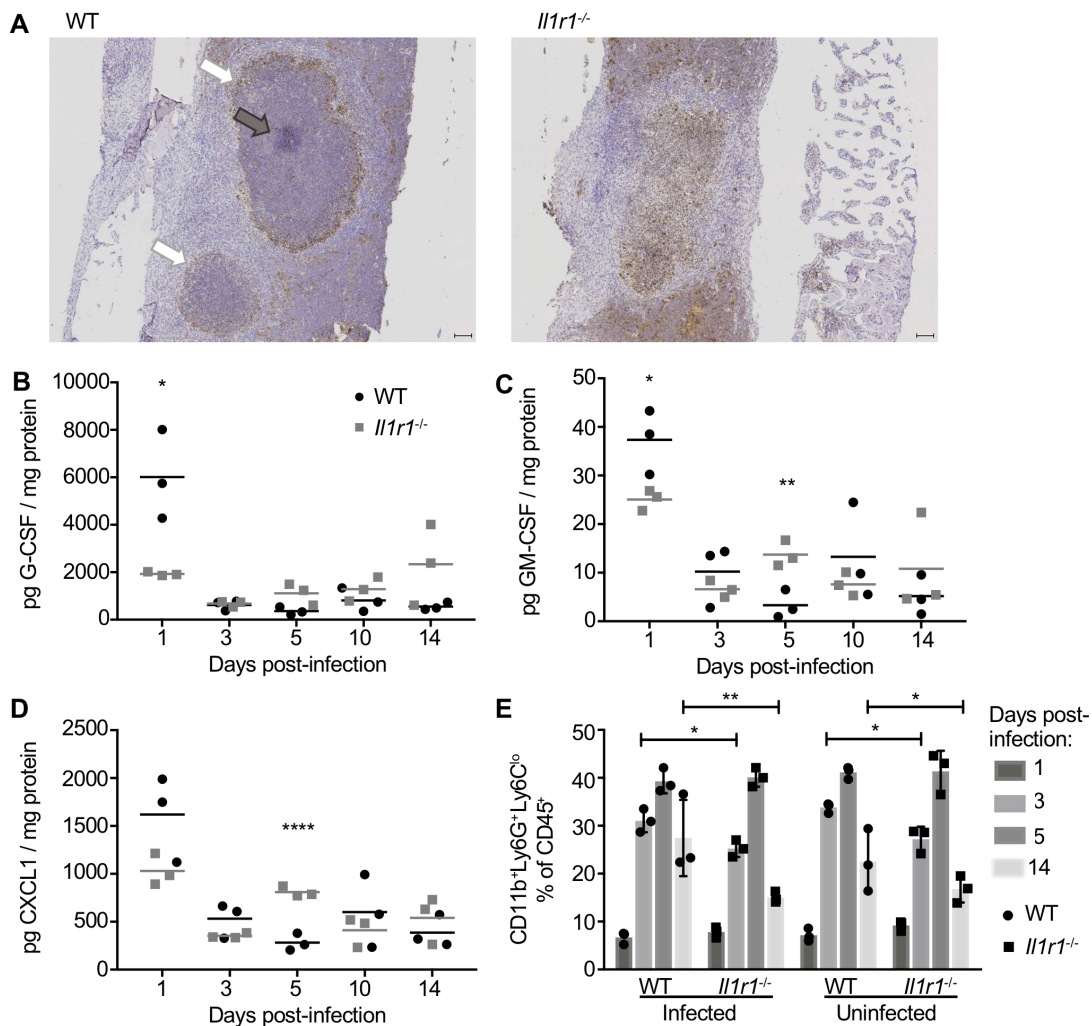
Figure 29. *Il1r1⁻/⁻* **mice have altered abscess structure, delayed granulocytic cytokine levels, and lower neutrophil abundance during *S. aureus* osteomyelitis. (A)** Femurs were harvested from female WT and *Il1r1⁻/⁻* mice ($n = 5$ per genotype) 14 days after *S. aureus* infection (10^6 CFUs). Harvested femurs were fixed in neutral buffered formalin, dehydrated in 70% ethanol, and decalcified in 20% EDTA before embedding in paraffin for sectioning. The infected femurs were sectioned through the medullary cavity and sections from each femur were stained for myeloperoxidase (MPO) to visualize MPO+ (brown) neutrophils and gross abscess architecture in WT (left) and *Il1r1⁻/⁻* (right) sections. Slides were scanned at 20X using a Leica SCN400 Slide Scanner and images were taken at 4X (scale bars = 100 μm) and are representative of $n = 5$ mice per genotype. Abscesses are indicated by white arrows and a *S. aureus* microcolony by a grey arrow. **(B-D)** After infection with 10^5 *S. aureus* CFUs, cytokine levels and relative neutrophil abundance were measured from femurs ($n = 3$ per genotype) harvested at days 1, 3, 5, 10, and 14 post-infection (cytokine analysis, **B-D**) or days 1, 3, 5, and 14 post-infection (flow cytometry, **E**). Cytokine levels in pg/mL were corrected for overall protein levels in the femur

115

homogenates as measured using a BCA assay. Depicted are select cytokines G-CSF **(B)**, GM-CSF **(C)**, and CXCL1 **(D)** from WT (black circles) and *Il1r1$^{-/-}$* (grey squares) femurs. **(E)** Relative neutrophil abundance was measured in bone marrow harvested from infected and contralateral, uninfected femurs of WT and *Il1r1$^{-/-}$* mice. Neutrophils are defined as CD45$^+$CD11b$^+$Ly6G$^+$Ly6C^{lo} and are reported as % of CD45$^+$ immune cells **(D)**. Symbols represent individual data points from each mouse (WT = circles; *Il1r1$^{-/-}$* = squares), horizontal lines or the top of each bar represent the mean, and error bars represent standard deviation. Multiple unpaired *t*-tests were used to compared pg cytokine/mg protein and neutrophil percentages between WT and *Il1r1$^{-/-}$* mice. * $p < 0.05$, ** $p < 0.01$, **** $p < 0.0001$. If not denoted with asterisks, statistical difference between genotypes was not significant.

Table 2. Cytokine levels in WT and *Il1r1*^{-/-} mice during *S. aureus* osteomyelitis.

Cytokine	WT infected (white)				
	Il1r1^{-/-} infected (grey)				
	(pg cytokine/mg protein)				
	Day 1	Day 3	Day 5	Day 10	Day 14
IL-1α	217.7 ± 60.2	226.9 ± 82.2	212.5 ± 242.3	544.1 ± 545.0	241.2 ± 76.6
	234.5 ± 40.2	346.6 ± 73.3	432.8 ± 243.2	693.3 ± 50.4	965.3 ± 826.0
IL-1β	500.1 ± 105.2*	408.5 ± 114.3	188.8 ± 146.7	199.9 ± 150.8	116.4 ± 34.5
	855.2 ± 93.8	402.5 ± 147.1	802.8 ± 471.2	314.2 ± 132.8	457.1 ± 305.2
IL-2	4.0 ± 0.5	1.4 ± 0.2	1.0 ± 0.2*	2.1 ± 0.6	2.0 ± 0.4
	4.6 ± 0.9	1.1 ± 0.1	1.7 ± 0.2	1.8 ± 0.1	2.1 ± 0.8
IL-3	0.5 ± 0.1	1.1 ± 0.2	1.3 ± 0.2	1.5 ± 0.5	1.5 ± 0.2
	0.7 ± 0.2	1.1 ± 0.4	2.5 ± 1.5	1.0 ± 0.1	1.3 ± 0.4
IL-4	2.4 ± 0.1	1.6 ± 0.1	1.3 ± 0.1*	2.4 ± 1.1	10.9 ± 6.5
	2.1 ± 0.2	1.8 ± 0.2	2.3 ± 0.5	2.8 ± 0.9	15.7 ± 18.2
IL-5	6.2 ± 1.8	2.3 ± 1.4	1.7 ± 1.8	3.3 ± 2.4	2.8 ± 1.6
	7.0 ± 3.4	3.7 ± 2.6	5.4 ± 3.2	5.2 ± 0.3	7.0 ± 3.6
IL-6	724.6 ± 227.9	151.0 ± 50.6	51.8 ± 4.6**	144.1 ± 114.8	68.1 ± 30.9
	502.1 ± 136.3	86.4 ± 17.7	173.9 ± 43.9	69.0 ± 13.4	118.1 ± 131.9
IL-7	3.1 ± 0.4	2.2 ± 0.3	2.1 ± 0.4*	3.0 ± 0.4	3.3 ± 0.3
	2.8 ± 0.6	2.2 ± 0.5	2.7 ± 0.2	3.0 ± 0.1	2.6 ± 0.7
IL-9	208.3 ± 18.8	116.3 ± 7.9	112.4 ± 10.5	153.0 ± 26.0	129.2 ± 25.2
	225.1 ± 41.3	103 ± 15.5	114.8 ± 15.9	133.2 ± 5.1	131.5 ± 20.9
IL-10	5.1 ± 0.7	5.4 ± 0.4	5.1 ± 0.5*	6.4 ± 2.4	7.2 ± 1.0
	5.6 ± 0.5	5.1 ± 1.1	8.4 ± 1.3	6.8 ± 0.8	10.0 ± 5.1
IL-12 p40	0.8 ± 0.0	17.9 ± 6.9	27.9 ± 6.4	21.1 ± 4.3	46.5 ± 22.9
	0.7 ± 0.1	20.4 ± 12.0	34.3 ± 13.5	18.9 ± 6.0	24.2 ± 9.5
IL-12 p70	9.8 ± 3.0	6.8 ± 1.1	8.3 ± 1.7	8.6 ± 4.4	8.2 ± 0.9
	6.3 ± 0.6	6.6 ± 2.2	7.9 ± 0.7	4.2 ± 1.1	6.1 ± 2.9
IL-15	16.9 ± 3.8	13.3 ± 4.3	9.0 ± 1.8**	14.8 ± 6.8	12.4 ± 1.0*
	16.1 ± 5.2	10.8 ± 2.8	17.5 ± 0.6	14.1 ± 1.1	12.3 ± 7.3
IL-17	4.6 ± 0.5	18.0 ± 6.4*	14.9 ± 10.9	233.5 ± 208.3	206.8 ± 43.2**
	4.5 ± 0.6	3.3 ± 1.5	29.5 ± 36.4	6.2 ± 2.4	9.3 ± 5.6
IFNγ	10.1 ± 1.7	6.3 ± 3.3	5.2 ± 2.0**	12.0 ± 8.2	12.0 ± 4.8
	10.0 ± 1.8	8.2 ± 2.1	20.1 ± 2.6	17.4 ± 5.2	16.8 ± 3.0
LIF	133.4 ± 11.5	99.3 ± 9.0	84.5 ± 31.8	111.2 ± 34.3	98.9 ± 12.2
	157.3 ± 28.1	92.5 ± 13.0	112.5 ± 24.1	111.7 ± 12.0	130.6 ± 32.0
TNFα	40.2 ± 5.7	56.4 ± 10.7	34.7 ± 16.5	64.9 ± 34.6	52.3 ± 5.2
	29.8 ± 5.1	53.2 ± 8.9	71.6 ± 24.7	60.5 ± 14.7	80.3 ± 33.1
G-CSF	6012.0 ± 1879.3*	624.0 ± 215.4	359.6 ± 165.8	809.4 ± 495.4	555.6 ± 161.3
	1928.9 ± 84.7	678.3 ± 120.2	1115.0 ± 454.3	1285.6 ± 504.4	2339.3 ± 1701.6

	WT infected (white)				
	Il1r1$^{-/-}$ infected (grey)				
	(pg cytokine/mg protein)				
Cytokine	Day 1	Day 3	Day 5	Day 10	Day 14
GM-CSF	37.3 ± 6.6*	10.2 ± 6.4	3.3 ± 2.9**	13.3 ± 10.0	5.2 ± 4.1
	25.1 ± 2.1	6.6 ± 1.7	13.7 ± 2.6	7.6 ± 2.4	10.8 ± 10.0
M-CSF	1898.9 ± 490.3	807.7 ± 651.3	761.0 ± 1010.1	92.2 ± 53.4	89.2 ± 27.4
	936.5 ± 354.7	702.6 ± 128.9	1452.5 ± 1163.2	119.0 ± 75.2	316.8 ± 344.4
VEGF	184.0 ± 26.9	360.1 ± 74.2	358.9 ± 56.7	365. 0 ± 169.5	334.2 ± 201.8
	187.4 ± 52.9	281.4 ± 103.4	306.3 ± 74.8	237.4 ± 58.5	179.1 ± 115.6
CCL2 / MCP-1	343.8 ± 95.7	178.8 ± 136.0	122.3 ± 126.5	63.6 ± 30.3	66.1 ± 2.2
	200.9 ± 36.4	113.0 ± 20.6	372.0 ± 144.2	73.2 ± 12.2	86.6 ± 62.1
CCL3 / MIP-1α	233.2 ± 42.0	258.6 ± 62.1	181.7 ± 82.5	319.3 ± 216.5	297.9 ± 5.04
	324.7 ± 75.3	332.5 ± 63.9	452.4 ± 177.2	487.1 ± 145.7	750.1 ± 421.1
CCL4 / MIP-1β	274.4 ± 70.1	181.2 ± 46.7	131.1 ± 66.0	305.0 ± 235.6	366.8 ± 90.3
	472.8 ± 126.5	274.2 ± 41.4	364.1 ± 168.6	410.9 ± 131.5	760.6 ± 441.9
CCL5 / RANTES	20.9 ± 3.1	25.2 ± 2.5*	42.2 ± 9.5	106.8 ± 63.2	89.8 ± 16.7
	22.1 ± 3.2	50.7 ± 13.8	64.5 ± 14.8	92.4 ± 30.8	97.9 ± 14.4
CCL11 / Eotaxin	178.6 ± 9.3	368.9 ± 35.9	289.3 ± 29.9*	421.9 ± 63.6	516.7 ± 61.4*
	164.2 ± 24.5	342.3 ± 35.1	395.8 ± 55.2	364.1 ± 33.4	322.3 ± 53.4
CXCL1 / KC	1619.2 ± 447.1	532.5 ± 178.8	281.7 ± 89.1***	602.0 ± 378.9	345.5 ± 165.4
	1029.8 ± 165.2	353.5 ± 27.3	809.6 ± 54.5	412.4 ± 156.7	541.3 ± 2453
CXCL2 / MIP-2	5713.9 ± 1425.8	7811.6 ± 3065.5	5648.5 ± 3960.1	6162.9 ± 4560.5	1977.1 ± 1209.6*
	6414.7 ± 918.3	7358.6 ± 2161.2	12454.7 ± 2926.9	12014.6 ± 569.7	10345.3 ± 4458.9
CXCL5 / LIX	364.3 ± 116.3	552.4 ± 241.3	399.8 ± 346.4	475.7 ± 290.3	336.9 ± 172.4
	393.0 ± 36.7	522.6 ± 113.9	873.3 ± 227.8	712.1 ± 262.4	683.0 ± 273.0
CXCL9 / MIG	121.7 ± 91.8	162.0 ± 24.4**	152.2 ± 37.2*	763.8 ± 596.5	712.7 ± 29.8
	92.1 ± 14.1	352.1 ± 60.6	673.1 ± 229.8	1301.7 ± 342.1	1042.2 ± 375.8
CXCL10 / IP-10	394.3 ± 369.1	290.8 ± 57.4	170.6 ± 42.0***	363.4 ± 151.8	312.1 ± 70.9
	214.8 ± 26.4	399.8 ± 42.8	594.5 ± 62.7	534.1 ± 78.2	412.8 ± 87.9

Female WT and *Il1r1$^{-/-}$* femurs were harvested at days 1, 3, 5, 10, and 14 post-infection with 10^5 *S. aureus* CFUs ($n = 3$ mice per timepoint). Cytokine data are reported as the mean pg cytokine/mg protein ± standard deviation, and were compared between infected WT and *Il1r1$^{-/-}$* mice using multiple *t*-tests. * $p < 0.05$, ** $p < 0.01$, *** $p < 0.001$.

To monitor neutrophil abundance during the course of osteomyelitis, bone marrow from infected and contralateral, uninfected WT and *Il1r1*$^{-/-}$ femurs at various time points after *S. aureus* infection was analyzed via flow cytometry **(Figure 30A-F)**. Neutrophils were identified as CD45$^+$CD11b$^+$Ly6G$^+$Ly6C^{lo} and reported as the percent of CD45$^+$ immune cells. At day 1 post-infection, WT and *Il1r1*$^{-/-}$ mice were found to have neutrophils comprising less than 10% of CD45$^+$ cells in the bone marrow. By day 3 post-infection, *Il1r1*$^{-/-}$ mice have significantly fewer neutrophils in the infected bone marrow compared to WT mice **(Figure 29E)**. Furthermore, differences between relative neutrophil abundance were also observed between WT and *Il1r1*$^{-/-}$ mice in the contralateral, uninfected femurs. Neutrophil abundance at day 5 post-infection is comparable between WT and *Il1r1*$^{-/-}$ genotypes, but again was significantly decreased in *Il1r1*$^{-/-}$ femurs at day 14 post-infection. Therefore, the data suggest that *Il1r1*$^{-/-}$ mice with *S. aureus* osteomyelitis have altered neutrophil responses, indicated by the significant decrease in relative neutrophil abundance at two timepoints post-infection.
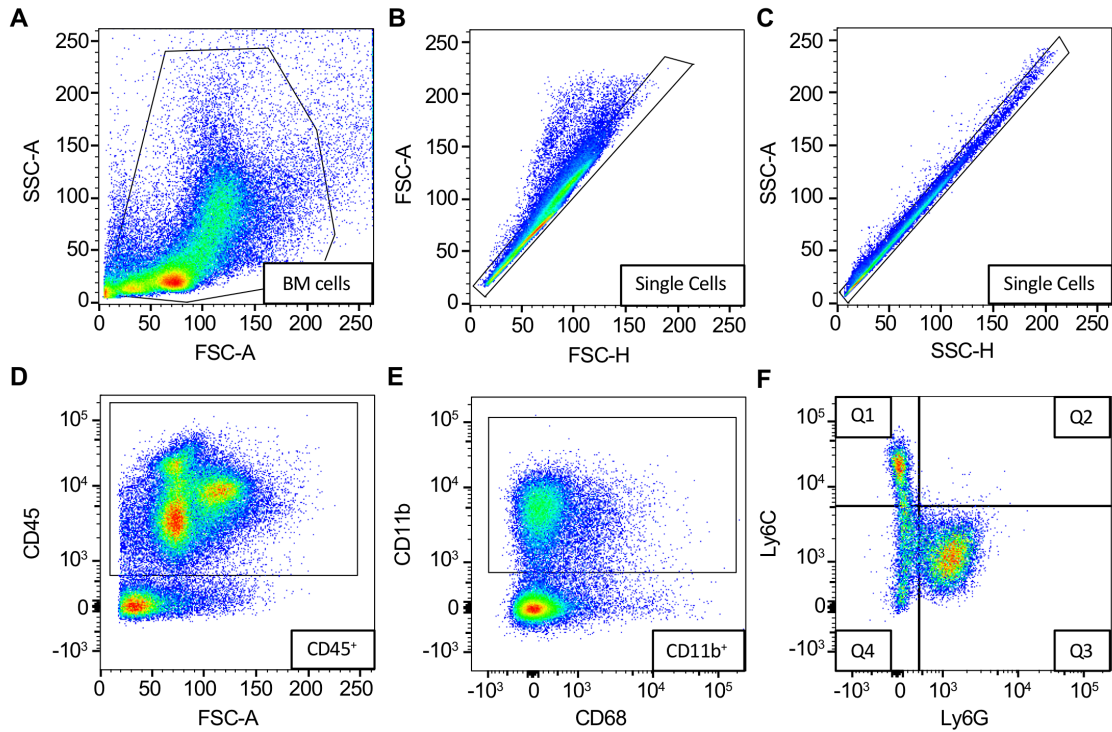
Figure 30. Flow cytometry gating scheme for identification of neutrophils. (A-F) WT and *Il1r1*$^{-/-}$ mice were infected with 10^5 *S. aureus* CFUs and at days 1, 3, 5, and 14 days after infection, the infected and contralateral, uninfected femurs were harvested and BM was collected for flow cytometry. Data shown here represent the gating scheme for each sample at each time point, where labels on plots can be identified by SSC = side scatter, FSC = forward scatter, A = area, H = height, or cellular marker conjugated to a fluorophore. BM cells were identified **(A)**, followed by two single-cell gates **(B, C)**, identification of CD45$^+$ cells **(D)**, CD11b$^+$ cells **(E)**, and finally the neutrophil population represented in quadrant 3 (Q3) as Ly6G$^+$Ly6C^{lo} **(F)**.

S. aureus promotes osteoclastogenesis and pathologic bone loss through IL-1R signaling

WT mice subjected to *S. aureus* osteomyelitis display significant cortical bone destruction and reactive bone formation at the site of infection, while sustaining alterations in osteoclast number and trabecular bone loss in the distal femur **(Figure 26A-I)** [31]. Given the important role of IL-1R signaling in skeletal cell differentiation and function *in vitro*, we hypothesized that pathologic bone remodeling during *S. aureus* osteomyelitis is mediated in part by IL-1R signaling. To test this hypothesis, we compared cortical bone remodeling between WT and *Il1r1*$^{-/-}$ mice using a lower dose (10^5 CFUs) *S. aureus* infection. At the site of infection, *Il1r1*$^{-/-}$ mice sustained increased cortical bone loss in comparison to WT mice **(Figure 31A and 31B)**. In areas adjacent to the cortical bone loss, *Il1r1*$^{-/-}$ mice had a dramatic increase in new bone formation, at nearly twice the volume formed in infected WT femurs **(Figure 31C)**, and these results were confirmed in littermate controls **(Figure 32A and 32B)**. Importantly, these data do not completely control for differences in bacterial burdens at the site of infection, where *Il1r1*$^{-/-}$ mice harbor higher bacterial burdens at day 5 post-infection with a lower inocula **(Figure 28E)**. However, *Il1r1*$^{-/-}$ mice do equilibrate bacterial burdens to the same level at WT mice by day 14 post-infection **(Figure 31D)**.
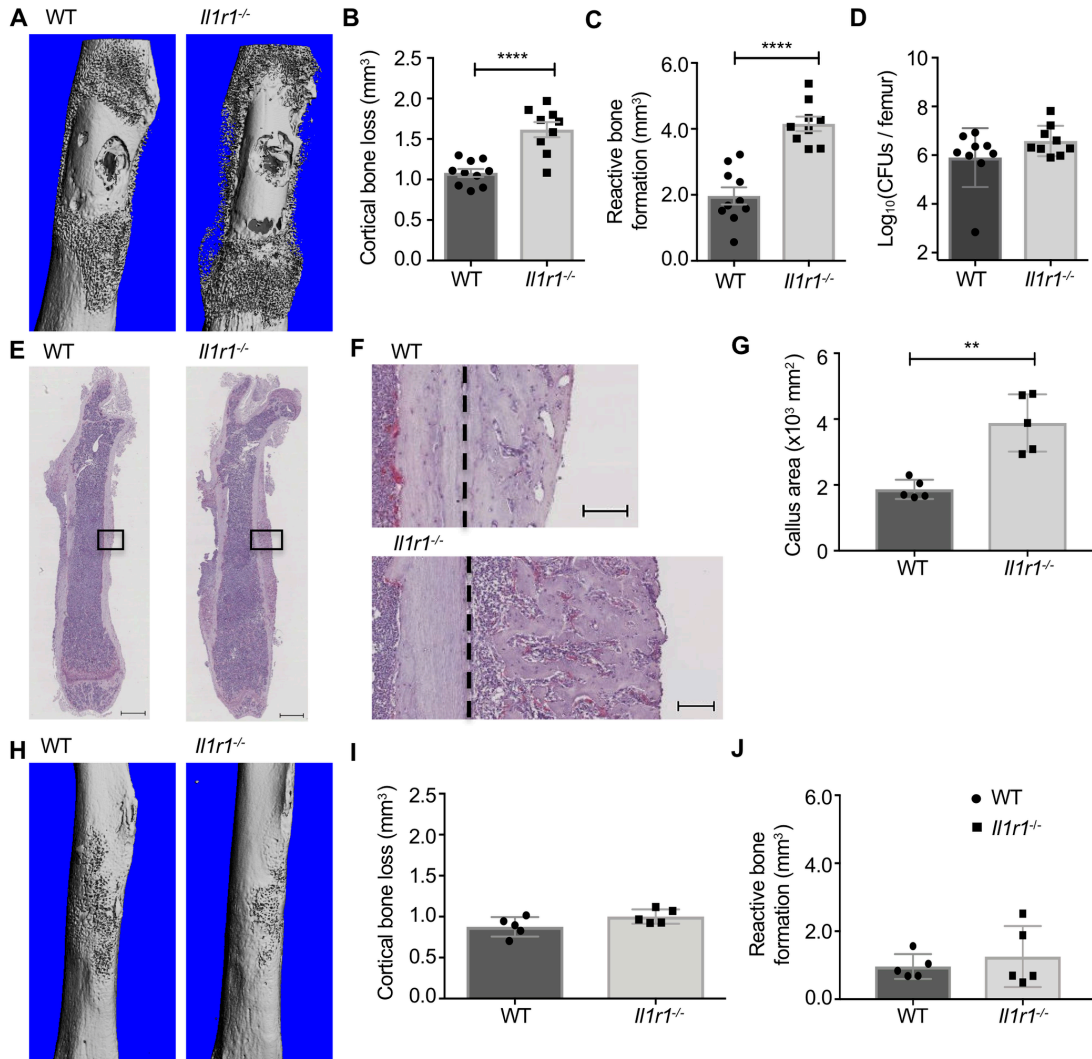
Figure 31. Loss of the IL-1R enhances cortical bone loss and reactive cortical bone formation during *S. aureus* osteomyelitis. (A-J) To determine changes in bone remodeling and final bacterial burdens, female mice were infected with *S. aureus* (10^5 CFUs: WT $n = 10$, *Il1r1*$^{-/-}$ $n = 9$; duplicate experiments for bone remodeling; WT $n = 9$, *Il1r1*$^{-/-}$ $n = 9$; duplicate experiments for CFU enumeration) or mock infected (WT $n = 5$, *Il1r1*$^{-/-}$ $n = 5$ for bone remodeling) with PBS. Femurs were harvested at day 14 post-infection and scanned using the μCT50. Representative anteroposterior views of *S. aureus* infected femurs **(A)** and mock infected femurs **(H)**. μCT three-dimensional analysis of cortical bone loss (mm^3) and reactive bone formation (mm^3) between *S. aureus* infected **(B, C)** and mock infected **(I, J)** WT and *Il1r1*$^{-/-}$ femurs. Bacterial burdens were quantified at day 14 post-infection from WT and *Il1r1*$^{-/-}$ femurs **(D)**. **(E, F)** After μCT analyses, histologic sections of the *S. aureus* infected femurs were prepared and TRAP-stained. Slides were scanned using a Leica SCN400 Slide Scanner, with representative images shown taken at 0.58X (scale bars = 1 mm) **(E)** with the region in the black box imaged at 4X (scale bars = 100 μm) **(F)**, with dashed black line demarcating the separation of intact cortical bone (left of dashed line) and the callus (right of dashed line). **(G)** Tissue IA 2.0

software was used to image callus area of infected femurs at 20X (10^5 CFUs; $n = 5$ per genotype). Symbols represent individual data points from each mouse (WT = circles; *Il1r1*^{-/-} = squares), the top line of each bar represents the mean, and error bars represent standard deviation. Unpaired *t*-tests were used to compare CFU burdens, µCT analyses, and Tissue IA 2.0 measurements between WT and *Il1r1*^{-/-} mice. ** $p < 0.01$, **** $p < 0.0001$.
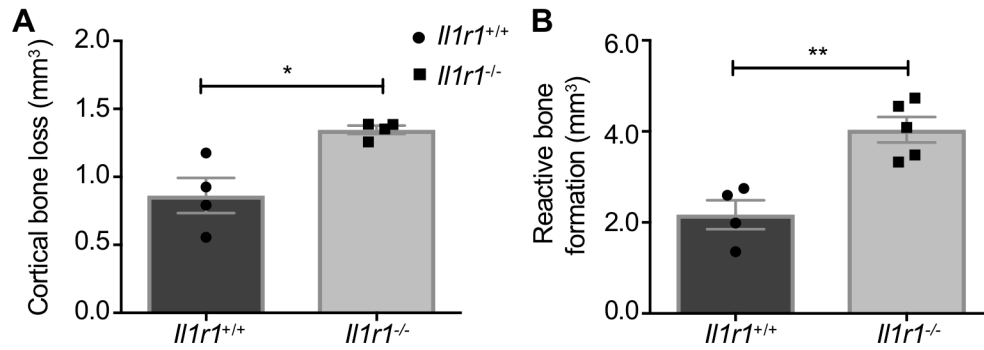
Figure 32. *Il1r1^{-/-}* **mice exhibit enhanced cortical bone loss and reactive bone formation relative to** *Il1r1^{+/+}* **littermates during** *S. aureus* **osteomyelitis. (A, B)** *Il1r1^{+/+}* and *Il1r1^{-/-}* littermate female mice were infected with 10^6 *S. aureus* CFUs (*Il1r1^{+/+}* $n = 5$, *Il1r1^{-/-}* $n = 4$,) to assess changes in cortical bone architecture. Femurs were harvested at day 14 post-infection and were scanned using the μCT50. **(A, B)** Cortical bone loss (mm³) **(A)** and reactive bone formation (mm³) **(B)** from infected *Il1r1^{+/+} and Il1r1^{-/-}* femurs were quantified using μCT analysis. Symbols represent individual data points from each mouse (*Il1r1^{+/+}* = circles, *Il1r1^{-/-}* = squares), the top line of each bar represents the mean, and error bars represent standard deviation. Unpaired *t*-tests were used to compare cortical bone loss and reactive bone formation between *Il1r1^{+/+}* and *Il1r1^{-/-}* mice. * $p < 0.05$, ** $p < 0.01$.

Histologic analyses revealed increased callus formation in infected *Il1r1⁻/⁻* femurs and also demonstrated qualitative differences in callus composition compared to infected WT femurs **(Figure 31E-G)**. In contrast to cortical bone remodeling changes during *S. aureus* infection, μCT analysis revealed no differences in cortical bone remodeling of a sterile bone defect at day 14 post-surgery, where mock infected WT and *Il1r1⁻/⁻* femurs had no significant differences in cortical bone measurements **(Figure 31H-J)**. Collectively, these data indicate that during *S. aureus* osteomyelitis, *Il1r1⁻/⁻* mice exhibit significantly altered cortical bone remodeling, with increased reactive bone formation, altered callus architecture, and greater cortical bone loss at the site of infection.

To elucidate the cellular changes driving differences in bone remodeling between WT and *Il1r1⁻/⁻* mice, we next analyzed trabecular bone remodeling during osteomyelitis. Histomorphometric analysis of trabecular bone was performed in both *S. aureus* infected femurs and contralateral, uninfected femurs from each genotype. Histomorphometry revealed that the infected femurs from WT mice had significantly lower trabecular BV/TV than contralateral, uninfected femurs **(Figure 33A)**. In contrast, infected femurs from *Il1r1⁻/⁻* mice showed no significant differences in BV/TV in comparison to the contralateral, uninfected femur, suggesting that these mice were protected from infection-associated trabecular bone loss despite having significantly higher bacterial burdens in the regions encompassing the trabecular bone over time **(Figure 33A; Figure 28E)**. To determine whether differences in osteoclast biology underlie the distinct trabecular bone remodeling parameters of WT and *Il1r1⁻/⁻* mice, we calculated the numbers of osteoclasts present on trabecular bone surfaces in both infected and contralateral, uninfected femurs. The infected femurs in WT mice displayed greater osteoclast numbers per bone perimeter (N.Oc/B.pm)

and osteoclast surface per bone surface (Oc.S/BS) compared to the contralateral, uninfected femurs, correlating with the infection-induced loss of trabecular bone volume **(Figure 33A-C)**. In contrast, the infected femurs from *Il1r1*^{-/-} mice showed no increase in N.Oc/B.pm or Oc.S/BS when compared to the contralateral, uninfected femur **(Figure 33B and 33C)**. These data suggest that *S. aureus* infection causes enhanced osteoclastogenesis in trabecular bone, which is dependent on intact IL-1R signaling and contributes to bone loss.
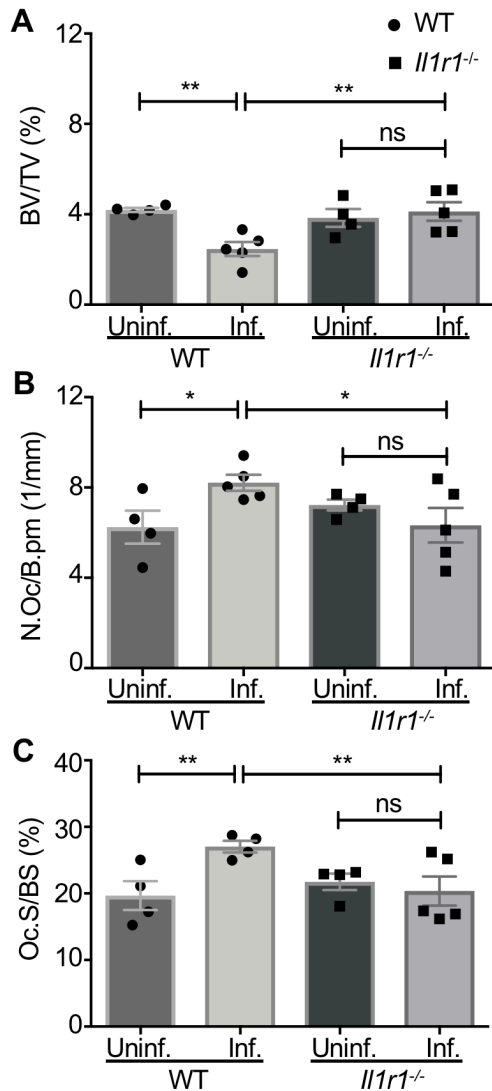
Figure 33. IL-1R contributes to infection-induced osteoclastogenesis during *S. aureus* osteomyelitis. (A-C) Following *S. aureus* infection (10^5 CFUs), female WT and *Il1r1*^{-/-} infected femurs (*n* = 5 per genotype per infection condition) and contralateral femurs from infected mice (*n* = 4 per genotype) were harvested, decalcified, processed for sectioning in paraffin, and TRAP-stained for histomorphometric analyses using OsteoMeasure software. Histomorphometric analyses of *S. aureus* infected femurs and contralateral femurs from infected mice were quantified to calculate the trabecular bone volume/total volume (BV/TV) (%) **(A)**, the number of osteoclasts per bone perimeter (N.Oc/B.pm) (1/mm) **(B)**, and the osteoclast surface per bone surface (Oc.S/BS) (%) **(C)** in the distal femur. Symbols represent individual data points from each mouse (WT = circles; *Il1r1*^{-/-} = squares), the top line of each bar represents the mean, and error bars represent standard deviation. All statistical comparisons used a two-way ANOVA and Fisher's Least Significant Difference (LSD) test to compare differences in trabecular bone composition of infected and contralateral, uninfected femurs of WT and *Il1r1*^{-/-} mice. * $p < 0.05$, ** $p < 0.01$, ns = not significant.

Histomorphometric analysis revealed that *S. aureus* infection enhances osteoclastogenesis and trabecular bone loss in an IL-1R-dependent manner. However, bone volume and remodeling are also significantly impacted by osteoblast function. In order to determine the contribution of osteoblasts toward altered bone homeostasis and trabecular bone loss during staphylococcal osteomyelitis, we measured bone mineralization in the trabecular bone of infected WT and *Il1r1*^{-/-} mice. No differences were observed in mineralizing surface, bone formation rate, or mineral apposition rate between WT and *Il1r1*^{-/-} mice **(Figure 34A-C)**. These data indicate that IL-1R signaling does not drive differences in trabecular osteoblastic function during *S. aureus* infection, and that the decrease in trabecular BV/TV is not a function of decreased osteoblastic bone formation.

S. aureus triggers osteoclastogenesis of RANKL-primed myeloid cells through MyD88 and IL-1R signaling

Staphylococcal infection causes bone loss and enhanced osteoclastogenesis in trabecular bone. Accordingly, we hypothesized that secreted bacterial factors might augment osteoclast differentiation. To test this hypothesis, we measured osteoclast differentiation of RANKL-primed myeloid progenitors after stimulation with *S. aureus* culture supernatant or a vehicle control. To avoid induction of cell death in myeloid cells, we used a *S. aureus* strain lacking the alpha-type PSMs, which we previously demonstrated are both necessary and sufficient for causing cell death when staphylococcal supernatants are applied to murine bone marrow-derived macrophages (BMMs) [31, 32].
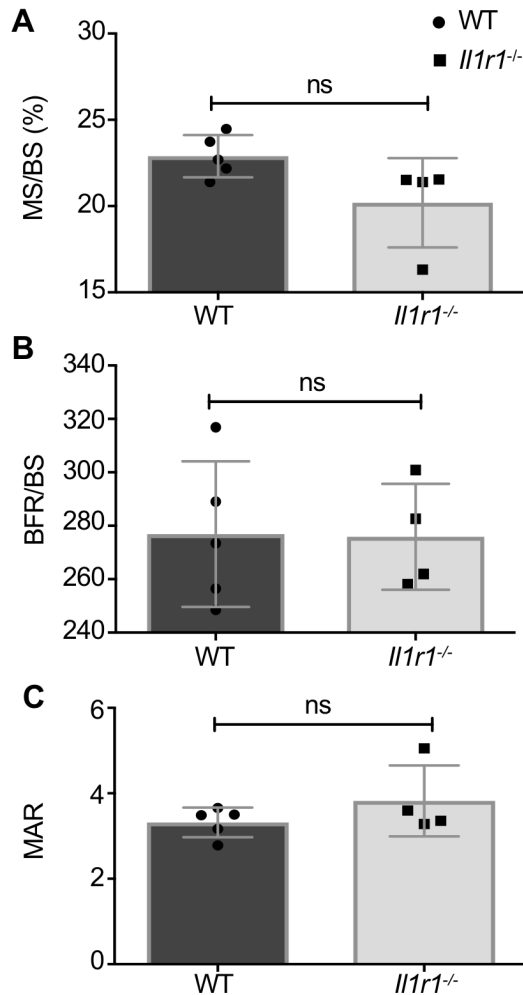
Figure 34. WT and *Il1r1*$^{-/-}$ mice have similar bone formation rates and osteoblast activity in trabecular bone during *S. aureus* osteomyelitis. (A-C) Female mice were infected with 10^5 *S. aureus* CFUs (WT $n = 5$, *Il1r1*$^{-/-}$ $n = 4$), with 20 mg/kg calcein injected intraperitoneally on days 8 and 12 post-infection. Femurs were harvested at day 14 post-infection, and embedded in poly(methyl methacrylate) for sectioning. Calcein incorporated into the trabecular bone, and single- and double-labeled fluorescent surfaces were traced relative to total bone surface using OsteoMeasure software. **(A-C)** OsteoMeasure software was used to calculate mineralizing surface per bone surface (MS/BS) (%) **(A)**, bone formation rate per bone surface (BFR/BS) **(B)**, and mineral apposition rate (MAR) **(C)** from WT and *Il1r1*$^{-/-}$ infected femurs. Symbols represent individual data points from each mouse (WT = circles, *Il1r1*$^{-/-}$ = squares), the top line of each bar represents the mean, and error bars represent standard deviation. Unpaired *t*-tests were used to compare measurements of osteoblast activity *in vivo* between infected WT and *Il1r1*$^{-/-}$ mice. ns = not significant.

As we saw in Chapter II, stimulation of RANKL-primed BMMs from WT mice with toxin-deficient supernatant can result in a dramatic increase in mature osteoclasts, as identified as TRAP$^+$ multinucleated cells, relative to vehicle control. To determine whether this bacterial enhancement of osteoclastogenesis was dependent on IL-1R signaling, we performed similar experiments with cells isolated from immunodeficient mice. We discovered that *Myd88$^{-/-}$*, *Il1r1$^{-/-}$*, and *Il1b$^{-/-}$* cells do not undergo *S. aureus*-mediated osteoclastogenesis to the same extent as WT cells **(Figure 35A, 35B, 35D; Figure 36)**. In fact, MyD88 was completely necessary for enhanced osteoclastogenesis in response to *S. aureus* supernatants. Cells unable to make the IL-1R or IL-1β were able to undergo some level of *S. aureus*-mediated osteoclastogenesis, but had significantly fewer TRAP$^+$ multinucleated cells than WT cells. Also, cells deficient in IL-1α displayed an enhanced ability to undergo *S. aureus*-mediated osteoclastogenesis, but the mechanism remains unclear **(Figure 35C and 36)**. Moreover, to test whether *S. aureus* stimulation prior to osteoclast commitment could inhibit subsequent RANKL-mediated osteoclastogenesis of these immunodeficient cells, we stimulated BMMs with *S. aureus* Δ*psm* supernatants before RANKL treatment for 5 days. The loss of MyD88 signaling completed ablated the ability of *S. aureus* to inhibit RANKL-mediated osteoclastogenesis, cells deficient in the IL-1R or IL-1β displayed some inhibition of osteoclast differentiation, and cells deficient in IL-1α were able to potently inhibit RANKL-mediated osteoclast formation, with almost no osteoclasts observed when treated with the highest dose of *S. aureus* Δ*psm* supernatants **(Figure 37A-E)**. Notably, cells unable to undergo MyD88 and IL-1R signaling are still able to differentiate into osteoclasts via canonical RANKL stimulation to the same extent **(Figure 38A-D)**.
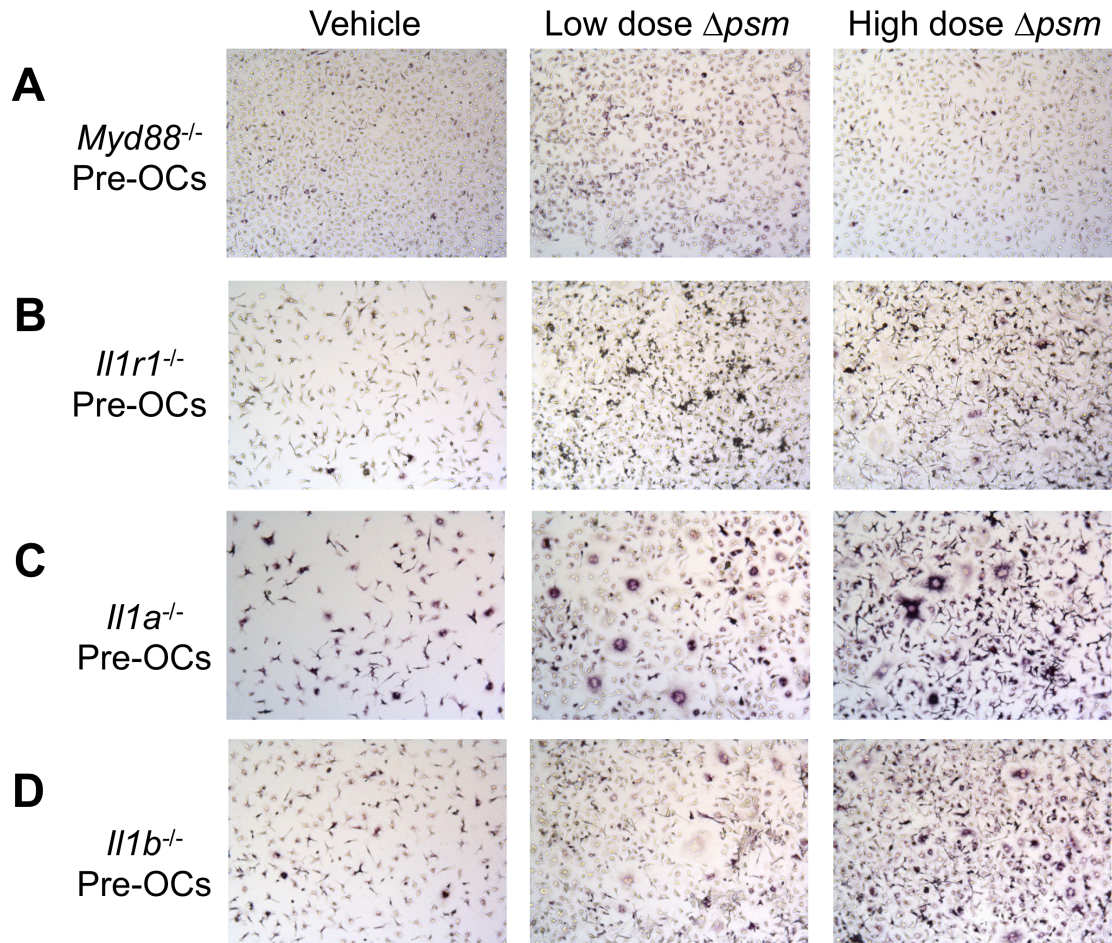
Figure 35. Enhancement of osteoclastogenesis by *S. aureus* supernatant is dependent on MyD88 and in part on IL-1R signaling pathways.

(A-D) Osteoclast precursors were generated from *Myd88*$^{-/-}$ **(A)**, *Il1r1*$^{-/-}$ **(B)**, *Il1a*$^{-/-}$ **(C)**, and *Il1b*$^{-/-}$ **(D)** primary BMMs plated at 50,000 cells per well by treating with M-CSF and RANKL for 2 days. After washing with PBS, the cells were stimulated with vehicle (RPMI; left column), Δpsm supernatant at 5% (middle column) or 25% (right column), and M-CSF. Cells were TRAP stained at day 6 and imaged at 10X.
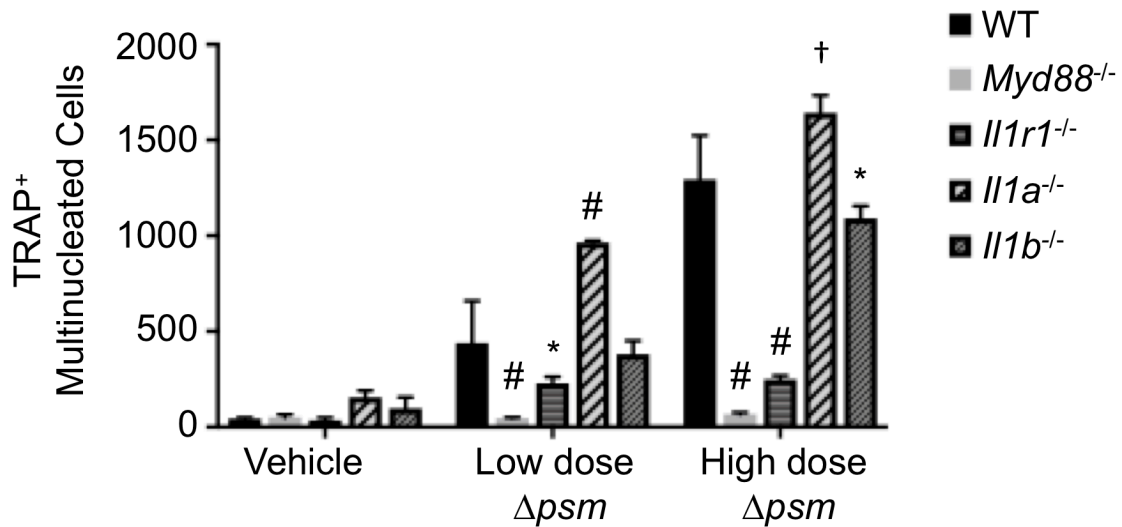
Figure 36. MyD88 and IL-1R signaling are required for enhancement of osteoclastogenesis by *S. aureus* supernatants.

TRAP^{+} multinucleated cells were quantified using OsteoMeasure software from WT, *MyD88^{-/-}*, *Il1r1^{-/-}*, *Il1a^{-/-}*, and *Il1b^{-/-}* cells ($n = 3$ wells per genotype), representative of triplicate experiments. A two-way ANOVA was used to compare genotype to WT and dosage effects of *S. aureus* Δ*psm* supernatant, with Dunnett's multiple comparisons test. * $p < 0.05$, † $p < 0.001$, # $p < 0.0001$.
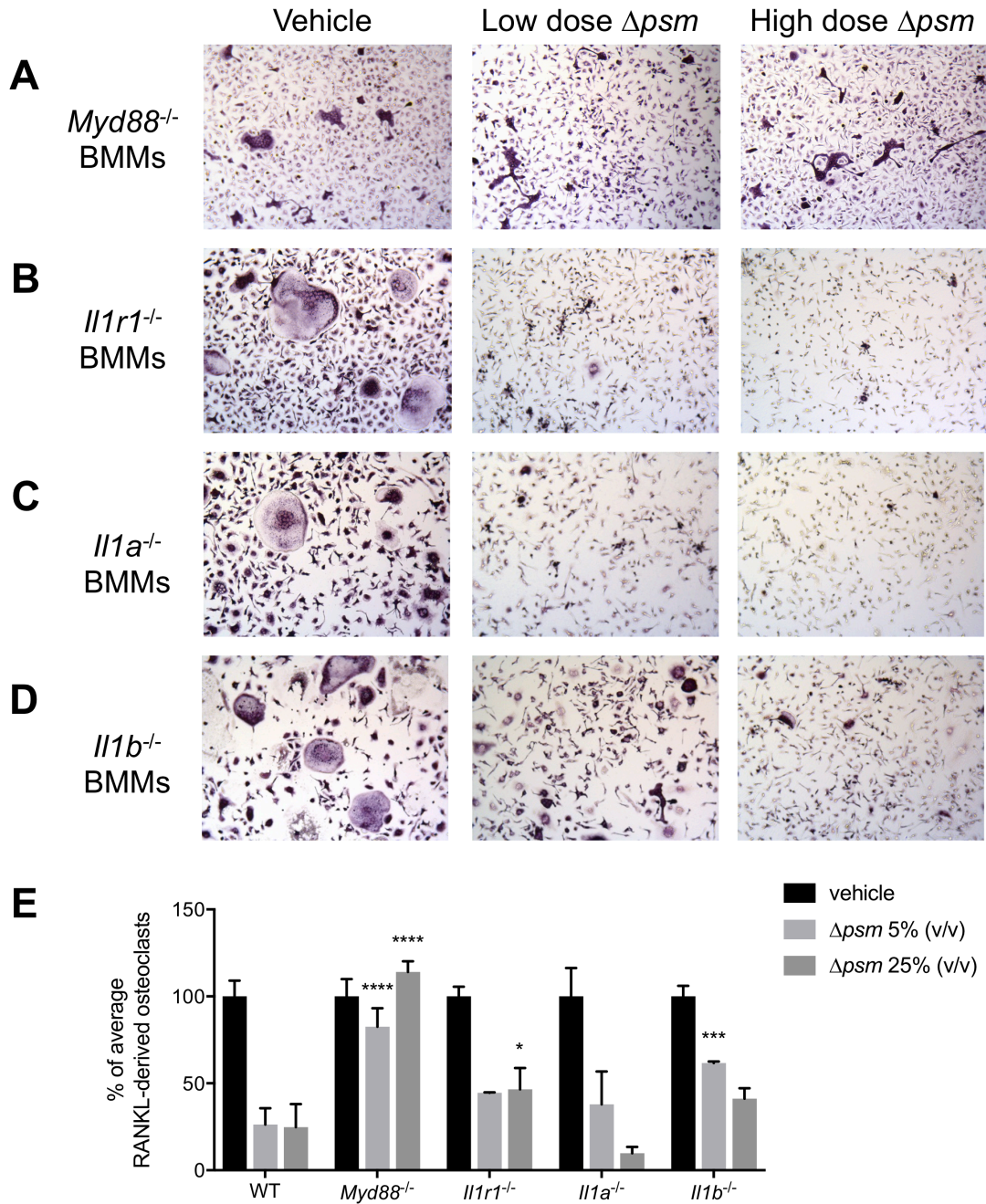
Figure 37. *S. aureus* stimulation of BMMs prior to RANKL treatment inhibits osteoclast differentiation and is dependent on MyD88 and in part on IL-1R signaling. (A-E) *Myd88*^{-/-} (A), *Il1r1*^{-/-} (B), *Il1a*^{-/-} (C), and *Il1b*^{-/-} (D) BMMs were plated at 50,000 cells per well and treated with M-CSF and vehicle (RPMI; left column) or Δ*psm* supernatant at 5% (middle column) or 25% (right column). After 24 hours of stimulation, cells were washed with PBS and fresh media was replenished with M-CSF and 35 ng/mL RANKL. At day 6 in culture, cells were TRAP stained and imaged at 10X. TRAP^{+} multinucleated cells were quantified, and the average vehicle-treated counts from each genotype was used to calculate the percent of average RANKL-derived osteoclasts (E).
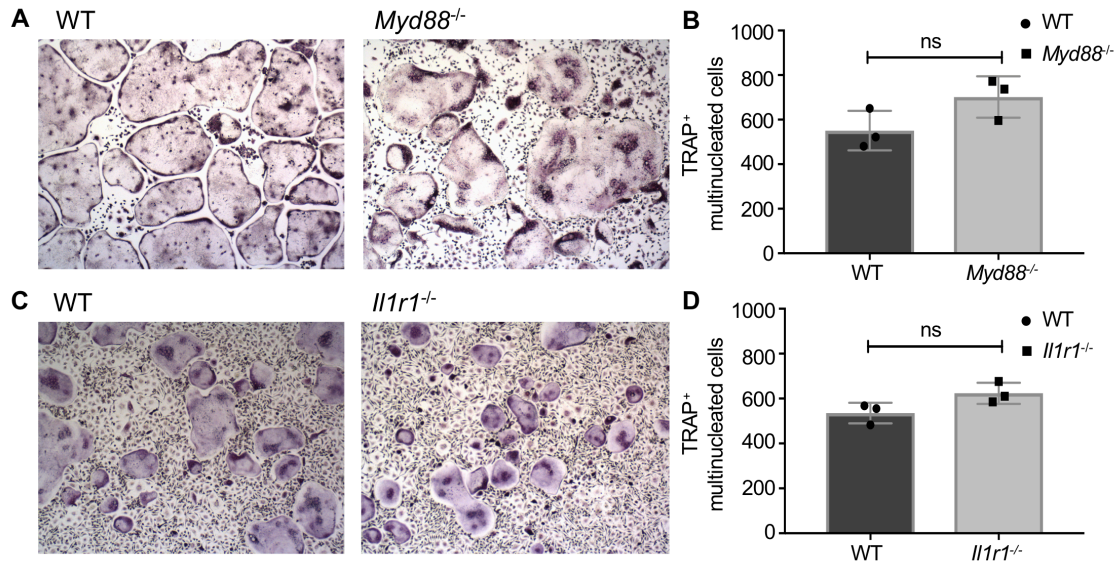
Figure 38. WT, *Myd88*-/-, and *Il1r1*-/- cells undergo RANKL-mediated osteoclastogenesis at similar levels. (A-D) WT, *Myd88*-/-, and *Il1r1*-/- BMMs were plated at 50,000 cells per well in a 96-well plate. Cell cultures were supplemented with 35 ng/mL RANKL and 1:20 CMG14-12 supernatant as an M-CSF source. Media and reagents were replenished on days 4 and 6 in culture (i.e. RANKL stimulation was continued for the entire experiment), and cells were fixed and stained for TRAP expression on day 7. **(A-D)** Cells were imaged at 10X **(A, C)** and TRAP+ multinucleated cells were counted using the OsteoMeasure software **(B, D)**. Symbols represent individual well counts from (WT = circles, *Myd88*-/- and *Il1r1*-/- = squares), the top of each bar represents the mean, and error bars represent standard deviation. Unpaired *t*-tests were used to compare cell counts between WT and *Myd88*-/- or *Il1r1*-/- cells. ns = not significant.

We next tested the role of IL-1 blockade on osteoclastogenesis using WT or *Il1r1*^{-/-} cells, with or without IL-1R antagonist (IL-1ra) treatment. In WT cells, IL-1ra treatment during RANKL pre-commitment and before *S. aureus* stimulation led to 50% fewer osteoclasts **(Figure 39)**. This decline in *S. aureus*-enhanced osteoclastogenesis results in differentiation to a similar level as is observed in *Il1r1*^{-/-} osteoclast precursors **(Figure 39)**. Moreover, IL-1ra treatment during Δ*psm* supernatant treatment did not affect the number of TRAP⁺ multinucleated cells, as compared to the BSA vehicle controls given at the same time **(Figure 39)**. In order to verify that IL-1ra treatment worked as expected in WT cells, we treated RANKL-committed osteoclast precursors with vehicle, IL-1β, or a combination of IL-1β and IL-1ra. In this assay we confirmed that IL-1β induced TRAP+ multinucleated cells from osteoclast precursors compared to vehicle, and also that IL-1ra treatment blocked this enhancement **(Figure 40A-C)**. Collectively, these observations indicate that MyD88 and the IL-1R are required for *S. aureus*-mediated enhancement of osteoclastogenesis. Therefore, although MyD88 and IL-1R are critical mediators of the anti-staphylococcal immune response, *S. aureus* infection also elicits osteoclast-mediated bone loss through MyD88 and IL-1R signaling pathways.
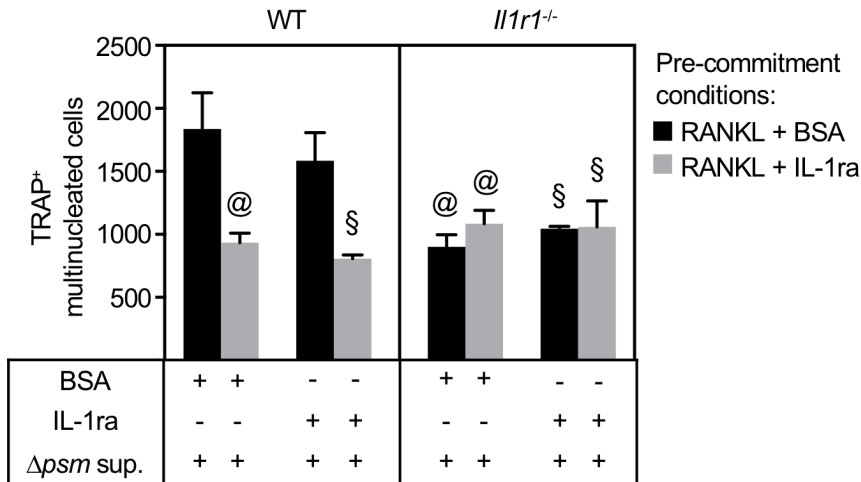
Figure 39. IL-1R signaling drives *S. aureus* enhancement of osteoclast differentiation *in vitro*. WT and *Il1r1$^{-/-}$* enriched BMMs were stimulated with 35 ng/mL exogenous RANKL for 2 days before stimulating with Δ*psm* supernatants for four days. In order to determine the contribution of IL-1 signaling in this assay, vehicle (0.1% low endotoxin BSA) or recombinant murine IL-1ra (1 μg/mL) were added during the 2 days of RANKL pre-commitment (BSA, black bars; IL-1ra, grey bars) or during the 4 days of Δ*psm* supernatant stimulation (indicated by + under each bar). The top line of each bar represents the mean and error bars represent standard deviation. A three-way ANOVA with Tukey's multiple comparisons test compared the effects of genotype, IL-1ra treatment during RANKL pre-commitment, and IL-1ra treatment during Δ*psm* supernatant stimulation. Statistical comparisons to WT cells pre-committed with RANKL + BSA and Δ*psm* supernatant + BSA (first black bar from the left) are reported as @ $p < 0.05$, or compared to WT cells pre-committed with RANKL + BSA and Δ*psm* supernatant + IL-1ra (second black bar from the left) are reported as § $p < 0.05$. Comparisons between all RANKL + IL-1ra pre-commitment conditions (grey bars) were non-significant
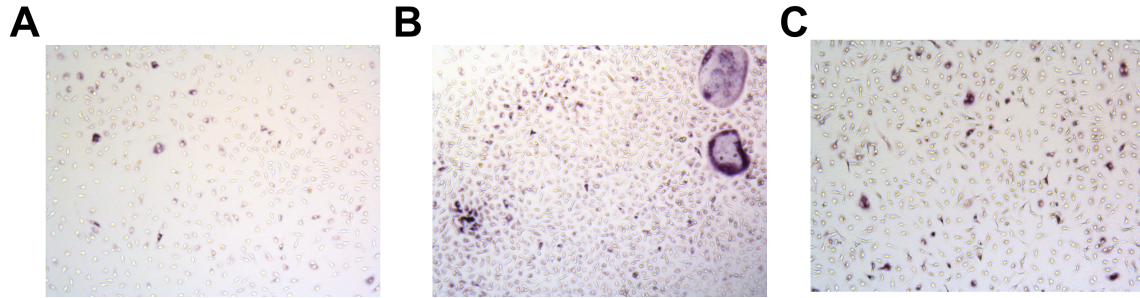
Figure 40. Osteoclast differentiation from precursor cells is promoted by IL-1β, and this can be blocked with IL-1ra. (A-C) WT osteoclast precursors were generated with M-CSF and RANKL for 2 days in culture, washed with PBS, after which fresh media and M-CSF were replenished with BSA vehicle **(A)**, 10 ng/mL recombinant murine IL-1β **(B)**, or simultaneously treated with 10 ng/mL recombinant murine IL-1β and 1 µg/mL IL-1ra **(C)**. Cells were TRAP stained at day 6 and imaged at 10X.

Discussion

Bacterial osteomyelitis is a debilitating invasive infection of bone that is accompanied by significant damage to skeletal tissues and the surrounding vasculature. Using a model of post-traumatic *S. aureus* osteomyelitis, we have detailed dramatic architectural and cellular bone remodeling alterations that accompany *S. aureus* infection. In prior research, we determined that some of the cortical bone loss observed during infection is due to *psm-* and *agr*-dependent mechanisms [31]. This observation is in keeping with the findings of Gillaspy et al., who used a rabbit model of osteomyelitis and observed significantly less bone pathology when infecting with an *agr* mutant [80]. However, the observation of residual bone pathology in mice infected with an *agr* mutant in our osteomyelitis model led us to postulate that host responses to bacterial infection may also contribute to bone loss. The focus of this work was therefore to delineate critical host responses to staphylococci in bone and to elucidate how an innate immune response might impact bone homeostasis.

In this study, we focused primarily on MyD88 and IL-1R signaling cascades given their established roles in innate immune responses against *S. aureus* in other models of infection [76, 77, 199, 264-269], in concert with the known effects of these signaling pathways on bone cell function [136, 140, 242, 261]. Additionally, patients with single nucleotide polymorphisms (SNPs) in *Myd88, Il1a,* and *Il1r1* genes have an increased risk of osteomyelitis and inflammatory joint disorders, further underscoring the importance of these immune pathways in skeletal homeostasis [102, 107, 108, 285-287].

A robust innate immune response was observed in *S. aureus* infected femurs, with abundant levels of pro-inflammatory cytokines IL-1α, IL-1β, IL-6, and TNFα detectable as

soon as one day after infection, similar to what has been reported in other musculoskeletal infection models [60, 180]. Many cytokines with increased abundance in infected versus mock infected femurs are encoded by IL-1 target genes, including IL-1α, IL-1β, IL-6, MCP-1 (CCL2), and the murine IL-8 homologs, KC (CXCL1) and MIP-2 (CXCL2) [288, 289]. In turn, IL-1 cytokines and IL-6 also promote the release of IL-17 and subsequent G-CSF production, both of which were highly abundant in *S. aureus* infected femurs [290]. These data suggest a role for IL-1 signaling in orchestrating downstream inflammatory responses to pathogens in bone. Growth factors and chemokines that support myeloid cell influx and expansion after infection, including M-CSF, G-CSF, MCP-1 (CCL2), MIP-1α (CCL3), MIP-1β (CCL4), KC (CXCL1) and MIP-2 (CXCL2), are also highly abundant in *S. aureus* infected femurs relative to mock infected femurs. This observation parallels other reports demonstrating increased levels of myeloid chemokines from osteoblasts after *S. aureus* infection, and a role of myeloid chemokines and growth factors in supporting osteoclastogenic bone degradation by promoting expansion of osteoclast precursor cells [291, 292]. Moreover, many of these chemokines have been shown to coordinate neutrophil responses during acute inflammation [293]. These data partially overlap with early cytokine signatures measured in a pin prosthetic implant model of *S. aureus* biofilm infection, with IL-1β, IL-6, TNFα, IL-12p70, and IL-17 detected in infected tissues. However local inflammation during biofilm infection was also characterized by increased abundance of IL-2 [294], which was not significantly elevated in our infection model. However, the development of a biofilm has been shown to attenuate the host pro-inflammatory response in a catheter *S. aureus* biofilm model, as measured by decreased levels of IL-1β, TNFα, CXCL2, and CCL2 [172]. Future studies should continue to

delineate how implant-associated biofilms skew the immune response during osteomyelitis.

The early increase in cardinal pro-inflammatory cytokines after *S. aureus* infection indicates that the post-traumatic model of osteomyelitis used in this study is most representative of acute osteomyelitis. However, the bone pathology visualized by day 14 post-infection has clear features suggestive of chronic infection, including significant reactive bone formation and the presence of sequestra [295]. Consistent with a possible shift from acute to chronic infection, we observed production of IFNγ and IL-17 at later time points post-infection, which could represent *S. aureus*-specific adaptive Th1/Th17 responses [294]. Delineating the cytokine milieu at later time points after infection will help to more comprehensively characterize the inflammation accompanying osteomyelitis in this model.

Based on the robust early inflammatory responses to *S. aureus* in bone coupled with the detection of multiple IL-1 associated cytokines, we focused on the role of MyD88 and IL-1R signaling in coordinating antibacterial defenses during osteomyelitis. Furthermore, since several cardinal pro-inflammatory cytokines, including IL-1, have direct effects on skeletal cell differentiation and function, we hypothesized that MyD88 and IL-1R-dependent signaling pathways would be necessary for control of bacterial proliferation during osteomyelitis, but that these same pathways might also contribute to pathogen-induced bone loss through actions on skeletal cells. To determine the contribution of MyD88 and IL-1R signaling towards antibacterial immune responses during *S. aureus* osteomyelitis, we infected mice globally deficient in MyD88, IL-1R, IL-1α, and IL-1β and measured bacterial burdens and morbidity. We found that MyD88 and IL-1R signaling are

required to control bacterial burdens in bone in mice infected with a high dose inoculum. Furthermore, even with a lower *S. aureus* inoculum, a timecourse experiment revealed that *Il1r1*$^{-/-}$ mice had a delay in ability to control bacterial burdens. In order to determine the relative contributions of IL-1 isoforms to IL-1R-mediated antibacterial immunity in bone, we infected *Il1a*$^{-/-}$ or *Il1b*$^{-/-}$ mice and compared bacterial burdens to those observed in WT and *Il1r1*$^{-/-}$ mice. Mice lacking either IL-1α or IL-1β sustained bacterial burdens not statistically different from bacterial burdens harbored by WT mice, but *Il1a*$^{-/-}$ and *Il1b*$^{-/-}$ mice both harbored significantly less bacterial CFUs than *Il1r1*$^{-/-}$ mice. These data suggest that the loss of both cytokines may be required to recapitulate the enhanced bacterial burdens in *Il1r1*$^{-/-}$ mice. Moreover, the extensive repertoire of innate receptors that signal through MyD88 (e.g. TLRs) likely promote a more effective antibacterial response to *S. aureus,* as MyD88 signaling is critical to prevent disseminated disease and death during osteomyelitis.

Our findings that MyD88 and IL-1R mediate antibacterial protection in bone are consistent with data from previous studies demonstrating that *Myd88*$^{-/-}$ and *Il1r1*$^{-/-}$ mice have enhanced susceptibility to bacterial infection in various experimental models [77, 78, 184, 278]. Several studies have also reported that IL-1R signaling contributes to the early influx of neutrophils and abscess formation to protect against *S. aureus* cutaneous and prosthetic joint infection [76, 77, 199, 207]. Elevated levels of GM-CSF, G-CSF, and CXCL1 in WT mice suggest that neutrophil influx and/or expansion is also a critical early response to *S. aureus* in bone to prevent continued bacterial replication and spread. Interestingly, the neutrophilic cytokine response was delayed in *Il1r1*$^{-/-}$ mice in response to *S. aureus,* which in congruent with other *Il1r1*$^{-/-}$ mouse models in response to

141

inflammatory stimuli [272-274]. Disorganized abscess architecture in $Il1r1^{-/-}$ infected femurs may indicate improper neutrophil mobilization without IL-1R signaling as an underlying mechanism for the inability to control bacterial burdens. Furthermore, we have previously shown that neutrophil depletion leads to significantly increased bacterial burdens during *S. aureus* osteomyelitis [32]. Here, we determined that relative neutrophil abundance was lower in $Il1r1^{-/-}$ mice at early and late time points in the infected femurs, suggesting that $Il1r1^{-/-}$ mice have altered systemic neutrophil responses that may correlate with alterations in G-CSF and GM-CSF data. Lower amounts of neutrophils in both the infected and contralateral, uninfected femurs of $Il1r1^{-/-}$ mice relative to WT mice support prior observations that $Il1r1^{-/-}$ mice have a defect in granulopoiesis [272-274]. Together these reports detail the importance of IL-1R signaling to protect against *S. aureus* bone infections by coordinating an effective anti-staphylococcal neutrophil response.

The inability of $Myd88^{-/-}$ and $Il1r1^{-/-}$ mice to mount appropriate anti-staphylococcal immune responses and the characteristic differences in bone remodeling between WT and $Il1r1^{-/-}$ mice led us to confirm these phenotypes with littermate controls bred heterozygously. Contradictory reports have detailed either no difference in bone mass of $Il1r1^{-/-}$ mice [296], low bone mass in $Il1r1^{-/-}$ mice [297], or greater bone mass in $Il1r1^{-/-}$ mice [139, 298] when compared to WT comparators. These studies used various WT comparators (129/J, 129/Sv, BALB/cA, C57BL/6), and also varied with respect to the assessment of mouse age and gender. Additionally, $Myd88^{-/-}$ mice have altered intestinal barrier function and differences in the microbiome, which can lead to differences in immune function and bone mass [75, 279, 281-284]. Therefore, breeding of heterozygous colonies allowed us to reduce the confounding influence of mouse genotype and

microbiome effects to confirm the importance of MyD88 and IL-1R signaling in antibacterial responses and bone remodeling.

To investigate the mechanisms by which *S. aureus* alters bone homeostasis to incite bone destruction and reactive bone formation, we measured cortical and trabecular changes in bone architecture via μCT, quantified changes in skeletal cell function and activity *in vivo* using standard bone histomorphometry, and cultured skeletal cells *in vitro* to determine how *S. aureus* influences skeletal cell differentiation. These data reveal that *S. aureus* osteomyelitis induces changes in bone turnover both locally at the inoculation site, as well as in more distal areas not grossly impacted by abscess formation, leading to the significant loss of cortical and trabecular bone. *Il1r1*$^{-/-}$ mice exhibited more dramatic cortical bone changes, which may be due to differences in bone remodeling processes between WT and *Il1r1*$^{-/-}$ mice, the fact that *Il1r1*$^{-/-}$ mice harbor increased bacterial burdens over the duration of infection, or a combination of these factors. Previous studies have shown that the loss of IL-1R and MyD88 signaling enhances healing of sterile bone defects [299], which may explain the enhanced volume of reactive callus formed on the cortical bone of *Il1r1*$^{-/-}$ mice in our findings. Although, we did not observe significant differences in osteoblast-mediated bone parameters in trabecular bone, it is possible that there are significant differences in osteoblast or pre-osteoblast differentiation and function in healing cortical bone (callus).

Trabecular bone is the major site of homeostatic bone remodeling [277], and bone loss here is thought to be multifactorial with potent contributions from inflammation, altered skeletal cell differentiation, and direct interaction with bacterial cells. With respect to the latter mechanisms, we detected viable *S. aureus* in the regions of the femur

143

encompassing trabecular bone throughout the course of infection. *S. aureus* infection enhanced the number of osteoclasts as well as the actively resorbing trabecular bone surface during osteomyelitis in WT mice, thereby corroborating previous observations of enhanced osteoclast surface from *S. aureus* infected human bone biopsies [300]. This may reflect, in part, direct interactions with *S. aureus* protein A which induces osteoclastogenesis through TNFR1 and EGFR [40]. However, other bacterial factors that directly enhance osteoclastogenesis *in vivo* remain to be determined. In contrast, *Il1r1*$^{-/-}$ mice were protected from enhanced osteoclastogenesis and trabecular bone loss. Excitingly, although *Il1r1*$^{-/-}$ mice harbored higher bacterial burdens throughout the course of infection, they did not exhibit trabecular bone loss or increased osteoclastogenesis relative to contralateral, uninfected femurs. Taken together, these *in vivo* bone remodeling data indicate that *S. aureus* osteomyelitis enhances osteoclastogenesis and triggers trabecular bone loss in WT mice, mainly through IL-1R-dependent effects on osteoclasts.

In vitro osteoclast differentiation assays further supported the observation of increased osteoclastogenesis in response to *S. aureus in vivo*, as staphylococcal supernatants significantly enhanced osteoclast formation from RANKL-primed WT precursor cells. These data corroborate other reports demonstrating that infection of host cells *in vitro* with live *S. aureus* enhances osteoclastogenesis and bone resorbing activity [241], and our *in vivo* data now provide evidence that this enhanced osteoclastogenesis translates to bone loss during infection. Mechanistically, genetic deletion of *Myd88, Il1r1,* and *Il1b* and molecular inhibition of IL-1R signaling were found to confer resistance to *S. aureus*-enhanced osteoclastogenesis. Consistent with previously published reports, endogenous IL-1 has been described to promote osteoclastogenesis *in vitro* through

144

synergistic signaling of the IL-1 and RANK receptors in the absence of infection [301]. Canonical osteoclast differentiation is initiated by RANK receptor signaling to activate the transcription factors NFATc1 and cFos, which in turn increase IL-1R expression. As we and others have shown, this allows IL-1 to signal osteoclast precursors to potentiate osteoclast formation by activating osteoclast-specific genes, and IL-1 has been reported to enhance "pathologically activated osteoclasts" that favor bone loss [136, 139, 140, 143, 242, 261, 301]. In the context of infection, *S. aureus* and specific staphylococcal toxins have been found to stimulate the production of IL-1 cytokines [302-304]. Moreover, IL-1 cytokines have been described to promote osteoclastogenesis *in vitro* and lead to bone destruction in murine models of rheumatoid arthritis and autoinflammatory disorders [140, 236, 242, 305, 306]. Therefore, these data are consistent with other observations and suggest that IL-1 signals onto osteoclast precursors to enhance osteoclastogenesis and trabecular bone resorption during infection. However, residual osteoclast formation observed in *Il1r1*^{-/-} cells suggests that while MyD88 is required for osteoclastogenesis in response to staphylococcal supernatant, there are both IL-1R-dependent and independent mechanisms involved. These *in vitro* studies support our findings that a major driver of bone loss during *S. aureus* osteomyelitis is coordinated by IL-1R-mediated osteoclast enhancement.

Data presented in this chapter highlight MyD88 and IL-1R signaling as critical pathways supporting anti-staphylococcal immunity in bone, but also implicate these signaling cascades in promoting bone loss during osteomyelitis. There are a few limitations of the experimental approach outlined in this study. We used globally deficient knockout mice to elucidate how MyD88-dependent IL-1R signaling impacts bone homeostasis and

anti-staphylococcal immunity. In certain *S. aureus* infection models, TLR2 and TLR9 have been shown to contribute to anti-staphylococcal immunity [188, 264, 278]. Given that the adapter protein MyD88 is necessary to relay signals from other upstream receptors including TLRs, Chapter IV will explore the relative contributions of other MyD88-dependent receptors in the pathogenesis of osteomyelitis. *In vitro* osteoclastogenesis assays imply that other MyD88-dependent receptors can sense and respond to components of *S. aureus* in culture to enhance osteoclastogenesis. Accordingly, osteoblast and osteoclast lineage cells have been shown to be activated *in vitro* through TLRs and IL-1R signaling to favor bone resorption [51, 55, 307]. During staphylococcal osteomyelitis, it remains unclear how much pathogen-induced bone loss occurs as result of direct osteoclast stimulation versus indirect perturbations of bone homeostasis that involve osteoblasts. This could be tested using MyD88 skeletal cell lineage specific knockout mice. Furthermore, the IL-1R-expressing target cells that stimulate anti-staphylococcal immunity and the source and isoform of IL-1 that promotes bone loss remain unclear.

Collectively, this chapter details the paradoxical roles of innate immune signaling pathways in the pathogenesis of osteomyelitis. Although MyD88 and IL-1R signaling elicit antibacterial responses during bone infection to protect against bacterial proliferation, dissemination, and systemic disease, they also contribute to host-mediated bone loss. Our findings also highlight a specific MyD88- and IL-1R-dependent mechanism of osteoclast enhancement, thereby uncovering a new mechanism for bone loss during *S. aureus* osteomyelitis.

CHAPTER IV

THE CONTRIBUTION OF TLR2 AND TLR9 TO

ANTIBACTERIAL IMMUNITY AND OSTEOCLAST

FORMATION DURING *S. AUREUS* OSTEOMYELITIS

Introduction

Many disease states significantly alter bone homeostasis and lead to bone loss by perturbing the equilibrium between osteoblasts that deposit new bone and osteoclasts that resorb bone [180, 235, 237]. Bone loss occurs when osteoclast differentiation is favored leading to excessive bone resorption [180], which can be seen during systemic inflammatory conditions such as rheumatoid arthritis and inflammatory bowel disease [237], as well as locally due to periodontal disease and joint inflammation [56, 235, 236]. As discussed in Chapter III, dramatic local inflammation occurs subsequent to the establishment of *S. aureus* osteomyelitis, and this inflammation causes bone loss [31, 308]. *S. aureus* contains conserved molecular patterns that are recognized by PRRs to initiate innate immune responses during infection. Skeletal cells express PRRs, although their contribution to changes in bone physiology and pathogen clearance have not been defined during osteomyelitis.

Though RANKL-dependent osteoclastogenesis is well defined as the canonical osteoclast differentiation pathway, immunologic crosstalk between other signaling pathways and transcription factors has been shown to promote osteoclastogenesis [234, 253]. Transcription factor activity and proinflammatory cytokine production downstream of PRRs have been implicated as potential mechanisms for non-canonical (RANKL-

independent) osteoclast differentiation, such as TNFα and IL-1β, as we have corroborated in Chapters II and III [51, 53, 57, 58, 144, 246, 253, 254]. Specifically, RANKL signaling on myeloid cells induces signaling cascades through TRAF6, NIK, IKK, p38, ERK, and JNK, activating non-canonical and canonical NFκB, AP-1, MITF, and NFATc1 transcription factors [247]. These differentiation pathways overlap with immune-mediated signaling and provide potential for crosstalk downstream of immune activation. In addition to the IL-1R, many TLRs (e.g., 1, 2, 6, 9) are upstream of TRAF6 and MyD88 and have been implicated in the anti-staphylococcal immune response [45]. Extracellular TLR1/2 and TLR2/6 heterodimers engage *S. aureus* lipoproteins [181, 182]. Additionally, *S. aureus* can stimulate endosomal TLR9 during bacterial replication following internalization into cells [183]. Downstream of TLR2 and TLR9, *S. aureus* activates signaling factors TRAF6, NIK, IKK and NFκB [61], all of which are also necessary during osteoclast differentiation.

Crosstalk between RANK receptor signaling and these immune pathways likely cause perturbations in osteoclastogenesis due to overlapping TRAF6 activation **(Figure 41)**. TRAF6 overexpression enhances osteoclastogenesis from precursor cells [254], but depending on the skeletal cell culture system, PRR ligation has variable outcomes. Our findings in Chapter III suggest that MyD88 plays a role in mediating *S. aureus*-enhancement and inhibition of osteoclastogenesis. These findings are supported by studies showing that PRR agonists can inhibit RANKL-naïve myeloid cells from subsequently becoming osteoclasts [51, 248, 250]. However, osteoclast differentiation is promoted if PRRs are activated on RANKL-committed osteoclast precursors [25, 51, 236, 240]. As we and other have shown, collectively these observations indicate that the effect of PRR ligation on osteoclast differentiation is complex, but once cells are primed with RANKL

PRR signaling appears to enhance osteoclastogenesis. However, the contribution of individual innate immune receptors to infection-associated osteoclastogenesis has not been studied in the context of *S. aureus* osteomyelitis.
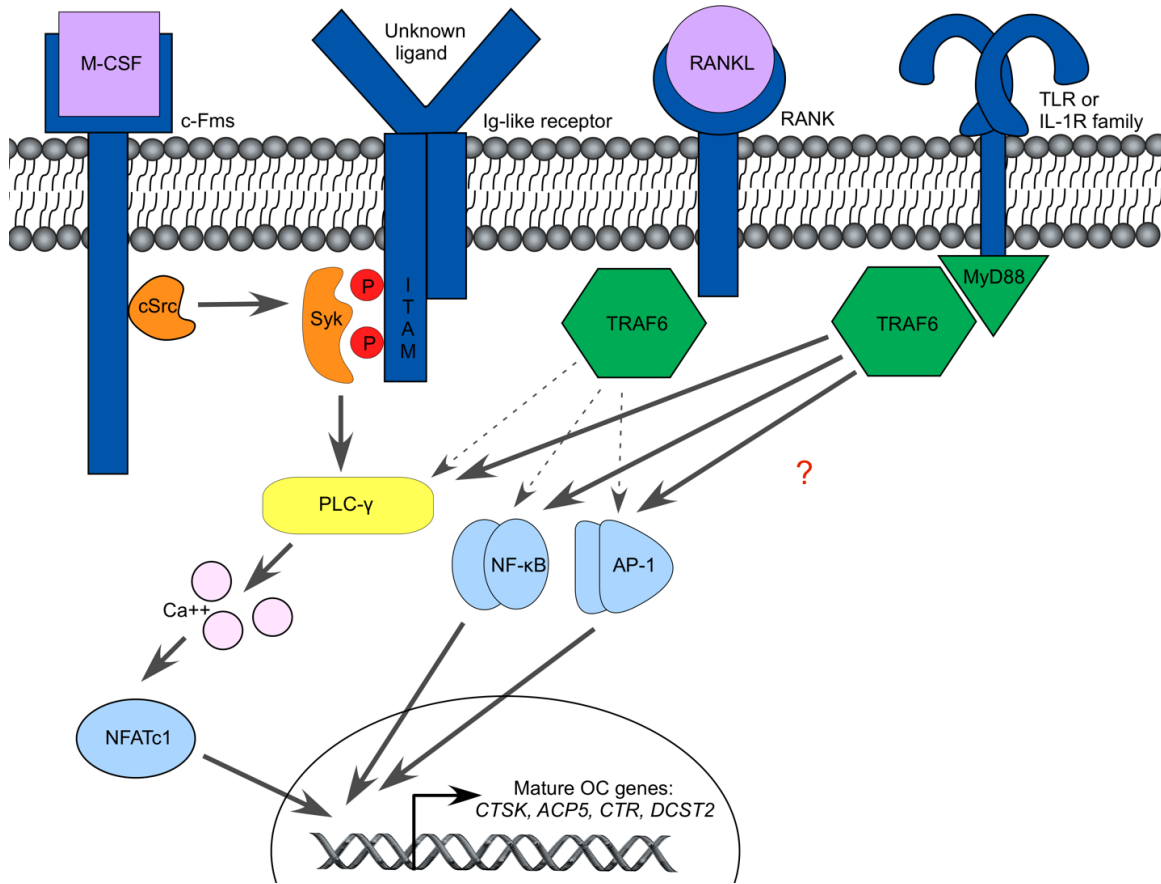
Figure 41. Osteo-immunologic crosstalk between RANK and MyD88-dependent receptors.
In a simplified schematic, osteoclastogenic signals through c-FMS, a co-stimulatory Ig-like receptor (OSCAR, TREM2), and RANK lead to cooperation between Syk kinase and TRAF6-mediated signaling to activate phospholipase C (PLC)-γ, cytoplasmic mobilization of calcium, and eventually activation of the canonical osteoclast transcription factor, NFATc1. However, TRAF6 signaling also occurs downstream of TLR and IL-1R family members through MyD88. Therefore, in the context of c-FMS and co-stimulatory receptors, either RANK or other MyD88-dependent receptors could lead to TRAF6 and transcription factors necessary for osteoclastogenesis. It has been established that RANK signaling (shown by dotted arrows) must first be activated to allow MyD88-dependent enhancement of osteoclast differentiation. Thus, the question remains, what does TRAF6 activate downstream of MyD88 (indicated by 3 black arrows to the left of the red question mark). In the nucleus, transcription factors may work together to induce osteoclast-specific genes such as *Ctsk* (cathepsin K), *Acp5* (tartrate-resistant acid phosphatase), *Ctr* (calcitonin receptor), and *Dcst2* (DC-STAMP), among others.

We speculate that innate recognition of PAMPs significantly influences physiologic bone remodeling and that skeletal cells sense and respond to both pathogenic microorganisms and the host microbiota. In support of this hypothesis, C3H/HeJ mice defective in TLR4 signaling have greater cortical thickness than C57BL/6 mice, and C3H/HeJ osteoblasts have a decreased RANKL response to LPS [309, 310]. These data suggest that some level of innate sensing is likely a normal part of homeostatic bone remodeling. However, the direct influence of PRRs or innate receptors on skeletal cells remains to be elucidated.

In this chapter, we explore whether or not the direct inoculation of *S. aureus* into the bone and absence of PRR signaling affect bone remodeling and immunity in the context of *S. aureus* osteomyelitis. As bone homeostasis is an equilibrium between both osteoblast and osteoclast lineage cells, we also begin to investigate how PRR sensing of *S. aureus* affects osteoblasts as well. Based on this background information, *we hypothesize that skeletal cells can sense and respond to innate immune stimuli to influence cytokine responses and osteoclast differentiation.* To test this hypothesis, we investigate how TLR2 and TLR9 influence *S. aureus*-altered osteoclastogenesis *in vitro*, as well as antibacterial immunity and bone remodeling in a murine model of *S. aureus* osteomyelitis.

Materials and methods

Ethics section

All experiments involving animals were reviewed and approved by the Institutional Animal Care and Use Committee at Vanderbilt University Medical Center on the animal protocols M12059 and M1800055. All experiments were performed according to NIH

guidelines, the Animal Welfare Act, and US Federal law. The murine model of osteomyelitis required inhalational anesthesia with isoflurane (1–5%). Post-operative analgesia (buprenorphine 0.5–0.1 mg/kg) was provided pre-operatively and every 8–12 hours for 48 hours post-infection. Mice were euthanized by CO_2 asphyxiation with secondary confirmation by cervical dislocation and observation of heart rate and breathing.

Bacterial strains and growth conditions

The toxin-deficient strain LAC$\Delta psm\alpha 1$-4 (Δpsm) was described previously and used for *in vitro* assays to prevent cytotoxicity in culture [31, 244]. To distinguish differences between toxin-induced and TLR-mediated bone remodeling, we infected a subset of mice with an *agr* deficient *S. aureus* strain. LACΔagr (Δagr) was described previously and induced only 50% of the bone loss compared to WT *S. aureus* during osteomyelitis [31]. All staphylococci were routinely grown on trypic soy agar (TSA) or shaking in tryptic soy broth (TSB) with 10 µg/mL erythromycin as needed.

Preparation of bacterial supernatants

To prepare concentrated bacterial supernatants, bacterial cells were grown overnight at 37°C with a 1:5 ratio of liquid media to flask size (250 mL or 1 L Erlenmeyer flask were used) and shaking at 180 rpm. The liquid media used for growth in this preparation was RPMI + 1% casamino acids. Three bacterial colonies per 50 mL of media were inoculated into each flask, and the flask was stoppered to create a hypoxic environment [32]. After 15 hours of growth, bacterial cultures were centrifuged at 8000 x g for 8 minutes at 4°C with a fixed angle rotor. Supernatants were pooled and filter

sterilized with a 0.22 μM filter. Amicon Ultra 50 mL concentration tubes were filled with 15 mL of the filter sterilized supernatant and centrifuged at 4000 x g for 30-45 minutes at 4°C. This was done three times in succession, decanting the filtrate each time, until the concentrated supernatant remaining above the filter reached 1.5 mL. Concentrated supernatants were then pooled, filter sterilized with a 0.22 μM filter, and aliquoted to freeze at -80°C for a single thaw and use.

Primary cell isolation and osteoclastogenesis assays

To obtain primary cells, 8- to 13-week old male mice were sacrificed by CO_2 asphyxiation, confirmed dead by observation, and cervically dislocated as a secondary method of euthanasia. Femurs from WT C57BL/6 mice were extracted and the muscle surrounding the femur was removed. Femurs were stored in PBS on ice until ready for skeletal cell isolation. To isolate whole bone marrow (WBM), the epiphyses (end) of femurs were cut off and discarded. To collect bone marrow cold, αMEM was flushed through the medullary cavity into a tube using a 27-gauge needle and 10 mL Luer-Lock syringe. Cells were pelleted at 1500 rpm for 5 minutes, and incubated for 10 minutes at room temperature in ACK Lysing Buffer. The reaction was quenched with 10 mL PBS, and cells were pelleted, counted, and either used in cell culture or frozen for future use.

WBM was cultured in DMEM supplemented with 10% FBS and 1X P/S, and was either used as a diverse cell population as isolated or used to enrich for bone marrow macrophages (BMMs) by plating between 8-13x10^6 cells per 10 cm dish in media supplemented with 100 ng/mL recombinant murine M-CSF for 4 days. After 4 days in

culture, enriched BMMs were scraped into a single cell suspension to plate for use or to freeze down for later use.

To isolate primary osteoblasts, the diaphysis (flushed of bone marrow) was cut lengthwise into strips, and then cut crosswise into small fragments. The minced bone tissue was washed three times in PBS by successive centrifugations at 1500 rpm for 5 minutes. Digestion media contains 20 mg of type II collagenase (Worthington Biochemical Corporation, Lakewood, NJ, #LS004176), and a final concentration of 0.01% Trypsin/EDTA in PBS. Bone fragments were incubated in 2 mL digestion media at 37°C for 45 minutes two times, and then washed three more times in PBS. Digested bone fragments were then added to a 10 cm dish with αMEM, 10% FBS, and 1X P/S. Importantly, only half of the media was replaced every 2-3 days to allow for cell-derived growth factors to remain in the media. Over time in culture, osteoblastic cells migrate out of the bone fragments. Between 10 and 14 days, cells are approximately 50-80% confluent. At this time bone fragments were discarded, and cells were trypsinized, plated for use, or frozen. All culture media was sterilized through a 0.22 μM filter, all FBS was heat-killed, and all primary cells were frozen in 90% FBS, 10% DMSO.

Osteoclast precursors were derived from enriched BMMs by treatment with 1:20 CMG14-12 supernatant (equivalent to 20 ng/mL recombinant murine M-CSF activity) and 35 ng/mL RANKL for 2 days [28]. Osteoclast precursors were stimulated with *S. aureus* supernatants for 4 days, or BMMs were stimulated with *S. aureus* supernatants for 24 hours before stimulation with RANKL for 5 days. All primary cells had continuous M-CSF treatment. On day 6 in culture, all RPMI- and *S. aureus*-stimulated osteoclastogenesis assays were fixed with a 4% formaldehyde and 0.05% Triton X-100 solution in PBS (10

minutes) and 1:1 acetone:ethanol (1 minute), before TRAP staining with reagents from the Acid Phosphatase, Leukocyte (TRAP) Kit (Sigma, Saint Louis, MO, 378A). TRAP$^+$ multinucleated cells were counted manually at 10X, with the assistance of OsteoMeasure software (OsteoMetrics, Inc., Decatur, GA) or by taking serial images of the entire well (18 total) and using the FIJI Cell Counter Plugin.

Post-traumatic osteomyelitis infection

The murine model of osteomyelitis was performed as described previously [31, 32]. C57BL/6J (Stock #: 000664) and *Tlr2*$^{-/-}$ (Stock #: 004650) mice were purchased through The Jackson Laboratory. *Tlr9*$^{-/-}$ mice were generated as described [311]. Mice were bred in house, which may account for mismatched numbers of animals in each replicate. The USA300 type *S. aureus* LAC clinical isolate or Δ*agr* was sub-cultured and prepared for infection inocula using OD$_{600}$ to target a concentration of approximately 1×10^6 CFUs in 2 μL of PBS. For some infections, the inoculum was diluted 1:10 to provide a dose of 1×10^5 CFUs. Osteomyelitis was induced in 7- to 8-week old female mice, following the introduction of a cortical bone defect using a 21G needle to reveal the medullary canal, into which 2 μL of bacterial suspension or PBS (mock-infection) was injected into the bone marrow cavity. Muscle fascia and skin were sutured and mice were given buprenorphine every 12 hours for 48 hours, with daily monitoring until the experimental end point.

CFU enumeration

At various time points throughout infection, tissues were harvested and homogenized using a BulletBlender and NAVY lysis tubes (Next Advance, Inc., Averill

Park, NY) at 4°C. Femurs were homogenized in CelLytic Buffer MT Cell Lysis Reagent (Sigma, Saint Louis, MO) to specifically lyse mammalian cells, and organs (liver, kidneys) were homogenized in PBS. Femur and organ homogenates were vortexed, serially diluted in PBS, and plated on TSA for bacterial enumeration. Following homogenization, femurs lysed in CellLytic Buffer were centrifuged at 4000 x g for 5 minutes to remove debris and the lysate was stored at -80°C for subsequent analysis.

Micro-computed tomography (µCT) of cortical and trabecular bone

Femurs were harvested 14 days post-infection and fixed for 48 hours in neutral buffered formalin at 4°C. Bones were analyzed using the Scanco Medical µCT50 and µCT Tomography V6.3-4 software (Scanco USA, Inc., Wayne, PA). Each scan included the diaphysis and distal epiphysis of each femur at 10 µm resolution (10mm, 10.0µm, 70kV, 200µA), resulting in 1088 slices for analysis and excluding the proximal epiphysis. Three-dimensional volumetric analyses were conducted by manually contouring transverse image slices in the region of interest. The diaphysis of each femur was comprised of 818 image slices. These image slices were used to quantify bone destruction and bone formation surrounding the cortical bone inoculation site. Trabecular bone measurements were obtained in the distal femur by advancing proximally past the growth plate 30 slices and 101 slices were manually contoured to include trabeculae and exclude the cortical bone, to measure trabecular bone volume/total volume (%).

Bone histology and histomorphometric analysis of trabecular bone

156

Following μCT data acquisition, fixed bones were dehydrated in 70% ethanol and decalcified for three days in 20% EDTA at 4°C. Decalcified bones were processed and embedded in paraffin and sectioned at 4μm thickness through the infectious nidus and bone marrow cavity using a Leica RM2255 microtome (Leica Biosystems, Buffalo Grove, IL). Sectioned femurs were stained with a modified hematoxylin and eosin (H&E) that included Orange G and Phloxine for enhanced bone contrast, tartrate-resistant acid phosphatase (TRAP) stain with hematoxylin counterstain. The region of interest in the distal femur included trabecular bone proximal to the growth plate. To quantify osteoclast number per bone perimeter in the distal femur, TRAP-stained histologic sections were analyzed using OsteoMeasure software (OsteoMetrics, Inc., Decatur, GA) and reported per ASBMR standards [276].

Cytokine detection via Luminex

Osteoblast infection and supernatant collection for cytokine analysis. To determine the how innate immune recognition alters the osteoblastic response to *S. aureus* infection, we infected the mc3T3 osteoblast cell line, as well as WT, *Myd88*^{-/-}, and *Tlr2*^{-/-} primary osteoblasts *in vitro*. Osteoblasts were plated at 5,000 cells per well in a 96-well plate and LAC and Δ*psm* strains were prepared for infection. An overnight culture of each was grown up to stationary phase, and subcultured 1:100 the following day. After 3 hours of growth at 37ºC with shaking at 180 rpm, the exponential phase culture was pelleted and bacterial cells were resuspended in PBS. Each bacterial suspension was adjusted by OD_{600} to approximately 5×10^8 bacterial cells/mL. A dilution was then calculated to target a multiplicity of infection (MOI) of 10.

Two hours prior to infection, cells were washed twice with PBS, and antibiotic-free media (αMEM with 10% FBS) was added to the cells. Bacterial cells at an MOI of 10 were added to each cell monolayer. Each infection condition had triplicate conditions from which to harvest host cell supernatants and calculate cytotoxicity. Cells were incubated at 37ºC and 5% CO_2 for 2 hours. Cells were washed twice with PBS, and media was added back with antibiotics (αMEM, 10% FBS, 1X P/S, and 10 µg/mL gentamicin). The following day, media was collected at 22 hours post-infection and pooled from each cell type and infection condition and stored at -80ºC. To assess the cytotoxic effect of *S. aureus* infection of osteoblasts, media solution containing 10% Cell Titer 96 Aqueous One Solution was added to each well. Plates were incubated at 37ºC 5% CO_2 for 2 hours at 37ºC, 5% CO_2, before reading optical density at 490 nm. Absorbance relative to PBS control was reported as a relative measure of viability of osteoblasts in each infection condition.

Luminex analysis. Supernatants or homogenates were thawed slowly at -20ºC overnight and at 4ºC two hours before setting up the assay. The Milliplex Map Kit - Mouse Cytokine/Chemokine Magnetic Bead Panel (EMD Millipore, Billerica, MA, MCYTOMAG-70K-PMX32) was used per the manufacturer's directions. Briefly, the 96-well plate was washed, samples were centrifuged to pellet particulate matter from supernatant, and quality controls and standards were prepared. To each well, standard, quality control, or sample was added. All standards, quality controls, and samples were run in duplicate. Beads were sonicated and added to each well. Plate was sealed, wrapped in foil, and left to shake overnight at 4ºC. The following day, with the use of a magnetic base, wells were washed with wash buffer, incubated in detection antibodies followed by

streptavidin-phycoerythrin, washed, and resuspended in sheath fluid. The samples were run using the FLEXMAP 3D™ xPONENT software (Luminex Corporation, Austin, TX). G-CSF failed to generate a standard curve for osteoblast cytokine analysis and was thus excluded. Data was analyzed by confirming quality control values, assessing standard curve generation, and verifying appropriate variance (CV) values between duplicate wells.

Results

TLR2 and TLR9 signaling influence *S. aureus*-mediated osteoclastogenesis *in vitro*

Other studies suggest that TRAF6 signaling alters osteoclast differentiation [254], and our own results show that depending on the timing and sequence of stimulation conditions (RANKL before *S. aureus* or *S. aureus* before RANKL), opposing cell differentiation phenotypes are observed. To assess what factors upstream of TRAF6 may be implicated in altering osteoclast differentiation, we used primary cells isolated from *Tlr2*⁻/⁻ and *Tlr9*⁻/⁻ mouse strains. To assess the roles of TLR2 and TLR9 in *S. aureus*-enhanced osteoclastogenesis from pre-osteoclasts and *S. aureus*-driven inhibition of osteoclast differentiation from BMMs, we used both BMMs and pre-committed osteoclast precursors for these assays. *Tlr2*⁻/⁻ cells did not undergo enhanced osteoclastogenesis in response to *S. aureus* stimulation and instead formed only TRAP⁺ mononuclear cells **(Figure 42A and Figure 43)**, similar to what was observed in *Myd88*⁻/⁻ cells (Chapter III). *Tlr9*⁻/⁻ pre-osteoclasts differentiated into multinucleated TRAP⁺ cells, but to a lesser extent than WT pre-osteoclasts **(Figure 42B and Figure 43)**. Similar trends were observed when we tested the ability of *S. aureus* to inhibit osteoclast differentiation from *Tlr2*⁻/⁻ and *Tlr9*⁻/⁻ cells. The loss of TLR2 completely ablated the ability of *S. aureus* supernatants to inhibit

159

RANKL-mediated osteoclastogenesis in BMMs, whereas BMMs deficient in TLR9 still displayed inhibition of osteoclast differentiation upon stimulation with *S. aureus* supernatants **(Figure 44A-C)**. These data suggest that in the myeloid lineage cells, MyD88 and TLR2 likely mediate the mechanisms by which *S. aureus* alters osteoclast differentiation. However, *Tlr9*$^{-/-}$ cells displayed enhanced osteoclastogenesis in response to *S. aureus* stimulation, although to a lesser extent than WT cells, and some level of *S. aureus*-mediated inhibition of osteoclasts, suggesting that TLR9 recognition and signaling may play an intermediate role as well.
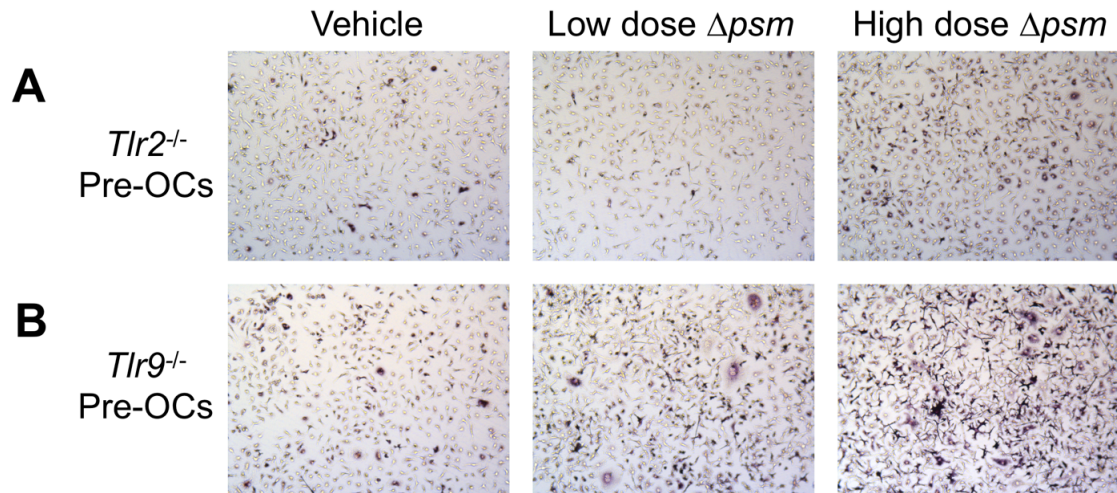
Figure 42. Enhancement of osteoclastogenesis by *S. aureus* supernatant is dependent on TLR2 and in part on TLR9.
(A-B) Osteoclast precursors were generated from *Tlr2*$^{-/-}$ **(A)** and *Tlr9*$^{-/-}$ **(B)** primary BMMs plated at 50,000 cells per well and treated with M-CSF and RANKL for 2 days. After washing cells with PBS, cells were stimulated with vehicle (RPMI; left column), or Δpsm supernatant at 5% (middle column) or 25% (right column) and M-CSF. Cells were TRAP stained at day 6 and imaged at 10X.
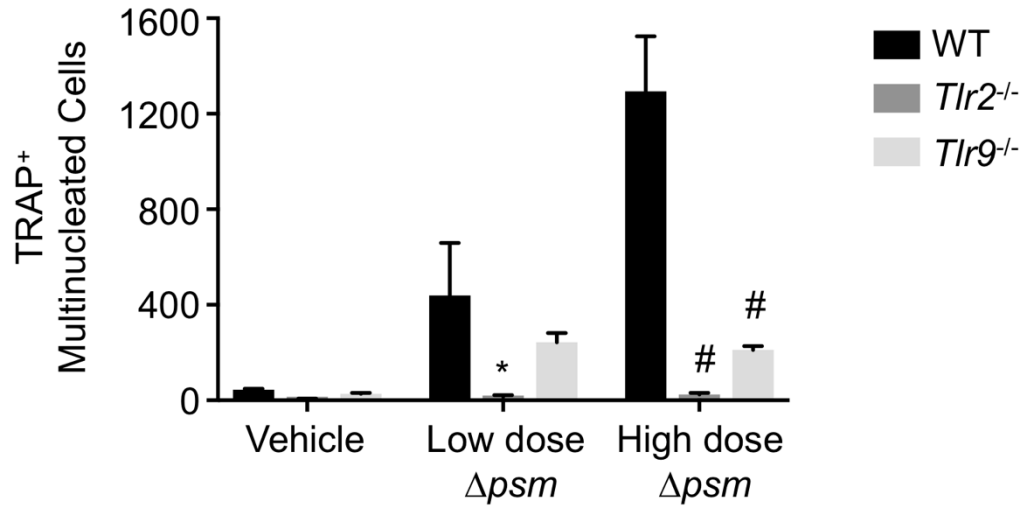
Figure 43. Quantification of *S. aureus*-mediated osteoclastogenesis from *Tlr2-/-* and *Tlr9-/-* osteoclast precursors.

TRAP^{+} multinucleated cells were quantified from WT, *Tlr2-/-*, and *Tlr9-/-* osteoclast precursor cells after stimulation with vehicle, low (5% v/v) or high (25% v/v) Δ*psm* supernatant doses (n = 3 wells per genotype) using OsteoMeasure software. Data are representative of triplicate experiments. A two-way ANOVA was used to compare genotype and dosage effects, with Dunnett's multiple comparisons test. * $p < 0.001$, # $p < 0.0001$.

| | Vehicle | Low dose Δ*psm* | High dose Δ*psm* |
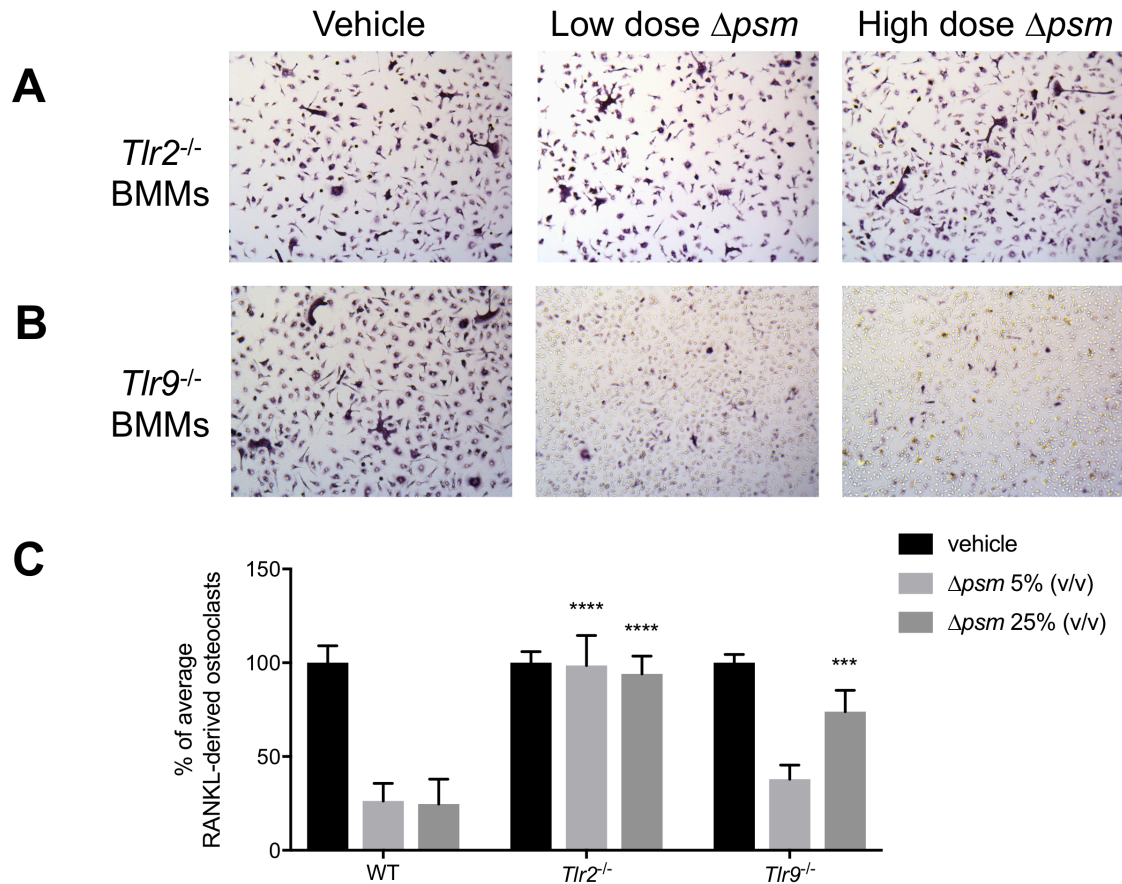
Figure 44. *S. aureus* **stimulation of BMMS prior to RANKL treatment inhibits osteoclastogenesis and is dependent on TLR and in part on TLR9.**
(A-C) *Tlr2⁻/⁻* (A) and *Tlr9⁻/⁻* (B) BMMs were plated at 50,000 cells per well and treated with M-CSF and vehicle (RPMI; left column) or Δ*psm* supernatant at 5% (middle column) or 25% (right column). After 24 hours of stimulation, cells were washed with PBS and fresh media was replenished with M-CSF and 35 ng/mL RANKL. At day 6 in culture, cells were TRAP stained and imaged at 10X. TRAP⁺ multinucleated cells were quantified, and the average vehicle-treated counts from each genotype was used to calculate the percent of average RANKL-derived osteoclasts (C).

Osteoblasts sense and respond to *S. aureus* infection *in vitro* through MyD88

Together, our data have implicated MyD88 and TLR2 sensing as the major pathways by which myeloid cell differentiation down the osteoclast lineage are perturbed. Thus far, we have not tested the ability of these pathways to alter cells of the osteoblast lineage, which are responsible for forming bone and further regulating osteoclastogenesis. To determine how the inflammatory response of osteoblasts is influenced by innate immune recognition of *S. aureus*, we infected osteoblasts isolated from WT mice or immunodeficient mice lacking MyD88 and TLR2. All osteoblasts remained viable 24 hours post-infection **(Figure 45A)**. This experiment was preliminary and triplicate wells were pooled together, preventing the ability to use statistical comparisons. All data described below are based solely on the magnitude of changes between mock-infection and infection, or between genotype. We found that WT mice had higher levels of many cytokines after *S. aureus* infection, including GM-CSF, IL-1α, IL-6, IL-9, IL-10, IL-13, IP-10, KC, LIF, LIX, MCP-1, MIP-1α, MIP-1β, MIP-2, RANTES, TNFα **(Figure 45D, 45F, 45K, 45M-N, 45Q, 45T-W, 45Y, 45AA-EE)**. The magnitude of some increases was relatively small, with changes within 10 pg/mL observed in eotaxin, IFNγ, IL-1β, IL-5, IL-12p70, and IL-15 **(Figure 45B, 45C, 45E, 45J, 45P, 45R)**. There were no differences (less than 1 pg/mL) in IL-2, IL-3, IL-4, IL-7, IL-12p40, IL-17, MIG, or VEGF between mock and infected WT cells **(Figure 45G-I, 45L, 45O, 45S, 45Z, 45FF)**, and M-CSF appeared to decrease with WT infection **(Figure 45X)**.
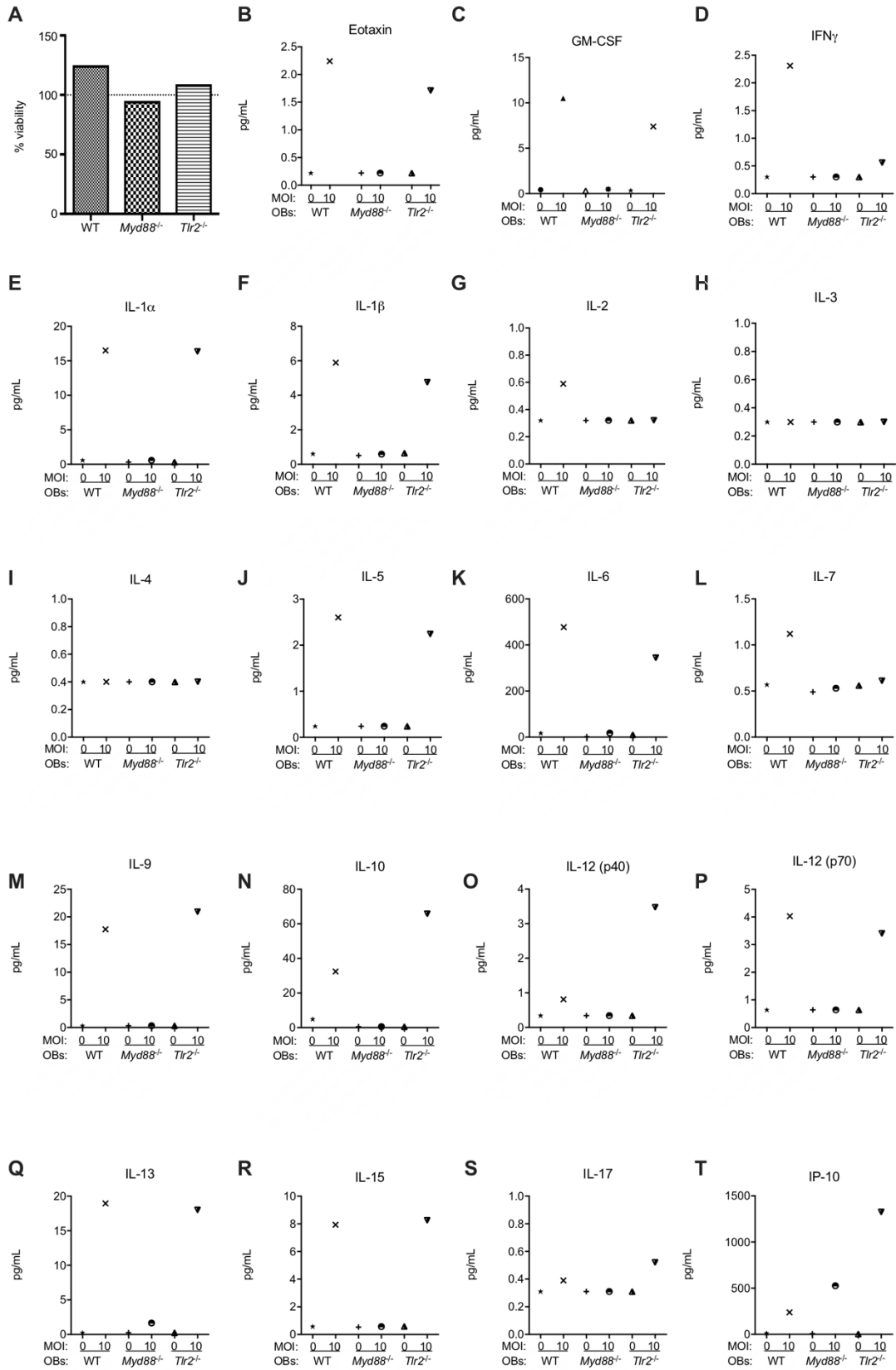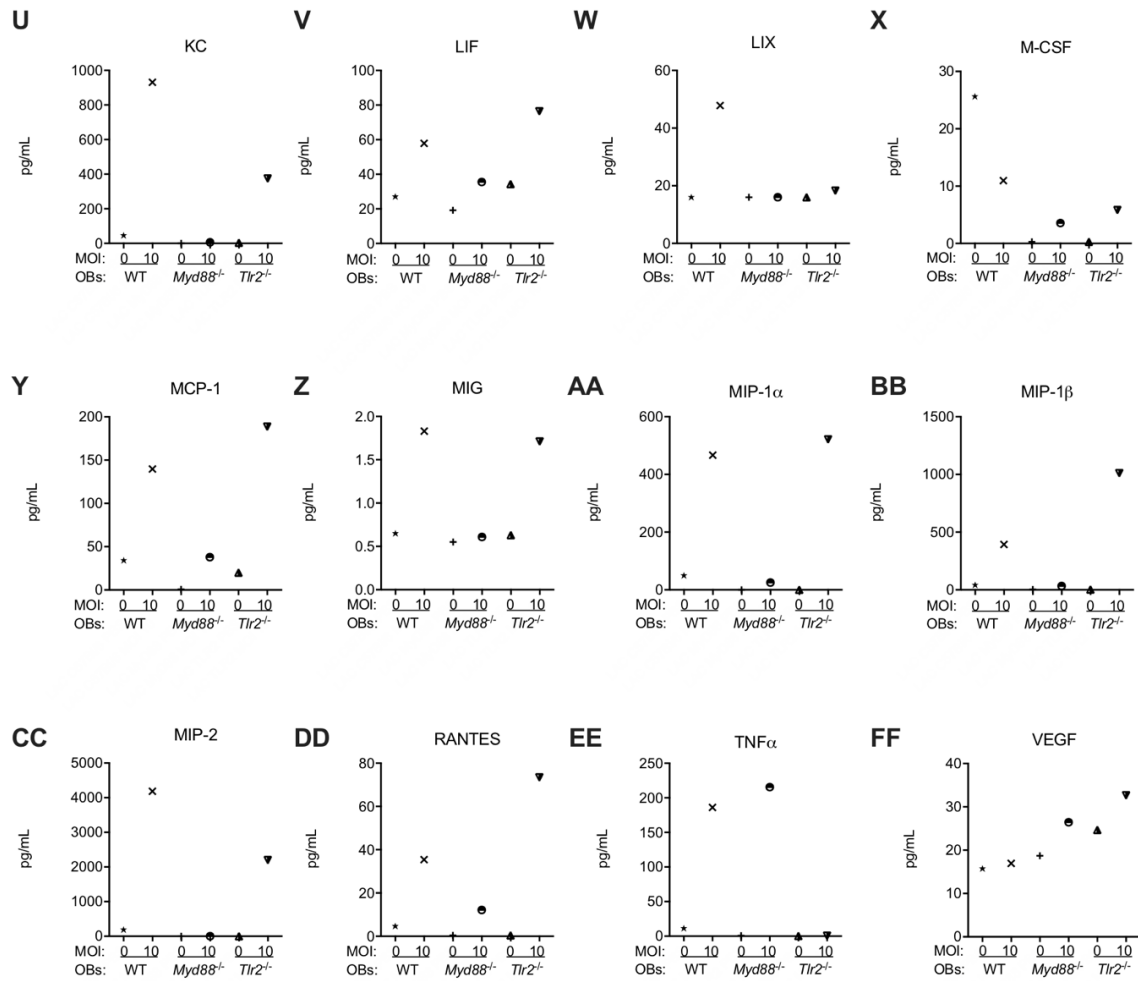
Figure 45. The role of MyD88 and TLR2 in cytokine responses of primary osteoblasts to *S. aureus* infection *in vitro*.

(A-FF) WT, *Myd88*⁻/⁻, and *Tlr2*⁻/⁻ osteoblasts (OBs) were plated at 5,000 cells per well in a 96-well plate and were mock-infected with PBS or infected with *S. aureus* LAC at a multiplicity of infection (MOI) of 10. At 2 hours, media containing antibiotics was added to cells to kill extracellular bacteria. Media was collected at 22 hours post-infection and pooled from 3 wells of the same cell type and infection condition and stored at -80ºC. To assess the cytotoxic effect of *S. aureus* infection of osteoblasts the following day, Cell Titer 96 Aqueous One Solution was read at 490 nm and absorbance relative to PBS control was reported to calculate relative viability of osteoblasts in each infection condition **(A)**. Pooled cell-free supernatants were run using the Luminex platform to quantify the abundance of individual cytokines **(B-FF)**.

In relation to WT osteoblasts, *Myd88*^{-/-} osteoblasts were less able to produce cytokines in response to *S. aureus* infection, showing discrepancies greater than 10 pg/mL in magnitude in only IP-10, LIF, MCP-1, MIP-1α, RANTES, and TNFα **(Figure 45T, 45V, 45Y, 45DD, 45EE)**. Despite drastic differences in WT and *Myd88*^{-/-} osteoblasts, *Tlr2*^{-/-} osteoblasts had a remarkably similar cytokine responses to *S. aureus* infection when compared to WT osteoblasts. Notably, some differences remained in that *Tlr2*^{-/-} osteoblasts produced lower levels of IFNγ, IL-2, IL-7, LIX, and TNFα in comparison to WT osteoblasts **(Figure 45D, 45G, 45L, 45EE)**. Unexpectedly, *Tlr2*^{-/-} osteoblasts produced some cytokines at higher abundance than WT osteoblasts following infection, including IL-10, IL-12p40, IP-10, LIF, MCP-1, MIP-1α, MIP-1β, RANTES, and VEGF **(Figure 45N, 45O, 45T, 45V, 45Y, 45AA, 45BB, 45DD, 45FF)**. These data suggest that osteoblasts show an early and robust inflammatory response to *S. aureus* infection, leading to the production of numerous cytokines and chemokines. Thus, the osteoblastic cytokine response to *S. aureus* is shaped by MyD88 and TLR2.

Early inflammation suggests an innate immune response is mounted during *S. aureus* bone infection

Our previous studies have shown that exoprotein- and toxin-deficient *S. aureus* strains retain some ability to dysregulate bone remodeling, implicating inflammation as a critical parameter that disrupts normal skeletal cell communication [31]. In order to determine whether cells local and distant to the site of infection are sensing and responding to infection by secreting cytokines, we compared cytokine levels from infected femurs and contralateral, uninfected femurs from the same mice to baseline levels of cytokines present

in femurs from healthy mice. We measured a panel of 32 cytokines over the course of 14 days. We sought to measure inflammatory responses that are produced locally in infected femurs, as well as systemic inflammation as measured in the contralateral femurs from infected mice.

In Chapter III, we observed that after osteomyelitis is established, *S. aureus* can disseminate to the contralateral femur. Here, we measured elevated levels of G-CSF and KC at day 1 post-infection in both the infected and the contralateral femurs **(Table 3)**. Specific to the infected femurs, GM-CSF, KC, and MIP-1α were significantly more abundant at days 1 and 4 **(Table 3)**. Similarly, LIF was elevated at days 1, 4, 7, and 10 post-infection, while eotaxin and TNFα were elevated at all days measured in the infected femurs **(Table 3)**. Conversely, IL-9 and LIX were decreased from baseline in both femurs **(Table 3)**. In a more acute manner, many cytokines were elevated in only infected femurs at day 1 post-infection, including IL-1β, IL-3, IL-5, IL-6, IL-7, IL-10, IL-12p40, IL-12p70, IL-15, MCP-1, MIP-1β, M-CSF, and MIP-2 **(Table 3)**. Furthermore, some cytokines, chemokines, and growth factors were more irregular in their expression signatures, with IP-10 increasing in femurs at days 4 and 10, IL-2 elevated at day 7, IL-17 increased at days 7 and 10, greater levels of IFNγ, IL-1α, RANTES, and VEGF at day 10, and more abundant levels of IL-4, MIP-1α, and MIP-1β at day 14 post-infection **(Table 3)**. Together, these data suggest that there is an abundant inflammatory response in the infected femur, but transient inflammation can be detected in the contralateral femurs as well.

Table 3. WT cytokine levels in non-infected femurs (baseline), infected femurs, and contralateral uninfected femurs from *S. aureus* infected mice.

Cytokine / Baseline	Infected Femur Cytokine Levels / Contralateral, Uninfected Femur Cytokine Levels				
	Day 1	Day 4	Day 7	Day 10	Day 14
G-CSF	7440.7 ± 1373.1****	306.7 ± 74.5	164.7 ± 78.6	124.3 ± 17.6	143.0 ± 64.3
6.7 ± 0.6	2900.7 ± 48.1****	78.8 ± 18.1	44.6 ± 8.6	31.2 ± 26.2	33.6 ± 27.5
Eotaxin	514.0 ± 10.4****	455.3 ± 9.1****	472.0 ± 45.0****	395.0 ± 4.0**	341.0 ± 99.4*
198.7 ± 28.0	456.0 ± 35.1****	443.7 ± 27.6****	385.0 ± 33.0***	330.7 ± 47.2*	270.7 ± 15.4
GM-CSF	73.5 ± 7.1****	51.7 ± 6.9**	43.8 ± 2.5	45.3 ± 4.9	45.1 ± 8.3
31.8 ± 5.0	40.1 ± 0.0	37.4 ± 5.5	38.3 ± 1.6	33.7 ± 4.7	34.1 ± 5.2
IFNy	18.1 ± 3.7	31.6 ± 20.1	16.0 ± 4.6	37.2 ± 15.8*	22.4 ± 2.7
13.3 ± 07	12.7 ± 1.2	12.2 ± 2.9	10.6 ± 2.2	10.5 ± 2.2	19.3 ± 2.0
IL-1α	143.0 ± 43.1	83.7 ± 10.1	76.4 ± 7.7	138.1 ± 62.8*	112.3 ± 19.9
79.0 ± 2.5	82.5 ± 4.2	60.6 ± 8.0	66.6 ± 8.6	64.9 ± 8.1	101.1 ± 8.8
IL-1β	424.7 ± 209.4****	126.3 ± 35.1	49.8 ± 15.4	65.0 ± 15.4	70.6 ± 15.0
47.1 ± 15.4	39.7 ± 11.4	25.9 ± 3.4	22.8 ± 4.7	20.3 ± 0.9	54.7 ± 18.3
IL-2	15.2 ± 2.3	9.4 ± 1.5	8.3 ± 1.1*	10.0 ± 1.7	15.1 ± 1.5
13.3 ± 0.4	12.2 ± 1.5	9.7 ± 1.6	8.6 ± 1.4*	9.0 ± 0.8	15.7 ± 2.4
IL-3	1.1 ± 0.1****	0.9 ± 0.2****	0.6 ± 0.0*	0.7 ± 0.1**	0.5 ± 0.1
0.3 ± 0.0	0.5 ± 0.1	0.6 ± 0.0*	0.5 ± 0.1	0.5 ± 0.1	0.4 ± 0.0
IL-4	2.6 ± 0.0	1.8 ± 0.3	1.4 ± 0.2	2.1 ± 0.8	5.2 ± 2.5**
1.78 ± 0.2	2.3 ± 0.4	2.0 ± 0.2	1.3 ± 0.2	1.4 ± 0.1	2.3 ± 0.3
IL-5	20.1 ± 5.2****	7.9 ± 1.8	5.9 ± 0.7	6.0 ± 0.7	6.6 ± 1.0
3.9 ± 0.9	9.1 ± 1.0	5.7 ± 0.9	5.9 ± 2.3	4.5 ± 1.0	5.2 ± 1.3
IL-6	465.3 ± 200.5****	129.2 ± 53.8	56.3 ± 22.5	60.5 ± 18.0	34.9 ± 13.5
15.7 ± 0.9	19.8 ± 1.2	12.7 ± 2.2	14.1 ± 2.1	12.9 ± 1.3	21.5 ± 1.9
IL-7	7.3 ± 1.3*	4.7 ± 0.9	5.2 ± 0.1	5.5 ± 0.8	4.6 ± 0.8
4.1 ± 0.9	4.0 ± 0.2	2.8 ± 0.2	4.3 ± 1.9	4.6 ± 0.6	5.4 ± 0.9

	Infected Femur Cytokine Levels				
	Contralateral, Uninfected Femur Cytokine Levels				
Cytokine	Day 1	Day 4	Day 7	Day 10	Day 14
Baseline					
IL-9	216.0 ± 56.3****	334.0 ± 46.0*	289.7 ± 29.1**	441.3 ± 51.0	541.0 ± 76.3
496.3 ± 40.5	201.3 ± 27.5****	290.3 ± 41.2**	291.7 ± 16.8**	391.0 ± 93.6	522.3 ± 62.7
IL-10	14.5 ± 3.6***	8.3 ± 2.2	6.1 ± 0.8	6.0 ± 1.1	9.2 ± 1.9
6.3 ± 0.5	7.7 ± 1.3	7.1 ± 1.1	4.8 ± 1.2	4.0 ± 0.1	8.1 ± 1.9
IL-12(p40)	21.2 ± 6.8****	12.7 ± 2.9*	4.7 ± 2.6	7.3 ± 1.4	2.9 ± 2.0
1.1 ± 0.0	5.7 ± 3.6	14.2 ± 3.9**	2.3 ± 1.3	6.3 ± 5.4	3.3 ± 2.8
IL-12(p70)	37.5 ± 3.3****	27.4 ± 2.3*	23.0 ± 1.9	23.8 ± 1.9	22.9 ± 1.4
20.5 ± 1.5	25.4 ± 2.1	21.6 ± 0.4	21.3 ± 3.0	22.7 ± 1.7	21.6 ± 1.8
LIF	114.0 ± 11.1****	81.5 ± 14.0****	69.3 ± 13.8****	58.1 ± 4.5**	41.2 ± 8.7
25.2 ± 6.6	47.6 ± 6.5	47.2 ± 5.5	34.2 ± 1.5	31.7 ± 6.0	25.0 ± 1.5
LIX	1189.3 ± 638.2	364.7 ± 75.5**	383.7 ± 73.3**	625.7 ± 178.6	2003.0 ± 177.8
1331.7 ± 48.4	576.3 ± 308.8	187.7 ± 110.6**	463.7 ± 98.2*	649.7 ± 292.2	1447.0 ± 286.0
IL-15	34.2 ± 8.8*	22.4 ± 5.0	20.4 ± 1.8	23.1 ± 3.0	28.7 ± 0.0
22.5 ± 2.2	21.4 ± 3.6	17.9 ± 2.4	19.1 ± 3.1	19.2 ± 0.6	31.3 ± 6.2
IL-17	6.6 ± 0.7	47.5 ± 13.6	104.4 ± 55.4****	97.7 ± 20.1***	46.5 ± 20.8
3.0 ± 0.4	3.1 ± 0.6	2.6 ± 0.3	2.5 ± 0.3	2.3 ± 0.3	4.5 ± 1.0
IP-10	124.0 ± 3.0	507.0 ± 202.9****	251.3 ± 36.0	366.3 ± 49.7*	268.3 ± 91.8
116.2 ± 23.3	91.4 ± 5.3	344.0 ± 51.0*	167.0 ± 16.8	144.3 ± 5.0	183.0 ± 67.1
KC	1352.7 ± 257.0****	352.7 ± 59.5*	219.0 ± 79.1	164.3 ± 18.7	109.8 ± 31.9
43.5 ± 1.9	350.3 ± 86.2*	107.8 ± 14.5	83.1 ± 6.2	62.6 ± 9.7	56.5 ± 4.8
MCP-1	412.7 ± 126.9****	88.6 ± 29.8	52.9 ± 8.8	43.6 ± 4.0	30.5 ± 12.8
15.0 ± 5.8	31.1 ± 7.8	28.1 ± 2.8	25.3 ± 11.0	15.2 ± 4.7	16.4 ± 4.4

| | Infected Femur Cytokine Levels | | | | |
| | Contralateral, Uninfected Femur Cytokine Levels | | | | |
Cytokine / Baseline	Day 1	Day 4	Day 7	Day 10	Day 14
MIP-1α	299.7 ± 75.8****	171.0 ± 23.8**	107.1 ± 27.7	115.4 ± 31.0	153.3 ± 69.1*
45.9 ± 3.0	49.7 ± 12.2	40.7 ± 9.3	33.9 ± 6.1	35.0 ± 1.7	54.7 ± 6.6
MIP-1β	223.7 ± 83.2****	105.2 ± 23.1	80.3 ± 13.1	88.3 ± 18.1	127.7 ± 51.6*
26.8 ± 5.5	28.9 ± 7.6	27.8 ± 46	26.0 ± 0.9	26.5 ± 2.4	35.9 ± 4.2
M-CSF	429.7 ± 149.7****	107.3 ± 54.0	53.8 ± 12.5	47.9 ± 6.4	59.4 ± 5.3
35.9 ± 10.3	67.1 ± 5.88	53.3 ± 4.6	100.2 ± 108.9	40.9 ± 5.2	44.2 ± 5.8
MIP-2	7815.1 ± 4479.2****	2180.7 ± 784.8	1032.3 ± 719.8	932.3 ± 409.2	542.0 ± 466.5
61.2 ± 6.0	90.8 ± 11.6	82.9 ± 11.6	68.9 ± 6.8	69.3 ± 15.1	68.1 ± 9.2
MIG	192.3 ± 76.1	848.3 ± 676.0	275.7 ± 64.1	657.0 ± 327.2	597.7 ± 116.9
191.1 ± 86.4	163.7 ± 64.6	266 ± 56.1	172.0 ± 76.7	122.7 ± 41.5	322.0 ± 92.7
RANTES	24.9 ± 7.9	38.1 ± 13.5	49.3 ± 3.7	59.9 ± 21.9*	50.5 ± 14.1
26.0 ± 9.4	23.0 ± 8.0	21.8 ± 1.1	44.9 ± 4.4	27.9 ± 1.1	40.4 ± 9.4
VEGF	28.0 ± 19.4	78.7 ± 13.2	90.8 ± 6.1	101.5 ± 47.2*	38.0 ± 20.2
34.6 ± 3.6	47.3 ± 15.2	92.3 ± 16.2	107.4 ± 19.3**	123.7 ± 15.9***	31.9 ± 6.4
TNFα	45.5 ± 15.1****	34.2 ± 2.3**	26.6 ± 3.5*	30.2 ± 7.2**	26.5 ± 14.0*
5.9 ± 0.8	11.2 ± 0.8	19.3 ± 1.0	13.5 ± 0.6	12.7 ± 3.1	10.4 ± 1.8

Uninfected femurs from WT mice ($n = 3$) or the infected and uninfected, contralateral femurs ($n = 3$ per time point) were harvested and homogenized in CelLytic Buffer. The resulting lysate was analyzed on the Luminex Platform using a 32-plex analyte Millipore kit. The quality control for IL-13 failed, and these data were excluded. Cytokine data are reported in pg/mL as mean ± standard deviation. A one-way ANOVA was performed using Tukey's multiple comparisons test for each cytokine, comparing baseline cytokine levels to infected and uninfected, contralateral femurs, where * $p < 0.05$, ** $p < 0.01$, *** $p < 0.001$, **** $p < 0.0001$.

TLR2 and TLR9 signaling are dispensable for control of staphylococcal burdens during osteomyelitis

Data in Chapter III revealed a critical role of MyD88 and the IL-1R in antibacterial responses to *S. aureus* in bone. However, many of the TLRs also require MyD88 for signaling, and we therefore sought to assess the role of TLRs known to sense S. aureus during osteomyelitis. To assess the antibacterial role of TLR2 during bone infection, we subjected WT and *Tlr2*$^{-/-}$ mice to *S. aureus* osteomyelitis. At day 14 post-infection, there was no difference in bacterial burdens recovered from the infected femur, kidneys, or liver when comparing WT and *Tlr2*$^{-/-}$ mice **(Figure 46A)**. After infection with a lower dose of *S. aureus*, WT and *Tlr2*$^{-/-}$ mice had similar bacterial burdens isolated at days 1, 2, 5, and 7 post-infection as well **(Figure 46B)**. In order to test whether TLR9 contributes to the control of bacterial burdens during osteomyelitis, both WT and *Tlr9*$^{-/-}$ mice were infected with *S. aureus*. Enumeration of bacterial burdens showed that *Tlr9*$^{-/-}$ mice had similar bacterial burdens in the infected femur to WT mice at day 14 post-infection **(Figure 46C)**. Collectively, these data suggest that TLR2 and TLR9 likely do not exclusively contribute to the reduction of *S. aureus* burdens in the bone during osteomyelitis.
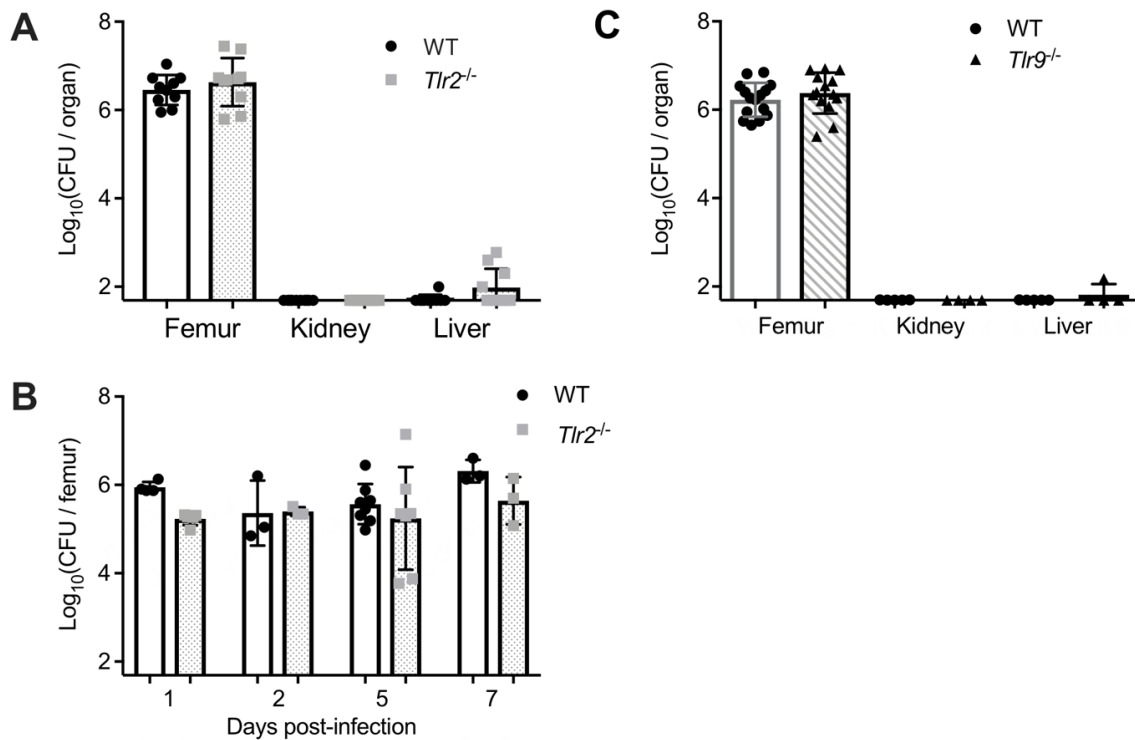
Figure 46. TLR2 and TLR9 signaling are dispensable for the control of staphylococcal burdens during osteomyelitis. (A-C) Female mice were infected with *S. aureus* at 10^6 **(A, C)** or 10^5 CFUs **(B)**. **(A, B)** WT and *Tlr2*$^{-/-}$ mice were infected with *S. aureus* in duplicate experiments and femurs and organs (WT $n = 10$, *Tlr2*$^{-/-}$ $n = 10$) were harvested at day 14 post-infection **(A)**. In duplicate experiments, femurs were harvested at day 1 (WT $n = 4$, *Tlr2*$^{-/-}$ $n = 5$), day 4 (WT $n = 3$, *Tlr2*$^{-/-}$ n = 3), day 5 (WT $n = 8$, *Tlr2*$^{-/-}$ $n = 7$), and day 7 (WT $n = 3$, *Tlr2*$^{-/-}$ $n = 3$) **(B)**. **(C)** WT and *Tlr9*$^{-/-}$ mice were infected with *S. aureus* in triplicate experiments and femurs (WT $n = 15$, *Tlr9*$^{-/-}$ $n = 14$) and organs (WT $n = 5$, *Tlr9*$^{-/-}$ $n = 4$) were harvested at day 14 post-infection. To compare bacterial burdens harvested between genotypes, t tests were used for each organ site. To compare CFUs harvested in femurs between genotype at each time point we used a one-way ANOVA with Sidak's multiple comparisons test. All comparisons were not statistically significant.

173

TLR2 and TLR9 do not alter bone remodeling during *S. aureus* osteomyelitis

In order to test the hypothesis that specific TLRs alter bone remodeling, we compared cortical and trabecular bone architecture between WT and *Tlr2*$^{-/-}$ mice after *S. aureus* osteomyelitis using microCT imaging **(Figure 47A)**. The extent of cortical and trabecular bone remodeling was similar between WT and *Tlr2*$^{-/-}$ mice at day 14 post-infection **(Figure 47B and 47C)**. Moreover, cellular histomorphometry of trabecular bone showed no difference in N.Oc/B.pm, indicating that no differences in osteoclast number were observed *in vivo* between WT and *Tlr2*$^{-/-}$ mice **(Figure 47D)**. To rule out bone remodeling changes strictly due to bacterial-induced bone cell death, we infected WT and *Tlr2*$^{-/-}$ mice with an *agr*-deficient *S. aureus* strain and analyzed femurs with microCT imaging **(Figure 48A)**. In comparison to the fully virulent WT *S. aureus* strain, *Tlr2*$^{-/-}$ mice infected with *agr*-deficient *S. aureus* had no significant differences in cortical or trabecular bone **(Figure 48B and 48C)**. These data confirm that TLR2 signaling does not contribute appreciably to infection-mediated bone remodeling at the site of infection or at sites distal to the infectious focus.

Figure 47. *Tlr2⁻ᐟ⁻* **mice infected with *S. aureus* show no differences in bone loss or osteoclast number compared to WT mice. (A-D)** Female WT and *Tlr2⁻ᐟ⁻* mice (*n* = 10 per genotype) were infected with 10^6 CFUs of *S. aureus* LAC in duplicate experiments. At day 14 post-infection, femurs were extracted and fixed in neutral buffered formalin for 48 hours. Femurs were scanned using the Scanco Medical μCT50 and the cortical bone around the site of infection was imaged at 10 μm resolution. One representative image from each genotype is pictured here **(A)**. Contouring of the cortical and trabecular bone regions quantified bone loss (mm³) **(B)** and bone volume/total volume (BV/TV, %) **(C)**. After scans were complete, femurs were dehydrated and stained for TRAP to visualize osteoclasts. The number of osteoclasts per bone perimeter (N.Oc/B.pm, 1/mm) were calculated in relation to trabecular bone in the distal femur **(D)**. Differences in bone remodeling and osteoclast number between genotypes were compared by *t* tests. All comparisons were not statistically significant.
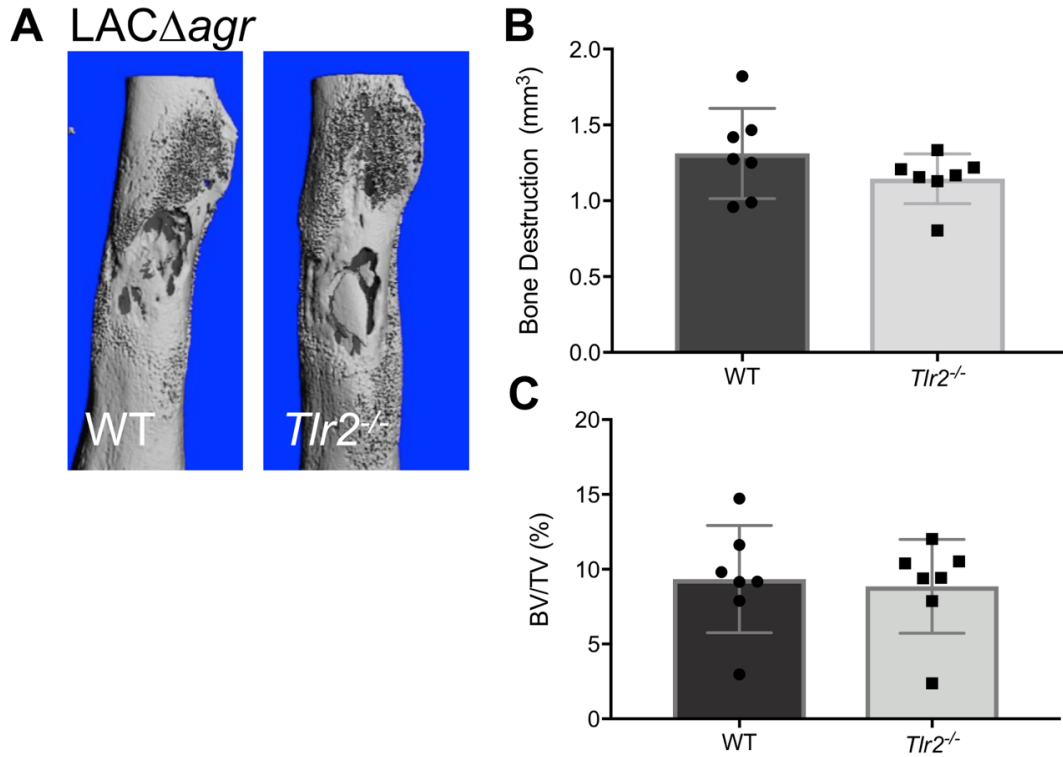
Figure 48. ***Tlr2*^{-/-} mice infected with a toxin-deficient strain of *S. aureus* (Δ*agr*) show no differences in bone loss compared to WT mice. (A-D)** Female WT and *Tlr2*^{-/-} mice (*n* = 7 per genotype) were infected with 10^6 CFUs of *S. aureus* Δ*agr*. At day 14 post-infection, femurs were extracted and fixed in neutral buffered formalin for 48 hours. Femurs were scanned using the Scanco Medical µCT50 and the cortical bone around the site of infection was imaged at 10 µm resolution. One representative image from each genotype is pictured here **(A)**. Contouring of the cortical and trabecular bone regions quantified bone loss (mm³) **(B)** and bone volume/total volume (BV/TV, %) **(C)**. Differences in bone remodeling between genotypes were compared by *t* tests. All comparisons were not statistically significant.

To assess whether bone remodeling was different between WT and *Tlr9*^{-/-} mice during *S. aureus* infection, we imaged infected bones via µCT **(Figure 49A)**. As observed in previous experiments with *Tlr2*^{-/-} mice, µCT analysis showed no significant difference in cortical or trabecular bone architecture at the site of infection **(Figure 49B and 49C)**. To determine whether there were alterations in resident osteoclast abundance in *Tlr9*^{-/-} mice, we measured osteoclast number per bone perimeter using histomorphometry. No differences were observed in relative osteoclast number between WT and *Tlr9*^{-/-} mice **(Figure 49D)**. These data indicate that *Tlr9*^{-/-} mice have similar outcomes as WT mice in response to *S. aureus* osteomyelitis, in the specific contexts of cortical bone loss, trabecular bone volume, and quantification of bone-resorbing osteoclasts. Collectively, these studies indicate that TLR9 or TLR2 deletion alone does not contribute to bone remodeling during *S. aureus* osteomyelitis.
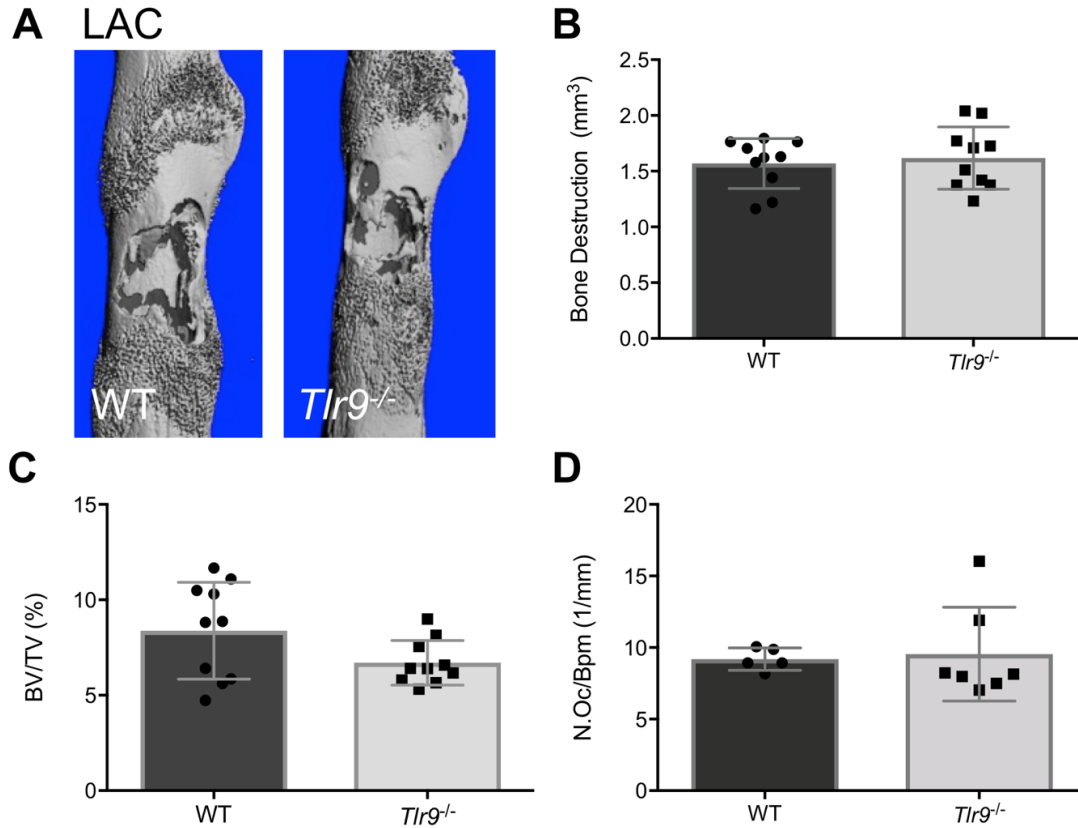
Figure 49. *Tlr9⁻/⁻* mice infected with *S. aureus* show no differences in bone loss or osteoclast number compared to WT mice. (A-D) Female WT and *Tlr9⁻/⁻* mice ($n = 10$ per genotype) were infected with 10^6 CFUs of *S. aureus* LAC in duplicate experiments. At day 14 post-infection, femurs were extracted and fixed in neutral buffered formalin for 48 hours. Femurs were scanned using the Scanco Medical µCT50 and the cortical bone around the site of infection was imaged at 10 µm resolution. One representative image from each genotype is pictured here **(A)**. Contouring of the cortical andx trabecular bone regions quantified bone loss (mm³) **(B)** and bone volume/total volume (BV/TV, %) **(C)**. After scans were complete, femurs (WT $n = 5$, *Tlr9⁻/⁻* $n = 7$) were dehydrated and stained for TRAP to visualize osteoclasts. The number of osteoclasts per bone perimeter (N.Oc/B.pm, 1/mm) were calculated in relation to trabecular bone in the distal femur **(D)**. Differences in bone remodeling and osteoclast number between genotypes were compared by *t* tests. All comparisons were not statistically significant.

Discussion

S. aureus contains conserved molecular patterns that are recognized by PRRs to initiate innate immune responses during infection. Osteoclast and osteoblast lineage cells express PRRs, although the full repertoire expressed at each differentiation state remains unclear [241, 250]. As we have shown in Chapter II, innate sensing of bacteria leads to activation of the transcription factor NFκB that is also involved in osteoclast differentiation. To test the role of the major *S. aureus*-recognizing PRRs upstream of NFκB on perturbation of osteoclastogenesis, we utilized primary cells harvested from mice lacking specific innate immune signaling components. We found that *S. aureus* enhancement or inhibition of osteoclastogenesis was completely dependent on the presence of TLR2. The loss of TLR9 did not completely prevent *S. aureus*-mediated osteoclastogenesis, but the extent of osteoclast formation was significantly less than that observed in WT cells. These data further support our results in Chapters II and III, wherein cell lines stimulated with purified TLR2 agonists and crude cell wall extracts enhance osteoclastogenesis in a MyD88-dependent manner. These data suggest that *S. aureus* lipoproteins or other cell wall components likely activate TLR2 and MyD88 on myeloid cells to alter the signaling pathways shared with skeletal cell differentiation pathways. Kassem et al. found that TLR2 enhances *S. aureus*-mediated osteoclastogenesis, but this occurs through increased RANKL production from osteoblasts [53], which are not present in our monoculture system of myeloid cells. Thus, *S. aureus* stimulation can lead to measurable changes in the ability of primary cells to undergo osteoclastogenesis, and these theories should be tested in more complex models as well.

Our data in Chapter III and other studies have characterized changes in inflammatory cytokines and chemokines after *S. aureus* bone infection *in vivo* [291, 292]. To expand on the findings characterizing cytokine levels only in infected femurs, we wanted to determine how cells local and distant to the site of infection were responding to infection. We compared secreted cytokine levels from infected femurs and contralateral, uninfected femurs from the same mice to baseline levels of cytokines present in femurs from healthy mice. We detected the early enrichment of growth factors and chemokines in both femurs from infected mice, including G-CSF, GM-CSF, and KC, which are characteristic of a granulopoietic response to bacterial infection [272-274]. In this study, we observed sustained levels of the cardinal pro-inflammatory cytokine TNFα in the infected femur over the two-week long infection. The infected femurs also had increased levels of myeloid chemoattractants MCP-1, MIP-1α, MIP-1β, and MIP-2, as well as IL-1α and IL-1β, but the contralateral uninfected femurs did not. These data suggest that over the course of bone infection, IL-1 and other inflammatory mediators are predominantly produced locally in the infected femur, and granuolopoiesis likely occurs early in both femurs after *S. aureus* osteomyelitis.

Many of the identified inflammatory cytokines produced downstream of PRR activation are proposed to stimulate bone resorption by inducing osteoclast differentiation [53, 144, 180, 237, 246, 253]. Because many cytokines influence bone remodeling *in vitro*, we hoped to define the role of MyD88 and TLR2 on osteoblasts in dictating the cytokine responses downstream of *S. aureus* infection. To do so, we conducted experiments to measure the cytokines produced following *S. aureus* infection of WT or immunodeficient osteoblasts. Importantly, these conclusions are based on magnitude alone and not statistical

comparisons, and this experiment needs to be repeated. However, we observed that WT osteoblasts made abundant levels of hallmark pro-inflammatory cytokines, IL-1α, IL-6, and TNFα, and also produced a large range of factors responsible for chemotaxis and expansion of other cell types, including GM-CSF, IL-9, IP-10, KC, MCP-1, MIP-1α, MIP-1β, MIP-2, and RANTES. In response to *S. aureus* infection, *Myd88*^{-/-} osteoblasts retained the ability to increase levels of LIF (which inhibits cell differentiation), TNFα, IP-10, MCP-1, and RANTES. The production of all other cytokines measured, including IL-1 and IL-6, were diminished, if not completely absent. *Tlr2*^{-/-} osteoblasts had similar cytokine responses to WT osteoblasts, although curiously, they did not produce the cytokines IFNγ, LIX, and TNFα, and they appeared to produce more abundant levels of some chemokines, including IP-10, RANTES, MCP-1 and MIP-1β. Accordingly, the osteoblast response to *S. aureus* infection details the necessity for MyD88 in order to mount a strong inflammatory cytokine response. Pro-inflammatory cytokines, myeloid growth factors, and chemokines present early after *S. aureus* osteomyelitis can promote differentiation of myeloid precursors into osteoclasts [138-141, 242, 291, 292]. Further analysis into perturbations of molecules that balance bone homeostasis, including RANKL and OPG, should also be considered in future studies given published reports of how altered RANKL:OPG ratios influence bone remodeling [53, 155, 236, 252].

Based on data of MyD88 mediating an inflammatory response in osteoblasts and *in vivo* (Chapter III), we next wanted to determine how TLRs that recognize *S. aureus* contribute to anti-staphylococcal immune responses *in vivo*. We hypothesized that recognition of *S. aureus* through TLRs would mediate bacterial clearance after bone infection. However, we saw no difference in the ability of *Tlr2*^{-/-} or *Tlr9*^{-/-} mice to clear

bacterial burdens, relative to WT mice. While the specific role of TLR2 on osteoblasts to mount a cytokine response remained unclear, our preliminary evidence suggests that the response of $Tlr2^{-/-}$ osteoblasts to *S. aureus* infection is remarkably similar to WT osteoblasts even at a relatively early 24-hour time point. Together, these data suggest that perhaps individual TLRs are dispensable for mounting a proper immune response, or that their role occurs so quickly after infection that we missed important differences. TLRs exhibit remarkable redundancy in their downstream signaling pathways and activation. Where $Myd88^{-/-}$ cells and mice exhibit dramatic phenotypes, including the loss of cytokine responses, perturbation of osteoclast differentiation, dissemination, and death, this is likely because they have prevented almost all TLRs and IL-1 receptors from responding to any of the corresponding stimuli. Thus, it is possible that we have not fully tested whether these individual pathways have functional overlap *in vivo*. One immediate avenue for future study is combinatorial knockout of TLR2 and TLR9 to assess for functional redundancy in the two major *S. aureus*-sensing TLRs.

Given that MyD88 and TLRs mediate *S. aureus*-perturbed osteoclastogenesis *in vitro*, we next measured bone remodeling in TLR-deficient mice during *S. aureus* osteomyelitis. In order to measure bone remodeling outcomes from infection, we quantified bone loss and osteoclast numbers in infected femurs from WT, $Tlr2^{-/-}$, and $Tlr9^{-/-}$ mice. We found that *in vitro* evidence of *S. aureus*-enhanced osteoclastogenesis in $Tlr2^{-/-}$ and $Tlr9^{-/-}$ cells did not predict osteoclastogenesis *in vivo* during *S. aureus* osteomyelitis. Specifically, we found no differences in the relative osteoclast number in trabecular bone between WT and $Tlr2^{-/-}$ or $Tlr9^{-/-}$ mice. Additionally, cortical bone loss occurred to the same extent between WT and $Tlr2^{-/-}$ or $Tlr9^{-/-}$ mice.

Collectively, data presented in this chapter describe that TLR2 and TLR9 do not mediate differences in the ability to control staphylococcal burdens, bone loss, or osteoclastogenesis in trabecular bone during osteomyelitis. While myeloid cells in culture respond directly to TLR ligands that influence their differentiation, the more complex cellular and inflammatory milieu *in vivo* likely diminishes these differences between WT and *Tlr2*$^{-/-}$ or *Tlr9*$^{-/-}$cells. We found that a majority of inflammation induced *in vivo* occurs locally in the infected femur, but granulopoiesis occurs systemically in response to *S. aureus*. We speculate that perhaps inflammation in TLR-deficient bones may still promote the influx of myeloid cells that subsequently serve as a reservoir of osteoclast precursors. Moreover, direct signaling through TLRs indicate robust abilities to modulate osteoclastogenesis, and thus, should be explored using more specific methods, such as a whole TLR-knockout mouse (*Unc93b1*) or a TLR2/9 double-knockout mouse. Here we demonstrate that, despite the mechanistic insights that can be gained in regards to TLR-mediated regulation of skeletal cell differentiation using *in vitro* systems, the *in vivo* environment creates additional complexities. In this chapter we found that, although TLR2 and TLR9 do not alter osteoclastogenesis or bone remodeling during *S. aureus* osteomyelitis, compelling *in vitro* data support myeloid sensing of TLRs to influence osteoclastogenesis.

A portion of the following section (*Chapter V, Summary and future directions*)

was originally published in *The Journal of Immunology.* (June 2018).

Brandt SL*, Putnam NE*, Cassat JE[#], Serezani CH[#]. 2018. Innate immunity to

Staphylococcus aureus: Evolving paradigms in soft tissue and invasive infections. *J

Immunol*. 200(12):3871-3880.

doi: 10.4049/jimmunol.1701574

CHAPTER V

SUMMARY AND FUTURE DIRECTIONS

Conclusions

Investigation into the physiology of bone remodeling affirms that skeletal and immune systems are interconnected. Research on bone infections has expanded research and findings in the area of osteoimmunology. In particular, my research has focused on *S. aureus* osteomyelitis. *S. aureus* is a leading cause of healthcare-associated infections and community-acquired *S. aureus* strains has also been shown to infect otherwise healthy individuals through strains [8, 312, 313]. Osteomyelitis can lead to serious complications from alterations in bone remodeling forming large areas of bone destruction, aberrant bone formation, and local vasculature damage. In this thesis, we hypothesized that sensing of *S. aureus* PAMPs and subsequent TLR and IL-1R signaling converges with osteoclastogenic differentiation pathways to enhance bone resorption, in addition to the ascribed roles for innate immune receptors towards the promotion of antibacterial responses. To address these questions, my thesis research has focused on (1) defining the bacterial components and innate immune receptors necessary to perturb osteoclastogenesis, (2) understanding how skeletal cells sense and respond to *S. aureus,* in terms of altering osteoclast differentiation and immune responses, (3) investigating innate immune host factors responsible for impacting bone remodeling during *S. aureus* osteomyelitis, (4) examining changes in inflammatory cytokines in response to *S. aureus* in bone, and (5) defining how innate immune receptors affect the anti-bacterial host response to *S. aureus* osteomyelitis. These goals have elucidated effects of *S. aureus* on bone at the cellular and organ level and

may describe common processes shared between sensing of the microbiota, infection, and inflammatory states.

Defining the bacterial stimuli and innate immune receptors necessary to perturb osteoclastogenesis

The data presented in Chapter II show how bacteria perturb osteoclast differentiation. We stimulated osteoclast precursors with synthetic TLR agonists, purified bacterial factors, crude cell wall extracts, and bacterial supernatants. We ultimately determined that both Gram-positive and Gram-negative PAMPs induce potent osteoclastogenic responses. For *S. aureus* specifically, cell wall and concentrated cell-free bacterial supernatants, purified lipoteichoic acid, and peptidoglycan were all capable of inducing osteoclastogenesis in RAW264.7 cells. Additionally, synthetic lipoproteins designed to engage TLR2 heterodimers, cell wall extracts, and bacterial supernatants all show patterns of NFκB transcription factor activation, a pathway necessary for osteoclastogenesis.

The bone biology literature has several contrasting papers classifying PRR agonists as either "stimulatory" or "inhibitory" towards osteoclast differentiation [25, 62, 75, 240, 248, 250]. While some researchers have compared the precursor cell populations used, timing of stimuli, or the effects of PRR agonists [51, 54, 55], there has not yet been a comprehensive study of how a clinically relevant strain of *S. aureus* perturbs osteoclastogenesis. Thus, my research into this area aimed to develop two different assay formats to allow for the investigation of both osteoclast enhancement and inhibition by bacterial stimuli. We have found that if BMMs are stimulated with bacterial supernatants,

they undergo changes consistent with the transcript repertoire of inflammatory M1 macrophages. Additionally, they are then inhibited from undergoing subsequent RANKL-mediated osteoclastogenesis. However, when given RANKL first, BMMs are activated to undergo osteoclast differentiation and become TRAP$^+$ mononuclear osteoclast precursors. When RANKL is removed, *S. aureus* can then provide signals to the cells to support continued osteoclastogenesis and the development of TRAP$^+$ multinucleated (mature) osteoclasts. Thus, recognition of *S. aureus* supernatants allows for cell fate decisions to skew the ability of the cells to differentiate down other lineages **(Figure 50)**. Furthermore, in Chapters II and III, we determined that *S. aureus*-enhanced osteoclastogenesis from osteoclast precursor cells is not dependent on paracrine signaling of TNFα and IL-1 cytokines produced in response to bacterial stimulation of cells in culture. These results indicate that NFκB activity alone is not sufficient to induce osteoclastogenesis, but that the RANKL cell program first needs to be activated.
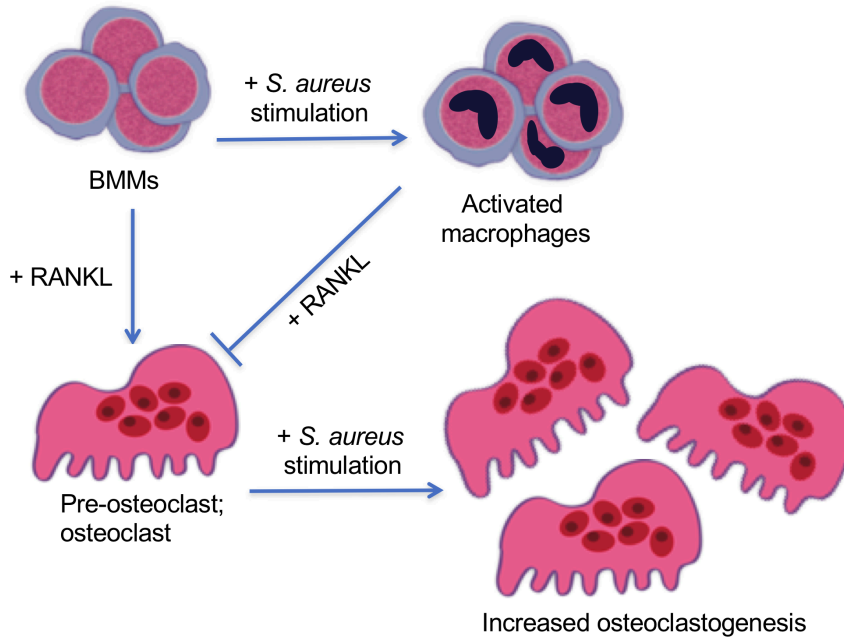
Figure 50. Myeloid-lineage cells sense and respond to *S. aureus* to influence osteoclast differentiation. When starting with an enriched BMM population in cell culture, these cells can be polarized to different extents depending on the order of stimuli seen. RANKL-priming forms osteoclast precursors, which allows subsequent *S. aureus* stimulation to increase osteoclast formation. However, *S. aureus*-priming of BMMs before RANKL treatment inhibits cells from forming osteoclast-lineage cells.

In Chapters III and IV, we determined that the *S. aureus* recognition on myeloid lineage cells influenced osteoclast differentiation in a manner dependent on MyD88 and TLR2. While cells deficient in TLR9, IL-1R, and IL-1β showed some osteoclast enhancement above baseline in response to *S. aureus* supernatants, the magnitude of osteoclasts differentiating in culture was diminished relative to WT cells. We next assessed the ability of *S. aureus* to prevent RANKL-mediated osteoclastogenesis in WT and immunodeficient cells, and the inverse was true for each cell type. *Myd88*$^{-/-}$ and *Tlr2*$^{-/-}$ myeloid cells evaded *S. aureus*-mediated osteoclast inhibition compared to WT cells first stimulated with *S. aureus* supernatants. *Tlr9*$^{-/-}$, *Il1r1*$^{-/-}$, and *Il1b*$^{-/-}$ myeloid cells limited the extent of, but did not completely impede, inhibition of RANKL-dependent osteoclastogenesis. In response to *S. aureus* supernatants, these data describe that osteoclast precursor cells of myeloid origin are dependent on signaling through MyD88 and TLR2 in order to perturb osteoclastogenesis. *S. aureus* supernatants are less able to influence myeloid cells that have lost expression of TLR9, IL-1R, and IL-1β, indicating that these innate immune receptors and cytokine play a role in mediating *S. aureus*-induced osteoclast changes. Together, these data describe a multifactorial approach to the ability of *S. aureus* to influence osteoclast differentiation.

Understanding how skeletal cells sense and respond to *S. aureus*

We have determined that osteoclast lineage cells differentially respond to *S. aureus* supernatants based on their differentiation state. We found that BMMs and osteoclast precursors retained similarities in the production of particular cytokines in response to *S. aureus* supernatants, including myeloid and T cell chemokines (MIP-1α, MIP-1β, MIP-2,

RANTES), anti-inflammatory IL-10, and the cardinal proinflammatory cytokines IL-6 and TNFα. However, as the BMMs skewed towards an M1 phenotype, osteoclast precursors took on a divergent cytokine profile. Osteoclast precursors were able to promote the production of granulocytic growth factors and chemokines (G-CSF and KC), as well as IL-2 which promotes the expansion of T cell populations, and MCP-1 to potentially promote additional myeloid cell influx. These data suggest that osteoclast lineage cells undergoing differentiation have an altered capacity to mount inflammatory responses.

We also interrogated the ability of *S. aureus* infection to induce inflammatory changes in primary osteoblasts, asking if MyD88 or TLR2 influence the osteoblastic immune response. Our results described that while deletion of MyD88 significantly hindered the ability of osteoblasts to mount an appropriate immune response, WT and *Tlr2⁻/⁻* osteoblasts had remarkably similar cytokine responses. WT osteoblasts had the greatest cytokine increases observed in IL-6, KC, MCP-1, MIP-1α, MIP-1β, MIP-2, and TNFα, among all cytokines measured. Thus, similar to cytokine responses elicited from BMMs and osteoclast precursors, early cytokine responses to *S. aureus* encouraged the production of pro-inflammatory cytokines and could support the influx of innate immune cells such as macrophages and neutrophils to promote bacterial clearance.

Investigating innate immune host factors responsible for impacting bone remodeling during *S. aureus* osteomyelitis

Investigation into bone remodeling in our laboratory has characterized cortical bone loss and the reactive bone callus during *S. aureus* osteomyelitis [31]. My research into bone remodeling has expanded these findings to characterize bone loss in the trabecular bone of

the distal femur with μCT imaging and histomorphometric analysis. One intriguing finding

from my work was that trabecular bone loss is accompanied by enhanced osteoclast number

and actively resorbing osteoclast surface. These data support what we and others have

observed *in vitro*, wherein stimulation of RANKL pre-committed osteoclasts with bacterial

products cause increased osteoclastogenesis. While many of my other investigations into

innate immune receptors began by assessing the role of MyD88, we did not conduct these

experiments with the knowledge that their underlying bone physiology is osteopenic,

meaning they have lower rates of both bone formation and bone resorption [75]. Instead,

we focused on three upstream receptors dependent on MyD88 signaling: TLR2, TLR9, and

IL-1R. TLR2 and TLR9 have been implicated in sensing extracellular and endosomal *S.

aureus*, and both receptors are reported to be expressed in skeletal cells [55, 75]. TLR2

sensing of *S. aureus* has been shown to directly enhance RANKL production from

osteoblasts [53]. Furthermore, the osteoblastic response to produce pro-inflammatory

cytokines and myeloid chemokines by our group and others [291, 314], suggest that these

factors are linked to enhanced bone loss [246, 292]. However, in mice deficient in TLR2

and TLR9, we did not observe any differences in cortical or trabecular bone remodeling in

response to *S. aureus*. These data indicate that even in the absence of TLR2 or TLR9, no

profound changes in bone remodeling were observed in response to *S. aureus* when

compared to WT mice. Compelling evidence has demonstrated a role for IL-1R signaling

in skeletal cell communication, but many studies have used exclusively *in vitro* systems,

while others have focused on how IL-1 influences bone remodeling in the absence of

infection or other inflammatory states [134, 136, 140, 242, 261, 262, 299]. We also utilized

in vitro assays to tease out mechanistic detail, that indicate IL-1R stimulation during

RANKL pre-commitment is important for developing osteoclast precursors. Work done in this thesis has expanded this body of knowledge to ask how the role of IL-1R to modulate bone remodeling occurs in a mouse model of infection. We found that $Il1r1^{-/-}$ mice were protected from the enhancement in relative osteoclast number and surface in the trabecular bone, and did not sustain a decrease in trabecular bone volume associated with *S. aureus* bone infection in WT mice. Furthermore, $Il1r1^{-/-}$ mice had an immense cortical bone remodeling callus formed along the diaphysis. Overall, these findings reveal that WT mice exhibit profound osteoclast-mediated trabecular bone loss during *S. aureus* osteomyelitis, while mice deficient in IL-1R signaling do not exhibit these changes. However, these data provide questions for future research, including elucidating mechanisms by which the dysregulated cortical bone callus forms and cortical bone loss occurs in $Il1r1^{-/-}$ mice, that may require new assays or tools to explore.

Examining changes in inflammatory cytokines in response to *S. aureus* osteomyelitis

One goal of my research was to define the inflammatory milieu in bone as it develops in response to *S. aureus*. While some researchers have focused on the roles and production of particular cytokines and chemokines *in vivo* [60, 292]*,* broad profiling of the changes in inflammation post-infection are lacking. To address this gap in the field, I first aimed to answer what cytokines are more plentiful in response to *S. aureus* infection, in comparison to bone healing observed during mock infection. *S. aureus* infected femurs had more abundant levels of pro-inflammatory cytokines IL-1α, IL-1β, IL-6, and TNFα than mock-infected femurs. *S. aureus* infected femurs also had increased levels of chemokines and growth factors responsible for myeloid and granulocytic cell chemotaxis and

expansion, including M-CSF, MCP-1, MIP-1α, MIP-1β, MIP-2, KC, and G-CSF. Cytokines measured in the infected femurs are indicative of an antibacterial response.

Comparison of infected femurs to mock infected femurs revealed cytokines and chemokines that are more abundant during *S. aureus* infection. However, these studies did not elucidate whether inflammation was localized to the site of infection or perhaps was systemically distributed throughout the infected animal. We therefore compared baseline cytokine values to those measured in the *S. aureus* infected femur or the uninfected, contralateral femur. These experiments revealed more abundant cytokine levels implicated in neutrophil chemotaxis and granulopoiesis, including G-CSF and KC at day 1 post-infection in both femurs, as well as GM-CSF at days 1 and 4 post-infection in the infected femur. While TNFα was elevated throughout the entire two-week timecourse in the *S. aureus* infected femur, many cytokines were only significantly increased in an acute manner (at day 1 post-infection). Finally, these studies elucidated the production of some cytokines commonly associated with T cell recruitment, expansion, and effector cell function, including RANTES, IP-10, IL-2, IFNγ, and IL-17. Our cytokine data consistently underscore the importance of IL-1 and TNFα production, neutrophil expansion and recruitment through G-CSF, GM-CSF, and KC, as well as the myriad of chemokines and cytokines associated with myeloid cell recruitment **(Figure 51, left column)**.
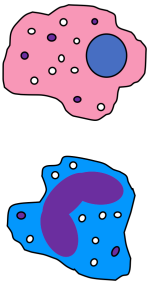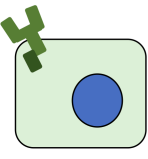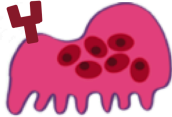
	Response to *S. aureus* osteomyelitis in C57BL/6 mice	Role of adapter protein MyD88 and upstream receptors TLR2, TLR9, and IL-1R
Inflammation / Innate Immunity	• Pro-inflammatory cytokines: IL-1α, IL-1β, IL-6, TNFα • Myeloid growth factors & chemokines: M-CSF, MCP-1, MIP-1α, MIP-1β, MIP-2 • Neutrophil expansion: G-CSF, GM-CSF, CXCL1 • Abscess formation	• MyD88: control of local *S. aureus* burdens, systemic bacterial spread, & mortality • IL-1R: control of local *S. aureus* burdens, neutrophil numbers, & abscess formation
Bone remodeling	• Increased osteoclastogenesis • Increased bone loss	• IL-1R promotes osteoclastogenesis and bone loss

Figure 51. *S. aureus* **osteomyelitis alters inflammation and bone remodeling, in part through IL-1R and MyD88.** WT mice, data comparing infected versus mock-infected femurs and infected versus contralateral femurs show consistent increases in cytokine abundance of pro-inflammatory cytokines, myeloid growth factors and chemokines, and granulocyte growth factors and chemokines. Normal immune responses to *S. aureus* are characterized by abscess formation in bone marrow and/or bone fragments. In trabecular bone, WT mice exhibited increased osteoclastogenesis and bone loss. We next assessed the antibacterial and bone remodeling effects using *Myd88*^{-/-}, *Tlr2*^{-/-}, *Tlr9*^{-/-}, and *Il1r1*^{-/-} mice. MyD88 and IL-1R were found to mediate the control of local bacterial burdens, osteoclastogenesis, and bone loss.

Defining how innate immune receptors affect the anti-bacterial host response to *S. aureus* osteomyelitis

In the post-traumatic model of murine osteomyelitis, the mouse is unable to completely clear *S. aureus* infection over the course of two weeks. WT mice harbor approximately 10^6 CFUs in the infected femurs at day 14 post-infection. Via histology, we can visualize *S. aureus* on living and dead fragments of bone or in the marrow space as a staphylococcal abscess community surrounded by a mature abscess. The mechanisms by which innate immune receptors allow bone cells to mount anti-staphylococcal immune responses has largely been explored *in vitro*. TLR2 has been shown to contribute to the production of antimicrobial peptides by osteoblasts [58, 65], and TLR9 promotes reactive oxygen species formation in these cells [66, 67]. However, roles for these TLRs against *S. aureus in vivo* remain minor [77, 172, 315]. IL-1 cytokines, however, have been found to contribute to anti-staphylococcal responses in several infection models [76, 77, 199, 207, 316]. Thus, the goal of this research was to determine how the MyD88-dependent receptors TLR2, TLR9, and IL-1R influence the anti-bacterial host response to *S. aureus* in bone.

We sought to more comprehensively investigate the role of MyD88 and its upstream receptors in osteomyelitis to control bacterial burdens at the site of infection, dissemination to other *S. aureus*-susceptible organs, mortality, and identification of innate immune cells in the infected femur via histology and flow cytometry. In these studies, we found that *Myd88^-/-* mice were extremely susceptible to *S. aureus* osteomyelitis. Without upstream signals transduced from TLRs and IL-1Rs, these immunodeficient mice had significant mortality rates and succumbed to infection due to dissemination of *S. aureus*. The *Myd88^-/-* mice that made it to day 14 post-infection (the experimental end point)

harbored higher *S. aureus* burdens in the bone as well. However, when *Tlr2*^{-/-} and *Tlr9*^{-/-} mice were subjected to *S. aureus* osteomyelitis, they had similar bacterial burdens as WT mice in the infected femurs and no dissemination. These data suggest that loss of a single TLR is not overtly detrimental to bacterial clearance or dissemination. In support of other findings that suggest IL-1R mediates bacterial clearance *in vivo* [76, 77, 199, 264-269], we found that IL-1R was responsible for the early clearance of bacterial burdens in the femur during *S. aureus* osteomyelitis. With a higher *S. aureus* inoculum, *Il1r1*^{-/-} mice were unable to control bacterial burdens to the same extent as WT mice by day 14 post-infection. We observed dysregulated abscess architecture in *Il1r1*^{-/-} mice that may have enabled the sustained high bacterial burdens. Additionally, with studies suggesting that IL-1R signaling is critical for a proper anti-staphylococcal neutrophil response [270-274], we investigated inflammatory mediators of neutrophil responses. We found that, *Il1r1*^{-/-} mice had a delayed ability to produce G-CSF, GM-CSF, and KC. These data suggest a defect in neutrophil expansion and recruitment, and via flow cytometry, *Il1r1*^{-/-} mice did have less neutrophils in the bone marrow at two days after infection. Interestingly, the decreased neutrophil abundance was detected in both the infected and the uninfected, contralateral femurs. These data indicate that IL-1R mice likely have a defect in granulopoiesis, leading to delayed clearance of *S. aureus* **(Figure 51, right column)**.

Remaining questions and future directions

The innate immune response to *S. aureus* dictates infection outcomes in a manner dependent on host genetics, comorbidities, and the tissue environment. Our research supports that skeletal cells participate in the induction of innate immunity and subsequent

tissue remodeling events. Future research should therefore investigate how tissue resident cells instigate immune responses through the elaboration of cytokines, the recruitment of phagocytes, and the production of antimicrobial compounds. At the same time, these studies must address the consequences of such immune activation on tissue homeostasis and remodeling, factors which play a large role in the morbidity of infectious diseases and the eventual recovery of a functional organ system. To this end, specific questions remain about the contribution of individual cell lineages to immunity in bone.

Areas of future research should include: (1) defining the role of immune responses mounted by osteoclast lineage cells at various differentiation states, (2) defining how crosstalk downstream of common PRR and tissue-specific signaling pathways affects skeletal cell communication and bone homeostasis, (3) addressing redundancy or compensation between TLRs, (4) determining mechanisms by which IL-1R contributes to altered bone remodeling during *S. aureus* osteomyelitis, (5) examining mechanisms of innate and adaptive immunity that limit morbidity from *S. aureus* osteomyelitis, and (6) develop methods to dissociate bacterial- versus immunologic-associated bone remodeling alterations.

Define the role of immune responses mounted by osteoclast lineage cells at various differentiation states

While the results in this thesis primarily focus on mature osteoclasts, results in Chapter II clearly describe differences in the inflammatory responses elicited by osteoclast lineage cells throughout differentiation. This data was preliminary in nature and leaves

many open areas of investigation regarding the role of osteoclast lineage cells (BMMs, osteoclast precursors, and mature osteoclasts) in response to *S. aureus* osteomyelitis.

1. **Define the ability of osteoclast-lineage cells to ingest and kill internalized bacterial**

As osteoclasts are also myeloid cells capable of phagocytosing large quantities of material [317], questions remain regarding what other macrophage-like qualities osteoclasts retain. Internalization of bacteria by professional phagocytes of the myeloid lineage such as macrophages, neutrophils, and dendritic cells, lead to the activation of intracellular killing mechanisms and antigen presentation [318]. However, it remains unclear how osteoclasts throughout their differentiation vary in the ability to internalize and kill *S. aureus*. Moreover, as we have observed differences in cytokine abundance in response to *S. aureus* between BMMs and osteoclast precursors, the capacity of mature osteoclasts to mount an immune response remains unknown.

2. **Define the innate immune receptor repertoire at each differentiation state**

The repertoire of TLRs expressed on mature osteoclasts and precursors throughout osteoclastogenesis remains unclear. While some published research has addressed this question, their findings have tested an incomplete repertoire of TLR protein expression or have focused on identifying only transcripts encoding various receptors [55, 75]. Osteoimmunology as a field would benefit from the delineation of protein expression of various TLRs as the ontogeny of osteoclast differentiation progresses. With specific interest in the response to *S. aureus*, changes in transcript expression and protein abundance in response to bacterial stimulation or infection would be informative.

3. **More clearly define immune responses and transcription factors activated downstream of *S. aureus* stimulation**

The characterization of innate immune receptor expression would allow for the use of TLR agonists to define how stimulation of an individual receptor or a combination of known receptors can activate transcription factors and production of cytokines. Of interest to this project are *S. aureus* specific ligands that promote osteoclastogenesis in RAW264.7 cells, that should first be repeated in primary cells. Next, this aim should focus on cytokines known to influence osteoclastogenesis and the pathways that activate transcription factors shared by osteoclast differentiation, including canonical and non-canonical NFκB, c-Fos, c-Jun, Pu.1, MITF, and NFATc1 [25-27, 233]. Activated transcription factors downstream of TLR activation should be determined using nuclear localization. Cytokines known to influence osteoclastogenesis should be measured following TLR activation and blocked during *in vitro* osteoclastogenesis assays. These studies will define potential mechanisms by which specific TLRs overlap with osteoclastogenic pathways cytokine production. Investigation into TLR-activated transcription factors may identify major pathways of crosstalk with osteoclastogenesis and provide insight into how skeletal cells are affected by *S. aureus*.

Define how crosstalk downstream of common PRR and tissue-specific signaling pathways affects skeletal cell communication and bone homeostasis

Osteoclastogenesis assays in this thesis highlight important innate immune receptors necessary to recognize *S. aureus* and influence myeloid lineage cells. However, the discrepancy between *in vitro* and *in vivo* osteoclast enumeration suggest that there are

other mechanisms that influence skeletal communication to promote osteoclastogenesis. As we have used mice completely deficient in each signaling component, it may be beneficial to model a more complex system *in vitro* to more precisely determine skeletal cell interactions. I propose the following experiments to test how skeletal interactions mediate responses to infectious stimuli *in vitro*.

1. **Co-culture assays**

Using a WBM co-culture system has allowed for communication between osteoblast and osteoclasts, whereby the osteoblasts in culture are able to produce factors for viability and RANKL to mediate osteoclastogenesis. WBM co-cultures would be established from cells from the same animal, thus we could compare cellular communication between WT and immunodeficient co-cultures in response to *S. aureus*. Thus, *S. aureus* stimulated WBM co-cultures may be used as a platform to determine the role of innate receptors on non-myeloid lineage cells on osteoclastogenesis. However, the gold standard co-culture assay would use neonatal calvarial cells from one mouse and BMMs from another, to represent osteoblast and osteoclast lineages, respectively. This assay would allow for the mixing of genotypes to determine how sensing of *S. aureus* by osteoblasts could lead to quantitative changes in the amount of osteoclast differentiation observed, or vice versa. It would be informative to determine the functional consequences of combinatorial receptor deletion on each lineage. Furthermore, these studies would be enlightened by experiments testing how the loss of innate receptors affects osteoblast ability to produce RANKL and OPG in monoculture.

2. **Functional assays**

A recent study by Shiratori et al. has described a phenotype known as the "pathologically activated osteoclast," which is the result of co-treatment of osteoclast precursors *in vitro* with RANKL and IL-1β [261]. Pathologically activated osteoclasts have been classified as having a greater functional capacity to resorb bone, relative to mature osteoclasts differentiated by RANKL alone. Findings by Shiratori et al. may further explain our own findings *in vivo*: that $Il1r1^{-/-}$ mice were protected from both enhancement in relative osteoclast numbers and osteoclast surface per bone perimeter in trabecular bone, but perhaps also lacked the formation of pathologically activated osteoclasts. Thus far, we have looked primarily at the ability to perturb differentiation itself through inhibition or enhancement of osteoclastogenesis. However, it is likely that if IL-1β enhances osteoclast function in terms of the quantity of bone being resorbed, this phenotype may also be dependent on TLR stimulation. By this rationale, it would then support experiments wherein co-stimulation with *S. aureus* supernatants alongside RANKL may influence osteoclast function differently than giving either stimulus alone. This could be tested *in vitro* with the development of bone resorption assays, utilizing commercially available OsteoAssay plates or dentin chip assays [261, 319]. In this assay, osteoclast precursors would be differentiated into mature osteoclasts on a mineralized matrix that could then be quantified for the amount of bone resorption.

3. Targeted inactivation of innate pathways in tissue resident cells

Our results have shown that MyD88 is necessary for *S. aureus*-induced increases in osteoclastogenesis *in vitro*. The precise roles of tissue resident cells in these signaling processes are beginning to be explored, and will be facilitated by new mammalian genetic models. To determine if MyD88 signal transduction is critical in skeletal cells during *S.*

aureus osteomyelitis, immune pathways that overlap with osteoclast differentiation could be targeted specifically in skeletal cells through genetic deletion. Skeletal cell-specific MyD88 knockout mice can be created with Cre-Lox breeding schemes. MyD88-floxed mice will be bred to *Ocn-cre* and *Ctsk-cre* mice to create mice with MyD88-deficient mature osteoblasts and osteoclasts, respectively. The creation of novel skeletal cell-specific knockout mice will allow us to determine the importance of MyD88 in skeletal cells during bone infection. Additionally, the role of MyD88 in skeletal cell precursor cells may be of interest. Cell-specific deletion of MyD88 in osteoblast and osteoclast precursors can be accomplished by crossing MyD88 floxed mice with *Osx-cre* or *LysM-cre* mice, respectively. However, these models are likely to have deletions in other cell lineages. Alternatively, BM transplants between WT and *Myd88*^{-/-} mice can be used to identify changes in MyD88 signaling through osteoclast precursors, as osteoblasts and mesenchymal cells are resistant to radioablation [320]. These genetic and experimental tools will be necessary to study the contribution of MyD88 in specific skeletal cells to bone remodeling *in vivo*.

Redundancy or compensation between TLRs

When testing a hypothesis with cells or a host that is deficient in a single receptor in the TLR family, the results can be theoretically confounded in two ways: (1) by the overlapping downstream activation shared with other TLRs and (2) the ubiquitous expression of other TLRs on nearly all host cell types. Within a given host cell, ligation of other TLRs may lead to the same or similar functional outcomes. The data from our *in vitro* osteoclastogenesis assays revealed several "intermediate" phenotypes, specifically in cells

deficient in TLR9 and IL-1R signaling. The shared signaling pathways through MyD88 and these intermediate phenotypes suggest that the method by which osteoclastogenesis is altered by *S. aureus* is multifactorial. Moreover, it is unclear whether cells that lack signaling through one TLR have other unrelated compensatory changes. In order to further address the hypothesis that *S. aureus*-sensing TLRs (specifically TLR2 and TLR9) play a role in antibacterial immunity and bone remodeling, two methods could be used that ameliorate these concerns. The creation of a double knockout mouse, deficient in both TLR2 and TLR9, may prevent compensatory signaling between the two individual TLRs. If perhaps, TLR9 activation in a *Tlr2*$^{-/-}$ mouse or TLR2 activation in a *Tlr9*$^{-/-}$ mouse prevented measurable differences in osteoclast number or immune responses *in vivo*, these changes would be elucidated in this mouse. However, it is well established that TLRs also respond to DAMPs, which are surely present in the context of cellular death and bone loss observed during *S. aureus* osteomyelitis. To test the more general role of TLR signaling without impacting IL-1R family signaling, the *Unc93b1*$^{-/-}$ mice could be used. *Unc93b1*$^{-/-}$ mice are effectively deficient in all TLR signaling, but retain signaling by IL-1, IL-18, and IL-33, which *Myd88*$^{-/-}$ mice lack [321]. Thus, the *Unc93b1*$^{-/-}$ mice deliver an animal model deficient in several TLRs whereby bone remodeling and histomorphometry can be assessed *in vivo*.

Determine mechanisms by which IL-1R contributes to altered bone remodeling during *S. aureus* osteomyelitis

In this thesis, IL-1R signaling was found to contribute to altered bone remodeling in cortical and trabecular bone. *Il1r1*$^{-/-}$ mice have fewer osteoclasts, exhibit less trabecular

bone loss, but also have a more extensive cortical bone callus formed around the inoculation site. To determine mechanisms by which IL-1R leads to altered bone remodeling during *S. aureus* osteomyelitis, μCT and histomorphometry should be compared between infected femurs from WT, *Il1r1$^{-/-}$*, *Il1a$^{-/-}$* and *Il1b$^{-/-}$* mice. Comparisons between bone remodeling data should determine if infected *Il1a$^{-/-}$* and *Il1b$^{-/-}$* femurs are similar to WT, if they phenocopy alterations in *Il1r1$^{-/-}$* mice, or if they display transitional results somewhere between the two. Moreover, the transcriptional activity of IL-1α may lead to effects not dependent on IL-1R, which may be elucidated using an *Il1a$^{-/-}$ Il1b$^{-/-}$* double knockout mouse. These proposed experiments may reveal if there is a primary IL-1 isoform contributing to altered bone remodeling during *S. aureus* osteomyelitis. While the mechanism behind the robust callus architecture observed in *Il1r1$^{-/-}$* mice remains unclear, it is possible that decreased bone resorption by osteoclasts in these mice led to a less actively remodeling callus. Additionally, enhanced bone formation has been shown in sterile bone healing in *Il1r1$^{-/-}$* mice [299], and it is possible that the increased callus size in Il1r1-/- mice with *S. aureus* osteomyelitis could reflect a mechanism by which bone heals over more quickly in the absence of IL-1R signaling.

Examine mechanisms of innate and adaptive immunity that limit morbidity from *S. aureus* osteomyelitis

The primary goal of this thesis was to test how sensing through a subset of MyD88-dependent innate immune receptors influenced antibacterial responses and bone remodeling. However, anti-staphylococcal immunity encompasses not only innate immune cell recruitment, but activation of innate immune cell effector functions, other immune

effectors such as AMPs and complement, and cells of the adaptive immune system. We have shown differences in neutrophil abundance supporting a mechanism of IL-1R-dependent antibacterial immunity in bone. This work raises the question as to how neutrophil activity and function is perturbed in response innate immune activation by *S. aureus*. In connection to work done in this thesis measuring various T cell cytokines in the infected bone, the development and functions of anti-staphylococcal effector T cells should be explored as well. As critical antibacterial immune responses are identified in bone, we should also investigate how they impact bone homeostasis, given that bone pathology is a significant driver of morbidity, mortality, and treatment failure. Data elucidated here will begin to fill gaps in knowledge regarding anti-staphylococcal innate and adaptive immune responses that are important during osteomyelitis.

Develop methods to dissociate bacterial- versus immunologic-associated bone remodeling alterations

Dysregulated bone remodeling occurs subsequent to *S. aureus* osteomyelitis. In this thesis, we began to address which innate immune receptors influence bone remodeling alterations. However, we are unable to conclude from results in this thesis what the degree of bone remodeling is dependent on bacterial factors versus immunologic changes. In order to dissociate between these two driving factors, new methods must be explored. New methods should be informed by similar studies that have intraperitoneally administered heat-killed WT or mutant bacteria or TLR agonists [79], or have used polyurethane scaffolds to release materials in close proximity to bone [322]. The contribution of bacterial components and inflammation on bone remodeling can be better parsed with the

combination of genetic mouse models, and testing inflammation or administration of bacterial components without active infection.

REFERENCES

1. Wertheim HF, Melles DC, Vos MC, van Leeuwen W, van Belkum A, Verbrugh HA, et al. The role of nasal carriage in *Staphylococcus aureus* infections. Lancet Infect Dis. 2005;5(12):751-62. PubMed PMID: 16310147.

2. Moran GJ, Krishnadasan A, Gorwitz RJ, Fosheim GE, McDougal LK, Carey RB, et al. Methicillin-resistant *S. aureus* infections among patients in the emergency department. N Engl J Med. 2006;355(7):666-74. PubMed PMID: 16914702.

3. Ray GT, Suaya JA, Baxter R. Incidence, microbiology, and patient characteristics of skin and soft-tissue infections in a U.S. population: A retrospective population-based study. BMC Infect Dis. 2013;13:252. Epub 2013/05/30. doi: 10.1186/1471-2334-13-252. PubMed PMID: 23721377; PubMed Central PMCID: PMCPMC3679727.

4. Newsom SW. Ogston's coccus. J Hosp Infect. 2008;70(4):369-72. PubMed PMID: 18952323.

5. Ogston A, British Medical Association. Scientific Grants Committee. Report upon micro-organisms in surgical diseases presented to the Scientific Grants Committee of the British Medical Association [microform]. London: British Medical Association,; 1881.

6. Hahn BL, Sohnle PG. Direct translocation of staphylococci from the skin surface to deep organs. Microb Pathog. 2013;63:24-9. doi: 10.1016/j.micpath.2013.05.012. PubMed PMID: 23747685; PubMed Central PMCID: PMCPMC3738190.

7. Huang H, Flynn NM, King JH, Monchaud C, Morita M, Cohen SH. Comparisons of community-associated methicillin-resistant *Staphylococcus aureus* (MRSA) and hospital-associated MSRA infections in Sacramento, California. J Clin Microbiol. 2006;44(7):2423-7. doi: 10.1128/JCM.00254-06. PubMed PMID: 16825359; PubMed Central PMCID: PMCPMC1489486.

8. CDC. Antibiotic resistance threats in the United States, 2013. 2013.

9. Cheng AG, DeDent AC, Schneewind O, Missiakas D. A play in four acts: *Staphylococcus aureus* abscess formation. Trends in microbiology. 2011;19(5):225-32. doi: 10.1016/j.tim.2011.01.007. PubMed PMID: 21353779; PubMed Central PMCID: PMC3087859.

10. Lew DP, Waldvogel FA. Osteomyelitis. Lancet. 2004;364(9431):369-79. doi: 10.1016/S0140-6736(04)16727-5. PubMed PMID: 15276398.

11. Clarke B. Normal bone anatomy and physiology. Clin J Am Soc Nephrol. 2008;3 Suppl 3:S131-9. doi: 10.2215/CJN.04151206. PubMed PMID: 18988698; PubMed Central PMCID: PMCPMC3152283.

12. Silver IA, Murrills RJ, Etherington DJ. Microelectrode studies on the acid microenvironment beneath adherent macrophages and osteoclasts. Exp Cell Res. 1988;175(2):266-76. PubMed PMID: 3360056.

13. Delaissé JM, Andersen TL, Engsig MT, Henriksen K, Troen T, Blavier L. Matrix metalloproteinases (MMP) and cathepsin K contribute differently to osteoclastic activities. Microsc Res Tech. 2003;61(6):504-13. doi: 10.1002/jemt.10374. PubMed PMID: 12879418.

14. Lacey DL, Timms E, Tan HL, Kelley MJ, Dunstan CR, Burgess T, et al. Osteoprotegerin ligand is a cytokine that regulates osteoclast differentiation and activation. Cell. 1998;93(2):165-76. PubMed PMID: 9568710.

15. Yasuda H, Shima N, Nakagawa N, Yamaguchi K, Kinosaki M, Mochizuki S, et al. Osteoclast differentiation factor is a ligand for osteoprotegerin/osteoclastogenesis-inhibitory factor and is identical to TRANCE/RANKL. Proc Natl Acad Sci U S A. 1998;95(7):3597-602. PubMed PMID: 9520411; PubMed Central PMCID: PMCPMC19881.

16. Udagawa N, Takahashi N, Yasuda H, Mizuno A, Itoh K, Ueno Y, et al. Osteoprotegerin produced by osteoblasts is an important regulator in osteoclast development and function. Endocrinology. 2000;141(9):3478-84. doi: 10.1210/endo.141.9.7634. PubMed PMID: 10965921.

17. Kong YY, Feige U, Sarosi I, Bolon B, Tafuri A, Morony S, et al. Activated T cells regulate bone loss and joint destruction in adjuvant arthritis through osteoprotegerin ligand. Nature. 1999;402(6759):304-9. doi: 10.1038/46303. PubMed PMID: 10580503.

18. O'Brien CA. Control of RANKL gene expression. Bone. 2010;46(4):911-9. Epub 2009/08/27. doi: 10.1016/j.bone.2009.08.050. PubMed PMID: 19716455; PubMed Central PMCID: PMCPMC2842447.

19. Li Y, Toraldo G, Li A, Yang X, Zhang H, Qian WP, et al. B cells and T cells are critical for the preservation of bone homeostasis and attainment of peak bone mass *in vivo*. Blood. 2007;109(9):3839-48. Epub 2007/01/03. doi: 10.1182/blood-2006-07-037994. PubMed PMID: 17202317; PubMed Central PMCID: PMCPMC1874582.

20. Bonewald LF. The amazing osteocyte. J Bone Miner Res. 2011;26(2):229-38. doi: 10.1002/jbmr.320. PubMed PMID: 21254230; PubMed Central PMCID: PMCPMC3179345.

21. Dougall WC, Glaccum M, Charrier K, Rohrbach K, Brasel K, De Smedt T, et al. RANK is essential for osteoclast and lymph node development. Genes Dev. 1999;13(18):2412-24. PubMed PMID: 10500098; PubMed Central PMCID: PMCPMC317030.

22. Kim N, Odgren PR, Kim DK, Marks SC, Choi Y. Diverse roles of the tumor necrosis factor family member TRANCE in skeletal physiology revealed by TRANCE deficiency and partial rescue by a lymphocyte-expressed TRANCE transgene. Proc Natl Acad Sci U S A.

2000;97(20):10905-10. doi: 10.1073/pnas.200294797. PubMed PMID: 10984520; PubMed Central PMCID: PMCPMC27122.

23. Mizuno A, Amizuka N, Irie K, Murakami A, Fujise N, Kanno T, et al. Severe osteoporosis in mice lacking osteoclastogenesis inhibitory factor/osteoprotegerin. Biochem Biophys Res Commun. 1998;247(3):610-5. PubMed PMID: 9647741.

24. Koga T, Inui M, Inoue K, Kim S, Suematsu A, Kobayashi E, et al. Costimulatory signals mediated by the ITAM motif cooperate with RANKL for bone homeostasis. Nature. 2004;428(6984):758-63. doi: 10.1038/nature02444. PubMed PMID: 15085135.

25. Boyce BF, Xiu Y, Li J, Xing L, Yao Z. NF-κB-mediated regulation of osteoclastogenesis. Endocrinol Metab (Seoul). 2015;30(1):35-44. doi: 10.3803/EnM.2015.30.1.35. PubMed PMID: 25827455; PubMed Central PMCID: PMCPMC4384681.

26. Novack DV. Role of NF-κB in the skeleton. Cell Res. 2011;21(1):169-82. Epub 2010/11/16. doi: 10.1038/cr.2010.159. PubMed PMID: 21079651; PubMed Central PMCID: PMCPMC3193402.

27. Takayanagi H, Kim S, Koga T, Nishina H, Isshiki M, Yoshida H, et al. Induction and activation of the transcription factor NFATc1 (NFAT2) integrate RANKL signaling in terminal differentiation of osteoclasts. Dev Cell. 2002;3(6):889-901. PubMed PMID: 12479813.

28. Takeshita S, Kaji K, Kudo A. Identification and characterization of the new osteoclast progenitor with macrophage phenotypes being able to differentiate into mature osteoclasts. J Bone Miner Res. 2000;15(8):1477-88. doi: 10.1359/jbmr.2000.15.8.1477. PubMed PMID: 10934646.

29. Yagi M, Ninomiya K, Fujita N, Suzuki T, Iwasaki R, Morita K, et al. Induction of DC-STAMP by alternative activation and downstream signaling mechanisms. J Bone Miner Res. 2007;22(7):992-1001. doi: 10.1359/jbmr.070401. PubMed PMID: 17402846.

30. de Mesy Bentley KL, Trombetta R, Nishitani K, Bello-Irizarry SN, Ninomiya M, Zhang L, et al. Evidence of *Staphylococcus aureus* deformation, proliferation, and migration in canaliculi of live cortical bone in murine models of osteomyelitis. J Bone Miner Res. 2017;32(5):985-90. Epub 2017/01/26. doi: 10.1002/jbmr.3055. PubMed PMID: 27933662; PubMed Central PMCID: PMCPMC5413415.

31. Cassat JE, Hammer ND, Campbell JP, Benson MA, Perrien DS, Mrak LN, et al. A secreted bacterial protease tailors the *Staphylococcus aureus* virulence repertoire to modulate bone remodeling during osteomyelitis. Cell Host Microbe. 2013;13(6):759-72. doi: 10.1016/j.chom.2013.05.003. PubMed PMID: 23768499; PubMed Central PMCID: PMCPMC3721972.

32. Wilde AD, Snyder DJ, Putnam NE, Valentino MD, Hammer ND, Lonergan ZR, et al. Bacterial hypoxic responses revealed as critical determinants of the host-pathogen outcome by TnSeq analysis of *Staphylococcus aureus* invasive infection. PLoS Pathog.

2015;11(12):e1005341. Epub 2015/12/18. doi: 10.1371/journal.ppat.1005341. PubMed PMID: 26684646; PubMed Central PMCID: PMCPMC4684308.

33.   Loughran AJ, Gaddy D, Beenken KE, Meeker DG, Morello R, Zhao H, et al. Impact of sarA and phenol-soluble modulins on the pathogenesis of osteomyelitis in diverse clinical isolates of *Staphylococcus aureus*. Infection and immunity. 2016;84(9):2586-94. doi: 10.1128/IAI.00152-16. PubMed PMID: 27354444.

34.   Tuchscherr L, Bischoff M, Lattar SM, Noto Llana M, Pförtner H, Niemann S, et al. Sigma factor SigB is crucial to mediate *Staphylococcus aureus* adaptation during chronic infections. PLoS pathogens. 2015;11(4):e1004870. Epub 2015/04/29. doi: 10.1371/journal.ppat.1004870. PubMed PMID: 25923704; PubMed Central PMCID: PMCPMC4414502.

35.   Wang Y, Cheng LI, Helfer DR, Ashbaugh AG, Miller RJ, Tzomides AJ, et al. Mouse model of hematogenous implant-related *Staphylococcus aureus* biofilm infection reveals therapeutic targets. Proceedings of the National Academy of Sciences of the United States of America. 2017;114(26):E5094-E102. Epub 2017/06/12. doi: 10.1073/pnas.1703427114. PubMed PMID: 28607050; PubMed Central PMCID: PMCPMC5495257.

36.   Horst SA, Hoerr V, Beineke A, Kreis C, Tuchscherr L, Kalinka J, et al. A novel mouse model of *Staphylococcus aureus* chronic osteomyelitis that closely mimics the human infection: An integrated view of disease pathogenesis. Am J Pathol. 2012;181(4):1206-14. PubMed PMID: 22902429.

37.   Mbalaviele G, Novack DV, Schett G, Teitelbaum SL. Inflammatory osteolysis: A conspiracy against bone. Journal of Clinical Investigation. 2017;127(6):2030-9. PubMed PMID: 28569732.

38.   Wagner JM, Jaurich H, Wallner C, Abraham S, Becerikli M, Dadras M, et al. Diminished bone regeneration after debridement of posttraumatic osteomyelitis is accompanied by altered cytokine levels, elevated B cell activity, and increased osteoclast activity. Journal of orthopaedic research : official publication of the Orthopaedic Research Society. 2017;35(11):2425-34. Epub 2017/03/24. doi: 10.1002/jor.23555. PubMed PMID: 28263017.

39.   Widaa A, Claro T, Foster TJ, O'Brien FJ, Kerrigan SW. *Staphylococcus aureus* protein A plays a critical role in mediating bone destruction and bone loss in osteomyelitis. PloS one. 2012;7(7):e40586. Epub 2012/07/11. doi: 10.1371/journal.pone.0040586. PubMed PMID: 22792377; PubMed Central PMCID: PMCPMC3394727.

40.   Mendoza Bertelli A, Delpino MV, Lattar S, Giai C, Llana MN, Sanjuan N, et al. *Staphylococcus aureus* protein A enhances osteoclastogenesis via TNFR1 and EGFR signaling. Biochim Biophys Acta. 2016;1862(10):1975-83. Epub 2016/07/28. doi: 10.1016/j.bbadis.2016.07.016. PubMed PMID: 27475257.

41. Thomer L, Schneewind O, Missiakas D. Pathogenesis of *Staphylococcus aureus* Bloodstream Infections. Annu Rev Pathol. 2016;11:343-64. PubMed PMID: 26925499.

42. Foster TJ, Geoghegan JA, Ganesh VK, Höök M. Adhesion, invasion and evasion: The many functions of the surface proteins of *Staphylococcus aureus*. Nat Rev Microbiol. 2014;12(1):49-62. doi: 10.1038/nrmicro3161. PubMed PMID: 24336184.

43. Alonzo F, 3rd, Torres VJ. The bicomponent pore-forming leucocidins of *Staphylococcus aureus*. Microbiol Mol Biol Rev. 2014;78(2):199-230. PubMed PMID: 24847020.

44. Powers ME, Bubeck Wardenburg J. Igniting the fire: *Staphylococcus aureus* virulence factors in the pathogenesis of sepsis. PLoS pathogens. 2014;10(2):e1003871. PubMed PMID: 24550724.

45. Josse J, Velard F, Gangloff SC. *Staphylococcus aureus* vs. osteoblast: Relationship and consequences in osteomyelitis. Front Cell Infect Microbiol. 2015;5:85. Epub 2015/11/26. doi: 10.3389/fcimb.2015.00085. PubMed PMID: 26636047; PubMed Central PMCID: PMCPMC4660271.

46. Heilmann C. Adhesion mechanisms of staphylococci. Adv Exp Med Biol. 2011;715:105-23. doi: 10.1007/978-94-007-0940-9_7. PubMed PMID: 21557060.

47. Bayles KW, Wesson CA, Liou LE, Fox LK, Bohach GA, Trumble WR. Intracellular *Staphylococcus aureus* escapes the endosome and induces apoptosis in epithelial cells. Infect Immun. 1998;66(1):336-42. PubMed PMID: 9423876; PubMed Central PMCID: PMCPMC107895.

48. Giese B, Glowinski F, Paprotka K, Dittmann S, Steiner T, Sinha B, et al. Expression of δ-toxin by *Staphylococcus aureus* mediates escape from phago-endosomes of human epithelial and endothelial cells in the presence of β-toxin. Cell Microbiol. 2011;13(2):316-29. Epub 2010/11/11. doi: 10.1111/j.1462-5822.2010.01538.x. PubMed PMID: 20946243.

49. Qazi SN, Counil E, Morrissey J, Rees CE, Cockayne A, Winzer K, et al. *agr* expression precedes escape of internalized *Staphylococcus aureus* from the host endosome. Infect Immun. 2001;69(11):7074-82. doi: 10.1128/IAI.69.11.7074-7082.2001. PubMed PMID: 11598083; PubMed Central PMCID: PMCPMC100088.

50. Grosz M, Kolter J, Paprotka K, Winkler AC, Schäfer D, Chatterjee SS, et al. Cytoplasmic replication of *Staphylococcus aureus* upon phagosomal escape triggered by phenol-soluble modulin α. Cell Microbiol. 2014;16(4):451-65. Epub 2013/11/12. doi: 10.1111/cmi.12233. PubMed PMID: 24164701; PubMed Central PMCID: PMCPMC3969633.

51. Bar-Shavit Z. Taking a toll on the bones: Regulation of bone metabolism by innate immune regulators. Autoimmunity. 2008;41(3):195-203. doi: 10.1080/08916930701694469. PubMed PMID: 18365832.

52. Kassem A, Henning P, Lundberg P, Souza PP, Lindholm C, Lerner UH. *Porphyromonas gingivalis* stimulates bone resorption by enhancing RANKL (receptor activator of NF-κB

ligand) through activation of Toll-like receptor 2 in osteoblasts. J Biol Chem. 2015;290(33):20147-58. Epub 2015/06/17. doi: 10.1074/jbc.M115.655787. PubMed PMID: 26085099; PubMed Central PMCID: PMCPMC4536425.

53. Kassem A, Lindholm C, Lerner UH. Toll-like receptor 2 stimulation of osteoblasts mediates *Staphylococcus aureus* induced bone resorption and osteoclastogenesis through enhanced RANKL. PLoS One. 2016;11(6):e0156708. Epub 2016/06/16. doi: 10.1371/journal.pone.0156708. PubMed PMID: 27311019; PubMed Central PMCID: PMCPMC4911171.

54. Zhang P, Liu J, Xu Q, Harber G, Feng X, Michalek SM, et al. TLR2-dependent modulation of osteoclastogenesis by *Porphyromonas gingivalis* through differential induction of NFATc1 and NF-kappaB. J Biol Chem. 2011;286(27):24159-69. Epub 2011/05/12. doi: 10.1074/jbc.M110.198085. PubMed PMID: 21566133; PubMed Central PMCID: PMCPMC3129197.

55. Krisher T, Bar-Shavit Z. Regulation of osteoclastogenesis by integrated signals from Toll-like receptors. J Cell Biochem. 2014;115(12):2146-54. doi: 10.1002/jcb.24891. PubMed PMID: 25079212.

56. Kim PD, Xia-Juan X, Crump KE, Abe T, Hajishengallis G, Sahingur SE. Toll-like receptor 9-mediated inflammation triggers alveolar bone loss in experimental murine periodontitis. Infect Immun. 2015;83(7):2992-3002. Epub 2015/05/11. doi: 10.1128/IAI.00424-15. PubMed PMID: 25964477; PubMed Central PMCID: PMCPMC4468549.

57. Warnke PH, Springer IN, Russo PA, Wiltfang J, Essig H, Kosmahl M, et al. Innate immunity in human bone. Bone. 2006;38(3):400-8. Epub 2005/11/02. doi: 10.1016/j.bone.2005.09.003. PubMed PMID: 16263346.

58. Varoga D, Tohidnezhad M, Paulsen F, Wruck CJ, Brandenburg L, Mentlein R, et al. The role of human beta-defensin-2 in bone. J Anat. 2008;213(6):749-57. doi: 10.1111/j.1469-7580.2008.00992.x. PubMed PMID: 19094191; PubMed Central PMCID: PMCPMC2666144.

59. Zhu C, Qin H, Cheng T, Tan HL, Guo YY, Shi SF, et al. *Staphylococcus aureus* supernatant induces the release of mouse β-defensin-14 from osteoblasts via the p38 MAPK and NF-κB pathways. Int J Mol Med. 2013;31(6):1484-94. Epub 2013/04/15. doi: 10.3892/ijmm.2013.1346. PubMed PMID: 23588388.

60. Yoshii T, Magara S, Miyai D, Nishimura H, Kuroki E, Furudoi S, et al. Local levels of interleukin-1beta, -4, -6 and tumor necrosis factor alpha in an experimental model of murine osteomyelitis due to *Staphylococcus aureus*. Cytokine. 2002;19(2):59-65. PubMed PMID: 12182840.

61. Wang Q, Dziarski R, Kirschning CJ, Muzio M, Gupta D. Micrococci and peptidoglycan activate TLR2-->MyD88-->IRAK-->TRAF-->NIK-->IKK-->NF-kappaB signal transduction pathway that induces transcription of interleukin-8. Infect Immun.

2001;69(4):2270-6. doi: 10.1128/IAI.69.4.2270-2276.2001. PubMed PMID: 11254583; PubMed Central PMCID: PMCPMC98155.

62.   Yang J, Ryu YH, Yun CH, Han SH. Impaired osteoclastogenesis by staphylococcal lipoteichoic acid through Toll-like receptor 2 with partial involvement of MyD88. J Leukoc Biol. 2009;86(4):823-31. Epub 2009/07/14. doi: 10.1189/jlb.0309206. PubMed PMID: 19602669.

63.   Zou W, Amcheslavsky A, Bar-Shavit Z. CpG oligodeoxynucleotides modulate the osteoclastogenic activity of osteoblasts via Toll-like receptor 9. J Biol Chem. 2003;278(19):16732-40. Epub 2003/02/28. doi: 10.1074/jbc.M212473200. PubMed PMID: 12611893.

64.   Marriott I, Rati DM, McCall SH, Tranguch SL. Induction of Nod1 and Nod2 intracellular pattern recognition receptors in murine osteoblasts following bacterial challenge. Infect Immun. 2005;73(5):2967-73. doi: 10.1128/IAI.73.5.2967-2973.2005. PubMed PMID: 15845503; PubMed Central PMCID: PMCPMC1087386.

65.   Chen Q, Hou T, Luo F, Wu X, Xie Z, Xu J. Involvement of toll-like receptor 2 and pro-apoptotic signaling pathways in bone remodeling in osteomyelitis. Cell Physiol Biochem. 2014;34(6):1890-900. Epub 2014/11/21. doi: 10.1159/000366387. PubMed PMID: 25503704.

66.   Mohamed W, Domann E, Chakraborty T, Mannala G, Lips KS, Heiss C, et al. TLR9 mediates *S. aureus* killing inside osteoblasts via induction of oxidative stress. BMC Microbiol. 2016;16(1):230. Epub 2016/10/03. doi: 10.1186/s12866-016-0855-8. PubMed PMID: 27716055; PubMed Central PMCID: PMCPMC5048406.

67.   Hamza T, Li B. Differential responses of osteoblasts and macrophages upon *Staphylococcus aureus* infection. BMC Microbiol. 2014;14:207. Epub 2014/07/25. doi: 10.1186/s12866-014-0207-5. PubMed PMID: 25059520; PubMed Central PMCID: PMCPMC4116603.

68.   Chauhan VS, Marriott I. Differential roles for NOD2 in osteoblast inflammatory immune responses to bacterial pathogens of bone tissue. J Med Microbiol. 2010;59(Pt 7):755-62. doi: 10.1099/jmm.0.015859-0. PubMed PMID: 20360399.

69.   Yang S, Takahashi N, Yamashita T, Sato N, Takahashi M, Mogi M, et al. Muramyl dipeptide enhances osteoclast formation induced by lipopolysaccharide, IL-1 alpha, and TNF-alpha through nucleotide-binding oligomerization domain 2-mediated signaling in osteoblasts. J Immunol. 2005;175(3):1956-64. PubMed PMID: 16034140.

70.   Shimada T, Park BG, Wolf AJ, Brikos C, Goodridge HS, Becker CA, et al. *Staphylococcus aureus* evades lysozyme-based peptidoglycan digestion that links phagocytosis, inflammasome activation, and IL-1beta secretion. Cell Host Microbe. 2010;7(1):38-49. doi: 10.1016/j.chom.2009.12.008. PubMed PMID: 20114027; PubMed Central PMCID: PMCPMC2818986.

71. Alippe Y, Wang C, Ricci B, Xiao J, Qu C, Zou W, et al. Bone matrix components activate the NLRP3 inflammasome and promote osteoclast differentiation. Sci Rep. 2017;7(1):6630. Epub 2017/07/26. doi: 10.1038/s41598-017-07014-0. PubMed PMID: 28747793; PubMed Central PMCID: PMCPMC5529467.

72. Copley LA. Pediatric musculoskeletal infection: Trends and antibiotic recommendations. The Journal of the American Academy of Orthopaedic Surgeons. 2009;17(10):618-26. PubMed PMID: 19794219.

73. Shirtliff ME, Mader JT. Acute septic arthritis. Clin Microbiol Rev. 2002;15(4):527-44. PubMed PMID: 12364368; PubMed Central PMCID: PMCPMC126863.

74. Verdrengh M, Carlsten H, Ohlsson C, Tarkowski A. Rapid systemic bone resorption during the course of *Staphylococcus aureus*-induced arthritis. J Infect Dis. 2006;194(11):1597-600. Epub 2006/10/18. doi: 10.1086/508751. PubMed PMID: 17083046.

75. Sato N, Takahashi N, Suda K, Nakamura M, Yamaki M, Ninomiya T, et al. MyD88 but not TRIF is essential for osteoclastogenesis induced by lipopolysaccharide, diacyl lipopeptide, and IL-1alpha. J Exp Med. 2004;200(5):601-11. doi: 10.1084/jem.20040689. PubMed PMID: 15353553; PubMed Central PMCID: PMCPMC2212746.

76. Bernthal NM, Pribaz JR, Stavrakis AI, Billi F, Cho JS, Ramos RI, et al. Protective role of IL-1β against post-arthroplasty *Staphylococcus aureus* infection. J Orthop Res. 2011;29(10):1621-6. Epub 2011/03/28. doi: 10.1002/jor.21414. PubMed PMID: 21445990; PubMed Central PMCID: PMCPMC3132302.

77. Miller LS, O'Connell RM, Gutierrez MA, Pietras EM, Shahangian A, Gross CE, et al. MyD88 mediates neutrophil recruitment initiated by IL-1R but not TLR2 activation in immunity against *Staphylococcus aureus*. Immunity. 2006;24(1):79-91. doi: 10.1016/j.immuni.2005.11.011. PubMed PMID: 16413925.

78. Hultgren OH, Svensson L, Tarkowski A. Critical role of signaling through IL-1 receptor for development of arthritis and sepsis during *Staphylococcus aureus* infection. J Immunol. 2002;168(10):5207-12. PubMed PMID: 11994477.

79. Kim J, Yang J, Park OJ, Kang SS, Kim WS, Kurokawa K, et al. Lipoproteins are an important bacterial component responsible for bone destruction through the induction of osteoclast differentiation and activation. J Bone Miner Res. 2013;28(11):2381-91. doi: 10.1002/jbmr.1973. PubMed PMID: 23633269.

80. Gillaspy AF, Hickmon SG, Skinner RA, Thomas JR, Nelson CL, Smeltzer MS. Role of the accessory gene regulator (*agr*) in pathogenesis of staphylococcal osteomyelitis. Infect Immun. 1995;63(9):3373-80. PubMed PMID: 7642265; PubMed Central PMCID: PMCPMC173464.

81. Crémieux AC, Saleh-Mghir A, Danel C, Couzon F, Dumitrescu O, Lilin T, et al. α-Hemolysin, not Panton-Valentine leukocidin, impacts rabbit mortality from severe sepsis with methicillin-resistant *Staphylococcus aureus* osteomyelitis. J Infect Dis.

2014;209(11):1773-80. Epub 2013/12/26. doi: 10.1093/infdis/jit840. PubMed PMID: 24376272.

82. Crémieux AC, Dumitrescu O, Lina G, Vallee C, Côté JF, Muffat-Joly M, et al. Panton-valentine leukocidin enhances the severity of community-associated methicillin-resistant *Staphylococcus aureus* rabbit osteomyelitis. PLoS One. 2009;4(9):e7204. Epub 2009/09/25. doi: 10.1371/journal.pone.0007204. PubMed PMID: 19779608; PubMed Central PMCID: PMCPMC2744873.

83. Zhang X, Ma YF, Wang L, Jiang N, Qin CH, Hu YJ, et al. A rabbit model of implant-related osteomyelitis inoculated with biofilm after open femoral fracture. Exp Ther Med. 2017;14(5):4995-5001. Epub 2017/09/19. doi: 10.3892/etm.2017.5138. PubMed PMID: 29201204; PubMed Central PMCID: PMCPMC5704256.

84. Robinson DA, Bechtold JE, Carlson CS, Evans RB, Conzemius MG. Development of a fracture osteomyelitis model in the rat femur. J Orthop Res. 2011;29(1):131-7. doi: 10.1002/jor.21188. PubMed PMID: 20602463.

85. Li B, Jiang B, Boyce BM, Lindsey BA. Multilayer polypeptide nanoscale coatings incorporating IL-12 for the prevention of biomedical device-associated infections. Biomaterials. 2009;30(13):2552-8. Epub 2009/02/12. doi: 10.1016/j.biomaterials.2009.01.042. PubMed PMID: 19215980; PubMed Central PMCID: PMCPMC3699876.

86. Khodaparast O, Coberly DM, Mathey J, Rohrich RJ, Levin LS, Brown SA. Effect of a transpositional muscle flap on VEGF mRNA expression in a canine fracture model. Plast Reconstr Surg. 2003;112(1):171-6. doi: 10.1097/01.PRS.0000066170.56389.27. PubMed PMID: 12832890.

87. Williams DL, Haymond BS, Woodbury KL, Beck JP, Moore DE, Epperson RT, et al. Experimental model of biofilm implant-related osteomyelitis to test combination biomaterials using biofilms as initial inocula. J Biomed Mater Res A. 2012;100(7):1888-900. Epub 2012/04/10. doi: 10.1002/jbm.a.34123. PubMed PMID: 22492534; PubMed Central PMCID: PMCPMC3360822.

88. Koschmieder R, Ritzerfield W, Homeyer L. [Addition of gentamicine to polymethyl methacrylate for therapy of infectious bone diseases. Expeimental *in vivo* tests]. Z Orthop Ihre Grenzgeb. 1975;113(1):147-9. PubMed PMID: 239496.

89. Wenke JC, Owens BD, Svoboda SJ, Brooks DE. Effectiveness of commercially-available antibiotic-impregnated implants. J Bone Joint Surg Br. 2006;88(8):1102-4. doi: 10.1302/0301-620X.88B8.17368. PubMed PMID: 16877615.

90. Rochford ETJ, Sabaté Brescó M, Zeiter S, Kluge K, Poulsson A, Ziegler M, et al. Monitoring immune responses in a mouse model of fracture fixation with and without *Staphylococcus aureus* osteomyelitis. Bone. 2016;83:82-92. Epub 2015/10/23. doi: 10.1016/j.bone.2015.10.014. PubMed PMID: 26525592.

91. Büren C, Hambüchen M, Windolf J, Lögters T, Windolf CD. Histological score for degrees of severity in an implant-associated infection model in mice. Arch Orthop Trauma Surg. 2019. Epub 2019/04/24. doi: 10.1007/s00402-019-03188-6. PubMed PMID: 31020411.

92. Pickett JE, Thompson JM, Sadowska A, Tkaczyk C, Sellman BR, Minola A, et al. Molecularly specific detection of bacterial lipoteichoic acid for diagnosis of prosthetic joint infection of the bone. Bone Res. 2018;6:13. Epub 2018/04/25. doi: 10.1038/s41413-018-0014-y. PubMed PMID: 29707402; PubMed Central PMCID: PMCPMC5916877.

93. Vidlak D, Kielian T. Infectious dose dictates the host response during *Staphylococcus aureus* orthopedic-implant biofilm infection. Infect Immun. 2016;84(7):1957-65. Epub 2016/06/23. doi: 10.1128/IAI.00117-16. PubMed PMID: 27091926; PubMed Central PMCID: PMCPMC4936354.

94. Kim HK, Missiakas D, Schneewind O. Mouse models for infectious diseases caused by *Staphylococcus aureus*. J Immunol Methods. 2014;410:88-99. PubMed PMID: 24769066.

95. Yoong P, Torres VJ. Animal models and imaging technologies: Paving the way towards insights into *Staphylococcus aureus*-induced osteomyelitis. Future Microbiol. 2013;8(12):1515-8. PubMed PMID: 24266351.

96. Cassat JE, Skaar EP. Recent advances in experimental models of osteomyelitis. Expert Rev Anti Infect Ther. 2013;11(12):1263-5. PubMed PMID: 24215241.

97. Niska JA, Meganck JA, Pribaz JR, Shahbazian JH, Lim E, Zhang N, et al. Monitoring bacterial burden, inflammation and bone damage longitudinally using optical and muCT imaging in an orthopaedic implant infection in mice. PLoS ONE [Electronic Resource]. 2012;7(10):e47397. PubMed PMID: 23082163.

98. Spaan AN, Schiepers A, de Haas CJ, van Hooijdonk DD, Badiou C, Contamin H, et al. Differential interaction of the staphylococcal toxins Panton-Valentine leukocidin and γ-hemolysin CB with human C5a receptors. J Immunol. 2015;195(3):1034-43. Epub 2015/06/19. doi: 10.4049/jimmunol.1500604. PubMed PMID: 26091719; PubMed Central PMCID: PMCPMC4506853.

99. Spaan AN, van Strijp JAG, Torres VJ. Leukocidins: Staphylococcal bi-component pore-forming toxins find their receptors. Nat Rev Microbiol. 2017;15(7):435-47. Epub 2017/04/19. doi: 10.1038/nrmicro.2017.27. PubMed PMID: 28420883; PubMed Central PMCID: PMCPMC5621924.

100. Prince A, Wang H, Kitur K, Parker D. Humanized mice exhibit increased susceptibility to *Staphylococcus aureus* pneumonia. J Infect Dis. 2017;215(9):1386-95. doi: 10.1093/infdis/jiw425. PubMed PMID: 27638942; PubMed Central PMCID: PMCPMC5853420.

101. Marciano BE, Spalding C, Fitzgerald A, Mann D, Brown T, Osgood S, et al. Common severe infections in chronic granulomatous disease. Clin Infect Dis. 2015;60(8):1176-83.

doi: 10.1093/cid/ciu1154. PubMed PMID: 25537876; PubMed Central PMCID: PMCPMC4400412.

102. von Bernuth H, Picard C, Jin Z, Pankla R, Xiao H, Ku CL, et al. Pyogenic bacterial infections in humans with MyD88 deficiency. Science. 2008;321(5889):691-6. doi: 10.1126/science.1158298. PubMed PMID: 18669862; PubMed Central PMCID: PMCPMC2688396.

103. Picard C, Puel A, Bonnet M, Ku CL, Bustamante J, Yang K, et al. Pyogenic bacterial infections in humans with IRAK-4 deficiency. Science. 2003;299(5615):2076-9. Epub 2003/03/13. doi: 10.1126/science.1081902. PubMed PMID: 12637671.

104. Israel L, Wang Y, Bulek K, Della Mina E, Zhang Z, Pedergnana V, et al. Human adaptive immunity rescues an inborn error of innate immunity. Cell. 2017;168(5):789-800 e10. PubMed PMID: 28235196.

105. Bonilla FA, Geha RS. 12. Primary immunodeficiency diseases. J Allergy Clin Immunol. 2003;111(2 Suppl):S571-81. PubMed PMID: 12592303.

106. Andrews T, Sullivan KE. Infections in patients with inherited defects in phagocytic function. Clin Microbiol Rev. 2003;16(4):597-621. PubMed PMID: 14557288; PubMed Central PMCID: PMCPMC207096.

107. Tsezou A, Poultsides L, Kostopoulou F, Zintzaras E, Satra M, Kitsiou-Tzeli S, et al. Influence of interleukin 1alpha (IL-1alpha), IL-4, and IL-6 polymorphisms on genetic susceptibility to chronic osteomyelitis. Clin Vaccine Immunol. 2008;15(12):1888-90. Epub 2008/10/29. doi: 10.1128/CVI.00209-08. PubMed PMID: 18971305; PubMed Central PMCID: PMCPMC2593176.

108. Asensi V, Alvarez V, Valle E, Meana A, Fierer J, Coto E, et al. IL-1 alpha (-889) promoter polymorphism is a risk factor for osteomyelitis. Am J Med Genet A. 2003;119A(2):132-6. doi: 10.1002/ajmg.a.20137. PubMed PMID: 12749050.

109. Holland SM. Chronic granulomatous disease. Hematol Oncol Clin North Am. 2013;27(1):89-99, viii. Epub 2012/11/22. doi: 10.1016/j.hoc.2012.11.002. PubMed PMID: 23351990; PubMed Central PMCID: PMCPMC3558921.

110. Picard C, von Bernuth H, Ghandil P, Chrabieh M, Levy O, Arkwright PD, et al. Clinical features and outcome of patients with IRAK-4 and MyD88 deficiency. Medicine (Baltimore). 2010;89(6):403-25. doi: 10.1097/MD.0b013e3181fd8ec3. PubMed PMID: 21057262; PubMed Central PMCID: PMCPMC3103888.

111. Menne EN, Sonabend RY, Mason EO, Lamberth LB, Hammerman WA, Minard CG, et al. *Staphylococcus aureus* infections in pediatric patients with diabetes mellitus. J Infect. 2012;65(2):135-41. doi: 10.1016/j.jinf.2012.04.001. PubMed PMID: 22490616.

112. Rich J, Lee JC. The pathogenesis of *Staphylococcus aureus* infection in the diabetic NOD mouse. Diabetes. 2005;54(10):2904-10. PubMed PMID: 16186391.

113. Bourke CD, Berkley JA, Prendergast AJ. Immune dysfunction as a cause and consequence of malnutrition. Trends Immunol. 2016. doi: 10.1016/j.it.2016.04.003. PubMed PMID: 27237815; PubMed Central PMCID: PMCPMC4889773.

114. Mihu CN, Schaub J, Kesh S, Jakubowski A, Sepkowitz K, Pamer EG, et al. Risk factors for late *Staphylococcus aureus* bacteremia after allogeneic hematopoietic stem cell transplantation: A single-institution, nested case-controlled study. Biol Blood Marrow Transplant. 2008;14(12):1429-33. doi: 10.1016/j.bbmt.2008.09.005. PubMed PMID: 19041067.

115. Drapeau CM, Angeletti C, Festa A, Petrosillo N. Role of previous hospitalization in clinically-significant MRSA infection among HIV-infected inpatients: Results of a case-control study. BMC Infect Dis. 2007;7:36. Epub 2007/04/30. doi: 10.1186/1471-2334-7-36. PubMed PMID: 17470274; PubMed Central PMCID: PMCPMC1868735.

116. Jones KD, Berkley JA. Severe acute malnutrition and infection. Paediatr Int Child Health. 2014;34 Suppl 1:S1-S29. doi: 10.1179/2046904714Z.000000000218. PubMed PMID: 25475887; PubMed Central PMCID: PMCPMC4266374.

117. Maraqa NF, Aigbivbalu L, Masnita-Iusan C, Wludyka P, Shareef Z, Bailey C, et al. Prevalence of and risk factors for methicillin-resistant *Staphylococcus aureus* colonization and infection among infants at a level III neonatal intensive care unit. Am J Infect Control. 2011;39(1):35-41. doi: 10.1016/j.ajic.2010.07.013. PubMed PMID: 21281885.

118. Rathore MH, Kline MW. Community-acquired methicillin-resistant *Staphylococcus aureus* infections in children. Pediatr Infect Dis J. 1989;8(9):645-7. PubMed PMID: 2797962.

119. Afessa B, Peters SG. Major complications following hematopoietic stem cell transplantation. Semin Respir Crit Care Med. 2006;27(3):297-309. doi: 10.1055/s-2006-945530. PubMed PMID: 16791762.

120. Fulop T, Tessier D, Carpentier A. The metabolic syndrome. Pathol Biol (Paris). 2006;54(7):375-86. doi: 10.1016/j.patbio.2006.07.002. PubMed PMID: 16904849.

121. Wicker LS, Clark J, Fraser HI, Garner VE, Gonzalez-Munoz A, Healy B, et al. Type 1 diabetes genes and pathways shared by humans and NOD mice. J Autoimmun. 2005;25 Suppl:29-33. Epub 2005/11/01. doi: 10.1016/j.jaut.2005.09.009. PubMed PMID: 16257508.

122. Pickup JC. Inflammation and activated innate immunity in the pathogenesis of type 2 diabetes. Diabetes Care. 2004;27(3):813-23. PubMed PMID: 14988310.

123. Lee YH, Pratley RE. The evolving role of inflammation in obesity and the metabolic syndrome. Curr Diab Rep. 2005;5(1):70-5. PubMed PMID: 15663921.

124. Wisse BE. The inflammatory syndrome: The role of adipose tissue cytokines in metabolic disorders linked to obesity. J Am Soc Nephrol. 2004;15(11):2792-800. doi: 10.1097/01.ASN.0000141966.69934.21. PubMed PMID: 15504932.

125. Hajishengallis G. Too old to fight? Aging and its toll on innate immunity. Mol Oral Microbiol. 2010;25(1):25-37. Epub 2010/03/23. doi: 10.1111/j.2041-1014.2009.00562.x. PubMed PMID: 20305805; PubMed Central PMCID: PMC2839454.

126. Bruunsgaard H, Pedersen M, Pedersen BK. Aging and proinflammatory cytokines. Curr Opin Hematol. 2001;8(3):131-6. PubMed PMID: 11303144.

127. Takahashi N, Akatsu T, Udagawa N, Sasaki T, Yamaguchi A, Moseley JM, et al. Osteoblastic cells are involved in osteoclast formation. Endocrinology. 1988;123(5):2600-2. doi: 10.1210/endo-123-5-2600. PubMed PMID: 2844518.

128. Perry HM, Skogen W, Chappel J, Kahn AJ, Wilner G, Teitelbaum SL. Partial characterization of a parathyroid hormone-stimulated resorption factor(s) from osteoblast-like cells. Endocrinology. 1989;125(4):2075-82. doi: 10.1210/endo-125-4-2075. PubMed PMID: 2791978.

129. Rodan GA, Martin TJ. Role of osteoblasts in hormonal control of bone resorption--A hypothesis. Calcif Tissue Int. 1981;33(4):349-51. PubMed PMID: 6271355.

130. Hofstetter W, Wetterwald A, Cecchini MC, Felix R, Fleisch H, Mueller C. Detection of transcripts for the receptor for macrophage colony-stimulating factor, c-fms, in murine osteoclasts. Proc Natl Acad Sci U S A. 1992;89(20):9637-41. PubMed PMID: 1409676; PubMed Central PMCID: PMCPMC50187.

131. Burger EH, van der Meer JW, Nijweide PJ. Osteoclast formation from mononuclear phagocytes: Role of bone-forming cells. J Cell Biol. 1984;99(6):1901-6. PubMed PMID: 6501407; PubMed Central PMCID: PMCPMC2113573.

132. Tsuda E, Goto M, Mochizuki S, Yano K, Kobayashi F, Morinaga T, et al. Isolation of a novel cytokine from human fibroblasts that specifically inhibits osteoclastogenesis. Biochem Biophys Res Commun. 1997;234(1):137-42. PubMed PMID: 9168977.

133. Simonet WS, Lacey DL, Dunstan CR, Kelley M, Chang MS, Lüthy R, et al. Osteoprotegerin: A novel secreted protein involved in the regulation of bone density. Cell. 1997;89(2):309-19. PubMed PMID: 9108485.

134. Horton JE, Raisz LG, Simmons HA, Oppenheim JJ, Mergenhagen SE. Bone resorbing activity in supernatant fluid from cultured human peripheral blood leukocytes. Science. 1972;177(4051):793-5. PubMed PMID: 5052733.

135. Arron JR, Choi Y. Bone versus immune system. Nature. 2000;408(6812):535-6. doi: 10.1038/35046196. PubMed PMID: 11117729.

136. Dewhirst FE, Stashenko PP, Mole JE, Tsurumachi T. Purification and partial sequence of human osteoclast-activating factor: Identity with interleukin 1 beta. J Immunol. 1985;135(4):2562-8. PubMed PMID: 3875658.

137. Gowen M, Wood DD, Ihrie EJ, McGuire MK, Russell RG. An interleukin 1 like factor stimulates bone resorption *in vitro*. Nature. 1983;306(5941):378-80. PubMed PMID: 6606132.

138. Nakashima T, Kobayashi Y, Yamasaki S, Kawakami A, Eguchi K, Sasaki H, et al. Protein expression and functional difference of membrane-bound and soluble receptor activator of NF-kappaB ligand: Modulation of the expression by osteotropic factors and cytokines. Biochem Biophys Res Commun. 2000;275(3):768-75. doi: 10.1006/bbrc.2000.3379. PubMed PMID: 10973797.

139. Lee YM, Fujikado N, Manaka H, Yasuda H, Iwakura Y. IL-1 plays an important role in the bone metabolism under physiological conditions. Int Immunol. 2010;22(10):805-16. Epub 2010/08/02. doi: 10.1093/intimm/dxq431. PubMed PMID: 20679512.

140. Jimi E, Shuto T, Koga T. Macrophage colony-stimulating factor and interleukin-1 alpha maintain the survival of osteoclast-like cells. Endocrinology. 1995;136(2):808-11. doi: 10.1210/endo.136.2.7835314. PubMed PMID: 7835314.

141. Zhang YH, Heulsmann A, Tondravi MM, Mukherjee A, Abu-Amer Y. Tumor necrosis factor-alpha (TNF) stimulates RANKL-induced osteoclastogenesis via coupling of TNF type 1 receptor and RANK signaling pathways. J Biol Chem. 2001;276(1):563-8. doi: 10.1074/jbc.M008198200. PubMed PMID: 11032840.

142. Lam J, Takeshita S, Barker JE, Kanagawa O, Ross FP, Teitelbaum SL. TNF-alpha induces osteoclastogenesis by direct stimulation of macrophages exposed to permissive levels of RANK ligand. J Clin Invest. 2000;106(12):1481-8. doi: 10.1172/JCI11176. PubMed PMID: 11120755; PubMed Central PMCID: PMCPMC387259.

143. Kim JH, Jin HM, Kim K, Song I, Youn BU, Matsuo K, et al. The mechanism of osteoclast differentiation induced by IL-1. J Immunol. 2009;183(3):1862-70. Epub 2009/07/08. doi: 10.4049/jimmunol.0803007. PubMed PMID: 19587010.

144. Wei S, Kitaura H, Zhou P, Ross FP, Teitelbaum SL. IL-1 mediates TNF-induced osteoclastogenesis. J Clin Invest. 2005;115(2):282-90. doi: 10.1172/JCI23394. PubMed PMID: 15668736; PubMed Central PMCID: PMCPMC544608.

145. Kotake S, Udagawa N, Takahashi N, Matsuzaki K, Itoh K, Ishiyama S, et al. IL-17 in synovial fluids from patients with rheumatoid arthritis is a potent stimulator of osteoclastogenesis. J Clin Invest. 1999;103(9):1345-52. doi: 10.1172/JCI5703. PubMed PMID: 10225978; PubMed Central PMCID: PMCPMC408356.

146. Sato K, Suematsu A, Okamoto K, Yamaguchi A, Morishita Y, Kadono Y, et al. Th17 functions as an osteoclastogenic helper T cell subset that links T cell activation and bone destruction. J Exp Med. 2006;203(12):2673-82. Epub 2006/11/06. doi:

10.1084/jem.20061775. PubMed PMID: 17088434; PubMed Central PMCID: PMCPMC2118166.

147. Frost A, Jonsson KB, Brändström H, Ljunghall S, Nilsson O, Ljunggren O. Interleukin (IL)-13 and IL-4 inhibit proliferation and stimulate IL-6 formation in human osteoblasts: Evidence for involvement of receptor subunits IL-13R, IL-13Ralpha, and IL-4Ralpha. Bone. 2001;28(3):268-74. PubMed PMID: 11248656.

148. Palmqvist P, Lundberg P, Persson E, Johansson A, Lundgren I, Lie A, et al. Inhibition of hormone and cytokine-stimulated osteoclastogenesis and bone resorption by interleukin-4 and interleukin-13 is associated with increased osteoprotegerin and decreased RANKL and RANK in a STAT6-dependent pathway. J Biol Chem. 2006;281(5):2414-29. Epub 2005/10/25. doi: 10.1074/jbc.M510160200. PubMed PMID: 16251181.

149. Yamada A, Takami M, Kawawa T, Yasuhara R, Zhao B, Mochizuki A, et al. Interleukin-4 inhibition of osteoclast differentiation is stronger than that of interleukin-13 and they are equivalent for induction of osteoprotegerin production from osteoblasts. Immunology. 2007;120(4):573-9. doi: 10.1111/j.1365-2567.2006.02538.x. PubMed PMID: 17343616; PubMed Central PMCID: PMCPMC2265899.

150. Wei S, Wang MW, Teitelbaum SL, Ross FP. Interleukin-4 reversibly inhibits osteoclastogenesis via inhibition of NF-kappa B and mitogen-activated protein kinase signaling. J Biol Chem. 2002;277(8):6622-30. Epub 2001/11/21. doi: 10.1074/jbc.M104957200. PubMed PMID: 11719504.

151. Evans KE, Fox SW. Interleukin-10 inhibits osteoclastogenesis by reducing NFATc1 expression and preventing its translocation to the nucleus. BMC Cell Biol. 2007;8:4. Epub 2007/01/19. doi: 10.1186/1471-2121-8-4. PubMed PMID: 17239241; PubMed Central PMCID: PMCPMC1781937.

152. Mohamed SG, Sugiyama E, Shinoda K, Taki H, Hounoki H, Abdel-Aziz HO, et al. Interleukin-10 inhibits RANKL-mediated expression of NFATc1 in part via suppression of c-Fos and c-Jun in RAW264.7 cells and mouse bone marrow cells. Bone. 2007;41(4):592-602. Epub 2007/06/13. doi: 10.1016/j.bone.2007.05.016. PubMed PMID: 17627913.

153. Williams RO, Feldmann M, Maini RN. Anti-tumor necrosis factor ameliorates joint disease in murine collagen-induced arthritis. Proc Natl Acad Sci U S A. 1992;89(20):9784-8. PubMed PMID: 1409699; PubMed Central PMCID: PMCPMC50217.

154. Keffer J, Probert L, Cazlaris H, Georgopoulos S, Kaslaris E, Kioussis D, et al. Transgenic mice expressing human tumour necrosis factor: A predictive genetic model of arthritis. EMBO J. 1991;10(13):4025-31. PubMed PMID: 1721867; PubMed Central PMCID: PMCPMC453150.

155. Polzer K, Joosten L, Gasser J, Distler JH, Ruiz G, Baum W, et al. Interleukin-1 is essential for systemic inflammatory bone loss. Ann Rheum Dis. 2010;69(1):284-90. doi: 10.1136/ard.2008.104786. PubMed PMID: 19196726.

156. Tamura T, Udagawa N, Takahashi N, Miyaura C, Tanaka S, Yamada Y, et al. Soluble interleukin-6 receptor triggers osteoclast formation by interleukin 6. Proc Natl Acad Sci U S A. 1993;90(24):11924-8. PubMed PMID: 8265649; PubMed Central PMCID: PMCPMC48097.

157. de la Mata J, Uy HL, Guise TA, Story B, Boyce BF, Mundy GR, et al. Interleukin-6 enhances hypercalcemia and bone resorption mediated by parathyroid hormone-related protein *in vivo*. J Clin Invest. 1995;95(6):2846-52. doi: 10.1172/JCI117990. PubMed PMID: 7769125; PubMed Central PMCID: PMCPMC295971.

158. Kudo O, Sabokbar A, Pocock A, Itonaga I, Fujikawa Y, Athanasou NA. Interleukin-6 and interleukin-11 support human osteoclast formation by a RANKL-independent mechanism. Bone. 2003;32(1):1-7. PubMed PMID: 12584029.

159. Koenders MI, Lubberts E, Oppers-Walgreen B, van den Bersselaar L, Helsen MM, Di Padova FE, et al. Blocking of interleukin-17 during reactivation of experimental arthritis prevents joint inflammation and bone erosion by decreasing RANKL and interleukin-1. Am J Pathol. 2005;167(1):141-9. doi: 10.1016/S0002-9440(10)62961-6. PubMed PMID: 15972960; PubMed Central PMCID: PMCPMC1603454.

160. Adamopoulos IE, Chao CC, Geissler R, Laface D, Blumenschein W, Iwakura Y, et al. Interleukin-17A upregulates receptor activator of NF-kappaB on osteoclast precursors. Arthritis Res Ther. 2010;12(1):R29. Epub 2010/02/18. doi: 10.1186/ar2936. PubMed PMID: 20167120; PubMed Central PMCID: PMCPMC2875663.

161. Fossiez F, Djossou O, Chomarat P, Flores-Romo L, Ait-Yahia S, Maat C, et al. T cell interleukin-17 induces stromal cells to produce proinflammatory and hematopoietic cytokines. J Exp Med. 1996;183(6):2593-603. PubMed PMID: 8676080; PubMed Central PMCID: PMCPMC2192621.

162. Jovanovic DV, Di Battista JA, Martel-Pelletier J, Jolicoeur FC, He Y, Zhang M, et al. IL-17 stimulates the production and expression of proinflammatory cytokines, IL-beta and TNF-alpha, by human macrophages. J Immunol. 1998;160(7):3513-21. PubMed PMID: 9531313.

163. Hwang SY, Kim JY, Kim KW, Park MK, Moon Y, Kim WU, et al. IL-17 induces production of IL-6 and IL-8 in rheumatoid arthritis synovial fibroblasts via NF-kappaB- and PI3-kinase/Akt-dependent pathways. Arthritis Res Ther. 2004;6(2):R120-8. Epub 2004/01/21. doi: 10.1186/ar1038. PubMed PMID: 15059275; PubMed Central PMCID: PMCPMC400429.

164. Wang R, Braughton KR, Kretschmer D, Bach TH, Queck SY, Li M, et al. Identification of novel cytolytic peptides as key virulence determinants for community-associated MRSA. Nat Med. 2007;13(12):1510-4. Epub 2007/11/11. doi: 10.1038/nm1656. PubMed PMID: 17994102.

165. Flammier S, Rasigade JP, Badiou C, Henry T, Vandenesch F, Laurent F, et al. Human monocyte-derived osteoclasts are targeted by staphylococcal pore-forming toxins and

superantigens. PLoS One. 2016;11(3):e0150693. Epub 2016/03/02. doi: 10.1371/journal.pone.0150693. PubMed PMID: 26934588; PubMed Central PMCID: PMCPMC4774977.

166.   Bocchini CE, Hulten KG, Mason EO, Gonzalez BE, Hammerman WA, Kaplan SL. Panton-Valentine leukocidin genes are associated with enhanced inflammatory response and local disease in acute hematogenous *Staphylococcus aureus* osteomyelitis in children. Pediatrics. 2006;117(2):433-40. doi: 10.1542/peds.2005-0566. PubMed PMID: 16452363.

167.   Claro T, Widaa A, McDonnell C, Foster TJ, O'Brien FJ, Kerrigan SW. *Staphylococcus aureus* protein A binding to osteoblast tumour necrosis factor receptor 1 results in activation of nuclear factor kappa B and release of interleukin-6 in bone infection. Microbiology. 2013;159(Pt 1):147-54. Epub 2012/11/15. doi: 10.1099/mic.0.063016-0. PubMed PMID: 23154968.

168.   Traber KE, Lee E, Benson S, Corrigan R, Cantera M, Shopsin B, et al. *agr* function in clinical *Staphylococcus aureus* isolates. Microbiology. 2008;154(Pt 8):2265-74. doi: 10.1099/mic.0.2007/011874-0. PubMed PMID: 18667559; PubMed Central PMCID: PMCPMC4904715.

169.   Yarwood JM, Schlievert PM. Quorum sensing in *Staphylococcus* infections. J Clin Invest. 2003;112(11):1620-5. doi: 10.1172/JCI20442. PubMed PMID: 14660735; PubMed Central PMCID: PMCPMC281656.

170.   Vuong C, Saenz HL, Götz F, Otto M. Impact of the *agr* quorum-sensing system on adherence to polystyrene in *Staphylococcus aureus*. J Infect Dis. 2000;182(6):1688-93. Epub 2000/10/13. doi: 10.1086/317606. PubMed PMID: 11069241.

171.   Meyle E, Stroh P, Günther F, Hoppy-Tichy T, Wagner C, Hänsch GM. Destruction of bacterial biofilms by polymorphonuclear neutrophils: Relative contribution of phagocytosis, DNA release, and degranulation. Int J Artif Organs. 2010;33(9):608-20. PubMed PMID: 20890882.

172.   Thurlow LR, Hanke ML, Fritz T, Angle A, Aldrich A, Williams SH, et al. *Staphylococcus aureus* biofilms prevent macrophage phagocytosis and attenuate inflammation *in vivo*. J Immunol. 2011;186(11):6585-96. Epub 2011/04/27. doi: 10.4049/jimmunol.1002794. PubMed PMID: 21525381; PubMed Central PMCID: PMCPMC3110737.

173.   Feuerstein R, Kolter J, Henneke P. Dynamic interactions between dermal macrophages and *Staphylococcus aureus*. J Leukoc Biol. 2017;101(1):99-106. doi: 10.1189/jlb.3MR0316-097RR. PubMed PMID: 27733573.

174.   Kobayashi SD, Malachowa N, DeLeo FR. Pathogenesis of *Staphylococcus aureus* abscesses. Am J Pathol. 2015;185(6):1518-27. doi: 10.1016/j.ajpath.2014.11.030. PubMed PMID: 25749135; PubMed Central PMCID: PMCPMC4450319.

175.   Ibrahim F, Khan T, Pujalte GG. Bacterial skin infections. Prim Care. 2015;42(4):485-99. doi: 10.1016/j.pop.2015.08.001. PubMed PMID: 26612370.

176. Mistry RD. Skin and soft tissue infections. Pediatr Clin North Am. 2013;60(5):1063-82. doi: 10.1016/j.pcl.2013.06.011. PubMed PMID: 24093896.

177. Miller LS. Toll-like receptors in skin. Adv Dermatol. 2008;24:71-87. PubMed PMID: 19256306; PubMed Central PMCID: PMCPMC2633625.

178. Bitschar K, Wolz C, Krismer B, Peschel A, Schittek B. Keratinocytes as sensors and central players in the immune defense against *Staphylococcus aureus* in the skin. J Dermatol Sci. 2017;87(3):215-20. doi: 10.1016/j.jdermsci.2017.06.003. PubMed PMID: 28655473.

179. Pasparakis M, Haase I, Nestle FO. Mechanisms regulating skin immunity and inflammation. Nat Rev Immunol. 2014;14(5):289-301. doi: 10.1038/nri3646. PubMed PMID: 24722477.

180. Walsh MC, Kim N, Kadono Y, Rho J, Lee SY, Lorenzo J, et al. Osteoimmunology: Interplay between the immune system and bone metabolism. Annu Rev Immunol. 2006;24:33-63. doi: 10.1146/annurev.immunol.24.021605.090646. PubMed PMID: 16551243.

181. Bubeck Wardenburg J, Williams WA, Missiakas D. Host defenses against *Staphylococcus aureus* infection require recognition of bacterial lipoproteins. Proc Natl Acad Sci U S A. 2006;103(37):13831-6. Epub 2006/09/05. doi: 10.1073/pnas.0603072103. PubMed PMID: 16954184; PubMed Central PMCID: PMCPMC1564215.

182. Tawaratsumida K, Furuyashiki M, Katsumoto M, Fujimoto Y, Fukase K, Suda Y, et al. Characterization of N-terminal structure of TLR2-activating lipoprotein in *Staphylococcus aureus*. J Biol Chem. 2009;284(14):9147-52. Epub 2009/02/13. doi: 10.1074/jbc.M900429200. PubMed PMID: 19218237; PubMed Central PMCID: PMCPMC2666565.

183. Liu L, Zhou X, Shi J, Xie X, Yuan Z. Toll-like receptor-9 induced by physical trauma mediates release of cytokines following exposure to CpG motif in mouse skin. Immunology. 2003;110(3):341-7. PubMed PMID: 14632662; PubMed Central PMCID: PMCPMC1783050.

184. Feuerstein R, Seidl M, Prinz M, Henneke P. MyD88 in macrophages is critical for abscess resolution in staphylococcal skin infection. J Immunol. 2015;194(6):2735-45. doi: 10.4049/jimmunol.1402566. PubMed PMID: 25681348.

185. Olaru F, Jensen LE. *Staphylococcus aureus* stimulates neutrophil targeting chemokine expression in keratinocytes through an autocrine IL-1alpha signaling loop. J Invest Dermatol. 2010;130(7):1866-76. doi: 10.1038/jid.2010.37. PubMed PMID: 20182449; PubMed Central PMCID: PMCPMC2886182.

186. Pietrocola G, Arciola CR, Rindi S, Di Poto A, Missineo A, Montanaro L, et al. Toll-like receptors (TLRs) in innate immune defense against *Staphylococcus aureus*. Int J Artif Organs. 2011;34(9):799-810. doi: 10.5301/ijao.5000030. PubMed PMID: 22094559.

187. van der Meer AJ, Achouiti A, van der Ende A, Soussan AA, Florquin S, de Vos A, et al. Toll-like receptor 9 enhances bacterial clearance and limits lung consolidation in murine pneumonia caused by methicillin resistant *Staphylococcus aureus*. Mol Med. 2016;22:292-9. Epub 2016/06/24. doi: 10.2119/molmed.2015.00242. PubMed PMID: 27508882; PubMed Central PMCID: PMCPMC5023514.

188. Hoebe K, Georgel P, Rutschmann S, Du X, Mudd S, Crozat K, et al. CD36 is a sensor of diacylglycerides. Nature. 2005;433(7025):523-7. doi: 10.1038/nature03253. PubMed PMID: 15690042.

189. Moriwaki M, Iwamoto K, Niitsu Y, Matsushima A, Yanase Y, Hisatsune J, et al. *Staphylococcus aureus* from atopic dermatitis skin accumulates in the lysosomes of keratinocytes with induction of IL-1α secretion via TLR9. Allergy. 2019;74(3):560-71. Epub 2018/11/12. doi: 10.1111/all.13622. PubMed PMID: 30269350.

190. Schaffler H, Demircioglu DD, Kuhner D, Menz S, Bender A, Autenrieth IB, et al. NOD2 stimulation by *Staphylococcus aureus*-derived peptidoglycan is boosted by Toll-like receptor 2 costimulation with lipoproteins in dendritic cells. Infect Immun. 2014;82(11):4681-8. doi: 10.1128/IAI.02043-14. PubMed PMID: 25156723; PubMed Central PMCID: PMCPMC4249339.

191. Parker D, Planet PJ, Soong G, Narechania A, Prince A. Induction of type I interferon signaling determines the relative pathogenicity of *Staphylococcus aureus* strains. PLoS Pathog. 2014;10(2):e1003951. doi: 10.1371/journal.ppat.1003951. PubMed PMID: 24586160; PubMed Central PMCID: PMCPMC3930619.

192. Kapetanovic R, Jouvion G, Fitting C, Parlato M, Blanchet C, Huerre M, et al. Contribution of NOD2 to lung inflammation during *Staphylococcus aureus*-induced pneumonia. Microbes Infect. 2010;12(10):759-67. doi: 10.1016/j.micinf.2010.05.003. PubMed PMID: 20493961.

193. Hruz P, Zinkernagel AS, Jenikova G, Botwin GJ, Hugot JP, Karin M, et al. NOD2 contributes to cutaneous defense against *Staphylococcus aureus* through alpha-toxin-dependent innate immune activation. Proc Natl Acad Sci U S A. 2009;106(31):12873-8. doi: 10.1073/pnas.0904958106. PubMed PMID: 19541630; PubMed Central PMCID: PMCPMC2722361.

194. Deshmukh HS, Hamburger JB, Ahn SH, McCafferty DG, Yang SR, Fowler VG, Jr. Critical role of NOD2 in regulating the immune response to *Staphylococcus aureus*. Infect Immun. 2009;77(4):1376-82. doi: 10.1128/IAI.00940-08. PubMed PMID: 19139201; PubMed Central PMCID: PMCPMC2663139.

195. Mizutani H, Black R, Kupper TS. Human keratinocytes produce but do not process pro-interleukin-1 (IL-1) beta. Different strategies of IL-1 production and processing in monocytes and keratinocytes. J Clin Invest. 1991;87(3):1066-71. doi: 10.1172/JCI115067. PubMed PMID: 1999487; PubMed Central PMCID: PMCPMC329902.

196. Kashem SW, Haniffa M, Kaplan DH. Antigen-presenting cells in the skin. Annu Rev Immunol. 2017;35:469-99. doi: 10.1146/annurev-immunol-051116-052215. PubMed PMID: 28226228.

197. Abtin A, Jain R, Mitchell AJ, Roediger B, Brzoska AJ, Tikoo S, et al. Perivascular macrophages mediate neutrophil recruitment during bacterial skin infection. Nat Immunol. 2014;15(1):45-53. doi: 10.1038/ni.2769. PubMed PMID: 24270515; PubMed Central PMCID: PMCPMC4097073.

198. Steen MB, Tuck FL, Selvan RS. Spontaneous activation of endothelial cells: A central role for endogenous IL-1alpha. In Vitro Cell Dev Biol Anim. 1999;35(6):327-32. doi: 10.1007/s11626-999-0082-9. PubMed PMID: 10476919.

199. Miller LS, Pietras EM, Uricchio LH, Hirano K, Rao S, Lin H, et al. Inflammasome-mediated production of IL-1beta is required for neutrophil recruitment against *Staphylococcus aureus in vivo*. J Immunol. 2007;179(10):6933-42. PubMed PMID: 17982084.

200. Wilkinson BJ, Kim Y, Peterson PK, Quie PG, Michael AF. Activation of complement by cell surface components of *Staphylococcus aureus*. Infect Immun. 1978;20(2):388-92. PubMed PMID: 669803; PubMed Central PMCID: PMCPMC421867.

201. van Kessel KP, Bestebroer J, van Strijp JA. Neutrophil-mediated phagocytosis of *Staphylococcus aureus*. Front Immunol. 2014;5:467. Epub 2014/09/26. doi: 10.3389/fimmu.2014.00467. PubMed PMID: 25309547; PubMed Central PMCID: PMCPMC4176147.

202. Laarman A, Milder F, van Strijp J, Rooijakkers S. Complement inhibition by gram-positive pathogens: Molecular mechanisms and therapeutic implications. J Mol Med (Berl). 2010;88(2):115-20. doi: 10.1007/s00109-009-0572-y. PubMed PMID: 20062962; PubMed Central PMCID: PMCPMC2832872.

203. Dumont AL, Nygaard TK, Watkins RL, Smith A, Kozhaya L, Kreiswirth BN, et al. Characterization of a new cytotoxin that contributes to *Staphylococcus aureus* pathogenesis. Mol Microbiol. 2011;79(3):814-25. Epub 2010/12/13. doi: 10.1111/j.1365-2958.2010.07490.x. PubMed PMID: 21255120; PubMed Central PMCID: PMCPMC3312031.

204. Kretschmer D, Gleske AK, Rautenberg M, Wang R, Köberle M, Bohn E, et al. Human formyl peptide receptor 2 senses highly pathogenic *Staphylococcus aureus*. Cell Host Microbe. 2010;7(6):463-73. doi: 10.1016/j.chom.2010.05.012. PubMed PMID: 20542250; PubMed Central PMCID: PMCPMC3417054.

205. Rathinam VA, Fitzgerald KA. Inflammasome complexes: Emerging mechanisms and effector functions. Cell. 2016;165(4):792-800. doi: 10.1016/j.cell.2016.03.046. PubMed PMID: 27153493; PubMed Central PMCID: PMCPMC5503689.

206. Netea MG, van de Veerdonk FL, van der Meer JW, Dinarello CA, Joosten LA. Inflammasome-independent regulation of IL-1-family cytokines. Annu Rev Immunol. 2015;33:49-77. doi: 10.1146/annurev-immunol-032414-112306. PubMed PMID: 25493334.

207. Cho JS, Guo Y, Ramos RI, Hebroni F, Plaisier SB, Xuan C, et al. Neutrophil-derived IL-1beta is sufficient for abscess formation in immunity against *Staphylococcus aureus* in mice. PLoS Pathog. 2012;8(11):e1003047. doi: 10.1371/journal.ppat.1003047. PubMed PMID: 23209417; PubMed Central PMCID: PMC3510260.

208. Sabroe I, Prince LR, Jones EC, Horsburgh MJ, Foster SJ, Vogel SN, et al. Selective roles for Toll-like receptor (TLR)2 and TLR4 in the regulation of neutrophil activation and life span. J Immunol. 2003;170(10):5268-75. PubMed PMID: 12734376.

209. Hayashi F, Means TK, Luster AD. Toll-like receptors stimulate human neutrophil function. Blood. 2003;102(7):2660-9. Epub 2003/06/26. doi: 10.1182/blood-2003-04-1078. PubMed PMID: 12829592.

210. Lotz S, Aga E, Wilde I, van Zandbergen G, Hartung T, Solbach W, et al. Highly purified lipoteichoic acid activates neutrophil granulocytes and delays their spontaneous apoptosis via CD14 and TLR2. J Leukoc Biol. 2004;75(3):467-77. Epub 2003/12/12. doi: 10.1189/jlb.0803360. PubMed PMID: 14673018.

211. Krishna S, Miller LS. Innate and adaptive immune responses against S*taphylococcus aureus* skin infections. Semin Immunopathol. 2012;34(2):261-80. doi: 10.1007/s00281-011-0292-6. PubMed PMID: 22057887.

212. Miller LS, Cho JS. Immunity against *Staphylococcus aureus* cutaneous infections. Nat Rev Immunol. 2011;11(8):505-18. doi: 10.1038/nri3010. PubMed PMID: 21720387.

213. Rigby KM, DeLeo FR. Neutrophils in innate host defense against *Staphylococcus aureus* infections. Semin Immunopathol. 2012;34(2):237-59. Epub 2011/11/12. doi: 10.1007/s00281-011-0295-3. PubMed PMID: 22080185; PubMed Central PMCID: PMCPMC3271231.

214. Martin CJ, Booty MG, Rosebrock TR, Nunes-Alves C, Desjardins DM, Keren I, et al. Efferocytosis is an innate antibacterial mechanism. Cell Host Microbe. 2012;12(3):289-300. doi: 10.1016/j.chom.2012.06.010. PubMed PMID: 22980326; PubMed Central PMCID: PMCPMC3517204.

215. Barker RN, Erwig LP, Hill KS, Devine A, Pearce WP, Rees AJ. Antigen presentation by macrophages is enhanced by the uptake of necrotic, but not apoptotic, cells. Clin Exp Immunol. 2002;127(2):220-5. PubMed PMID: 11876743; PubMed Central PMCID: PMCPMC1906351.

216. Guerra FE, Borgogna TR, Patel DM, Sward EW, Voyich JM. Epic Immune battles of history: Neutrophils vs. *Staphylococcus aureus*. Front Cell Infect Microbiol. 2017;7:286.

doi: 10.3389/fcimb.2017.00286. PubMed PMID: 28713774; PubMed Central PMCID: PMCPMC5491559.

217.   Harrison CJ. Innate immunity as a key element in host defense against methicillin resistant *Staphylococcus aureus*. Minerva Pediatr. 2009;61(5):503-14. Epub 2009/10/02. PubMed PMID: 19794376.

218.   Okumura CY, Nizet V. Subterfuge and sabotage: Evasion of host innate defenses by invasive gram-positive bacterial pathogens. Annu Rev Microbiol. 2014;68:439-58. doi: 10.1146/annurev-micro-092412-155711. PubMed PMID: 25002085; PubMed Central PMCID: PMCPMC4343215.

219.   Buvelot H, Posfay-Barbe KM, Linder P, Schrenzel J, Krause KH. *Staphylococcus aureus,* phagocyte NADPH oxidase and chronic granulomatous disease. FEMS Microbiol Rev. 2017;41(2):139-57. doi: 10.1093/femsre/fuw042. PubMed PMID: 27965320.

220.   Beavers WN, Skaar EP. Neutrophil-generated oxidative stress and protein damage in *Staphylococcus aureus*. Pathog Dis. 2016;74(6). doi: 10.1093/femspd/ftw060. PubMed PMID: 27354296.

221.   Bogdan C. Nitric oxide and the immune response. Nat Immunol. 2001;2(10):907-16. doi: 10.1038/ni1001-907. PubMed PMID: 11577346.

222.   Li C, Li H, Jiang Z, Zhang T, Wang Y, Li Z, et al. Interleukin-33 increases antibacterial defense by activation of inducible nitric oxide synthase in skin. PLoS Pathog. 2014;10(2):e1003918. doi: 10.1371/journal.ppat.1003918. PubMed PMID: 24586149; PubMed Central PMCID: PMCPMC3930573.

223.   Zhao YT, Guo JH, Wu ZL, Xiong Y, Zhou WL. Innate immune responses of epididymal epithelial cells to *Staphylococcus aureus* infection. Immunol Lett. 2008;119(1-2):84-90. doi: 10.1016/j.imlet.2008.05.002. PubMed PMID: 18571736.

224.   Kobayashi Y. Neutrophil biology: An update. EXCLI J. 2015;14:220-7. doi: 10.17179/excli2015-102. PubMed PMID: 26600743; PubMed Central PMCID: PMCPMC4650944.

225.   Greenlee-Wacker M, DeLeo FR, Nauseef WM. How methicillin-resistant *Staphylococcus aureus* evade neutrophil killing. Curr Opin Hematol. 2015;22(1):30-5. doi: 10.1097/MOH.0000000000000096. PubMed PMID: 25394313; PubMed Central PMCID: PMCPMC4343318.

226.   Yipp BG, Petri B, Salina D, Jenne CN, Scott BN, Zbytnuik LD, et al. Infection-induced NETosis is a dynamic process involving neutrophil multitasking *in vivo*. Nat Med. 2012;18(9):1386-93. doi: 10.1038/nm.2847. PubMed PMID: 22922410; PubMed Central PMCID: PMCPMC4529131.

227. Brinkmann V, Reichard U, Goosmann C, Fauler B, Uhlemann Y, Weiss DS, et al. Neutrophil extracellular traps kill bacteria. Science. 2004;303(5663):1532-5. doi: 10.1126/science.1092385. PubMed PMID: 15001782.

228. Thammavongsa V, Missiakas DM, Schneewind O. *Staphylococcus aureus* degrades neutrophil extracellular traps to promote immune cell death. Science. 2013;342(6160):863-6. doi: 10.1126/science.1242255. PubMed PMID: 24233725; PubMed Central PMCID: PMCPMC4026193.

229. Singer AJ, Talan DA. Management of skin abscesses in the era of methicillin-resistant *Staphylococcus aureus*. N Engl J Med. 2014;370(11):1039-47. doi: 10.1056/NEJMra1212788. PubMed PMID: 24620867.

230. Brandt SL, Klopfenstein N, Wang S, Winfree S, McCarthy BP, Territo PR, et al. Macrophage-derived LTB4 promotes abscess formation and clearance of *Staphylococcus aureus* skin infection in mice. PLoS Pathog. 2018;14(8):e1007244. Epub 2018/08/13. doi: 10.1371/journal.ppat.1007244. PubMed PMID: 30102746; PubMed Central PMCID: PMCPMC6107286.

231. Cheng AG, Kim HK, Burts ML, Krausz T, Schneewind O, Missiakas DM. Genetic requirements for *Staphylococcus aureus* abscess formation and persistence in host tissues. FASEB journal : official publication of the Federation of American Societies for Experimental Biology. 2009;23(10):3393-404. doi: 10.1096/fj.09-135467. PubMed PMID: 19525403; PubMed Central PMCID: PMC2747682.

232. Tucker KA, Reilly SS, Leslie CS, Hudson MC. Intracellular *Staphylococcus aureus* induces apoptosis in mouse osteoblasts. FEMS Microbiol Lett. 2000;186(2):151-6. doi: 10.1111/j.1574-6968.2000.tb09096.x. PubMed PMID: 10802163.

233. Takayanagi H. Osteoimmunology: Shared mechanisms and crosstalk between the immune and bone systems. Nat Rev Immunol. 2007;7(4):292-304. doi: 10.1038/nri2062. PubMed PMID: 17380158.

234. Oeckinghaus A, Hayden MS, Ghosh S. Crosstalk in NF-κB signaling pathways. Nat Immunol. 2011;12(8):695-708. Epub 2011/07/19. doi: 10.1038/ni.2065. PubMed PMID: 21772278.

235. Redlich K, Smolen JS. Inflammatory bone loss: pathogenesis and therapeutic intervention. Nat Rev Drug Discov. 2012;11(3):234-50. Epub 2012/03/01. doi: 10.1038/nrd3669. PubMed PMID: 22378270.

236. Braun T, Zwerina J. Positive regulators of osteoclastogenesis and bone resorption in rheumatoid arthritis. Arthritis Res Ther. 2011;13(4):235. Epub 2011/07/28. doi: 10.1186/ar3380. PubMed PMID: 21861862; PubMed Central PMCID: PMCPMC3239343.

237. Martin TJ, Romas E, Gillespie MT. Interleukins in the control of osteoclast differentiation. Crit Rev Eukaryot Gene Expr. 1998;8(2):107-23. PubMed PMID: 9714893.

238.   Evans CA, Jellis J, Hughes SP, Remick DG, Friedland JS. Tumor necrosis factor-alpha, interleukin-6, and interleukin-8 secretion and the acute-phase response in patients with bacterial and tuberculous osteomyelitis. J Infect Dis. 1998;177(6):1582-7. PubMed PMID: 9607836; PubMed Central PMCID: PMCPMC3034154.

239.   Klosterhalfen B, Peters KM, Tons C, Hauptmann S, Klein CL, Kirkpatrick CJ. Local and systemic inflammatory mediator release in patients with acute and chronic posttraumatic osteomyelitis. J Trauma. 1996;40(3):372-8. PubMed PMID: 8601852.

240.   Meghji S, Crean SJ, Hill PA, Sheikh M, Nair SP, Heron K, et al. Surface-associated protein from *Staphylococcus aureus* stimulates osteoclastogenesis: possible role in *S. aureus*-induced bone pathology. Br J Rheumatol. 1998;37(10):1095-101. PubMed PMID: 9825749.

241.   Trouillet-Assant S, Gallet M, Nauroy P, Rasigade JP, Flammier S, Parroche P, et al. Dual impact of live *Staphylococcus aureus* on the osteoclast lineage, leading to increased bone resorption. J Infect Dis. 2015;211(4):571-81. Epub 2014/07/08. doi: 10.1093/infdis/jiu386. PubMed PMID: 25006047.

242.   Jimi E, Nakamura I, Duong LT, Ikebe T, Takahashi N, Rodan GA, et al. Interleukin 1 induces multinucleation and bone-resorbing activity of osteoclasts in the absence of osteoblasts/stromal cells. Exp Cell Res. 1999;247(1):84-93. doi: 10.1006/excr.1998.4320. PubMed PMID: 10047450.

243.   Boles BR, Thoendel M, Roth AJ, Horswill AR. Identification of genes involved in polysaccharide-independent *Staphylococcus aureus* biofilm formation. PLoS One. 2010;5(4):e10146. Epub 2010/04/14. doi: 10.1371/journal.pone.0010146. PubMed PMID: 20418950; PubMed Central PMCID: PMCPMC2854687.

244.   Kaito C, Saito Y, Nagano G, Ikuo M, Omae Y, Hanada Y, et al. Transcription and translation products of the cytolysin gene *psm-mec* on the mobile genetic element SCC*mec* regulate *Staphylococcus aureus* virulence. PLoS Pathog. 2011;7(2):e1001267. Epub 2011/02/03. doi: 10.1371/journal.ppat.1001267. PubMed PMID: 21304931; PubMed Central PMCID: PMCPMC3033363.

245.   Cao F, Zhou W, Liu G, Xia T, Liu M, Mi B, et al. Peptidoglycan promotes osteoclastogenesis via TLR2-mediated activation of the NF-κB/NFATc1 signaling pathway. Am J Transl Res. 2017;9(11):5022-30. Epub 2017/11/15. PubMed PMID: 29218100; PubMed Central PMCID: PMCPMC5714786.

246.   Sabokbar A, Mahoney DJ, Hemingway F, Athanasou NA. Non-canonical (RANKL-independent) pathways of osteoclast differentiation and their role in musculoskeletal diseases. Clin Rev Allergy Immunol. 2016;51(1):16-26. doi: 10.1007/s12016-015-8523-6. PubMed PMID: 26578261.

247.   Boyle WJ, Simonet WS, Lacey DL. Osteoclast differentiation and activation. Nature. 2003;423(6937):337-42. doi: 10.1038/nature01658. PubMed PMID: 12748652.

248. Ji JD, Park-Min KH, Shen Z, Fajardo RJ, Goldring SR, McHugh KP, et al. Inhibition of RANK expression and osteoclastogenesis by TLRs and IFN-gamma in human osteoclast precursors. J Immunol. 2009;183(11):7223-33. Epub 2009/11/04. doi: 10.4049/jimmunol.0900072. PubMed PMID: 19890054; PubMed Central PMCID: PMCPMC2783334.

249. Zhao B, Ivashkiv LB. Negative regulation of osteoclastogenesis and bone resorption by cytokines and transcriptional repressors. Arthritis Res Ther. 2011;13(4):234. Epub 2011/07/28. doi: 10.1186/ar3379. PubMed PMID: 21861861; PubMed Central PMCID: PMCPMC3239342.

250. Takami M, Kim N, Rho J, Choi Y. Stimulation by toll-like receptors inhibits osteoclast differentiation. J Immunol. 2002;169(3):1516-23. PubMed PMID: 12133979.

251. Haas DW, McAndrew MP. Bacterial osteomyelitis in adults: Evolving considerations in diagnosis and treatment. Am J Med. 1996;101(5):550-61. PubMed PMID: 8948280.

252. Glass DA, Bialek P, Ahn JD, Starbuck M, Patel MS, Clevers H, et al. Canonical Wnt signaling in differentiated osteoblasts controls osteoclast differentiation. Dev Cell. 2005;8(5):751-64. doi: 10.1016/j.devcel.2005.02.017. PubMed PMID: 15866165.

253. Kim N, Kadono Y, Takami M, Lee J, Lee SH, Okada F, et al. Osteoclast differentiation independent of the TRANCE-RANK-TRAF6 axis. J Exp Med. 2005;202(5):589-95. doi: 10.1084/jem.20050978. PubMed PMID: 16147974; PubMed Central PMCID: PMCPMC2212875.

254. Kadono Y, Okada F, Perchonock C, Jang HD, Lee SY, Kim N, et al. Strength of TRAF6 signalling determines osteoclastogenesis. EMBO Rep. 2005;6(2):171-6. doi: 10.1038/sj.embor.7400345. PubMed PMID: 15678156; PubMed Central PMCID: PMCPMC1299255.

255. Lee SE, Chung WJ, Kwak HB, Chung CH, Kwack KB, Lee ZH, et al. Tumor necrosis factor-alpha supports the survival of osteoclasts through the activation of Akt and ERK. J Biol Chem. 2001;276(52):49343-9. Epub 2001/10/23. doi: 10.1074/jbc.M103642200. PubMed PMID: 11675379.

256. Kobayashi K, Takahashi N, Jimi E, Udagawa N, Takami M, Kotake S, et al. Tumor necrosis factor alpha stimulates osteoclast differentiation by a mechanism independent of the ODF/RANKL-RANK interaction. J Exp Med. 2000;191(2):275-86. doi: 10.1084/jem.191.2.275. PubMed PMID: 10637272; PubMed Central PMCID: PMCPMC2195746.

257. Ukai T, Yumoto H, Gibson FC, Genco CA. Macrophage-elicited osteoclastogenesis in response to bacterial stimulation requires Toll-like receptor 2-dependent tumor necrosis factor-alpha production. Infect Immun. 2008;76(2):812-9. Epub 2007/11/12. doi: 10.1128/IAI.01241-07. PubMed PMID: 17998311; PubMed Central PMCID: PMCPMC2223461.

258. Pfeilschifter J, Chenu C, Bird A, Mundy GR, Roodman GD. Interleukin-1 and tumor necrosis factor stimulate the formation of human osteoclastlike cells *in vitro*. J Bone Miner Res. 1989;4(1):113-8. doi: 10.1002/jbmr.5650040116. PubMed PMID: 2785743.

259. Berendt T, Byren I. Bone and joint infection. Clin Med (Lond). 2004;4(6):510-8. PubMed PMID: 15656476.

260. Birt MC, Anderson DW, Bruce Toby E, Wang J. Osteomyelitis: Recent advances in pathophysiology and therapeutic strategies. J Orthop. 2017;14(1):45-52. Epub 2016/10/26. doi: 10.1016/j.jor.2016.10.004. PubMed PMID: 27822001; PubMed Central PMCID: PMCPMC5090239.

261. Shiratori T, Kyumoto-Nakamura Y, Kukita A, Uehara N, Zhang J, Koda K, et al. IL-1β induces pathologically activated osteoclasts bearing extremely high levels of resorbing activity: A possible pathological subpopulation of osteoclasts, accompanied by suppressed expression of kindlin-3 and talin-1. J Immunol. 2018;200(1):218-28. Epub 2017/11/15. doi: 10.4049/jimmunol.1602035. PubMed PMID: 29141864.

262. Jandinski JJ. Osteoclast activating factor is now interleukin-1 beta: Historical perspective and biological implications. J Oral Pathol. 1988;17(4):145-52. PubMed PMID: 3139850.

263. Brandt SL, Putnam NE, Cassat JE, Serezani CH. Innate Immunity to *Staphylococcus aureus:* Evolving paradigms in soft tissue and invasive infections. J Immunol. 2018;200(12):3871-80. doi: 10.4049/jimmunol.1701574. PubMed PMID: 29866769; PubMed Central PMCID: PMCPMC6028009.

264. Takeuchi O, Hoshino K, Akira S. Cutting edge: TLR2-deficient and MyD88-deficient mice are highly susceptible to *Staphylococcus aureus* infection. J Immunol. 2000;165(10):5392-6. PubMed PMID: 11067888.

265. Cho JS, Guo Y, Ramos RI, Hebroni F, Plaisier SB, Xuan C, et al. Neutrophil-derived IL-1β is sufficient for abscess formation in immunity against *Staphylococcus aureus* in mice. PLoS Pathog. 2012;8(11):e1003047. Epub 2012/11/29. doi: 10.1371/journal.ppat.1003047. PubMed PMID: 23209417; PubMed Central PMCID: PMCPMC3510260.

266. Hanke ML, Angle A, Kielian T. MyD88-dependent signaling influences fibrosis and alternative macrophage activation during *Staphylococcus aureus* biofilm infection. PLoS One. 2012;7(8):e42476. Epub 2012/08/03. doi: 10.1371/journal.pone.0042476. PubMed PMID: 22879997; PubMed Central PMCID: PMCPMC3411753.

267. Kielian T, Bearden ED, Baldwin AC, Esen N. IL-1 and TNF-alpha play a pivotal role in the host immune response in a mouse model of *Staphylococcus aureus*-induced experimental brain abscess. J Neuropathol Exp Neurol. 2004;63(4):381-96. PubMed PMID: 15099027.

268. Kielian T, Phulwani NK, Esen N, Syed MM, Haney AC, McCastlain K, et al. MyD88-dependent signals are essential for the host immune response in experimental brain abscess.

J Immunol. 2007;178(7):4528-37. PubMed PMID: 17372011; PubMed Central PMCID: PMCPMC2094730.

269. Xiong J, Burkovetskaya M, Karpuk N, Kielian T. IL-1RI (interleukin-1 receptor type I) signalling is essential for host defence and hemichannel activity during acute central nervous system bacterial infection. ASN Neuro. 2012;4(3). Epub 2012/04/18. doi: 10.1042/AN20120008. PubMed PMID: 22414156; PubMed Central PMCID: PMCPMC3328864.

270. Stork LC, Peterson VM, Rundus CH, Robinson WA. Interleukin-1 enhances murine granulopoiesis *in vivo*. Exp Hematol. 1988;16(2):163-7. PubMed PMID: 3257444.

271. Nakai S, Aihara K, Hirai Y. Interleukin-1 potentiates granulopoiesis and thrombopoiesis by producing hematopoietic factors *in vivo*. Life Sci. 1989;45(7):585-91. PubMed PMID: 2671565.

272. Ueda Y, Cain DW, Kuraoka M, Kondo M, Kelsoe G. IL-1R type I-dependent hemopoietic stem cell proliferation is necessary for inflammatory granulopoiesis and reactive neutrophilia. J Immunol. 2009;182(10):6477-84. doi: 10.4049/jimmunol.0803961. PubMed PMID: 19414802; PubMed Central PMCID: PMCPMC2780360.

273. Cain DW, Snowden PB, Sempowski GD, Kelsoe G. Inflammation triggers emergency granulopoiesis through a density-dependent feedback mechanism. PLoS One. 2011;6(5):e19957. Epub 2011/05/31. doi: 10.1371/journal.pone.0019957. PubMed PMID: 21655273; PubMed Central PMCID: PMCPMC3104996.

274. Beaulieu LM, Lin E, Mick E, Koupenova M, Weinberg EO, Kramer CD, et al. Interleukin 1 receptor 1 and interleukin 1β regulate megakaryocyte maturation, platelet activation, and transcript profile during inflammation in mice and humans. Arterioscler Thromb Vasc Biol. 2014;34(3):552-64. Epub 2014/01/23. doi: 10.1161/ATVBAHA.113.302700. PubMed PMID: 24458711; PubMed Central PMCID: PMCPMC4070375.

275. Horai R, Asano M, Sudo K, Kanuka H, Suzuki M, Nishihara M, et al. Production of mice deficient in genes for interleukin (IL)-1alpha, IL-1beta, IL-1alpha/beta, and IL-1 receptor antagonist shows that IL-1beta is crucial in turpentine-induced fever development and glucocorticoid secretion. J Exp Med. 1998;187(9):1463-75. PubMed PMID: 9565638; PubMed Central PMCID: PMCPMC2212263.

276. Dempster DW, Compston JE, Drezner MK, Glorieux FH, Kanis JA, Malluche H, et al. Standardized nomenclature, symbols, and units for bone histomorphometry: A 2012 update of the report of the ASBMR Histomorphometry Nomenclature Committee. J Bone Miner Res. 2013;28(1):2-17. doi: 10.1002/jbmr.1805. PubMed PMID: 23197339; PubMed Central PMCID: PMCPMC3672237.

277. Kini U, Nandeesh BN. Physiology of bone formation, remodeling, and metabolism. Radionuclide and Hybrid Bone Imaging.: Springer: Berlin; 2012.

278. Kielian T, Haney A, Mayes PM, Garg S, Esen N. Toll-like receptor 2 modulates the proinflammatory milieu in *Staphylococcus aureus*-induced brain abscess. Infect Immun. 2005;73(11):7428-35. doi: 10.1128/IAI.73.11.7428-7435.2005. PubMed PMID: 16239543; PubMed Central PMCID: PMCPMC1273898.

279. Frantz AL, Rogier EW, Weber CR, Shen L, Cohen DA, Fenton LA, et al. Targeted deletion of MyD88 in intestinal epithelial cells results in compromised antibacterial immunity associated with downregulation of polymeric immunoglobulin receptor, mucin-2, and antibacterial peptides. Mucosal Immunol. 2012;5(5):501-12. Epub 2012/04/11. doi: 10.1038/mi.2012.23. PubMed PMID: 22491177; PubMed Central PMCID: PMCPMC3422608.

280. Villano JS, Rong F, Cooper TK. Bacterial infections in *Myd88*-deficient mice. Comp Med. 2014;64(2):110-4. PubMed PMID: 24674585; PubMed Central PMCID: PMCPMC3997288.

281. Sjögren K, Engdahl C, Henning P, Lerner UH, Tremaroli V, Lagerquist MK, et al. The gut microbiota regulates bone mass in mice. J Bone Miner Res. 2012;27(6):1357-67. doi: 10.1002/jbmr.1588. PubMed PMID: 22407806; PubMed Central PMCID: PMCPMC3415623.

282. Novince CM, Whittow CR, Aartun JD, Hathaway JD, Poulides N, Chavez MB, et al. Commensal gut microbiota immunomodulatory actions in bone marrow and liver have catabolic effects on skeletal homeostasis in health. Sci Rep. 2017;7(1):5747. Epub 2017/07/18. doi: 10.1038/s41598-017-06126-x. PubMed PMID: 28720797; PubMed Central PMCID: PMCPMC5515851.

283. Yan J, Herzog JW, Tsang K, Brennan CA, Bower MA, Garrett WS, et al. Gut microbiota induce IGF-1 and promote bone formation and growth. Proc Natl Acad Sci U S A. 2016;113(47):E7554-E63. Epub 2016/11/07. doi: 10.1073/pnas.1607235113. PubMed PMID: 27821775; PubMed Central PMCID: PMCPMC5127374.

284. Li JY, Chassaing B, Tyagi AM, Vaccaro C, Luo T, Adams J, et al. Sex steroid deficiency-associated bone loss is microbiota dependent and prevented by probiotics. J Clin Invest. 2016;126(6):2049-63. Epub 2016/04/25. doi: 10.1172/JCI86062. PubMed PMID: 27111232; PubMed Central PMCID: PMCPMC4887186.

285. Knight J. Polymorphisms in tumor necrosis factor and other cytokines as risks for infectious diseases and the septic syndrome. Curr Infect Dis Rep. 2001;3(5):427-39. PubMed PMID: 11559463.

286. McDowell TL, Symons JA, Ploski R, Førre O, Duff GW. A genetic association between juvenile rheumatoid arthritis and a novel interleukin-1 alpha polymorphism. Arthritis Rheum. 1995;38(2):221-8. PubMed PMID: 7848312.

287. Na Y, Bai R, Zhao Z, Wei Y, Li D, Wang Y, et al. IL1R1 gene polymorphisms are associated with knee osteoarthritis risk in the Chinese Han population. Oncotarget.

2017;8(3):4228-33. doi: 10.18632/oncotarget.13935. PubMed PMID: 27980229; PubMed Central PMCID: PMCPMC5354826.

288. Weber A, Wasiliew P, Kracht M. Interleukin-1 (IL-1) pathway. Sci Signal. 2010;3(105):cm1. Epub 2010/01/19. doi: 10.1126/scisignal.3105cm1. PubMed PMID: 20086235.

289. Hol J, Wilhelmsen L, Haraldsen G. The murine IL-8 homologues KC, MIP-2, and LIX are found in endothelial cytoplasmic granules but not in Weibel-Palade bodies. J Leukoc Biol. 2010;87(3):501-8. Epub 2009/12/09. doi: 10.1189/jlb.0809532. PubMed PMID: 20007247.

290. Kuwabara T, Ishikawa F, Kondo M, Kakiuchi T. The role of IL-17 and related cytokines in inflammatory autoimmune diseases. Mediators Inflamm. 2017;2017:3908061. Epub 2017/02/20. doi: 10.1155/2017/3908061. PubMed PMID: 28316374; PubMed Central PMCID: PMCPMC5337858.

291. Bost KL, Bento JL, Petty CC, Schrum LW, Hudson MC, Marriott I. Monocyte chemoattractant protein-1 expression by osteoblasts following infection with *Staphylococcus aureus* or *Salmonella*. J Interferon Cytokine Res. 2001;21(5):297-304. doi: 10.1089/107999001300177484. PubMed PMID: 11429160.

292. Dapunt U, Maurer S, Giese T, Gaida MM, Hänsch GM. The macrophage inflammatory proteins MIP1α (CCL3) and MIP2α (CXCL2) in implant-associated osteomyelitis: Linking inflammation to bone degradation. Mediators Inflamm. 2014;2014:728619. Epub 2014/03/25. doi: 10.1155/2014/728619. PubMed PMID: 24795505; PubMed Central PMCID: PMCPMC3984830.

293. Wengner AM, Pitchford SC, Furze RC, Rankin SM. The coordinated action of G-CSF and ELR + CXC chemokines in neutrophil mobilization during acute inflammation. Blood. 2008;111(1):42-9. Epub 2007/10/10. doi: 10.1182/blood-2007-07-099648. PubMed PMID: 17928531; PubMed Central PMCID: PMCPMC2575836.

294. Prabhakara R, Harro JM, Leid JG, Harris M, Shirtliff ME. Murine immune response to a chronic *Staphylococcus aureus* biofilm infection. Infect Immun. 2011;79(4):1789-96. Epub 2011/01/31. doi: 10.1128/IAI.01386-10. PubMed PMID: 21282411; PubMed Central PMCID: PMCPMC3067568.

295. Kumar V, Abbas A, Aster J. Robbins and Cotran Pathologic Basis of Disease. 9 ed: Elsevier; 2014.

296. Vargas SJ, Naprta A, Glaccum M, Lee SK, Kalinowski J, Lorenzo JA. Interleukin-6 expression and histomorphometry of bones from mice deficient in receptors for interleukin-1 or tumor necrosis factor. J Bone Miner Res. 1996;11(11):1736-44. doi: 10.1002/jbmr.5650111117. PubMed PMID: 8915781.

297. Bajayo A, Goshen I, Feldman S, Csernus V, Iverfeldt K, Shohami E, et al. Central IL-1 receptor signaling regulates bone growth and mass. Proc Natl Acad Sci U S A.

2005;102(36):12956-61. Epub 2005/08/26. doi: 10.1073/pnas.0502562102. PubMed PMID: 16126903; PubMed Central PMCID: PMCPMC1200265.

298. Simsa-Maziel S, Zaretsky J, Reich A, Koren Y, Shahar R, Monsonego-Ornan E. IL-1RI participates in normal growth plate development and bone modeling. Am J Physiol Endocrinol Metab. 2013;305(1):E15-21. Epub 2013/04/16. doi: 10.1152/ajpendo.00335.2012. PubMed PMID: 23592480.

299. Martino MM, Maruyama K, Kuhn GA, Satoh T, Takeuchi O, Müller R, et al. Inhibition of IL-1R1/MyD88 signalling promotes mesenchymal stem cell-driven tissue regeneration. Nat Commun. 2016;7:11051. Epub 2016/03/22. doi: 10.1038/ncomms11051. PubMed PMID: 27001940; PubMed Central PMCID: PMCPMC4804175.

300. Wang Y, Liu X, Dou C, Cao Z, Liu C, Dong S, et al. Staphylococcal protein A promotes osteoclastogenesis through MAPK signaling during bone infection. J Cell Physiol. 2017;232(9):2396-406. Epub 2017/03/31. doi: 10.1002/jcp.25774. PubMed PMID: 28185243; PubMed Central PMCID: PMCPMC5485048.

301. Lee SK, Gardner AE, Kalinowski JF, Jastrzebski SL, Lorenzo JA. RANKL-stimulated osteoclast-like cell formation in vitro is partially dependent on endogenous interleukin-1 production. Bone. 2006;38(5):678-85. Epub 2005/11/23. doi: 10.1016/j.bone.2005.10.011. PubMed PMID: 16309985.

302. Holzinger D, Gieldon L, Mysore V, Nippe N, Taxman DJ, Duncan JA, et al. *Staphylococcus aureus* Panton-Valentine leukocidin induces an inflammatory response in human phagocytes via the NLRP3 inflammasome. J Leukoc Biol. 2012;92(5):1069-81. Epub 2012/08/14. doi: 10.1189/jlb.0112014. PubMed PMID: 22892107; PubMed Central PMCID: PMCPMC3476237.

303. Craven RR, Gao X, Allen IC, Gris D, Bubeck Wardenburg J, McElvania-Tekippe E, et al. *Staphylococcus aureus* alpha-hemolysin activates the NLRP3-inflammasome in human and mouse monocytic cells. PLoS One. 2009;4(10):e7446. Epub 2009/10/14. doi: 10.1371/journal.pone.0007446. PubMed PMID: 19826485; PubMed Central PMCID: PMCPMC2758589.

304. Muñoz-Planillo R, Franchi L, Miller LS, Núñez G. A critical role for hemolysins and bacterial lipoproteins in *Staphylococcus aureus*-induced activation of the Nlrp3 inflammasome. J Immunol. 2009;183(6):3942-8. Epub 2009/08/28. PubMed PMID: 19717510; PubMed Central PMCID: PMCPMC2762867.

305. Takayanagi H. Osteoimmunology and the effects of the immune system on bone. Nat Rev Rheumatol. 2009;5(12):667-76. Epub 2009/11/03. doi: 10.1038/nrrheum.2009.217. PubMed PMID: 19884898.

306. Lukens JR, Gross JM, Calabrese C, Iwakura Y, Lamkanfi M, Vogel P, et al. Critical role for inflammasome-independent IL-1β production in osteomyelitis. Proc Natl Acad Sci U S A. 2014;111(3):1066-71. Epub 2014/01/06. doi: 10.1073/pnas.1318688111. PubMed PMID: 24395792; PubMed Central PMCID: PMCPMC3903206.

307. Kubatzky KF, Uhle F, Eigenbrod T. From macrophage to osteoclast - How metabolism determines function and activity. Cytokine. 2018. Epub 2018/06/15. doi: 10.1016/j.cyto.2018.06.013. PubMed PMID: 29914791.

308. Putnam NE, Fulbright LE, Curry JM, Ford CA, Petronglo JR, Hendrix AS, et al. MyD88 and IL-1R signaling drive antibacterial immunity and osteoclast-driven bone loss during *Staphylococcus aureus* osteomyelitis. PLoS Pathog. 2019;15(4):e1007744. Epub 2019/04/12. doi: 10.1371/journal.ppat.1007744. PubMed PMID: 30978245.

309. Kikuchi T, Matsuguchi T, Tsuboi N, Mitani A, Tanaka S, Matsuoka M, et al. Gene expression of osteoclast differentiation factor is induced by lipopolysaccharide in mouse osteoblasts via Toll-like receptors. J Immunol. 2001;166(5):3574-9. PubMed PMID: 11207318.

310. Raum K, Hofmann T, Leguerney I, Saïed A, Peyrin F, Vico L, et al. Variations of microstructure, mineral density and tissue elasticity in B6/C3H mice. Bone. 2007;41(6):1017-24. Epub 2007/09/07. doi: 10.1016/j.bone.2007.08.042. PubMed PMID: 17931992.

311. Hemmi H, Takeuchi O, Kawai T, Kaisho T, Sato S, Sanjo H, et al. A Toll-like receptor recognizes bacterial DNA. Nature. 2000;408(6813):740-5. doi: 10.1038/35047123. PubMed PMID: 11130078.

312. Lowy FD. *Staphylococcus aureus* infections. N Engl J Med. 1998;339(8):520-32. doi: 10.1056/NEJM199808203390806. PubMed PMID: 9709046.

313. Carrel M, Perencevich EN, David MZ. USA300 methicillin-resistant *Staphylococcus aureus*, United States, 2000-2013. Emerg Infect Dis. 2015;21(11):1973-80. doi: 10.3201/eid2111.150452. PubMed PMID: 26484389; PubMed Central PMCID: PMCPMC4622244.

314. Bost KL, Bento JL, Ellington JK, Marriott I, Hudson MC. Induction of colony-stimulating factor expression following *Staphylococcus* or *Salmonella* interaction with mouse or human osteoblasts. Infect Immun. 2000;68(9):5075-83. PubMed PMID: 10948128; PubMed Central PMCID: PMCPMC101742.

315. Mullaly SC, Kubes P. The role of TLR2 *in vivo* following challenge with *Staphylococcus aureus* and prototypic ligands. J Immunol. 2006;177(11):8154-63. PubMed PMID: 17114491.

316. Liese J, Rooijakkers SH, van Strijp JA, Novick RP, Dustin ML. Intravital two-photon microscopy of host-pathogen interactions in a mouse model of *Staphylococcus aureus* skin abscess formation. Cell Microbiol. 2013;15(6):891-909. Epub 2012/12/24. doi: 10.1111/cmi.12085. PubMed PMID: 23217115.

317. Wang W, Ferguson DJ, Quinn JM, Simpson AH, Athanasou NA. Osteoclasts are capable of particle phagocytosis and bone resorption. J Pathol. 1997;182(1):92-8. doi:

10.1002/(SICI)1096-9896(199705)182:1<92::AID-PATH813>3.0.CO;2-E.   PubMed PMID: 9227347.

318.   Nagl M, Kacani L, Müllauer B, Lemberger EM, Stoiber H, Sprinzl GM, et al. Phagocytosis and killing of bacteria by professional phagocytes and dendritic cells. Clin Diagn Lab Immunol. 2002;9(6):1165-8. PubMed PMID: 12414745; PubMed Central PMCID: PMCPMC130096.

319.   Prates TP, Taira TM, Holanda MC, Bignardi LA, Salvador SL, Zamboni DS, et al. NOD2 contributes to *Porphyromonas gingivalis*-induced bone resorption. J Dent Res. 2014;93(11):1155-62. Epub 2014/09/19. doi: 10.1177/0022034514551770. PubMed PMID: 25239844; PubMed Central PMCID: PMCPMC4293770.

320.   Dominici M, Rasini V, Bussolari R, Chen X, Hofmann TJ, Spano C, et al. Restoration and reversible expansion of the osteoblastic hematopoietic stem cell niche after marrow radioablation. Blood. 2009;114(11):2333-43. Epub 2009/05/11. doi: 10.1182/blood-2008-10-183459. PubMed PMID: 19433859; PubMed Central PMCID: PMCPMC2745851.

321.   Sivick KE, Arpaia N, Reiner GL, Lee BL, Russell BR, Barton GM. Toll-like receptor-deficient mice reveal how innate immune signaling influences *Salmonella* virulence strategies. Cell Host Microbe. 2014;15(2):203-13. doi: 10.1016/j.chom.2014.01.013. PubMed PMID: 24528866; PubMed Central PMCID: PMCPMC3979597.

322.   Hendrix AS, Spoonmore TJ, Wilde AD, Putnam NE, Hammer ND, Snyder DJ, et al. Repurposing the nonsteroidal anti-inflammatory drug diflunisal as an osteoprotective, antivirulence therapy for *Staphylococcus aureus* osteomyelitis. Antimicrob Agents Chemother. 2016;60(9):5322-30. Epub 2016/08/22. doi: 10.1128/AAC.00834-16. PubMed PMID: 27324764; PubMed Central PMCID: PMCPMC4997817.